

CONVERGENCE OF NEURODEVELOPMENTAL DISORDER RISK
GENES ON COMMON SIGNALING PATHWAYS

CONVERGENCE OF NEURODEVELOPMENTAL DISORDER RISK
GENES ON COMMON SIGNALING PATHWAYS

By

BRIANNA UNDA, BSc (Honours)

A Thesis Submitted to the School of Graduate Studies in
partial Fulfillment of the Requirements for the Degree Doctor of Philosophy

McMaster University

© Copyright Brianna Unda, December 2020

DOCTOR OF PHILOSOPHY (2020)
Science—Biochemistry

McMASTER UNIVERSITY
Hamilton, ON

TITLE	Convergence of neurodevelopmental risk genes on common signaling pathways
AUTHOR	Brianna Unda, B.Sc. (McMaster University)
SUPERVISOR	Dr. Karun K. Singh
NUMBER OF PAGES	cccviii, 308

LAY ABSTRACT

Neurodevelopmental disorders result from disruptions to early brain development and include autism spectrum disorder (ASD), developmental delay (DD), epilepsy, and schizophrenia (SZ). These disorders affect more than 3% of children worldwide and can have a significant impact on an individual's quality of life, including an increased risk of death in some cases. There is currently a lack of understanding of how these disorders develop and how to effectively treat them. Neurodevelopmental disorders are thought to arise from alterations in the connections between brain cells (neurons) and one of the major risk factors for these disorders is having certain variations in regions of the genome (DNA sequences), with more than 1000 of these risk variants having been identified so far. In this thesis, we analyzed how genetic risk factors interact in neurons to regulate neural connectivity. We discovered that risk variants found in individuals with different disorders actually work together to regulate similar processes important for neural connectivity, which suggests that distinct disorders may share a common underlying cause. Additionally, we established the importance of a new ASD risk gene and discovered that it interacts with other known risk genes to regulate neural connectivity. This thesis provides new insights into the processes in the brain that lead to neurodevelopmental disorders and has implications for future development of effective therapies for individuals affected by these disorders.

ABSTRACT

Neurodevelopmental disorders (NDDs) are a heterogeneous set of disorders that are characterized by early disruptions to brain development and include autism spectrum disorder (ASD), attention deficit/hyperactivity disorder (ADHD), developmental delay (DD), intellectual disability (ID), epilepsy and schizophrenia (SZ). Although thousands of genetic risk variants have been identified, there is a lack of understanding of how they impact cellular and molecular mechanisms that underlie the clinical presentation and heterogeneity of NDDs. To investigate this, we used a combination of cellular, molecular, bioinformatic and omics methods to study NDD-associated molecular pathways in distinct neuronal populations. First, we studied the interaction between the high-confidence SZ risk genes *DISC1* and *NRG1-ErbB4* in cortical inhibitory neurons and found that *NRG1-ErbB4* functions through *DISC1* to regulate dendrite growth and excitatory synapses onto inhibitory neurons. Next, we studied the 15q13.3 microdeletion, a recurrent copy number variation (CNV) that is associated with multiple NDDs. Using a heterozygous mouse model [*Df(h15q13)/+*] and human sequencing data we identified *OTUD7A* (encoding a deubiquitinase) as an important gene driving neurodevelopmental phenotypes in the 15q13.3 microdeletion syndrome. Due to the paucity of literature on the function of *OTUD7A* in the brain, we used a proximity-labeling approach (BioID2) to elucidate the *OTUD7A* protein interaction network (PIN) in cortical neurons, and to examine how patient mutations affect the *OTUD7A* PIN. We found that the *OTUD7A* PIN was enriched for postsynaptic and axon initial segment proteins, and that distinct patient mutations have shared and distinct effects on the *OTUD7A* PIN. Further, we identified the interaction of *OTUD7A* with a high-confidence bipolar risk gene *ANK3*, which encodes AnkyrinG. We identified decreased levels of AnkyrinG in *Df(h15q13)/+* neurons, and synaptic phenotypes were rescued by increasing AnkyrinG levels or targeting the Wnt pathway. Future investigation should include examination of the role of *OTUD7A* deubiquitinase activity in neural development.

ACKNOWLEDGEMENTS

First and foremost, I would like to thank my supervisor, Dr. Karun Singh, who has continued to believe in my abilities even at times when I don't. Starting out my graduate studies in a newly formed lab, although stressful at times, allowed me to push myself intellectually and taught me how to think critically and problem solve. Although the lab has grown, his "open door" policy has remained, and is always open to chatting about science or life. Over the years he has given me full license to explore my ideas and has allowed me to drive my projects independently. His passion for pushing the boundaries in the field of neuroscience through collaboration and new techniques is truly inspiring and I know I will take the lessons I've learned with me to my future academic endeavors.

I would also like to thank my committee members Dr. Deda Gillespie and Dr. Jonathan Schertzer who have taken this seven-year journey with me and provided insightful feedback which has shaped the trajectory of my research.

I would like to express my gratitude to all past and present members of the lab and the institute, who not only are excellent team members but have also become cherished friends without whom I would not be sane today. Vickie, thank you for taking me under your wing when I started in the lab and helping me through stressful manuscript writing and revisions. Michelle, Annie and Savannah, thank you for always supporting me and making my time as a graduate student a fun experience.

To all of my friends and family, thank you for understanding my crazy lab schedule and my dedication to my work. Your continual love and support have been a constant motivation for me. A special thanks goes to Taylor Jeffrey, who has been a constant support during my thesis writing process.

Last but not least, I would like to thank my grandmother, Viris Brown. I attribute all of my successes to your unwavering support and encouragement throughout my life. Although you are no longer with us, you have remained my number one motivation to push myself harder and to always strive to be the best person I can possibly be.

TABLE OF CONTENTS

LAY ABSTRACT	iii
ABSTRACT	iv
ACKNOWLEDGEMENTS.....	v
TABLE OF CONTENTS	vi
LIST OF FIGURES AND TABLES	ix
LIST OF ABBREVIATIONS	xiii
CHAPTER 1: INTRODUCTION.....	1
1.1 Neurodevelopmental disorders (NDDs).....	1
1.1.2 Schizophrenia (SZ).....	2
1.1.3 Autism Spectrum Disorder (ASD).....	3
1.2 Genetics of NDDs	5
1.2.1 Rare inherited variants and De Novo variants	7
1.2.2 Copy Number Variations (CNVs)	8
1.2.3 SFARI Genes.....	9
1.3 Pathophysiology of NDDs	10
1.3.1 Cortical brain development	10
1.3.2 Excitatory/Inhibitory (E/I) imbalance underlies NDD pathophysiology.....	12
1.3.3 Axonal pathology in NDDs.....	14
1.3.4 Excitatory synaptic connectivity is altered in NDDs	15
1.3.5 Cortical inhibitory interneuron pathophysiology.....	18
1.3.6 Mouse models of NDDs.....	22
1.4 Overcoming challenges in NDD research with new techniques.....	24
1.4.1 Hypothesis-based and discovery-based methods.....	24
1.4.2 Transcriptomics.....	25
1.4.3 Proteomics.....	26
1.4.4 Identifying protein interaction networks (PINs) using proximity-labeling proteomics.....	29
1.4.5 Applying next-generation sequencing (NGS) and omics to CNV analysis.....	32
1.5 Thesis Objectives	34
CHAPTER 2: NEUREGULIN-1 REGULATES CORTICAL INHIBITORY NEURON DENDRITE AND SYNAPSE GROWTH THROUGH DISC1.....	41
2.1 ABSTRACT	44

2.2 INTRODUCTION	45
2.3 MATERIALS AND METHODS	48
2.4 RESULTS.....	54
2.4.1 shRNA Knockdown of DISC1 Inhibits NRG1-Mediated Dendrite and Excitatory Synapse Growth of Cortical Inhibitory Neurons	54
2.4.2 NRG1 Regulates DISC1 Expression and Localization to Glutamatergic Synapses in Cortical Inhibitory Neurons.....	55
2.4.3 NRG1 Functions through DISC1 to Regulate Glutamatergic Synaptogenesis onto Cortical Inhibitory Neurons.....	57
2.4.4 NRG1 Functions through DISC1 to Regulate Dendrite Growth in Cortical Inhibitory Neurons ...	59
2.4.5 ErbB4 and DISC1 Interact in Cortical Inhibitory Neurons	60
2.5 DISCUSSION.....	62
2.6 CONCLUSION	67
2.7 REFERENCES	75
2.8 SUPPLEMENTARY FIGURE.....	85
CHAPTER 3: <i>OTUD7A</i> REGULATES NEURODEVELOPMENTAL PHENOTYPES IN THE 15Q13.3 MICRODELETION SYNDROME	87
3.1 ABSTRACT	90
3.2 INTRODUCTION	90
3.3 MATERIAL AND METHODS	95
3.4 RESULTS.....	106
3.4.1 Df(h15q13)/+ Mice Show Defects in Forebrain Development Including Abnormalities in Dendritic Spines and Dendrite Growth	106
3.4.2 OTUD7A Is a Candidate Driver Gene in the 15q13.3 Microdeletion	108
3.4.3 Expression and Localization of OTUD7A in Neurons	113
3.4.4 Rescue of Spine and Dendrite Phenotypes in Df(h15q13)/+ Excitatory Neurons by OTUD7A..	114
3.4.5 An ASD-Associated De Novo Mutation in OTUD7A Impairs Dendrite and Spine Growth.....	115
3.4.6 OTUD7A Is the Predominant Gene Regulating Dendrite Spine Development	116
3.5 DISCUSSION.....	117
3.6 REFERENCES	133
3.7 SUPPLEMENTAL DATA.....	148
CHAPTER 4: PROXIMITY-LABELING PROTEOMICS OF THE 15Q13.3 MICRODELETION GENE <i>OTUD7A</i> IDENTIFIES SHARED NEURODEVELOPMENTAL DISORDER SIGNALING NETWORKS THROUGH ANK3	157
4.1 ABSTRACT	158
4.2 INTRODUCTION	159
4.3 MATERIALS AND METHODS	164
4.3 RESULTS.....	176

4.3.1 Df(h15q13)/+ cortical neurons show decreased spontaneous firing and bursting patterns	176
4.3.2 Df(h15q13)/+ dendritic spine phenotypes, but not dendrite complexity phenotypes, can be rescued by expression of an epilepsy-associated OTUD7A patient mutation.....	177
4.3.3 Establishing a neuron-specific in vitro BiOLD2 proximity-labelling proteomics system	179
4.3.4 Elucidation of a neuron-specific OTUD7A protein interaction network using proximity labelling proteomics	186
4.3.5 Shared and Distinct Effects of de novo patient mutations on the OTUD7A PIN and functional networks	188
4.3.6 OTUD7A binds the ANKRD and spectrin-binding domains of ANKG and shares a common protein interaction network.....	190
4.3.7 AnkrynG protein levels and localization are altered in Df(h15q13)/+ cortical neurons	192
4.3.8 Exogenous expression of AnkyrinG rescues synaptic phenotypes in Df(h15q13)/+ cortical neurons.....	194
4.3.9 Targeted GSK-3 inhibition with CHIR-99021 rescues neuronal bursting deficits in Df(h15q13)/+ cortical neurons.....	195
4.4 DISCUSSION.....	195
4.4.1 Persistent deficits in neural network activity in a 15q13.3 microdeletion mouse model	196
4.4.2 Shared and distinct effects of patient mutations on synaptic connectivity.....	197
4.4.3 Identification of a novel neuronal OTUD7A protein interaction network that is impacted by patient mutations.....	198
4.4.4 OTUD7A and AnkyrinG protein interaction networks converge on a network of spectrin cytoskeleton and axonal proteins.....	201
4.4.5 AnkyrinG reduction underlies synaptic deficits in 15q13.3 microdeletion mouse neurons	203
4.4.6 GSK-3 inhibition rescues persistent neural activity deficits in a 15q13.3. microdeletion mouse model.....	205
4.5 SIGNIFICANCE.....	206
4.6 SUPPLEMENTARY FIGURES.....	225
CHAPTER 5: DISCUSSION AND FUTURE DIRECTIONS.....	235
5.1 Convergence of two Schizophrenia-linked pathways in cortical inhibitory neuron development.....	235
5.2 Identifying Synaptic Phenotypes in a mouse model of the 15q13.3 Microdeletion	239
5.3 A multimodal approach to Pinpointing disease-driving genes in the 15q13.3 Microdeletion.....	242
5.4 Pleiotropy as a mechanism of CNV Expression in the 15q13.3 Microdeletion	246
5.4.1 A novel OTUD7A protein interactome at the postsynaptic density and the axon initial segment	247
5.4.2 Studying NDD-associated mutations to understand clinical heterogeneity	248
5.4.3 Convergence of OTUD7A with known NDD-associated pathways	249
5.5 Future Directions.....	253
5.5.1 A multi-model approach to studying CNVs.....	253
5.5.2 Convergence of the ubiquitin proteasome system (UPS) with synaptic and NDD-related Pathways.....	254
5.6 Significance.....	260
REFERENCES.....	261

LIST OF FIGURES AND TABLES**CHAPTER 1**

- Figure 1:** Schematic of Human Brain Development. **38**
- Figure 2:** Mechanisms underlying excitation/inhibition imbalance in neurodevelopmental disorders. **39**
- Figure 3:** Diverse dendritic spine pathology in neurodevelopmental disorders. **40**
- Figure 4:** Proximity-labeling proteomic methods. **41**

CHAPTER 2

- Figure 1:** NRG1 regulates DISC1 expression and localization to excitatory synaptic terminals in cortical inhibitory neurons. **68**
- Figure 2:** NRG1 functions through DISC1 to regulate glutamatergic synaptogenesis onto cortical inhibitory neurons. **70**
- Figure 3:** NRG1 functions through DISC1 to regulate cortical inhibitory neuron dendrite growth. **72**
- Figure 4:** ErbB4 and DISC1 physically interact in cortical inhibitory neurons. **73**
- Figure S1:** shRNA knockdown of DISC1 inhibits NRG1-mediated dendrite and excitatory synapse growth of cortical inhibitory neurons. **85**

CHAPTER 3

- Figure 1:** Overview of the 15q13.3 Microdeletion and CHRNA7/OTUD7A Overlapping Deletion. **121**
- Figure 2:** *Df(h15q13)/+* Mice Have Defects in Dendritic Spine Development and Neuronal Morphology. **122**
- Figure 3:** Identification of *OTUD7A* as a Driver Gene of the 15q13.3 Microdeletion. **124**
- Figure 4:** Reduced Expression of *OTUD7A* Contributes to Spine and Dendrite Defects in *Df(h15q13)/+* Mice. **126**
- Figure 5:** An Autism Spectrum Disorder-Linked *De Novo* Mutation in *OTUD7A* Disrupts Dendritic Spine Development and Neuronal Morphology. **128**
- Figure 6:** *OTUD7A* Is the Predominant Gene in the 15q13.3 Microdeletion Regulating Dendritic Spine Development. **130**
- Table 1:** Individual ASD-Affected Case subjects with De Novo Mutations Found near or within *OTUD7A*. **132**
- Figure S1:** A 15q13.3 mouse model (*Df(h15q13)/+*) has defects in forebrain signaling pathways. **149**
- Figure S2:** *Df(h15q13)/+* mice have defects in dendritic spine development. **150**
- Figure S3:** Analysis of overlapping deletions and gene expression in the human 15q13.3 region. **151**
- Figure S4:** *In silico* analysis reveals a *de novo* ASD-linked mutation near *OTUD7A* occurs in the binding region of the transcription factor *EZH2*. **153**

- Figure S5:** Dendritic spine analysis in Df(h15q13)/+ cultured neurons expressing OTUD7A WT or the de novo OTUD7A Asn492_Lys494del mutation. **154**
- Table S3:** Number of cases from each cohort, phenotypic ascertainment and the controls. **156**

CHAPTER 4

- Figure 1:** Persistent synaptic deficits in Df(h15q13)/+ cortical neurons. **208**
- Figure 2:** The OTUD7A protein-interaction network is enriched for postsynaptic and axon initial segment proteins. **210**
- Figure 3:** Effects of patient mutations on the OTUD7A protein interaction network. **212**
- Figure 4:** AnkyrinG binds OTUD7A and shares a protein interaction network. **214**
- Figure 5:** AnkyrinG levels are decreased in Df(h15q13)/+ neurons and are modulated by OTUD7A. **216**
- Figure 6:** AnkyrinG nanodomains are decreased in the dendrites and dendric spines of Df(h15q13)/+ cortical neurons. **218**
- Figure 7:** Rescue of synaptic phenotypes through exogenous AnkyrinG expression or targeted inhibition of GSK-3. **220**
- Table 1:** Proteins with SAINT scores ≥ 0.6 in the WT OTUD7A, OTUD7AN492_K494del, and OTUD7AL23F BioID2 datasets. **222**

- Table 2:** List of proteins shared between OTUD7A-BioID2 list of proteins with SAINT scores ≥ 0.6 and proteins identified in the Hamdan et al., 2020 AIS-BioID2 study. **223**
- Table 3:** Category 1,2 and S (syndromic) SFARI genes shared with WT OTUD7A-BioID2 list of proteins with SAINT scores ≥ 0.6 . **224**
- Figure S1:** Analysis of overexpressed tagged OTUD7A constructs. **225**
- Figure S2:** Validation of BioID2 constructs in HEK 293 cells. **227**
- Figure S3:** Validation of transduced lentiviral BioID2 construct expression and localization in neurons. **228**
- Figure S4:** PSD95-BioID2 identified known PSD95 interactors. **230**
- Figure S5:** Top OTUD7A-BioID2 hits. **232**
- Figure S6:** Validation of AnkyrinG-190-BioID2 construct expression. **233**
- Figure S7:** Endogenous OTUD7A protein expression in 3XFLAG-Otud7a mouse cortex across development. **234**

LIST OF ABBREVIATIONS

AAV	Adeno-associated virus
AIS	Axon initial segment
AMPA	α -Amino-3-hydroxy-5-methyl-4-isoxazolepropionic acid
ANK3	Ankyrin-3
ANKRD	Ankyrin repeat domain
APEX	Engineered ascorbate peroxidase
ASD	Autism spectrum disorder
BioID	Proximity-dependent biotin identification
CHRNA7	Cholinergic receptor, nicotinic, alpha 7
CNTNAP2	Contactin Associated Protein 2
CNV	Copy number variation
CRD	Cysteine-rich domain
DD	Developmental delay
DE	Differential expression
DGV	Database of genomic variants
DISC1	Disrupted in Schizophrenia 1
DISC1DN	Disrupted in Schizophrenia 1-Dominant negative
DISC1FL	Disrupted in Schizophrenia 1- Full length
DIV	Day <i>in vitro</i>
DLG4	Discs large MAGUK scaffold protein 4
DLX6	Distal-less homeobox 6

DSM	Diagnostic and Statistical Manual
DUB	Deubiquitinase
E/I	Excitatory/inhibitory
FMR1	Fragile X mental retardation 1
fMRI	Functional magnetic resonance imaging
GABA	Gamma aminobutyric acid
GAD67	Glutamic acid decarboxylase
GFP	Green fluorescent protein
GO	Gene ontology
GRIA2	Glutamate ionotropic receptor AMPA type subunit 2
GRIN2B	Glutamate receptor, ionotropic, N-methyl D-aspartate 2B
GSEA	Gene set enrichment analysis
GSK-3	Glycogen synthase kinase 3
hSYN	human Synapsin 1 promoter
ID	Intellectual disability
iN	Induced neuron
IP	Immunoprecipitation
iPSC	Induced pluripotent stem cell
IUE	<i>In utero</i> electroporation
KD	Kinase dead
KEGG	Kyoto Encyclopedia of Genes and Genomes

KI	Knock-in
KO	Knockout
LC-MS	Liquid chromatography mass spectrometry
LCR	Low copy repeat
LOF	Loss-of-function
MEA	Multielectrode array
mEPSC	Miniature excitatory postsynaptic current
mIPSC	Miniature inhibitory postsynaptic current
MOI	Multiplicity of infection
mPFC	Medial prefrontal cortex
MRI	Magnetic resonance imaging
MS	Mass spectrometry
NAHR	Non-Allelic homologous recombination
NDD	Neurodevelopmental disorder
NGS	Next generation sequencing
NLS	Nuclear localization sequence
NMDA	N-Methyl-D-aspartate
NPC	Neural progenitor cell
NRG1	Neuregulin-1
OCD	Obsessive compulsive disorder
OTUD7A	OTU deubiquitinase 7A
PBS	Phosphate buffered saline

PDD-NOS	Pervasive developmental disorder- not otherwise specified
PIN	Protein interaction network
PLA	Proximity ligation assay
PPI	Protein-protein interaction
PSD	Postsynaptic density
PSD95	Postsynaptic density protein 95
PTM	Post-translational modification
PV	Parvalbumin
RAC1	Ras-related C3 botulinum toxin substrate 1
SAINT	Significance Analysis of Interactome
SCN1A	Sodium channel, voltage-gated, type I, alpha subunit
SCN2A	Sodium channel protein type 2 subunit alpha
SFARI	Simons Foundation Autism Research Initiative
SHANK2	SH3 and multiple ankyrin repeat domains 2
SHANK3	SH3 and multiple ankyrin repeat domains 3
shRNA	Short hairpin RNA
SNAP-25	Synaptosomal-associated protein, 25kDa

SNP	Single nucleotide polymorphism
SNV	Single nucleotide variant
SPTAN1	Spectrin Alpha, Non-Erythrocytic 1
SST	Somatostatin
STRING	Search Tool for the Retrieval of Interacting Genes
SVZ	Subventricular zone
SYNGAP1	Synaptic Ras GTPase activating protein 1
SZ	Schizophrenia
UBE3A	Ubiquitin-protein ligase E3A
UPS	Ubiquitin proteasome system
VGLUT1	Vesicular glutamate transporter 1
WES	Whole exome sequencing
WGCNA	Weighted gene co-expression network analysis
WGS	Whole genome sequencing
Wnt	Wingless-related integration site
WT	Wild-type
Y2H	Yeast-2-Hybrid

CHAPTER 1: INTRODUCTION

1.1 Neurodevelopmental disorders (NDDs)

Neurodevelopmental disorders are a prevalent and heterogeneous group of disorders involving disruption to brain development that lead to poor psychosocial outcomes in affected individuals (Arim et al., 2015). Although the term has been used to describe a wide range of disorders, the diagnostic and statistical manual of mental disorders 5 (DSM-5) provides the gold standard for grouping mental health disorders. The DSM-V includes the following disorders under the category of neurodevelopmental disorders: intellectual disabilities, communication disorders, autism spectrum disorder (ASD), attention-deficit/hyperactivity disorder (ADHD), Specific learning disorder, motor disorders, and other neurodevelopmental disorders (American Psychiatric Association, 2013). The grouping and labeling of disorders based solely on clinical presentation is both a strength and weakness of the DSM-5; although it provides a standardized method of diagnosis between clinicians, it largely neglects underlying causes that may lead to differential grouping of disorders. Recent research from the past decade, including the emergence of next generation high throughout sequencing methods, have begun to uncover the immensely complex genetic and molecular differences and similarities between NDDs which are not apparent at the level of clinical presentation. The genetics underlying NDDs are complex and research is only beginning to scratch the surface. One of the most puzzling observations has been that many different mutations in different genes can all result in the same NDD; conversely, mutations in the same gene can result in a wide range of NDDs and symptoms. Therefore, it is likely that there is a level of

convergence and regulation above the level of genes, and likely at the level of molecular signaling pathways, that underlies the pathophysiology of NDDs.

1.1.2 Schizophrenia (SZ)

Despite efforts and advances in research and community support, schizophrenia remains one of the most debilitating *health* conditions in industrialized countries (Goeree et al., 2005; Lomholt et al., 2019) Schizophrenic individuals have a shorter lifespan compared to the general population, which is partially due to increased rates of suicide (Hor & Taylor, 2010; Lomholt et al, 2019). This chronic and prevalent neuropsychiatric disorder is estimated to affect up to 1% of the population world-wide (Goeree et al., 2005).

Although the age of onset is typically late-adolescence to early adulthood it is widely accepted that the pathogenesis of the disorder begins in early development (Castle & Murray, 1993; Gogtay et al., 2011). The disorder is also highly heritable; the chance of developing schizophrenia increases with increasing relatedness to the schizophrenic individual (Singh et al., 2014). In the DSM5, schizophrenia is listed under the category Schizophrenia Spectrum and Other Psychotic Disorders and is characterized by three main types of symptoms: positive symptoms, negative symptoms, and cognitive symptoms. Positive symptoms include visual and auditory hallucinations, delusions, and disorganized thoughts. Negative symptoms include social withdrawal, lack of motivation, flat affect, and inability to experience pleasure. Cognitive symptoms include working memory and attention deficits. Antipsychotic drugs are currently the first-line of treatment for schizophrenia. Many antipsychotic drugs improve positive symptoms in

patients; however they are not as successful at treating negative and cognitive symptoms (van Os & Kapur et al., 2009; Remington et al., 2016). Additionally, antipsychotics are associated with many side effects. While these side effects are less common in patients taking atypical antipsychotics, other side effects such as weight gain are common, increasing the risk of diabetes and heart disease (Mitchell et al., 2013). Psychosocial therapies, such as cognitive behavioural therapy, family intervention therapy, and social skills training, are also currently used. A combination of treatments is increasingly becoming regarded as the most effective way of attempting to tackle the many symptoms of this complex disorder (Patterson et al., 2008; Tiihonen et al., 2019). Despite the fact that many antipsychotic drugs improve psychotic symptoms, none have been shown to greatly improve overall psychosocial functionality (Swartz et al., 2007; Remington et al., 2016). It is clear that there is still a long way to go and many improvements to be made to existing treatments. This is mainly due to the lack of knowledge of schizophrenia etiology. While many theories exist, the underlying molecular pathways mediating the development of this disease are currently unknown. Therefore, it is imperative that these pathways be studied to discover potential molecular targets and eventually more effective and safer treatments for schizophrenic individuals.

1.1.3 Autism Spectrum Disorder (ASD)

Autism Spectrum Disorder (ASD) describes a set of neurodevelopmental disorders (NDDs) ranging in severity and characterized by persistent deficits in social communication and social interaction as well as restricted and repetitive behaviours,

interests or activities (Miles, 2011). The previous version of the DSM (DSM-4) categorized children with ASD into three distinct categories: Autistic disorder, Asperger's syndrome, and pervasive developmental disorder- not otherwise specified (PDD-NOS) (Miles, 2011). However, the updated DSM-5, published in 2013, now describes children with ASD under the broad category of autism spectrum disorder (Brentani et al., 2013). Diagnosis typically occurs after 4 years of age, although deficits in communication, which can manifest as a lack of smiling, pointing and babbling, can be observed as early as 6 months of age (Miles et al., 2011). Prevalence estimates report that as many 1 in 54 children are diagnosed with ASD (Maenner et al., 2020). ASD is also reported to be 4.3 times as prevalent in boys compared to girls, highlighting a strong sex bias (Maenner et al., 2020). A strong genetic component to ASD etiology has been widely acknowledged since early twin studies showing high concordance rates between monozygotic twins (Folstein & Rutter, 1977; Hallmayer et al., 2011; Sandin et al., 2014), and modern genetic techniques have continued to discover an unprecedented level of complexity in the genetic architecture of ASD. However, there is still a lack of understanding of how this genetic landscape impacts ASD etiology and pathophysiology. Currently, there are no treatments that cure or treat the core symptoms of ASD, although some behavioural therapies and medications can improve functioning in patients (McPheeters et al., 2011; Virtues-Ortega, 2010). This necessitates the need for valid model systems to study the molecular mechanisms of ASD and other NDDs, which will aid in the development of targeted drug therapies.

1.2 Genetics of NDDS

It is widely accepted that both genetic and environmental factors contribute to the development of NDDs. For much of history, the genetic underpinnings of these disorders remained an intractable area of research due to the lack of available tools to detect these genetic abnormalities. Since then, ever improving sequencing methods have shown that not only do genetics make up a significant proportion of risk for NDDs, but that the genetic architecture of these disorders is much more complex than anticipated. There are many perturbations to the genome that may contribute to the development and pathophysiology of ASD, such as insertions, deletions, single nucleotide variants (SNVs) or copy number variations (CNVs) (O'Roak et al., 2012; Pinto et al., 2014; Yuen et al., 2016), and these variants can be inherited or *de novo*.

The advent of genome wide association studies (GWAS) over a decade ago marked a turning point for studying NDD genetics, particularly in schizophrenia research. In GWAS studies, thousands to millions of genetic variants across the genomes of many individuals are tested to identify genotype-phenotype associations. The goal is to identify genetic loci which confer risk for a particular disorder. Early iterations of this method relied solely on DNA chip-based microarrays that identified the frequency of various single nucleotide variants (SNVs) present in the population (Tam et al., 2019). Those SNVs that are present in > 1% of the population are termed single nucleotide polymorphisms (SNPs) or common variants. The frequency of a given SNV in a population is measured using the minor allele frequency (MAF). A SNV with a low MAF value is considered to be a rare variant (Bush & Moore, 2012). SNP arrays remain an

attractive and widely used sequencing tool due to its affordability and reliability.

However, there are some major limitations to this method. Since it is based on a CHIP array, the genomic coverage is low and restricted mostly to common variants in well-studied or sequenced populations (Tam et al., 2019). Therefore, it is not suitable for identifying rare variants. This presents a large problem, since it is thought that common variants, which have small effect sizes on their own, make up only one to two thirds of the heritability of complex traits, with the rest caused by rare variants with large individual effect sizes (Stein et al., 2013). Although SNP arrays are still widely used, researchers have shifted towards using whole genome sequencing (WGS) or whole exome sequencing (WES) to identify variants associated with disease. These methods are able to analyze the entire genome or exome of a given organism and are a type of next generation sequencing (NGS) or high throughput sequencing (HTS) (Wilfert et al., 2017). In a typical WGS experiment, genomic DNA is first fragmented and pairs of primers are used to produce reads of each DNA fragment, which are then assembled to reconstruct the genome. The number of unique reads that include a given nucleotide is referred to as read depth or sequencing depth. The higher the depth, the more accurate the sequencing (Troost et al., 2018). NGS methods are able to identify all types of genetic variants, including rare variants and structural variants (Yuen et al., 2017). The wide-spread use of NGS has pushed the field of genetics forward and has identified many previously unknown NDD risk variants.

1.2.1 Rare inherited variants and De Novo variants

An important application of WGS and WES has been the identification of both rare inherited and *de novo* mutations in NDDs. While inherited variants are passed directly from parent to offspring, *de novo* variants are newly identified in the affected individual. They are not present in the somatic cells of either parent of the affected individual (proband) and can occur either during gamete formation or very early in embryonic development. *De novo* mutations range from single nucleotide changes to large genomic deletions or duplications (Wilfert et al., 2017). WGS of probands and their families allows researchers to determine whether a variant is inherited or *de novo*. This is a very important distinction; since *de novo* variants are unique to the affected individual, they are more likely to contribute to disease. The Simons Simplex collection is a repository of genetic samples from 2600 families, each including one child affected by ASD and their unaffected parents and/or siblings. Studies using samples from this collection have discovered that there is an enrichment of missense and nonsense *de novo* mutations in probands relative to unaffected sibling controls, suggesting that *de novo* variants are pathogenic and have a large individual effect size (Guo et al., 2018; Turner et al., 2017). While common variants are thought to make up about 50% of ASD risk, *de novo* variants are estimated to make up about 3% of ASD risk. The remaining risk of ASD is attributed to unknown genetics, environmental factors and interactions between risk factors (Gaugler et al., 2014). *De novo* variants typically have very large individual effect sizes and therefore provide an opportunity to study specific molecular pathways that are causally involved with NDDs (Ruzzo et al., 2019).

1.2.2 Copy Number Variations (CNVs)

One of the most strongly associated chromosomal abnormalities associated with ASD and other NDDs are copy number variations (CNVs), which are regions of the genome that are deleted or duplicated, resulting in an abnormal number of copies of genes within the affected region (Kaminsky et al., 2011). These regions are typically greater than 1 kilobase (Kb) in size and can include a large number of genes. CNVs on the smaller end of the spectrum (<5 Mb) are classified as microdeletions/microduplications, based on the fact that they are too small to be resolved through karyotyping (Freeman et al., 2007). CNVs typically occur at areas of the genome which have acquired segmental duplications throughout evolution, leading to areas of low copy repeats (LCRs), which share more than 90% sequence identity with more than one genomic region. These areas are hotspots for a mechanism known as non-allelic homologous recombination (NAHR). Because of their high sequence similarity, recombination between misaligned sequences at LCRs can occur, leading to deletions, duplications or inversions of large regions of the genome (Gu et al., 2008). Importantly, an early study analyzing genetic data from a large human dataset showed that while SNPs and CNVs captured about 80% and 20% of the total detected genetic variation in human gene expression, respectively, there was very little overlap between the two signals (Stranger et al., 2007). This provided early evidence that CNVs are unique and important determinants of complex genetic traits. Approximately 4-10% of individuals with ASD have reported *de novo* CNVs, compared to only 1-2% of their neurotypical siblings. Inherited CNVs also contribute to ASD risk, with a prevalence of 3% in affected individuals (Vicari et al., 2019). A small proportion of recurrent CNVs

are syndromic, meaning that they are sufficient to cause a highly reproducible set of symptoms, such as the 7q11.23 region causing Williams Syndrome and the 15q11.2-q13 deletion/duplication leading to Prader-Willi/Angelman syndrome. However, the majority of pathogenic CNVs display variable expressivity, leading to broad and heterogeneous phenotypic outcomes (Morris et al., 2015; Thibert et al., 2013) Examples of CNVs that are strongly associated with multiple NDDs are 1q21.1, 15q13.3, 22q11.2, and 16p11.2 (Hiroi et al., 2013; Moreira et al., 2014; Niarchou et al., 2019; Qiao et al., 2016; Sharp et al., 2008). A recent large study genotyped 2691 NDD probands (ASD, SZ, ADHD and OCD) and 1769 family members, and found clinically relevant CNVs in all cohorts. They also noted that some genes were impacted by CNVs in multiple disorders, suggesting that CNVs impacting the same genes may contribute to multiple NDDs (Zarrei et al., 2019).

1.2.3 SFARI Genes

The Simons Foundation Autism Research Initiative (SFARI) is an organization that aims for the better understanding, diagnosis and treatment of ASD. SFARI projects include cohorts of individuals with ASD from the Simons Simplex Collection and Simons Variation in Individuals Project. SFARI integrates data from various genetic and molecular ASD studies and uses this information to score ASD risk genes based on the strength of the evidence linking them to ASD. This represents the largest database of curated genes with links to ASD, including 960 scored genes. The genes are separated into 4 categories: syndromic, category 1 (High confidence), category 2 (strong candidate), or category 3 (suggestive evidence) (Abrahams et al., 2013). The syndromic risk genes

are genes that are implicated in idiopathic autism, such as *FMRI* in fragile X syndrome, and *UBE3A* in Angelman syndrome. High confidence (category 1) genes are clearly implicated in ASD by the presence of at least three *de novo* “likely-gene-disrupting” mutations reported in the literature. Many of these also display statistically significant mutation frequency compared to controls with genome-wide significance. There are currently 192 category 1 high confidence genes encoding proteins with a wide range of molecular functions, including the DNA helicase CHD8, sodium channel subunit SCN2A, scaffold proteins SHANK3 and ANK3, and phosphatase PTEN. Category 2 includes genes with two reported *de novo* “likely-gene-disrupting” mutations with consistent evidence in the literature linking it to ASD. Finally, category 3 is the lowest confidence category and includes genes with a single reported *de novo* “likely gene-disrupting” mutation and unreplicated findings in the literature. This is the largest category, with 483 genes, highlighting the need for more studies to investigate the molecular consequences of many newly identified ASD-linked genes (Abrahams et al., 2013). These types of studies tend to lag behind those of human genetic sequencing studies and keeping up with the large amounts of genetic data that is available through NGS poses a daunting task.

1.3 Pathophysiology of NDDs

1.3.1 Cortical brain development

The cerebral cortex is the thin outer layer of the brain that mediates higher-order cognitive thought and processing. The cortex is where neural integration of signals from

other areas of the brain takes place and plays a key role in attention, perception, memory and language. There is a growing amount of evidence to suggest that disruptions to the development of neural circuits in the cortex during critical periods of development underlie the etiology and pathophysiology of NDDs (Leblanc & Fagiolini, 2011; Varghese et al., 2017). The 14-16 billion neurons that reside in the cortex are precisely organized into layers and columns through a complex and spatiotemporally ordered series of events in fetal development (Figure 1). The development of the cortical layers occurs through 3 main processes: cell proliferation, neuronal migration and cortical organization. The cortical layers are formed in an inside-out manner, whereby early born neurons make up the deeper layers and later born neurons make up the superficial layers. The specification of neuronal layering patterns is thought to occur through various molecular cues (Tau & Peterson, 2010; Subramanian et al., 2020). Disruption in certain genes involved in neuronal migration has also been associated with ASD. For example, contactin-associated protein-like 2 (CNTNAP2) gene is a strong candidate gene for ASD that is important for regulation of neuronal migration, and multiple variants in CNTNAP2 have been discovered in patients with ASD and other NDDs (Gdalyahu et al., 2015; Peñagarikano et al., 2011). As the neurons migrate, they begin to develop actin rich protrusions called neurites. The longest of these will become the axon, while the rest will become the dendrites. The neurons connect to one another locally and begin to project myelinated axons which form the cortical white matter. This includes the axon tracts that make up the corpus callosum, the thick bundle of axons that connects the two hemispheres (Subramanian et al., 2020). Unlike excitatory pyramidal neurons, which

originate in the ventricular zone, cortical inhibitory neurons originate in a region of the ventral telencephalon called the ganglionic eminences. These neurons then migrate tangentially into the cortex where they form synaptic connections with other inhibitory and excitatory neurons (Wonders & Anderson, 2006). The final step of the process, cortical organization, starts concurrently with neuronal migration and continues beyond fetal development into postnatal development. This involves the formation and extension of neuronal process, which become the axon and dendrites, followed by formation and pruning of synaptic contacts between neurons. Synaptic density increases rapidly after birth to a level 50% higher than that is seen in adulthood, and is followed by a period of synaptic elimination. Synaptic elimination or pruning and remodeling continues into adolescence in humans, showing that the human brains remains relatively plastic beyond early development (Sakai, 2016; Subrmanian et al., 2020). The formation of these early cortical neuronal circuits is essential for the proper functioning of the brain later in life, and disruption during any of these developmental stages can lead to neurodevelopmental disorders. Over the years, hundreds of genes involved in neurite and synapse development and function have been identified as being linked to various NDDs. As such, synaptic connectivity is a major area of study in NDD research.

1.3.2 Excitatory/Inhibitory (E/I) imbalance underlies NDD pathophysiology

The brain maintains homeostasis through a finely tuned balance of excitation and inhibition, which is carried out through a variety of compensatory mechanisms (Figure 2), and loss of this balance is one of the leading theories of NDD pathophysiology (Gao &

Penzes, 2015). In the cerebral cortex, one mechanism is carried out at the level of cell type specificity, mainly through the opposing actions of glutamatergic excitatory neurons and GABA-ergic inhibitory neurons (Le Roux et al, 2006). The majority of neurons in the cortex (~80%) are excitatory, and have a distinct pyramidal shape. These neurons release the neurotransmitter glutamate from the pre-synaptic terminal of the axon which binds to receptors located in a specialized protein-rich structure called the post-synaptic density (PSD) on the postsynaptic neuron. The excitatory PSD is composed of a dense set of over 100 proteins, including ion channels, receptors, scaffold proteins and intracellular signaling proteins. These proteins work in concert in response to both extracellular and intracellular stimuli to maintain typical neuronal function (Chen et al., 2008; Kaizuka & Takumi, 2018). The most well-studied of these is the scaffold protein PSD95, which anchors the NMDA and AMPA glutamate receptors at the cell surface and serves as a docking site for various intracellular proteins (Kim & Sheng, 2004). Inhibitory neurons release the neurotransmitter GABA, which makes a neuron less likely to fire, and acts to modulate and fine tune excitatory signaling (Le Magueresse et al., 2013). Changes in numbers, protein expression, localization, and morphology of both cell types have been shown to be linked to NDD pathology, which will be detailed in the following sections. Additionally, aberrant functioning of the specialized neuronal process, the axon and dendrites also have a major impact on the balance of excitation and inhibition in the brain, leading to disruptions in brain development and function.

1.3.3 Axonal pathology in NDDs

The axon is the specialized neuronal process that conducts electrical signals away from the cell body to the axon terminal, where vesicles containing neurotransmitters are released into the synaptic cleft. During neuronal migration, neurons polarize and adapt a bipolar morphology, forming the axonal and somato-dendritic compartments. The axon extends and is guided by various extracellular and intracellular cues to a specified destination. Following this, the axon branches and establishes contacts with postsynaptic partners, where it plays a vital role in synaptic transmission (Lewis et al., 2013). Human imaging studies have shown that the corpus callosum is often reduced in individuals with ASD (McFadden & Minshew, 2013) and have identified white matter alterations in individuals with schizophrenia (Stampfli et al., 2019).

The axon is composed of a periodic submembrane actin/spectrin cytoskeleton and a uniform microtubule structure. The proximal axon contains a highly organized specialized structure called the axon initial segment (AIS). This axonal compartment acts as a diffusion barrier between the axonal compartment and the rest of the cell. The AIS is the site of axon potential initiation and is enriched for voltage-gated sodium channels and potassium channels (Leterrier, 2018). These ion channels are anchored to the plasma membrane by AnkyrinG (encoded by *ANK3*), which acts as a scaffold bridging the plasma membrane, actin/spectrin cytoskeleton and the microtubules. Known as the master regulator of the AIS, AnkyrinG clusters along the proximal axon early in development, and then recruits other AIS components. Disruptions in AnkyrinG result in complete disorganization of the AIS and is implicated in various NDDs, such as bipolar disorder

and ASD (SFARI category 1) (Hedstrom et al., 2008; Leussis et al., 2012; Yang et al., 2019). ANK3, as well as other axonal and AIS genes have been implicated in neurodevelopmental disorders, and in particular, epilepsy. For example, mutations in SCN1A (encoding the voltage-gated sodium channel Nav1.1) lead to disorder known as Dravet syndrome, a severe form of intractable childhood onset epilepsy (Cetica et al., 2017). Mutations in SPTAN1 (encoding the AIS enriched alpha II spectrin protein) lead to West syndrome, which is characterized by infantile spasms and intellectual disability (Syrbe et al., 2017). Current research is aimed at understanding the impact of these variants on protein and cellular function in order to develop therapies for currently intractable forms of epilepsy.

1.3.4 Excitatory synaptic connectivity is altered in NDDs

Pyramidal cells receive excitatory inputs at tiny dendritic actin-rich dendritic protrusions, called dendritic spines, each containing a postsynaptic density (PSD). The PSD is a specialized compartment opposed to the plasma membrane of dendritic spines that is composed of diverse proteins including ion channels, receptors, scaffold proteins and signaling proteins (Chen et al., 2008; Kim et al., 2004). PSD proteins make up a large proportion of known NDD risk genes, including scaffold proteins (DLG4, SHANK3, SHANK2), glutamate receptors (GRIA2, GRIN2B), intracellular signaling proteins (SYNGAP1, UBE3A) and adhesion proteins (NRXN1), and the organization of the PSD has been found to be altered in models of NDDs (Clement et al., 2013; O'Connor et al., 201; Penzes et al., 2011). Each pyramidal neuron has thousands of dendritic spines,

allowing for integration of many excitatory inputs. During development, dendritic spines are highly dynamic, with constant formation and pruning of spines, reflecting the plastic nature of synaptic connectivity (Hotulainen & Hoogenraad, 2010; Star et al., 2002).

Dendritic spines are generally classified into four morphological types: mushroom, thin, stubby and filopodia (Figure 3). Mushroom-shaped spines are considered to be the most mature morphology with a characteristic wide head with large PSD and narrow neck, allowing micro-compartmentalization of calcium and other important post-synaptic secondary messengers during synaptic transmission. In contrast, thin spines have smaller PSDs and, due to their smaller size, have a greater potential for synaptic strengthening; therefore, thin spines are sometimes referred to as “learning” spines, and may drive synaptic plasticity in the developing and adult brain. In the adult cortex, only ~25% of spines are mushroom shaped, whereas >65% are thin, with the number of thin spines decreasing with age. Stubby spines have a small squat morphology, and are considered to be functionally immature. Lastly, filopodia spines are long and extremely thin protrusions which don't contain a typical PSD (Bourne & Harris, 2008; Hotulainen & Hoogenraad, 2010). Changes in density and maturity of dendritic spines are thought to correlate with changes in synaptic function and are therefore an area of intense investigation in regard to NDDs (Penzes et al., 2011).

One of the most well supported theories of the etiology of NDDs is that defects in excitatory synaptic connectivity and plasticity underlie these disorders. Although schizophrenia is not classified as a developmental disorder in the DSM-5, there is ample genetic and biological evidence to suggest that it arises due to a disorder of brain

development (Birnbaum & Weinberger, 2017). This hypothesis has also been supported by studies that show that early disruptions to the fetus *in utero*, such as maternal infection, increase the risk of developing schizophrenia (Cannon et al., 2002). Through retrograde analysis, patient studies reveal that schizophrenic patients showing cognitive impairments also displayed cognitive deficits in their childhood years (Reichenberg et al., 2010). Additionally, sequencing studies have identified a large amount of shared genetic risk and overlap of pathogenic mechanisms between schizophrenia and neurodevelopmental disorders such as ASD and ID (Chisholm et al., 2015). Taken together, studies such as these suggest that schizophrenia may result as a manifestation of neurodevelopmental insults acquired thorough embryonic and post-natal development. Magnetic Resonance Imaging (MRI) studies have been instrumental in uncovering brain structural changes in individuals after their first psychotic episode but before beginning treatment. These studies consistently show reductions in volume of the lateral ventricles, hippocampus and cortical grey matter at the time of diagnosis (Steen et al., 2006). One possible explanation for this loss in brain volume is reduced neural connectivity or synapses (sites of neural transmission). Supporting this theory are post-mortem studies which show reduced expression of dendrite protein markers such as synaptosomal-associated protein 25 (SNAP-25) and microtubule associated protein 2 (MAP2) in patient brains (Young et al., 1998). Post-mortem analyses also reveal reduced dendrite length and dendritic spine density in pyramidal excitatory neurons in the frontal cortex of schizophrenic patients (Broadbelt et al., 2002; Young et al., 1998). Reduced dendritic spine density is one of the consistent findings from postmortem analysis of brain tissue

from individuals with schizophrenia (Garey et al., 1998; Rosoklija et al., 2002; Sweet et al., 2009; Konopaske et al., 2014) Conversely, early studies of post-mortem human brains from ASD patients show an increase in dendritic spine density on cortical layer 2 pyramidal neurons (Hutsler & Zhang., 2010). Interestingly, studies also show a pattern of hyper-connectivity within brain regions and hypoconnectivity between brain regions, and newer imaging studies of individuals with ASD have corroborated this data (Geschwind & Levitt., 2007; Li et al., 2020; Varghese et al., 2017) . Mouse models of ASD have found both increases and decreases in neural connectivity, depending on the genetic model used, further highlighting the complexity of the genetic architecture of ASD pathophysiology (Varghese et al., 2017). However, it is unclear as to whether dendritic spine formation, pruning, or a combination of both are the cause of these changes in dendritic spine density. Overall the current state of knowledge on excitatory neuron pathology in NDDs reveals a high degree of overlap between NDD pathological mechanisms and highlights the need to further study how risk factors for different NDDs converge on these mechanisms.

1.3.5 Cortical inhibitory interneuron pathophysiology

Although they make up only approximately 20% of the neurons in the cortex, inhibitory neurons play a significant role in proper cortical development and function (Wonders et al, 2006). Unlike excitatory cortical projection neurons, which originate in the ventricular zone, cortical inhibitory neurons originate in a region of the ventral telencephalon called the ganglionic eminences. These neurons then migrate tangentially into the cortex where

they form synaptic connections with other inhibitory and excitatory neurons (Wonders et al., 2006). Gamma amino butyric acid (GABA) released from GABA-ergic inhibitory neurons is the primary source of inhibition in the cortex. However, during early development, GABA's effects are depolarizing due to the predominant expression of Na-K-Cl cotransporter 1 (NKCC1), which causes accumulation of chloride ions inside cells, resulting in chloride ion extrusion and depolarization upon GABA receptor activation (Le Magueresse & Monyer, 2013). There is evidence that this depolarizing GABA plays a role in the developing cortex by negatively regulating stem cell proliferation in the subventricular zone (SVZ) and acting as a chemoattractant for the migration of cells from the SVZ to the cortical plate (Behar et al., 2001). There is also evidence that GABA-ergic inhibitory neurons can fine tune glutamatergic synapses (Lim et al., 2018), which is crucial for proper neural network circuitry. Inhibitory neurons may also define the timing of critical periods of experience-dependent neural plasticity in the developing brain (Yaeger et al., 2019). Inhibitory neurons are extremely heterogeneous, and nearly all cortical inhibitory neurons express one of three non-overlapping markers: parvalbumin (PV), somatostatin (SST) or ionotropic serotonin receptor 5HT3a (5HT3aR). They are further classified within these groups based on morphology and firing patterns (Lim et al., 2018). Unlike excitatory neurons, inhibitory neurons primarily make synapses onto dendritic shafts, cell bodies and axons. However, application of newer higher resolution imaging techniques have revealed that up to 30% of inhibitory synapses contact dendritic spines, which are always located next to an excitatory synapse.

One of the longest-standing theories of schizophrenia pathophysiology is the NMDAR hypofunction hypothesis. This theory postulates that NMDA receptor dysfunction, particularly on GABA-ergic interneurons, resulting in reduced inhibitory control of pyramidal neurons and toxic levels of excitatory activity from pyramidal neurons (Nakazawa et al., 2012; Nakazawa & Sapkota, 2020). In one study, freely moving awake rats were injected with the NMDAR inhibitor drug MK801, and individual inhibitory and excitatory neurons were extracellularly recorded. Remarkably, inhibitory neurons showed an immediate decrease in firing rate, which was followed by an increase in pyramidal neuron firing (Homayoun & Moghaddam, 2007). This study suggests that NMDAR inhibition may predominantly affect inhibitory neurons, and that it indirectly leads to increased pyramidal neuron firing through disinhibition. Studies on post-mortem brain tissue from schizophrenic individuals have revealed reduced expression of inhibitory markers, such as glutamic acid decarboxylase 67 (GAD67) and parvalbumin (PV) in PV+ neurons in the prefrontal cortex (Kalus et al., 2002). Schizophrenic individuals have been shown to display altered cortical gamma-rhythms during perceptual tasks and increases in gamma frequency oscillations are also highly correlated with the presence of positive symptoms in schizophrenic individuals (Grutzner et al., 2013; Sun et al., 2013). Interestingly, cortical gamma rhythms are primarily driven by fast-spiking PV+ interneurons and are believed to be associated with cognitive functions such as attention and working memory, which are typically deficient in schizophrenia (Cardin et al., 2009). An increase in E/I balance is also the leading theory of epilepsy pathophysiology, as spontaneous seizures are characterized by hypersynchronous firing between networks on

neurons in the brain. Loss of inhibitory neuron function is regarded as a main component driving increased E/I balance leading to seizure activity (Rao & Lowenstein, 2015). Dravet syndrome is an example of a severe form of childhood epilepsy in which inhibitory interneurons are regarded as the most likely pathological mechanism. Dravet syndrome is associated with mutations in the SCN1A gene, leading to inhibition of inhibitory neurons and subsequent hyperexcitability in the brains (Connolly, 2016). SCN1A is also a high-confidence ASD risk gene (SFARI category 1), further highlighting the importance of inhibitory neurons in heterogeneous clinical phenotypes. Animal models of ASD have consistently displayed defects in inhibitory neuron development and function. A recent meta-analysis of 4 different ASD mouse models showed a consistent decrease in inhibitory post-synaptic currents (IPSCs) in L2/3 pyramidal neurons in somatosensory cortex of all 4 models (Antoine et al., 2019). Furthermore, optogenetic stimulation of either PV+ inhibitory neurons or excitatory pyramidal neurons in a mouse model of the ASD risk gene CNTNAP2 showed that increasing excitability of inhibitory neurons or decreasing excitability of pyramidal neurons rescued deficits in social behavior and hyperactivity in this mouse model (Selimbeyoglu et al., 2017). This study provides evidence of an increased E/I ratio in ASD and suggests that this circuit can be modulated for therapeutic purposes. Additionally, many genes encoding proteins important for inhibitory signaling, including the inhibitory scaffold protein gephyrin, GABA receptor GABRA3, the GABA transporter SLC6A1, and inhibitory neuron migration (DLX6) have been identified as strong ASD candidate risk genes (Wang et al.,

2018). Overall, multiple lines of evidence have highlighted an important role for inhibitory neurons in brain homeostasis and NDD pathophysiology.

1.3.6 Mouse models of NDDs

Mouse models remain one of the most widely used model systems to study NDDs due to sequence conservation of many genes between mouse and human, as well as the feasibility of genetic manipulation. Additionally, genetic mouse models are advantageous compared to *in vitro* cell based systems due to the ability to control and observe the effects of genetic manipulations across time (developmental stages) and space (distinct brain regions), as well as the ability to measure changes in neuronal circuit function and behavioural endophenotypes that recapitulate symptoms in human patients. Mouse models aim to satisfy three validation criteria: predictive, construct and face validity. In other words: how well the model can be used to predict unknown aspects of the disease in humans, how well the human genetic deletion is faithfully replicated in the mouse and how well the model recapitulates characteristic human phenotypes associated with the disorder (Nestler & Hyman, 2010). As such, genetic mouse models of NDDs undergo a battery of behavioural, genetic and molecular phenotyping before being considered a valid model for studying the human disease (Silverman et al., 2010).

The rapid pace of disease-associated candidate gene identification through next-generation sequencing has also led to a boom in the number of genetic mouse models created to study NDD pathophysiology. These include single-gene knockout (KO), mutation knock-in (KI), or heterozygous/homozygous CNV models. Mouse models of

many of the ASD-risk genes discovered through WES and WGS have demonstrated alterations in E/I balance and display defects in phenotypes such as dendrite growth, dendritic spine morphology, synaptic function, and NDD-like behaviours in animal models (Crawley, 2012; Lee et al., 2017). Single gene KOs have been particularly instrumental in studying syndromic forms of ASD, such as FragileX syndrome (Hulbert et al., 2016). For example, studies reporting on a FMR1 KO mouse model consistently show an increase in dendritic spine density as well abnormal social behaviours, cognitive deficits and increased repetitive behaviours (Kazdoba et al., 2014). Other ASD gene KO models, such as the CNTNAP2 mouse, have shown decreased dendritic spine density along with ASD-like behaviours (Lazaro et al., 2019). Although there seem to be gene-specific differences in the direction of spine density abnormalities, changes in spine dynamics are consistently associated with ASD-like behaviors in NDD-risk gene KO mouse models. The large number of *de novo* and rare inherited variants identified in individuals has necessitated the need to model these mutations to determine the impact on protein and cellular function. Studying these variants can also shed light on how different mutations in the same gene can contribute to different disorders. One study examined this by comparing two SHANK3 mutations: an ASD-linked mutation and a Schizophrenia-linked mutation. They found that each mutation had both shared and distinct effects on synaptic and behavioural phenotypes, providing a framework for understanding how disease in patients with mutations in the same gene may develop (Zhou et al, 2016). Mouse models have been instrumental in understanding how NDD-associated CNVs impact molecular, cellular and behavioural development and to pin-point disease-causing

genes within CNVs. Mouse models for 16p11.2, 22q11.2, and 15q13.3 have been characterized, and are starting to be used to identify disease-driving genes, which will be crucial to our understanding how CNVs lead to disease (Fejgin et al., 2014; Pucilowska et al., 2015; Hiroi et al., 2013).

1.4 Overcoming challenges in NDD research with new techniques

1.4.1 Hypothesis-based and discovery-based methods

Historically, most of the research done in the field of NDDs has stemmed from observation-driven hypotheses, involving specific studies of one gene at a time. Although many important discoveries have been made in this way, the advent of NGS in the last decade made it impossible for molecular and cellular research to keep up in this manner. How is it possible to sort through the rapidly growing number of identified NDD risk genes and investigate them mechanistically individually? Additionally, it has become clear that many genetic risk loci are shared between different NDDs, suggesting that common networks involved in fundamental neurodevelopmental processes underlying multiple disorders are likely at the root of these disorders. This has presented a challenge that would be extremely difficult to overcome using conventional methods. Discovery-based methods provide an exciting solution to this problem. As the name suggests, the goal of this approach is to discover things that were previously unknown and to see relationships between elements on a global scale. Also known as “omics”, this includes genomics, transcriptomics, proteomics, and metabolomics, which all have one thing in common; they all involve the generation of extremely large datasets of information on the

molecular signature of a biological system (Hasin et al.,2017). In this way, the entire transcriptome or proteome of an organ or cell type can be analyzed both qualitatively and quantitatively, and this information can then be used to develop further hypotheses regarding the mechanistic underpinnings of the findings. The omics field has provided a way to analyze disease states and altered physiological states at a global scale. It has also been used widely in the cancer field to subtype tumors based on biomarkers in order to more effectively treat them. In recent years, molecular subtyping has been recognized by the NDD field as a potential new way to classify NDDs, based on genotype-phenotype associations, rather than classical symptom-based groupings, in the hopes that this classification methods will lead to more effective treatments (Stessman et al., 2016).

1.4.2 Transcriptomics

RNA sequencing allows for the quantitative and qualitative analysis of the entire transcriptome of cells. It is most widely used to analyze differential gene expression (DEG) between groups. Briefly, RNA sequencing starts with extraction of RNA from tissue, mRNA enrichment and fragmentation, cDNA synthesis and library prep. Short adaptors are ligated to each fragment for PCR amplification. These fragments are then sequenced and computational methods are performed to align and assemble the sequencing reads to the transcriptome. These reads are then quantified, filtered and normalized between groups and undergoes statistical tests to identify changes that have a high likelihood of being biologically relevant (Chao et al., 2019). This process is gene set enrichment analysis (GSEA) which is a computational method to determine whether

different sets of genes show statistically significant differences in gene expression (Subramanian et al., 2005). These DEGs can then be grouped into biologically relevant functional networks using large bioinformatic data bases. The most significantly changed networks can then be investigated in more detail. RNA Sequencing has been used to identify novel signaling pathways in NDD mouse models and human cell-based models (Hoffman et al, 2017; Wu et al., 2016).

1.4.3 Proteomics

Proteomics is the large-scale study of proteins in biological systems and allows for quantitative and qualitative analysis of the proteome. Although RNA sequencing has uncovered many altered signaling pathways in NDDs, studies have shown some discordance between results from transcriptomic and proteomic studies (Abraham et al., 2019). This is somewhat expected, since there are many steps on the path from mRNA to mature protein, including translation, protein folding and post-translational modifications (PTMs) such as phosphorylation, methylation, acetylation, ubiquitination, glycosylation, S-nitrosylation and palmitoylation, which can alter protein activity (Deribe et al., 2010). The actions and interactions of proteins are by and large the main effectors of cellular processes, backing the argument that analysis of the proteome is a more accurate depiction of the molecular underpinnings of a system.

A typical proteomics experiment begins with protein isolation through cell/tissue lysis, and specific subcellular compartments can be enriched using fractionation. Proteins are then enzymatically digested to produce peptide fragments. These peptides are separated

through liquid chromatography, ionized and sprayed into a mass spectrometer. Two levels of MS measurements take place in tandem: MS1, which measures the mass to charge ratio (m/z) of peptide molecular ions and MS2, which analyzes the specific fragmentation ion pattern of each peptide ion. This allows for peptides to later be identified with high confidence, which can then be mapped to proteins. The signal intensity of these peptides can be used to estimate the relative abundance of each protein in a sample (Silva et al., 2006). Although label-free MS quantification methods are still widely used, many researchers have turned to label-based quantification methods. One example is the Stable Isotope Labeling by Amino Acids in Cell Culture (SILAC) technique, in which isotope-labeled amino acids are added to cell culture media and are incorporated into newly synthesized proteins (Ong et al., 2002). Label-based methods are faster, since samples are combined prior and therefore requires only one MS run, and has also been shown to be more precise for low abundance proteins. However, label-free methods provide higher proteome coverage (Patel et al., 2009). Therefore, the type of quantitative proteomics method to choose varies based on the specific question being asked. Various computational tools exist to normalize, filter and perform statistical testing of proteomics data (Tyanova et al., 2016). Functional analysis is carried out in a similar manner to RNA Seq workflows, using large annotated databases such as GO, KEGG, Reactome or STRING to identify networks.

In neuroscience and NDD research, proteomics can help answer a wide range of questions, including ones regarding spatial and temporal dynamics of proteins in different regions of the brain and subcellular compartments. Various proteomic studies have

revealed the composition of the PSD in various species, brain regions, and disease states, identifying hundreds of previously unknown PSD proteins. In one study, the PSD was enriched from post-mortem brain samples from bipolar disorder patients and neurotypical controls, and were used to compare the PSD proteome between groups. Of the 2033 proteins identified, 288 were found to be differentially expressed, including proteins involved in mitochondrial function, oxidative phosphorylation, protein translation and calcium signaling (Focking et al, 2016). In another study, PSDs were isolated from the striatum and hippocampus of control and SHANK3 mutant mice, and label-free MS was used to compare the proteomes of each brain region and genotype. They discovered that although both regions showed significantly altered proteins between controls and mutants, there were region specific differences in affected pathways (Reim et al., 2017). Quantitative proteomics can also be used to analyze PTMs through specific purification methods prior to MS. PTMs are important regulators of protein function and activity and play a role in neurological disorders (Arrington et al., 2017; Kelley et al., 2019). Phospho-proteomics maps the global phosphorylation of the proteome, and can be used to not only identify new phosphorylation sites on proteins but also quantitatively compare the phosphorylation status of proteins from multiple samples. SILAC-MS of enriched phospho-peptides from mouse Fmr1 KO mouse embryonic fibroblasts revealed multiple changes to the MAPK, mTOR, Wnt, and p53 signaling pathways (Matic et al., 2014). Overall, quantitative proteomics has led to the discovery of many new NDD-pathways and allowed for spatial and temporal analysis of the proteomes of NDD models.

1.4.4 Identifying protein interaction networks (PINs) using proximity-labeling proteomics

Interactions between proteins regulate the complexity of cellular signaling pathways and interactions between those pathways. As mentioned previously, interactions between genetic variants and associated pathways are thought to underlie NDD etiology and can explain some of the complexity of these disorders. Conventional proteomic methods are suitable for studying the global proteome of a system and measures relative levels of proteins. However, studying protein interaction networks can provide information on how proteins functionally interact with each other in particular cellular compartments and contexts and can help formulate new hypotheses about protein function.

The traditional method for studying protein interactions is the yeast two hybrid (Y2H) screen, which employs the use of a bait and a library of prey proteins. When a bait and prey fragment come within a certain proximity of each other, this allows for the transcription and expression of a reporter gene that can be observed in the yeast.

However, this method is inherently biased because of the use of a prepared library and is typically used to confirm direct binding of proteins. This method is also not adapted for use in other eukaryotic systems (Mehla et al., 2017). Co-immunoprecipitation involves the use of an antibody against a protein of interest to pull down the protein from a lysed sample of cells or tissue. An antibody against a presumptive protein interactor is used to detect if it was pulled down with the protein of interest. This method can be used in both cells and tissue samples, making it more versatile than Y2H. Additionally, immunoprecipitation (IP) can be paired with quantitative mass spectrometry on the

affinity purified sample (Morris et al., 2014). However, because affinity purification occurs after cell lysis, protein degradation and interaction strength changes can occur depending on lysis conditions. Additionally, the quality of the antibody can be extremely variable and can greatly affect the sensitivity of the experiment. Other methods, such as the proximity ligation assay (PLA) allow for endogenous visualization of protein interactions, allowing for spatial resolution of protein interactions. However, this method also relies on the availability of appropriate antibodies and is low-throughput (Weibrecht et al., 2010).

Proximity-dependent labeling coupled to MS has become a valuable method for identifying protein-protein interactions (PPIs) in living cells. This method allows for the detection of endogenous protein interaction networks (PINs) in live cells by enzymatically labelling proteins prior to harvesting, followed by mass spectrometry (MS) (Han et al., 2018). Labelling *in vivo* reduces artifacts that can occur with traditional IP methods due to the presence of detergents and protein degradation during lysing steps. Proximity labeling is able to identify weak and transient interactions, which are typically hard to capture using traditional techniques. The two most widely used proximity labeling techniques that have been developed both rely on labeling of proximal proteins with biotin (Figure 4). Biotin shows strong affinity for streptavidin, allowing for efficient affinity capture following labeling (Sano et al., 1998). The first method that was developed involves the tagging of a protein of interest with the engineered BirA* biotin ligase (BioID) with a catalytic site mutation that allows it to nonspecifically tag proteins in close proximity with biotin (Roux et al., 2012). Another method was subsequently

developed which involves the tagging of a protein of interest to the engineered ascorbate peroxidase (APEX) (Rhee et al., 2013). BirA* uses ATP to create active biotin that labels lysine residues, while APEX uses biotin-phenol that is activated by hydrogen peroxide and labels tyrosine residues (Roux et al., 2012; Hwang & Espenshade, 2016). APEX and BioID have been used to map cellular compartments and signaling pathways in mammalian cells lines such as HEK293 cells (Fazal et al., 2019; Liu et al., 2018; Roux et al., 2012; Schopp & Bethune, 2018; Youn et al., 2018). Two studies have used APEX on cultured cortical neurons and have been used to identify novel proteins in the synaptic cleft and subcellular localization of RNA (Fazal et al., 2019; Ting et al., 2016). To date, there are three studies that have utilized BioID in the brain or cultured neurons. Two studies delivered BioID-tagged synaptic proteins virally *in vivo* using adeno-associated virus (AAV); one mapped excitatory and inhibitory synaptic proteomes in the mouse brain while the other characterized the interactome of a novel regulator of the cytoskeleton at the synapse (Spence et al., 2019; Uezu et al., 2016). The most recent study used AAV packaged BioID constructs to map the axon-initial segment (AIS) proteome in cultured mouse cortical neurons (Hamdan et al., 2020). While BioID constructs can be introduced *in vitro* using either lentivirus or AAV, *in vivo* BioID requires the use of AAV with small packaging size limitations, preventing the study of larger proteins. Many large scaffolding proteins and receptors are implicated in neuronal function and NDDs, highlighting the importance of packaging size considerations when designing BioID experiments.

Although APEX and BioID are powerful tools for identifying PPIs, they each have their own advantages and limitations. APEX cannot be used *in vivo* due to toxicity of the biotin-phenol activator hydrogen peroxide. Additionally, APEX labels tyrosine residues, which are among the least abundant amino acids in proteins and therefore can result in missed labeling (Rhee et al., 2013). Alternatively, BioID requires only ATP and biotin, and labels one of the most common amino acids, lysine. However, BioID has been shown to have reduced activity in the endoplasmic reticulum compared to other proximity labeling methods (May et al., 2020). BioID can be used in *in vitro* or *in vivo* models and, because lysine is one of the most common amino acids, has a higher chance of labeling more proteins within its active biotinylation radius (Roux et al., 201). However, the incubation and label time required for BioID is much longer compared to APEX (hours vs minutes) (Chen, 2017). For this reason, BioID is more suitable for identifying a history of interacting proteins, while APEX can capture more dynamic changes in protein interactions. A newer version of BioID, called TurboID, allows biotin labeling within a 10-min time frame, creating the opportunity to study dynamic changes in PINs *in vivo* and *in vitro* (Branon et al., 2013). Therefore, the appropriate proximity-labeling technique varies greatly depending on the specific question being asked.

1.4.5 Applying next-generation sequencing (NGS) and omics to CNV analysis

Studying CNVs poses a unique challenge given that multiple genes are affected. In order to pinpoint disease driving genes within these deletions or duplications, hypotheses are traditionally formed based on the existing literature. However, this method is inherently

biased and precludes the identification of novel genes involved in brain development and NDD etiology. A less biased alternative is to use CRISPR-Cas9 technology to knock each of these affected genes out in a wildtype background and assess phenotypes related to the full CNV; if any individual gene or combination of gene KOs result in a similar phenotype, it suggests that these genes may be disease-driving. Similarly, rescue experiments can be done by re-introducing each gene individually to cells containing the full deletion. However, for CNVs with many genes, this approach is slow, labor intensive and very expensive.

One way to provide a fast and unbiased starting point for investigation is to use bioinformatic methods to predict which genes in the deletion may be important. In 2014, Dr. Stephen Scherer's team at SickKids (Toronto, CA) devised an algorithm that identifies so-called brain-critical exons (Uddin et al., 2014). These exons are expressed highly in the brain, are protected from accumulation of deleterious mutations in healthy individuals and are enriched for deleterious mutations in ASD individuals. This tool can therefore be used to pinpoint potential disease driving genes in CNVs and has been applied to determine which genes could be driving disease phenotypes in NDDs (Wassman et al., 2019). Another method is to analyze WGS and WES from NDD families and determine if any of the genes in the deletion contain likely protein disrupting *de novo* mutations, as these genes have a higher likelihood of being important for disease etiology (Guo et al., 2018; Turner et al., 2017). Another approach is to use omics-based methods to support literature-based hypotheses regarding putative disease-driving genes in a CNV. For example, proteomic analysis identified altered mitochondrial pathways in a 22q11.2

microdeletion mouse model, in which 9 out of 30 deleted genes are known mitochondrial genes, supporting the hypothesis that some or all of these genes may play a role in this CNV model.

Once one or more disease driving genes are identified, a new challenge arises; if there is little to no literature on the molecular and cellular function of the protein product of the identified gene(s), it may be hard to develop appropriate hypothesis-based experiments. This is where discovery-based experimental designs can be very useful. For example, a genetic mouse model of the protein of interest can be developed and can be compared to a full CNV mouse model to validate the role of disease-driving genes in the CNV phenotype. To understand the molecular underpinnings of altering the dosage of this gene, proteomics can be performed to gain an unbiased global understanding of the signaling pathways that are affected in the model. Additionally, proximity-labeling proteomics can be performed for the protein of interest to identify molecular targets and to investigate convergence with known NDD associated pathways. Using a combination of these tools can greatly accelerate the identification and study of novel disease-driving genes in NDDs, leading to molecular targets for future therapeutic development.

1.5 Thesis Objectives

The overall objective of my PhD thesis was to identify and study novel molecular mechanisms and signaling pathway interactions involved in brain development and NDD etiology. I employed the use of a variety of cellular, biochemical and discovery-based

methods to accomplish this. This objective was further divided into three broad aims, which will be the focus of the following three chapters in this dissertation.

Aim 1: My first aim was to investigate the novel interaction between two high confidence schizophrenia-linked signaling pathways regulating the development of cortical inhibitory neurons. Neuregulin-1 (NRG1) and its receptor ErbB4 are SZ risk genes with established roles in cortical inhibitory neuron development, but the downstream mechanism of regulation had not been fully explored (Buonanno, 2010; Fazzari et al., 2010; Mei et al., 2008). Disrupted in Schizophrenia 1 (DISC1) is another well-established schizophrenia risk gene that was first discovered in a Scottish pedigree with a high prevalence of schizophrenia and other psychiatric disorders as a balanced translocation between chromosomes 1 and 11 (1q42.1;11q14.8) (Brandon & Sawa, 2011; Chubb et al., 2008; Millar et al., 2000). Although DISC1 had not been specifically studied in cortical inhibitory neurons, previous studies suggested that it may play a role in this cell type (Lee et al., 2013). Using techniques such as inhibitory-neuron specific shRNA mediated knockdown, quantitative immunofluorescence, co-immunoprecipitation and PLA, we elucidated a functional and physical interaction between DISC1 and Nrg1-ErbB4. Specifically, we showed that NRG1-ErbB4 signaling functions through DISC1 to regulate the development of dendrite growth and excitatory synapse formation onto inhibitory neurons using inhibitory neuron-specific expression of a dominant negative DISC1 mutant that models the Scottish mutation. This work was published in *Neural Plasticity* in October 2016 and I am the first author of this study.

Aim2: My second aim was to characterize neurodevelopmental phenotypes in a mouse model of the 15q13.3 microdeletion and to pinpoint disease-driving genes in this CNV. The 15q13.3 microdeletion is a recurrent CNV that is associated with intellectual disability (ID), epilepsy, developmental delay (DD), schizophrenia and ASD (Pagnamenta et al., 2009; Shinawi et al., 2009; Stefansson et al., 2008). Although a mouse model of this CNV had been behaviourally characterized, there were no studies investigating the neurodevelopmental or synaptic impacts, nor were there any candidate driver genes (Fejgin et al., 2014). We discovered that pyramidal neurons from the 15q13.3 microdeletion mouse model displayed immature neuronal morphology and altered forebrain development signaling pathways. Through a collaboration with Dr. Stephen Scherer's lab (SickKids Hospital, Toronto, CA), we used genetic and bioinformatic techniques to pinpoint one of the genes, *OTUD7A*, as a potential disease-driving gene in the 15q13.3 microdeletion. Further, rescue experiments revealed that *OTUD7A*, but not an ASD-associated *de novo* *OTUD7A* mutation, was sufficient to rescue neurodevelopmental phenotypes in this model. The results of this work were published in *The American Journal of Human Genetics* (AJHG) in February 2018. I am a co-first author on this study, along with Dr. Mohammed Uddin who was a postdoctoral fellow in Dr. Stephen Scherer's lab at the time. Our study, along with a co-published study from Dr. Christian Schaaf's lab led to the inclusion of *OTUD7A* as a category 2 SFARI ASD risk gene.

Aim 3: Finally, in my third aim, we further investigated the molecular function of the 15q.13.3 microdeletion driver gene *OTUD7A* in neurons. *OTUD7A* encodes a deubiquitinase which removes ubiquitin molecules from target proteins (Mevissen et al., 2013). However, *OTUD7A* has not been previously studied in the brain. Using proximity proteomics, we compared the protein interactome of *OTUD7A* and two NDD-associated *De Novo* *OTUD7A* mutations. We discovered that the *OTUD7A* protein interaction network was enriched for proteins localized to the postsynaptic density and the AIS, and that patient mutations had shared and distinct effects on the *OTUD7A* protein interactome. One of the top BioID2 hits was *ANK3*, a high-confidence bipolar and ASD risk gene which encodes the scaffold protein AnkyrinG, which plays important roles at the AIS and dendritic spines (Luoni et al., 2016; Smith et al, 2014). Biochemical experiments in brain samples confirmed binding between *OTUD7A* and AnkyrinG, and we showed that AnkyrinG levels are decreased in dendritic spines and dendrites of 15q13.3^{+/-} neurons. We were also able to rescue synaptic phenotypes in the 15q13.3 microdeletion mouse model through re-expression of AnkyrinG or targeting an AnkyrinG associated pathway. The results of this study are currently being prepared for submission to *Nature Genetics*.

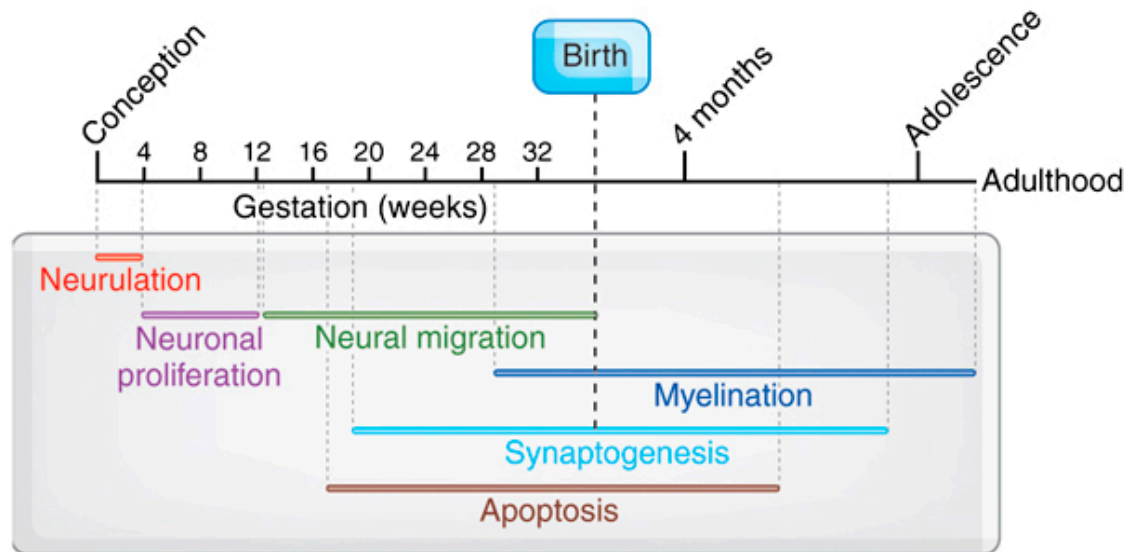


Figure 1. Schematic of Human Brain Development

Brain development occurs through a series of overlapping events from conception through to adulthood. Early processes such as neurulation, neuronal proliferation and migration are complete by birth. Processes such as Synaptogenesis, apoptosis (pruning) and myelination begin before birth and continue into adulthood. Figure adapted from Tau & Peterson, 2010.

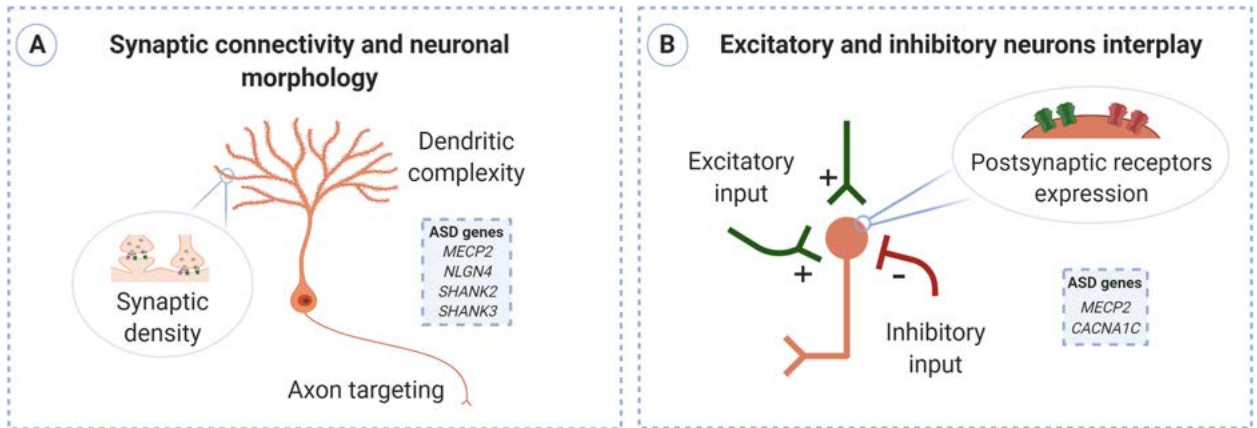


Figure 2. Mechanisms underlying excitation/inhibition imbalance in

neurodevelopmental disorders. (A) The formation and maintenance of neuronal

connectivity requires the proper development and function of specialized neuronal

structures: synapses, dendrites, and axons. (B) Excitatory/ inhibitory balance is

maintained through the interplay between excitatory and inhibitory neuron function.

Alterations of the processes shown in (A) and (B) have been found in models of ASD risk

genes. Figure adapted from Culotta & Penzes, 2020.

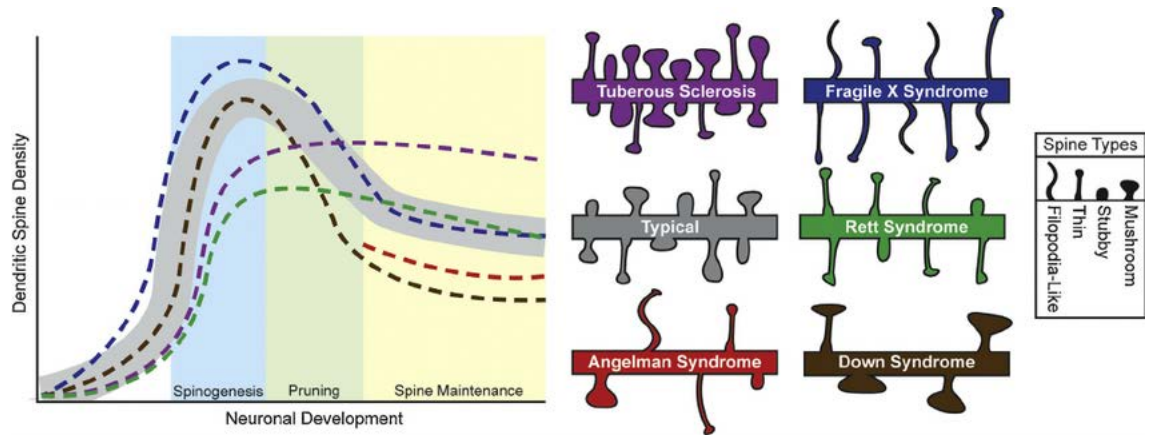


Figure 3. Diverse dendritic spine pathology in neurodevelopmental disorders.

Dendritic spines are formed during early development, followed by an elimination process known as pruning, after which spines are largely maintained into adulthood.

Dendritic spines go through dynamic morphological changes during development and are classified into 4 morphological groups: Mushroom (mature), stubby (immature), thin and filopodia. Alterations to dendritic spines during spine formation, pruning and maintenance have been observed in neurodevelopmental disorders. Figure adapted from Phillips & Pozzo-Miller, 2014.

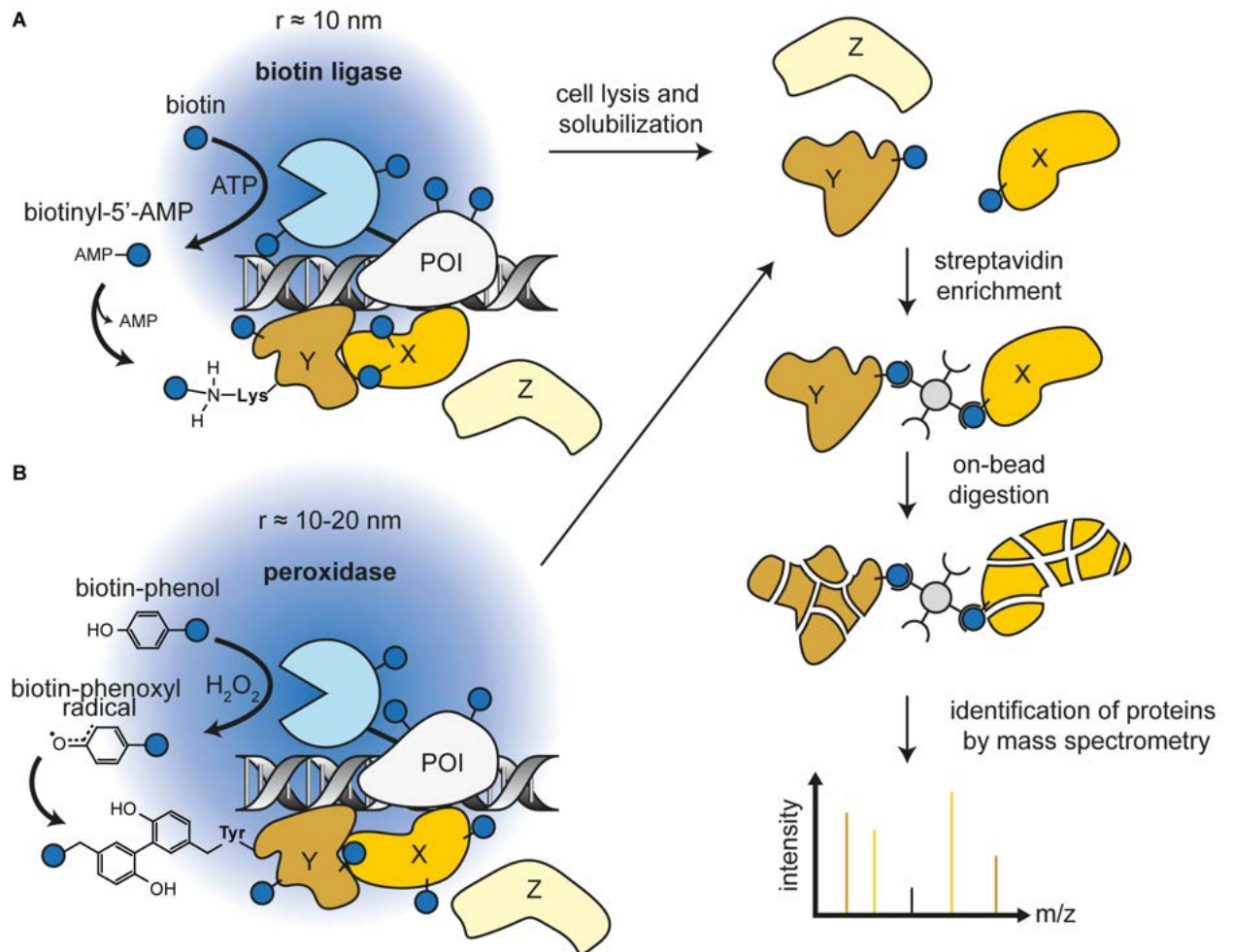


Figure 4. Proximity-labeling proteomic methods. (A) BioID involves the tagging of a protein of interest (POI) to the promiscuous biotin ligase BirA*. Addition of biotin leads to the creation of the reactive intermediate biotinyl-5'-AMP that targets lysine residues on proximal proteins. (B) APEX involves the tagging of a POI to a peroxidase, and addition of hydrogen peroxide leads to the creation of a reactive intermediate that targets tyrosine residues on proximal proteins. Tagged proteins from either method can be pulled down with streptavidin beads, digested and identified through mass spectrometry. Figure adapted from Ummethum & hamper, 2020.

CHAPTER 2: NEUREGULIN-1 REGULATES CORTICAL INHIBITORY NEURON
DENDRITE AND SYNAPSE GROWTH THROUGH DISC1

Brianna K. Unda,^{1,2} Vickie Kwan,^{1,2} and Karun K. Singh^{1,2}

*¹Stem Cell and Cancer Research Institute, McMaster University, Hamilton, ON, Canada
L8S 4K1*

*²Department of Biochemistry and Biomedical Sciences, McMaster University, Hamilton,
ON, Canada L8S 4K1*

Correspondence should be addressed to Karun K. Singh; singhk2@mcmaster.ca Received
16 April 2016; Revised 5 July 2016; Accepted 5 September 2016 Academic Editor:

Andreas M. Grabrucker

Copyright © 2016 Brianna K. Unda et al. “This is an open access article distributed under
the Creative Commons Attribution License, which permits unrestricted use, distribution,
and reproduction in any medium, provided the original work is properly cited.”

PREFACE

This manuscript was published in *Neural Plasticity* on October 25, 2016. It has been
slightly modified to match the formatting of this thesis. Dr. Karun Singh and Brianna
Unda designed the study. All experiments were performed by Brianna Unda, with
assistance from Vickie Kwan. Data were analyzed and figures were prepared by Brianna
Unda. Brianna Unda and Dr. Karun Singh wrote the manuscript.

ACKNOWLEDGEMENTS

The authors would like to thank Dr. Gordon Fishell for the DLX5/6-GFP construct and Dr. Graziella Di Cristo for the P_{G67}-GFP construct. This work was supported by grants from Natural Sciences and Engineering Research Council of Canada (NSERC), the J. P. Bickell Foundation, and the Scottish Rite Charitable Foundation to Karun K. Singh.

2.1 ABSTRACT

Cortical inhibitory neurons play crucial roles in regulating excitatory synaptic networks and cognitive function and aberrant development of these cells have been linked to neurodevelopmental disorders. The secreted neurotrophic factor Neuregulin-1 (NRG1) and its receptor ErbB4 are established regulators of inhibitory neuron connectivity, but the developmental signalling mechanisms regulating this process remain poorly understood. Here, we provide evidence that NRG1-ErbB4 signalling functions through the multifunctional scaffold protein, Disrupted in Schizophrenia 1 (DISC1), to regulate the development of cortical inhibitory interneuron dendrite and synaptic growth. We found that NRG1 increases inhibitory neuron dendrite complexity and glutamatergic synapse formation onto inhibitory neurons and that this effect is blocked by expression of a dominant negative DISC1 mutant, or DISC1 knockdown. We also discovered that NRG1 treatment increases DISC1 expression and its localization to glutamatergic synapses being made onto cortical inhibitory neurons. Mechanistically, we determined that DISC1 binds ErbB4 within cortical inhibitory neurons. Collectively, these data suggest that a NRG1-ErbB4-DISC1 signalling pathway regulates the development of cortical inhibitory neuron dendrite and synaptic growth. Given that NRG1, ErbB4, and DISC1 are schizophrenia-linked genes, these findings shed light on how independent risk factors may signal in a common developmental pathway that contributes to neural connectivity defects and disease pathogenesis.

2.2 INTRODUCTION

Proper functioning of the central nervous system requires a fine balance between excitatory and inhibitory neurotransmission [1]. Cortical inhibitory neurons, classified by their expression of the inhibitory neurotransmitter gamma aminobutyric acid (GABA), comprise 10–25% of neurons in the cortex and are the primary source of inhibition [2]. Cortical inhibitory neurons play major roles in neural development and are important for processes such as fine-tuning of glutamatergic synapse formation and function and defining the timing of critical periods of experience-dependent neural plasticity in the developing brain [3, 4]. Cortical inhibitory neurons are also regulators of high frequency gamma oscillations, which are thought to underlie cognitive processes such as working memory and attention [5–7]. There is also abundant evidence that deficits in the development and function of cortical inhibitory neurons are involved in neurodevelopmental disorders such as epilepsy, schizophrenia, and autism spectrum disorders (ASDs) [1, 8–13]. Therefore, understanding the molecular pathways that regulate inhibitory neuron development may shed light on how their function is disrupted in these disorders. In this regard, the morphological development of cortical inhibitory neurons is governed by both extracellular (e.g., neuronal activity [14] and NRG1 [15–17]) and intracellular signalling molecules (e.g., the distal-less homeobox (Dlx) family of transcription factors [18]), which regulate the branching of dendrites and formation of synapses. However, the underlying signalling pathways governing inhibitory neuron development and, consequently, how these processes may be affected in neurodevelopmental disorders are still poorly understood.

Multiple studies have implicated a crucial role for the Neuregulin-1- (NRG1-) ErbB4 signalling pathway in the development of cortical inhibitory neurons. Furthermore, several linkage and genetic association studies have identified the genes encoding both of these proteins as risk factors for schizophrenia [19–23]. NRG1 is a neurotrophic factor that binds to and activates the ErbB family of receptor tyrosine kinases on target neurons [24, 25]. In the mouse cortex, ErbB4 is predominantly expressed in GABA-ergic inhibitory neurons, with lower expression levels in excitatory neurons [17, 26–28]. Biological functions of the NRG1-ErbB4 signalling pathway in inhibitory neuron development include processes such as neuronal migration, dendrite growth, synapse formation, and neurotransmitter receptor expression [15, 16, 29–31]. For example, application of NRG1 to cortical neuronal cultures results in increased dendrite growth and excitatory synaptogenesis onto inhibitory neurons [15, 16], and inhibitory neuron-specific ErbB4 knockout mice display decreased excitatory synaptogenesis onto cortical inhibitory neurons [30]. One of the mechanisms by which NRG1-ErbB4 signalling regulates these processes is through activation of Kalirin-7, a gene previously implicated in schizophrenia [15, 32, 33]. However, there is little known about other signalling molecules downstream of NRG1-ErbB4 in this context. Disrupted in Schizophrenia 1 (DISC1) is another putative schizophrenia risk gene [34–41], and many lines of evidence suggest that it may functionally and/or physically interact with the NRG1-ErbB4 signalling pathway [15, 17, 30, 40–47]. DISC1 was first identified as a balanced translocation between chromosomes 1 and 11 (1q42.1; 11q14.8) in a Scottish pedigree with a high prevalence of schizophrenia and other psychiatric disorders [32, 33]. The

functional consequence of this translocation is unknown. Previous studies suggest that it may work as a dominant negative protein [48–50], while another study suggests the disease mechanism may be haploinsufficiency [51] with the possibility of novel transcripts being generated due to the translocation [52]. The DISC1 gene encodes a scaffold protein that is expressed in the developing and adult brain and shares many roles in neurodevelopment with the NRG1-ErbB4 pathway [15, 46, 48, 50, 53, 54]. Conditional inhibitory neuron-specific ErbB4 knockout mice and DISC1 genetic mouse models display similar morphological deficits in brain development as well as behavioural phenotypes such as abnormal sensorimotor gating, working memory, and sociability [17, 30, 40–43, 50]. Additionally, ErbB4 and DISC1 share common binding partners at the postsynaptic density of excitatory synapses (e.g., postsynaptic density-95 (PSD95) and Kalirin-7) suggesting that they may physically or functionally interact [15, 44, 45]. A study by Seshadri and colleagues demonstrated that treatment of primary mouse cortical neurons with NRG1 increased DISC1 expression in the neurites of cortical neurons [49]. However, this effect was primarily mediated by ErbB2/3, suggesting that a novel NRG1-ErbB2/3 pathway regulates DISC1 expression in cortical excitatory neurons [49]. More recently, a study by the Sawa laboratory demonstrated that, in the mature mouse cortex, there is a functional relationship between NRG1, ErbB4, and DISC1 in the regulation of synaptic plasticity in inhibitory neurons [55]. However, whether this relationship is established during inhibitory neuron development and how the Scottish DISC1 mutation impacts this process have not been experimentally interrogated.

Here, we show that NRG1 functions through DISC1 to regulate the development of dendrite growth and excitatory synapse formation onto inhibitory neurons using inhibitory neuron-specific expression of a dominant negative DISC1 mutant that models the Scottish mutation. Furthermore, we provide evidence that treatment of primary mouse cortical cultures with NRG1 increases DISC1 levels and localization to glutamatergic synapses in the primary dendrites of inhibitory neurons. Finally, we provide evidence that ErbB4 binds to DISC1, suggesting that, in developing inhibitory neurons, NRG1-ErbB4 signals through DISC1. Together these results show that two candidate schizophrenia risk pathways functionally interact to regulate the development of cortical inhibitory neuron morphology.

2.3 MATERIALS AND METHODS

Antibodies and Constructs

The following primary antibodies were used in this study: goat anti-DISC1 N-terminus (N-16) (Santa Cruz Biotechnology; IF/PLA 1 : 100, WB 1 : 500), rabbit anti-ErbB4 C-terminus (C-18) (Santa Cruz Biotechnology; PLA 1 : 100, WB 1 : 100), guinea pig anti-VGLUT1 (EMD Millipore; IF 1 : 1000, WB 1 : 3000), anti-GAD65&67 (Millipore; 1 : 1000), mouse anti-GFP (Santa Cruz Biotechnology; IP 1 : 1000), rabbit anti- β -actin (Cell Signaling Technologies; IB 1 : 1000), anti-mouse IgG (IP 1 : 1000), and chicken anti-GFP (Aves Labs Inc.; IF 1 : 1000). All secondary antibodies (anti-goat cy5, anti-guinea pig cy3, and anti-chicken 488; Jackson ImmunoResearch; IF 1 : 500, anti-rabbit-HRP, anti-mouse-HRP; GE Life Sciences; IB 1 : 5000) were raised in donkey. The DLX5/6-

GFP construct was a gift from De Marco García et al. [14]. The control shRNA, DISC1 shRNA, and DISC1-GFP constructs were created as described previously [56]. The PG67-GFP construct was a gift from Dr. Graziella Di Cristo [57, 58]. The PG67-DISC1FL and PG67-DISC1DN constructs were generated by GeneArt (Life Technologies). The full-length mouse DISC1 gene (DISC1FL) (RefSeq NC 000074.6) and a C-terminal truncated mutant in which the C-terminal 257 amino acids are deleted (DISC1DN) [50] were assembled from synthetic oligonucleotides and/or PCR products. Each fragment was cloned separately into the PG67-GFP vector (kanR) using *PacI* and *PmeI* cloning sites, resulting in constructs containing the promoter of GAD67 upstream of the DISC1FL or DISC1DN coding sequence. The plasmid DNA was then purified from transformed bacteria. The ErBb4 plasmid and ErbB4 KD plasmid were gifts from Yardena Samuels (pcDNA3.1-ErbB4: Addgene plasmid #29527, pcDNA3.1- ErbB4 kinase dead: Addgene plasmid #29533).

Cell Culture, Transfection, and Treatment

Primary cortical neurons were cultured as follows. Cortices were dissected out of CD1 mouse (Charles River) embryonic brains at E16. Dissociation was aided by incubation in 0.3 mg/mL Papain (Worthington Biochemical)/400 U/mL DNase I (Invitrogen) in 1x Hanks Buffered Saline Solution (HBSS) for 20 minutes at 37°C, followed by light trituration. Cells were seeded onto 0.1 mg/mL Poly-D-Lysine (BD Sciences)/3.3 μ g/mL Laminin (Sigma)-coated cover slips (Matsunami) in 12-well plates at a density of $\sim 0.8\text{--}1 \times 10^6$ cells/well in plating media containing Neurobasal medium, 10% Fetal Bovine

Serum, 1% Penicillin/Streptomycin, and 2 mM L-Glutamine (Invitrogen). After 1.5 hours, media was changed to serum-free feeding media containing Neurobasal medium, 2% B27 supplement, 1% Penicillin/Streptomycin, and 2 mM L-Glutamine. At DIV2–4, cultures were treated with 1 μ M Cytosine β -D-arabinofuranoside hydrochloride (Ara-C) (Sigma) to inhibit glial cell proliferation. Cultures were maintained at 37°C, 5% CO₂. All media components were from Gibco unless otherwise specified. Transfections were performed at DIV7 using Lipofectamine LTX and Plus reagents (Invitrogen) according to the manufacturer's instructions.

HEK 293 FT cells were cultured in Dulbecco's Modified Eagle Medium (Fisher Scientific) supplemented with 10% FBS and 1% Glutamax (Fisher Scientific) and were passaged every 2–4 days. HEK 293 FT cell transfections were performed using Lipofectamine 2000 (Invitrogen) according to the manufacturer's instructions.

Primary neurons were treated with 5 nM Recombinant Human NRG1 β 1/HRG1 β 1 EGF Domain (R&D Systems) dissolved in phosphate-buffered saline (PBS) on DIV19 and an equal volume of PBS was used as a vehicle control. For western blotting, primary cortical cultures were treated with 5 nM NRG1 on DIV3 and 4, and scraped into lysis buffer on DIV5. For Duolink Proximity Ligation Assays, cells were treated with NRG1 β 1 or PBS for 5 minutes prior to fixation. HEK 293 FT cells were treated with 10 nM Human NRG1 β 1/HRG1 β 1 EGF Domain for 5 minutes at 37°C. Following treatment, cells were placed on ice, washed with ice-cold PBS, and scraped into lysis buffer.

Coimmunoprecipitation and Western Blotting

Protein lysates were prepared by cell scraping in lysis buffer (150 mM NaCl, 1% Triton X-100, 50 mM Tris-Cl, and cOmplete mini protease inhibitor cocktail (Roche)). 25 μ L protein G dynabeads (Fisher Scientific) were incubated with 5 μ g primary antibody or IgG control antibody for 1 h at 4°C. Lysates were then incubated with the bead-Ab conjugate for 1 h at 4°C. The beads were then washed three times with lysis buffer and then boiled in sample buffer for 5 minutes. For western blotting, 20 μ L of sample was loaded in a 8% Tris-Glycine gel and run at room temperature, followed by transfer to a PVDF membrane (Thermo Scientific). Membranes were blocked for 1 h in 3% milk in 1x TBST and incubated with primary antibody overnight and then with secondary antibody (donkey anti- mouse or anti-rabbit HRP, GE Healthcare) for 1 h at room temperature before exposure using a ChemiDoc MP system (BioRad).

Immunocytochemistry and Quantification

On DIV21, cells on glass cover slips were fixed in 4% formaldehyde in PBS for 20 minutes at room temperature. Cells were washed in PBS, followed by blocking in Blocking/Permeabilization solution consisting of 10% Donkey Serum (Cedarlane) and 0.3% Triton X-100 (Fisher Scientific) in PBS for 1 hour at room temperature. Incubation in primary antibodies was performed at 4°C overnight with gentle agitation. Cells were then washed in PBS, followed by incubation with secondary antibodies in 50% Blocking/Permeabilization solution at room temperature with gentle agitation for 1.5 hours. Cells were then washed in PBS and were mounted on VistaVision glass microscope slides (VWR) using Prolong Gold antifade reagent (Life Technologies).

Cover slips were allowed to dry overnight before being imaged on a Zeiss LSM700 confocal microscope. For puncta analyses, images were manually thresholded using ImageJ such that each image within an experiment was thresholded to the same value. The “Particle Analysis” tool in ImageJ was used to count the number of individual puncta from the cell body and two to three dendritic sections per cell (10–40 μm^2) of primary dendrites adjacent to the cell body. Sholl analysis was performed in ImageJ. The Straight Line tool was used to draw a line 200 μm in length starting from the centre of the soma. The Sholl analysis plugin (<http://labs.biology.ucsd.edu/ghosh/software/ShollAnalysis.pdf>) was used to make concentric circles increasing at a constant radius of 10 μm and to count the number of intersections.

Duolink Proximity Ligation Assay (PLA)

The PLA was performed using Duolink *In Situ* Red reagents (Sigma). Cortical neurons were seeded onto poly-D-Lysine/Laminin- coated cover slips in 24-well plates ($\sim 3.5 \times 10^5$ cells/well) or 12-well plates ($\sim 1 \times 10^6$ cells/well). After treatment on DIV21, the cortical neurons were fixed with 4% formaldehyde in PBS at room temperature for 20 minutes. Cells were washed in 1x PBS 3 times, 8 minutes each, followed by blocking in Blocking/Permeabilization solution consisting of 10% Donkey Serum (Cedarlane) and 0.3% Triton X-100 (Fisher Scientific) in PBS for 1 hour at room temperature. Incubation in primary antibodies was performed at 4°C overnight with gentle agitation. Primary antibodies were omitted in the control PLA condition. Samples were washed in 1x Wash Buffer A (supplied with the kit) at room temperature 2 times, 5 minutes each, followed by

incubation with a mixture containing the two PLA probes diluted in 50% Blocking/Permeabilization Solution in a humidified chamber at 37°C for 1 hour. The cells were again washed in 1x Wash Buffer A at room temperature 2 times, for 5 minutes. The ligation reaction was performed in a humidified chamber at 37°C for 30 minutes, followed by washing in 1x Wash Buffer A 2 times, 5 minutes each. The cells were then incubated with the amplification- polymerase solution for 100 minutes at 37°C in a darkened humidified chamber. The cells were then washed with 1x Buffer B (supplied with the kit) 2 times, 10 minutes each, followed by a 1 minute wash with 0.01x buffer B at room temperature. Cover slips were then mounted onto VistaVision glass microscope slides (VWR) using mounting media with DAPI (supplied with the kit). Images were acquired on a Zeiss LSM700 confocal microscope using a 63x objective. The PLA signal density (identified as red dots) was quantified in the cell body and 3 primary dendrites per cell from manually thresholded maximum intensity projections of three to seven Z-stacks (1 μm step size) per image using ImageJ.

Statistical Analysis

Quantified data are presented as mean \pm SEM and analyzed using GraphPad PRISM 6. Statistical comparisons between two groups were made using unpaired student's *t*-tests. Comparisons between multiple groups were made using one-way analysis of variance (ANOVA), with Tukey's *post hoc* tests to identify significant differences between groups. Probability (*p*) values of less than 5% were considered significant.

2.4 RESULTS

2.4.1 shRNA Knockdown of DISC1 Inhibits NRG1-Mediated Dendrite and Excitatory Synapse Growth of Cortical Inhibitory Neurons

We used mixed primary cortical neuron cultures derived from E16/17 mouse embryos as our model system, which contains both excitatory and inhibitory neurons. To label and identify cortical inhibitory neuron, we transfected cultured neurons with a plasmid that expresses green fluorescent protein (GFP) under an enhancer element of the distal-less homeobox (DLX) 5 gene, which is expressed in the majority of forebrain inhibitory neurons [14]. We then cotransfected previously validated control shRNA or DISC1 shRNA plasmids together with DLX5/6-GFP into day *in vitro* (DIV) 7 neurons [56]. We treated cultures with NRG1 (or PBS control) for two days beginning at DIV19 and analyzed cells at DIV21. We found that knocking down DISC1 expression caused no change in the puncta density of the excitatory presynaptic marker, vesicular glutamate transporter 1 (VGLUT1), in both the cell body and primary dendrites compared to control shRNA-treated neurons (Supplementary Figures 1A–C in Supplementary Material available online at <http://dx.doi.org/10.1155/2016/7694385>). Furthermore, we found that the control shRNA-expressing neurons treated with NRG1 showed an increase in VGLUT1 puncta density in the primary dendrites, in line with a previous report [16] (Figures 1(a) and 1(c)). To determine if DISC1 plays a role in this process, we knocked down DISC1 in neurons treated with NRG1 and discovered that the NRG1-mediated increase in VGLUT1 puncta density was completely abolished (Supplementary Figures 1A–C).

Next we determined if NRG1 regulates dendritic growth of cortical inhibitory neurons through DISC1. Using the same cultures for analysis, we imaged the complete dendritic morphology of individual GFP-labelled cortical inhibitory neurons. Using Sholl analysis, we determined that knocking down DISC1 led to a decrease in dendritic morphology in PBS-treated cells (Supplementary Figures 1D–F). Furthermore, we determined that NRG1 treatment for two days led to an increase in dendritic morphology, which was abolished when DISC1 expression was decreased using shRNA (Supplementary Figures 1D–F). Taken together, these results suggest that NRG1 regulates the dendritic and synaptic growth of cortical inhibitory neurons and requires DISC1 expression to mediate these effects.

2.4.2 NRG1 Regulates DISC1 Expression and Localization to Glutamatergic Synapses in Cortical Inhibitory Neurons

The results in Supplementary Figure 1 suggest that NRG1 regulates cortical inhibitory dendrite and synapse growth; however, a caveat of these experiments is that DISC1 was knocked down nonspecifically in both excitatory and inhibitory neurons since we used cultures. Therefore, in our subsequent experiments we specifically manipulated DISC1 levels in cortical inhibitory neurons with a construct that uses the glutamic acid decarboxylase (GAD67) promoter to drive separate expression of GFP and DISC1 (P_{GAD67}-GFP). GAD67 is expressed in all forebrain GABA-ergic neurons as it is the rate-limiting enzyme in the conversion of glutamate to GABA [59]. Furthermore, it has been reported that the majority of DLX5-expressing cortical inhibitory neurons also express

GAD67 [14]. Immunostaining of cortical cultures transfected with P_{G67}-GFP confirmed that GFP-positive neurons expressed endogenous GAD67 (Figure 1(a)). Given the potential relationship between NRG1 and DISC1 we uncovered, we wanted to determine if NRG1 treatment specifically regulates DISC1 expression in cortical inhibitory neurons. It has been previously shown that NRG1 treatment of cortical neuron cultures leads to an increase in DISC1 levels via an ErbB2/3-mediated mechanism, most likely reflecting DISC1 levels in excitatory neurons as they make up 80–90% of cortical neuron cultures [49]. Therefore, we hypothesized that NRG1 also regulates DISC1 expression levels and localization specifically within inhibitory neurons. Using quantitative immunofluorescence, we first detected that two days of NRG1 treatment (starting at DIV19) of developing cultures caused a significant increase in DISC1 levels in the primary dendrites and the cell body of DIV21 cortical inhibitory neurons compared to vehicle treatment (PBS) (Figures 1(b), 1(c), and 1(f)), suggesting that the growth effects of NRG1 on inhibitory neurons may require DISC1. Given this result, we next asked whether the NRG1-induced increase in DISC1 expression is localized to excitatory synapses on inhibitory neurons by staining for VGLUT1. The numbers of VGLUT1 or double-positive DISC1/VGLUT1 puncta on the cell body and primary dendrites of P_{G67}-GFP positive inhibitory neurons were quantified. We found that NRG1 treatment led to a significant increase in the number of VGLUT1-positive excitatory synapses on both the cell body and primary dendrites (Figures 1(b), 1(d), and 1(g)). Furthermore, we found a significant increase in double-positive DISC1/VGLUT1 puncta on the cell body and primary dendrites on cortical inhibitory neurons (Figures 1(b), 1(e), and 1(h)). These data

indicate that NRG1 stimulation is sufficient to increase DISC1 levels and localize its expression to excitatory synapses formed on inhibitory neurons. Additionally, western blotting of cultured cortical neurons treated with NRG1 on DIV3 and 4 showed a slight increase in VGLUT1 and DISC1 levels compared to vehicle (PBS) treated cultures, although this was not significant (Figure 1(i)).

2.4.3 NRG1 Functions through DISC1 to Regulate Glutamatergic Synaptogenesis onto Cortical Inhibitory Neurons

In the mouse brain, the NRG1 receptor ErbB4 is primarily localized to GABA-ergic interneurons in the postsynaptic densities receiving glutamatergic input, where it regulates excitatory synapse formation and maturation [17]. To investigate whether DISC1 works downstream of NRG1-ErbB4 to regulate excitatory synapse formation onto cortical inhibitory neurons, we examined VGLUT1 immunofluorescence in primary cortical cultures. Cortical cultures were transfected with P_{G67}-GFP on DIV 7 and treated with NRG1 or PBS for two days, starting on DIV 19. Cultures were then fixed and analyzed on DIV21. Quantification of discrete puncta of VGLUT1 immunoreactivity in DIV21 cortical inhibitory neurons expressing P_{G67}-GFP revealed that NRG1 treatment caused a significant increase in puncta density on both the cell body and primary dendrites (Figures 2(b)–2(d)). Coexpression of P_{G67}-GFP with a plasmid expressing full length mouse DISC1 under control of the GAD67 promoter (P_{G67}-DISC1FL) revealed that expression of DISC1FL in inhibitory neurons at baseline conditions (PBS) had no effect on VGLUT1 puncta density compared to P_{G67}-GFP-only controls (Figures 2(b)–

2(d)). To study the Scottish DISC1 mutation, we used a C-terminal truncated mouse DISC1 mutant (DISC1DN) (Figure 2(a)). The stop codon of this mutant occurs at the orthologous region of the translocation breakpoint found in the human DISC1 Scottish pedigree [50]. When overexpressed in mice, this mutant has been shown to act in a dominant negative manner by binding to and redistributing wild-type (WT) DISC1, causing defects in neural migration, dendrite formation, and reduced cortical parvalbumin levels [50, 53, 54]. We cotransfected P_{G67}-GFP with a plasmid expressing DISC1DN under control of the GAD67 promoter (P_{G67}-DISC1DN) and compared its expression to DISC1FL in cortical inhibitory neurons and found no gross differences in expression levels (Figure 2(c)). In subsequent experiments with the DISC1FL and DISC1DN plasmids, we found that expression of DISC1DN in inhibitory neurons at baseline conditions (PBS) significantly decreased VGLUT1 puncta on the primary dendrites, but not in the cell body (Figures 2(d) and 2(e)), suggesting that the DISC1Scottish mutation impairs excitatory synaptogenesis onto cortical inhibitory neurons at baseline conditions. We then performed the same experiment in the presence of NRG1 stimulation for 2 days (starting at DIV19). We discovered that expression of P_{G67}-DISC1DN completely blocked the NRG1-induced increase in VGLUT1 puncta density on both primary dendrite shafts and the cell body (Figures 2(d) and 2(e)). These data indicate that inhibiting DISC1 specifically in cortical inhibitory neurons blocks NRG1-induced effects on glutamatergic synaptogenesis. Taken together, these results implicate a cell-autonomous role for NRG1-DISC1 signalling in developing cortical inhibitory neurons. However, it is important to note that while the truncated DISC1 mimics the Scottish mutation discovered in patients,

our overexpression paradigm does not recapitulate allele heterozygosity as patients have one intact DISC1 allele.

2.4.4 NRG1 Functions through DISC1 to Regulate Dendrite Growth in Cortical

Inhibitory Neurons

Given our identification of a developmental relationship between NRG1 and DISC1 in excitatory synaptogenesis on inhibitory neurons, we examined whether this extends to neuronal morphology. Although both NRG1 and DISC1 have been found to independently regulate dendrite growth in cortical neurons, it is still unknown whether they regulate this process together [15, 48]. Therefore, to elucidate a functional interaction between NRG1 and DISC1 in cortical inhibitory neurons dendrite growth, we examined the effects of expression of P_{G67}-DISC1FL or P_{G67}-DISC1DN at baseline (PBS) and NRG1 treatment conditions. Cortical cultures were cotransfected with P_{G67}-GFP and either P_{G67}-DISC1FL or P_{G67}-DISC1DN at DIV7. Cultures were then treated with either NRG1 or PBS on DIV19 and fixed and analyzed on DIV21. Sholl analysis revealed that, at baseline conditions, expression of P_{G67}-DISC1FL had no significant effect on dendrite growth, whereas P_{G67}-DISC1DN expression significantly decreased dendrite growth (Figures 3(a)–3(c)). Similar to previous reports, we found that stimulation of cultures with NRG1 increased inhibitory neuron dendrite growth and complexity (Figures 3(a)–3(c)). We next asked whether this NRG1- dependent effect requires DISC1 function. Sholl analysis revealed that expression of P_{G67}-DISC1FL or P_{G67}-DISC1DN blocked the NRG1-induced effects on dendrite growth, causing a

significant decrease in dendrite growth compared to the P_{G67} control under NRG1 treatment conditions (Figures 3(a)– 3(c)). These data suggest that the DISC1DN mutant affects dendrite growth specifically in cortical inhibitory neurons, implicating a cell-autonomous role of DISC1 in regulating dendrite growth in this cell type. In addition, the observation that overexpression of either full-length DISC1 or mutant truncated DISC1 inhibited NRG1-induced dendrite growth demonstrates the complexities of NRG1 signalling.

2.4.5 ErbB4 and DISC1 Interact in Cortical Inhibitory Neurons

Our data thus far suggest that NRG1 requires DISC1 for certain aspects of inhibitory neuron dendrite and glutamatergic synapse growth; however, we do not know whether DISC1 functions directly downstream of ErbB4, the receptor for NRG1. DISC1 and ErbB4 share many binding partners at the postsynaptic density [15, 44, 45]; therefore, we hypothesized that DISC1 may physically interact with ErbB4. A recent study demonstrated that DISC1 plays a role in regulating the interaction between ErbB4 and the postsynaptic protein, PSD95 particularly in the mature cortex [55]. However, whether DISC1 binds the ErbB4 receptor specifically within developing inhibitory neurons, and if NRG1 regulates this process, remains unknown. We first took a biochemical approach to test this using a heterologous cell system (HEK293 FT cells). We expressed ErbB4, kinase dead ErbB4 (ErbB4 KD), or DISC1-GFP alone or DISC1-GFP + ErbB4 or DISC1-GFP+ ErbB4 KD in HEK293 cells, immunoprecipitated for GFP, and used an ErbB4 antibody to determine binding to DISC1. We found that when DISC1-GFP and

ErbB4 were expressed together in HEK293 cells, we detected an interaction between the two proteins, demonstrating that they can directly bind one another (Figure 4(a), asterisks). Interestingly, we found this interaction was reduced when a kinase dead version of ErbB4 was expressed, indicating DISC1 may require NRG1 activation of ErbB4 for intracellular binding (Figure 4(a)). However, the interaction between DISC1 and ErbB4 was not changed in the presence of NRG1 stimulation likely because the overexpressed ErbB4 receptor self-dimerizes, causing transactivation [60]. While these experiments indicate ErbB4 can bind DISC1, these results do not extend to inhibitory neurons. Considering that only 10–25% of cultured cortical neurons are inhibitory neurons, traditional coimmunoprecipitation experiments would not be able to detect interactions specifically within inhibitory neurons. Therefore we used an alternative technique to overcome this problem and examined the interaction specifically in P_{G67}-GFP-positive cultured inhibitory neurons.

To do this, we performed a Proximity Ligation Assay (PLA) on DIV21 cortical cultures transfected with P_{G67}-GFP on DIV7 (Figures 4(b)–4(d)). PLA is a method that allows for visualization of endogenous protein-protein interactions in fixed cells and results in a punctate fluorescent signal where the proteins are within 40 nm of each other. Analysis of PLA signal density in cortical inhibitory neurons expressing P_{G67}-GFP revealed that NRG1 caused a significant increase in PLA signal density compared to PBS-treated controls in both the cell body and primary dendrites (Figures 4(b)–4(d)). Signal density in PBS treated cells was no different than that of the control PLA condition, in which primary antibodies were omitted (Figures 4(b)–4(d)). We also detected PLA signal

outside of the GFP-inhibitory neuron, which we attribute to DISC1 binding to the low levels of ErbB4 in excitatory neurons (Figure 4(b), lower left panel). Taking the biochemical and PLA results together, they demonstrate that ErbB4 binds to DISC1 and that NRG1 stimulation increases this interaction in developing cortical inhibitory neurons. This suggests that DISC1 may be recruited to activated ErbB4 upon NRG1 binding to ErbB4 and is a part of the initial signalling cascade downstream of NRG1-ErbB4 during development.

2.5 DISCUSSION

The development of cortical inhibitory neurons is crucial for normal cognitive processes, and disrupted development and function of these cells are strongly implicated in neurodevelopmental and psychiatric disorders. However, since their development is not well understood, it is important to gain a better understanding of the signalling mechanisms that regulate inhibitory dendrite and synapse growth. Our study reveals that NRG1-ErbB4 signalling functions through DISC1 to regulate dendrite growth and excitatory synapse formation on cortical inhibitory neurons. Specifically, we found that NRG1 stimulation increases DISC1 levels and its localization to excitatory synapses in the primary dendrites of cortical inhibitory neurons, a mechanism that may underlie the developmental effects of NRG1 on dendrite growth and excitatory synaptogenesis onto cortical inhibitory neurons. Furthermore, we show that NRG1-ErbB4 signals through DISC1 to developmentally regulate excitatory synaptogenesis onto cortical inhibitory neurons. Third, we show that NRG1- ErbB4 signals through DISC1 to regulate the

development of dendrite growth in cortical inhibitory neurons. Finally, we show that NRG1 stimulation promotes binding of ErbB4 to DISC1 in cortical inhibitory neurons. The results from this study are consistent with other *in vitro* NRG1 studies, which show that NRG1 regulates dendrite growth and excitatory synaptogenesis onto cortical inhibitory interneurons [15, 16]. *In vivo* data from two different conditional neocortical inhibitory neuron-specific ErbB4 knock-out mouse models displaying decreased VGLUT1 puncta density on hippocampal interneurons further corroborates our findings [17, 30]. The data in the present study provide a potential mechanism mediating the effects of NRG1 signalling in cortical inhibitory neuron development, whereby DISC1 functions downstream of NRG1-ErbB4 signalling. A previous study by Cahill et al. in 2012 elucidated a mechanism whereby NRG1-ErbB4 signalling regulates dendrite growth in cortical inhibitory interneurons by disinhibiting the RAC1- GEF Kalirin-7 [15]. Interestingly, Kalirin-7 is also a binding partner of DISC1 at the postsynaptic density (PSD) [46], suggesting that ErbB4, DISC1, and Kalirin-7 may form a functional complex in cortical inhibitory neurons to regulate dendrite growth, and provides an avenue for further research into the downstream mechanisms of NRG1 signalling.

In this study, we examined a potential mechanism by which DISC1 mediates the effects of NRG1-ErbB4 signalling, in which NRG1-ErbB4 signalling regulates DISC1 levels in the primary dendrites of cortical inhibitory neurons. This is consistent with a study by Seshadri and colleagues in 2010 which showed that treatment of primary mouse cortical neurons with NRG1 increased the expression of the 130 kDa isoform of DISC1 in the primary dendrites of cortical neurons [49]. However, this effect was found to be mediated

by ErbB2/3 heterodimers and likely reflects the large numbers of excitatory neurons from cortical cultures (~80–90%) since they did not isolate inhibitory neurons [49].

Furthermore, because ErbB4 expression is much higher in inhibitory neurons than in excitatory neurons [17, 26–28], it is not surprising that NRG1 regulation of DISC1 levels in excitatory neurons would require ErbB2/3 and not ErbB4. We have also shown that NRG1 stimulation increases colocalization of DISC1 with VGLUT1 in cortical inhibitory neurons, suggesting that NRG1 stimulation localizes DISC1 to developing excitatory synapses contacting inhibitory neurons. Therefore, our study provides the first evidence that NRG1 regulates DISC1 expression and localization in developing cortical inhibitory neurons. However, whether this is carried out at the transcriptional, translational, or posttranslational level remains to be elucidated in future studies.

The role of DISC1 in psychiatric disorders remains controversial; however, many biological studies have shown that DISC1 plays important roles in cortical development [44, 46, 50, 55, 56]. There have been few studies examining the function of DISC1 in cortical inhibitory neurons [61, 62]; therefore what role it plays in their development is still not well understood. Our study provides the first report of DISC1 regulating dendrite growth and glutamatergic synapse formation specifically in cortical inhibitory neurons during neurodevelopment. We show using a P_{G67}-DISC1DN construct, which expresses a dominant negative form of DISC1 in GABA-ergic neurons, that DISC1 regulates dendrite growth in a cell-autonomous fashion. Furthermore, inhibitory-specific expression of a dominant negative DISC1 mutant and inhibitory-specific overexpression of full length DISC1 were both able to abolish NRG1-induced effects on dendritic arborisation,

suggesting that an optimal level of NRG1-ErbB4 signalling is necessary for proper dendrite growth. This hypothesis is supported by a study in which two mutant NRG1 mouse strains, one with elevated cysteine-rich domain- (CRD-) NRG1 levels in cortical pyramidal neurons and one with reduced CRD-NRG1 levels, were both able to disrupt excitatory-inhibitory balance of neurotransmission [63]. In contrast, expression of the dominant negative DISC1 mutant, but not full-length DISC1, was able to block NRG1-induced effects on glutamatergic synaptogenesis onto cortical inhibitory neurons in the present study. This suggests that NRG1-ErbB4-DISC1 signalling may mediate its effects on dendrite growth and excitatory synapse development via two different mechanisms in cortical inhibitory neurons. NRG1- ErbB4 signalling has been found to mediate synapse maturation and dendrite growth via two distinct mechanisms in hippocampal mouse cultures [57]. Specifically, regulation of the maturity of synapses contacting ErbB4-positive hippocampal neurons by ErbB4 was dependent on the extracellular domain and PDZ motif, whereas the tyrosine kinase domain was not required [57]. In contrast, ErbB4 regulated dendrite growth via its tyrosine kinase domain and PI3 kinase signalling [57]. DISC1 may carry out different functions downstream of NRG1-ErbB4 stimulation depending on its interaction with different ErbB4 domains (PDZ or tyrosine kinase domain) or its interaction with other ErbB4 binding proteins that preferentially bind to either the PDZ or tyrosine kinase domain.

ErbB4 and DISC1 share common binding partners at the postsynaptic density, including PSD95 and Kalirin-7 [15, 46, 47]. However, a physical interaction between ErbB4 and DISC1 has not been examined thus far in primary inhibitory neurons due to the difficulty

in isolating a large number of purified cells (devoid of excitatory neurons). Here, using an alternative technique (Proximity Ligation Assay), we have shown that NRG1 stimulation promotes binding of ErbB4 to DISC1 in cortical inhibitory neurons. Further investigation is needed to determine which protein domains are important for this interaction and for NRG1-induced effects on cortical inhibitory neuron development and whether Kalirin-7 is also involved in this complex. Additionally, it will be important to understand the potential mechanisms underlying a developmental switch for DISC1 regulating ErbB4 signalling during development versus the mature cortex, as these roles may be opposite. While our study provides a mechanism for NRG1 function during inhibitory neuron development, it highlights potential differences with NRG1 signalling in the mature cortex. Seshadri et al. recently reported that DISC1 negatively regulates ErbB4 signalling, where, upon removal of DISC1, there is increased phosphorylation of ErbB4 and binding to PSD95 [55]. These results are in contrast to the results of our study, which suggests that DISC1 positively regulates ErbB4 signalling. However this can potentially be explained by a difference in the time point examined in brain function, since we examined neurodevelopmental ages while the Seshadri et al. study examined inhibitory neuron function in the mature cortex. Furthermore, the difference in approach to disrupt DISC1 function could also explain potential differences. For example, our study used a dominant negative form of DISC1 that models the Scottish mutation, whereas the Seshadri et al. study used shRNA and a DISC1 knockout transgenic mouse model. This also highlights that the Scottish mutation may not be accurately modeled by a complete loss of DISC1 function. Future studies are necessary to tease apart the exact mechanism

of NRG1-ErbB4 regulation by DISC1 across different developmental and adult time points of inhibitory neuron function.

2.6 CONCLUSION

In conclusion, this study elucidated the novel convergence of NRG1-ErbB4 signalling and DISC1 onto a common signalling pathway regulating the development of cortical inhibitory neurons. As NRG1, ErbB4, and DISC1 are all candidate schizophrenia-associated risk genes [19–21, 23, 34–41], the results of this study not only shed light on the molecular mechanisms governing the normal development of cortical inhibitory neurons but also may provide insight into the aberrant processes underlying psychiatric disorders.

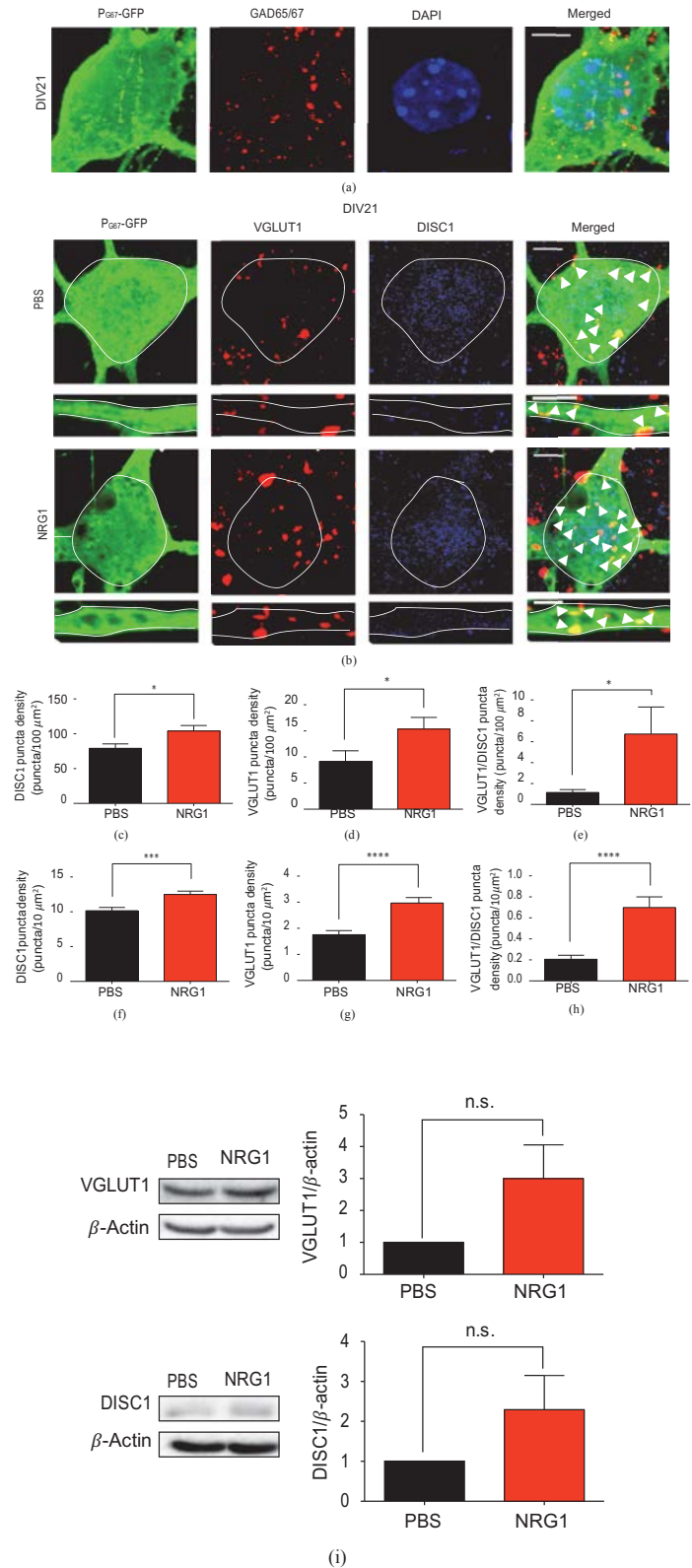


Figure 1: NRG1 regulates DISC1 expression and localization to excitatory synaptic terminals in cortical inhibitory neurons. (a) Representative image of GAD65&67 staining (red) in DIV21 cortical inhibitory neurons transfected with P_{G67}-GFP on DIV7. Images were acquired at 63x. Scale bar = 5 μ m. (b) Representative images of immunofluorescent staining of DISC1 (blue) and VGLUT1 (red) in DIV21 cortical inhibitory neurons transfected with P_{G67}-GFP on DIV7 and treated with NRG1 β or PBS for 2 days. Cultures were also stained for GFP to enhance the GFP signal (green). Images were acquired at 63x. Scale bars = 5 μ m (cell body zoom image) and 2 μ m (dendrite zoom image). Arrowheads indicate double-positive colocalized VGLUT1/DISC1 puncta. NRG1 treatment results in an increase in VGLUT1 puncta density, DISC1 puncta density, and double-positive colocalized VGLUT1/DISC1 puncta density in the cell body (c–e) and in the primary dendrites (f–h). Significance determined using an unpaired student's *t*-test. Error bars represent standard error of the mean, *n* = 25 cells (2-3 primary dendrites/cell) per condition from 5 experiments, **p* < 0.05, ****p* < 0.001, and *****p* < 0.0001. (i) Western blot for VGLUT1 (top) and DISC1 (bottom) in cultured cortical neurons treated with NRG1 for 2 days starting at DIV3 and then lysed at DIV5. *N* = 3 separate mouse litters. Student's *t*-test.

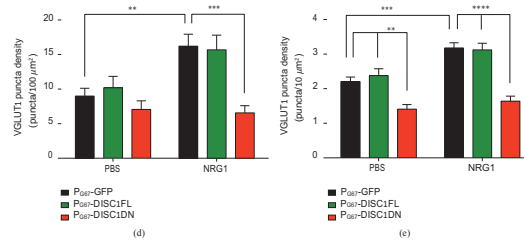
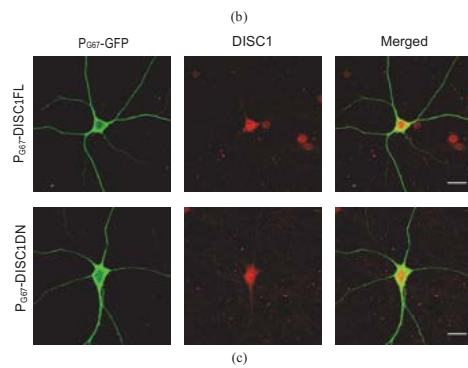
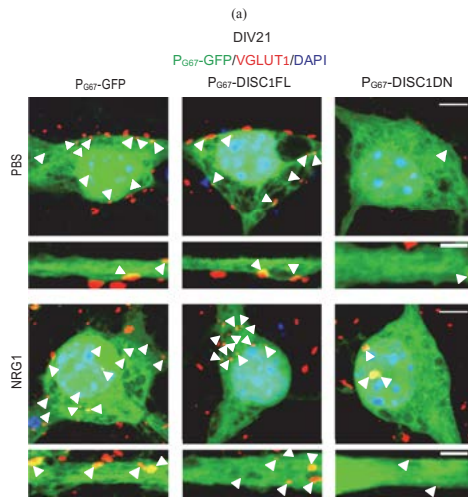
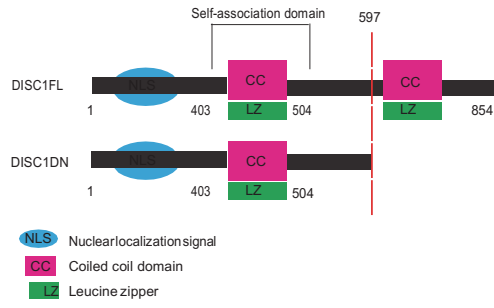


Figure 2: NRG1 functions through DISC1 to regulate glutamatergic synaptogenesis onto cortical inhibitory neurons. (a) Schematic of the mouse DISC1^{FL} protein and DISC1^{DN} truncated mutant protein. (b) Representative images of immunofluorescence staining of VGLUT1 in DIV21 cortical inhibitory neurons cotransfected with P_{G67}-GFP and P_{G67}-DISC1^{FL} or P_{G67}-DISC1^{DN} on DIV7. Cells were treated with NRG1 β or PBS for 2 days. Cultures were stained for GFP to enhance the GFP signal. Images were acquired at 63x. Scale bars = 5 μ m (cell body zoom image), 2 μ m (dendrite zoom image). Arrowheads indicate VGLUT1 puncta colocalized with P_{G67}-GFP. (c) Representative images of immunofluorescent staining of DISC1 in DIV21 cortical inhibitory neurons transfected with P_{G67}-GFP and P_{G67}-DISC1^{FL} or P_{G67}-DISC1^{DN} on DIV7. NRG1 β treatment caused a significant increase in VGLUT1 puncta density in the cell body (d) and primary dendrites (e) which was blocked by expression of P_{G67}-DISC1^{DN}. Significance determined using a one-way analysis of variance (ANOVA) with Tukey's *post hoc* tests. Error bars represent standard error of the mean, $n = 27-50$ cells (2-3 primary dendrites/cell) per condition from 3 experiments, ** $p < 0.01$, *** $p < 0.001$, and **** $p < 0.0001$.

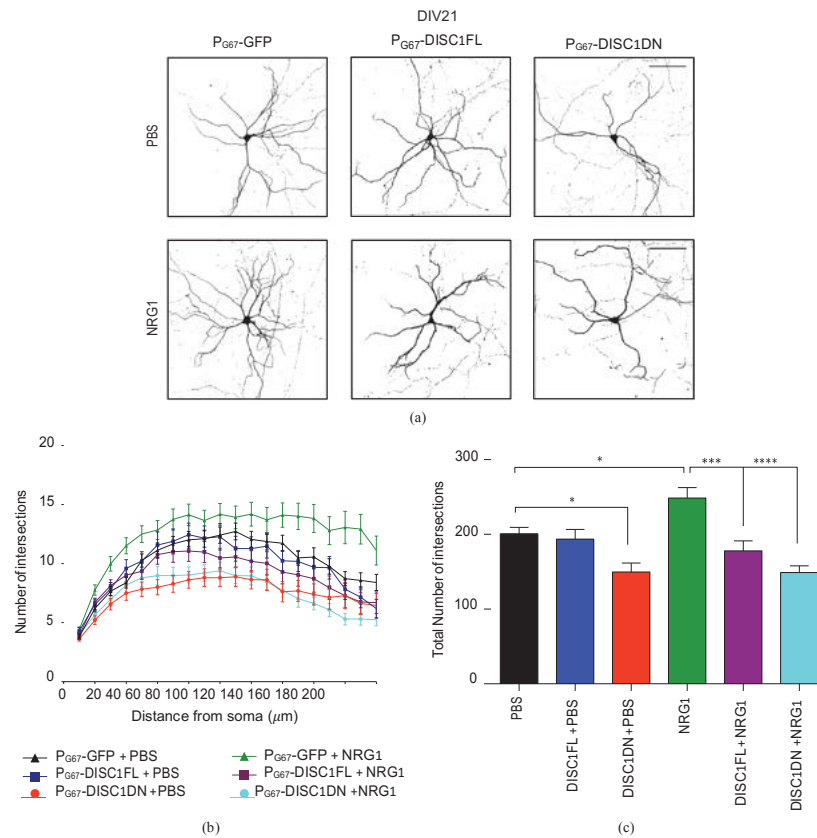
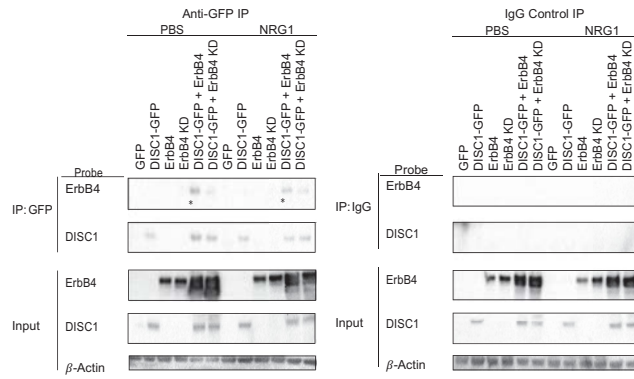
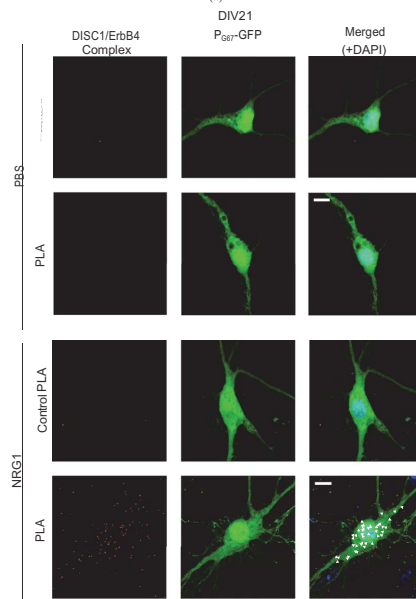


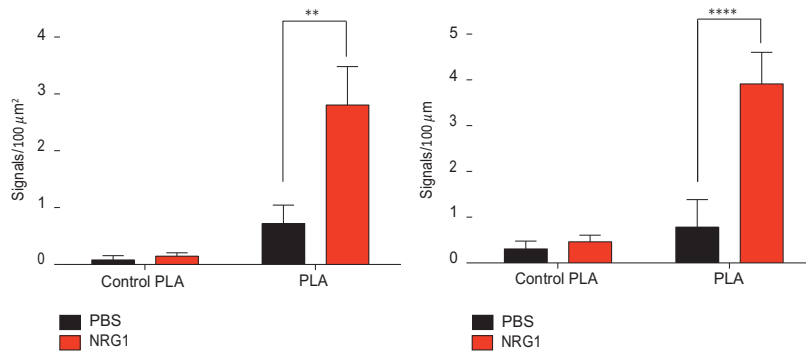
Figure 3: NRG1 functions through DISC1 to regulate cortical inhibitory neuron dendrite growth. (a) Representative images of DIV21 cortical inhibitory neurons cotransfected with P_{G67}-GFP and P_{G67}-DISC1FL or P_{G67}-DISC1DN on DIV7. Cells were treated with PBS (top panels) or NRG1 β (bottom panels) for 2 days. Cultures were stained for GFP to enhance to GFP signal. Images were acquired at 20x. Scale bar = 100 μ m. (b) Dendrite growth was analyzed by Sholl analysis using ImageJ. (c) At baseline conditions (PBS treatment), expression of P_{G67}-DISC1DN resulted in a significant decrease in total dendrite growth compared to P_{G67}-GFP controls; expression of P_{G67}-DISC1FL had no effect compared to P_{G67}-GFP controls. In cells treated with NRG1 β , both P_{G67}-DISC1FL and P_{G67}-DISC1DN caused a significant decrease in total dendrite growth compared to P_{G67}-GFP controls. Significance determined using a one-way analysis of variance (ANOVA) with Tukey's *post hoc* tests. Error bars represent standard error of the mean, $n = 34$ – 54 cells per condition from 3 experiments; * $p < 0.05$, *** $p < 0.001$, and **** $p < 0.0001$.



(a)



(b)



(c)

(d)

Figure 4: ErbB4 and DISC1 physically interact in cortical inhibitory neurons. (a) Co-IP of DISC1-GFP and ErbB4 in lysates from HEK293 FT cells transfected with ErbB4, ErbB4 KD, or DISC1-GFP alone or with DISC1-GFP + ErbB4 or DISC1-GFP + ErbB4 KD, with or without NRG1 treatment. Left panel: western blot for ErbB4 and DISC1-GFP in anti-GFP (DISC1) precipitates and input. Right panel: western blot for ErbB4 and DISC1-GFP in anti IgG control precipitates and input. DISC1-GFP binds ErbB4 in both PBS and NRG1 conditions (left panel, asterisks). Binding is reduced with DISC1-GFP and kinase dead ErbB4 (ErbB4 KD) (left panel). No binding was observed in the IgG control precipitates (right panel). (b) Proximity Ligation Assay (PLA) was performed in DIV21 cortical inhibitory neurons transfected with P_{G67}-GFP on DIV7 and treated with NRG1 β or PBS for 5 min prior to fixation. Primary antibodies were omitted in the control PLA condition. Representative images were acquired at 63x. Scale bars = 10 μ m. NRG1 β treatment significantly increased the number of PLA signals in the cell body. Arrowheads indicate PLA signals colocalized with P_{G67}-GFP positive neurons (c) and the primary dendrites (d). Significance determined using a one-way analysis of variance (ANOVA) with Tukey's *post hoc* tests. Error bars represent standard error of the mean, $n = 6-15$ cells (2-3 primary dendrites/cell) per condition from 3 experiments; ** $p < 0.01$, **** $p < 0.0001$.

2.7 REFERENCES

1. O. Yizhar, L. E. Fenno, M. Prigge et al., “Neocortical excitation/inhibition balance in information processing and social dysfunction,” *Nature*, vol. 477, no. 7363, pp. 171–178, 2011.
2. H. Markram, M. Toledo-Rodriguez, Y. Wang, A. Gupta, G. Silberberg, and C. Wu, “Interneurons of the neocortical inhibitory system,” *Nature Reviews Neuroscience*, vol. 5, no. 10, pp. 793–807, 2004.
3. C. Le Magueresse and H. Monyer, “GABAergic interneurons shape the functional maturation of the cortex,” *Neuron*, vol. 77, no. 3, pp. 388–405, 2013.
4. T. Toyoizumi, H. Miyamoto, Y. Yazaki-Sugiyama, N. Atapour, T. K. Hensch, and K. D. Miller, “A theory of the transition to critical period plasticity: inhibition selectively suppresses spontaneous activity,” *Neuron*, vol. 80, no. 1, pp. 51–63, 2013.
5. J. A. Cardin, M. Carlén, K. Meletis et al., “Driving fast-spiking cells induces gamma rhythm and controls sensory responses,” *Nature*, vol. 459, no. 7247, pp. 663–667, 2009.
6. G. Buzsáki and X.-J. Wang, “Mechanisms of gamma oscillations,” *Annual Review of Neuroscience*, vol. 35, no. 1, pp. 203–225, 2012.
7. P. J. Uhlhaas and W. Singer, “Abnormal neural oscillations and synchrony in schizophrenia,” *Nature Reviews Neuroscience*, vol. 11, no. 2, pp. 100–113, 2010.
8. A. Guidotti, J. Auta, J. M. Davis et al., “Decrease in reelin and glutamic acid decarboxylase67 (GAD67) expression in schizophrenia and bipolar disorder: a

- postmortem brain study,” *Archives of General Psychiatry*, vol. 57, no. 11, pp. 1061–1069, 2000.
9. J. R. Glausier, K. N. Fish, and D. A. Lewis, “Altered parvalbumin basket cell inputs in the dorsolateral prefrontal cortex of schizophrenia subjects,” *Molecular Psychiatry*, vol. 19, no. 1, pp. 30–36, 2014.
 10. J. A. Brown, T. S. Ramikie, M. J. Schmidt et al., “Inhibition of parvalbumin-expressing interneurons results in complex behavioral changes,” *Molecular Psychiatry*, vol. 20, no. 12, pp. 1499–1507, 2015.
 11. K. K. A. Cho, R. Hoch, A. T. Lee, T. Patel, J. L. R. Rubenstein, and V. S. Sohal, “Gamma rhythms link prefrontal interneuron dysfunction with cognitive inflexibility in *dlx5/6^{+/-}* mice,” *Neuron*, vol. 85, no. 6, pp. 1332–1343, 2015.
 12. Z. Xie, D. P. Srivastava, H. Photowala et al., “Kalirin-7 controls activity-dependent structural and functional plasticity of dendritic spines,” *Neuron*, vol. 56, no. 4, pp. 640–656, 2007.
 13. P. Kalus, J. Bondzio, A. Federspiel, T. J. Müller, and W. Zschratte, “Cell-type specific alterations of cortical interneurons in schizophrenic patients,” *NeuroReport*, vol. 13, no. 5, pp. 713–717, 2002.
 14. N. V. De Marco García, T. Karayannis, and G. Fishell, “Neuronal activity is required for the development of specific cortical interneuron subtypes,” *Nature*, vol. 472, no. 7343, pp. 351–355, 2011.

15. M. E. Cahill, K. A. Jones, I. Rafalovich et al., “Control of interneuron dendritic growth through NRG1/erbB4-mediated kalirin-7 disinhibition,” *Molecular Psychiatry*, vol. 17, no. 1, pp. 99–107, 2012.
16. A. K. Ting, Y. Chen, L. Wen et al., “Neuregulin 1 promotes excitatory synapse development and function in GABAergic interneurons,” *The Journal of Neuroscience*, vol. 31, no. 1, pp. 15–25, 2011.
17. P. Fazzari, A. V. Paternain, M. Valiente et al., “Control of cortical GABA circuitry development by Nrg1 and ErbB4 signalling,” *Nature*, vol. 464, no. 7293, pp. 1376–1380, 2010.
18. Y. Wang, C. A. Dye, V. Sohal et al., “Dlx5 and Dlx6 regulate the development of parvalbumin-expressing cortical interneurons,” *The Journal of Neuroscience*, vol. 30, no. 15, pp. 5334–5345, 2010.
19. H. Stefansson, E. Sigurdsson, V. Steinthorsdottir et al., “Neuregulin 1 and susceptibility to schizophrenia,” *American Journal of Human Genetics*, vol. 71, no. 4, pp. 877–892, 2002.
20. H. Stefansson, J. Sarginson, A. Kong et al., “Association of neuregulin 1 with schizophrenia confirmed in a Scottish population,” *American Journal of Human Genetics*, vol. 72, no. 1, pp. 83–87, 2003.
21. A. J. Law, J. E. Kleinman, D. R. Weinberger, and C. S. Weickert, “Disease-associated intronic variants in the ErbB4 gene are related to altered ErbB4 splice-variant expression in the brain in schizophrenia,” *Human Molecular Genetics*, vol. 16, no. 2, pp. 129–141, 2007.

22. T. Walsh, J. M. McClellan, S. E. McCarthy et al., “Rare structural variants disrupt multiple genes in neurodevelopmental pathways in schizophrenia,” *Science*, vol. 320, no. 5875, pp. 539–543, 2008.
23. N. Norton, V. Moskvina, D. W. Morris et al., “Evidence that interaction between neuregulin 1 and its receptor erbB4 increases susceptibility to schizophrenia,” *American Journal of Medical Genetics—Neuropsychiatric Genetics*, vol. 141, no. 1, pp. 96–101, 2006.
24. D. Meyer, T. Yamaal, A. Garratt et al., “Isoform-specific expression and function of neuregulin,” *Development*, vol. 124, no. 18, pp. 3575–3586, 1997.
25. L. Mei and K.A. Nave, “Neuregulin-ERBB signaling in the nervous system and neuropsychiatric diseases,” *Neuron*, vol. 83, no. 1, pp. 27–49, 2014.
26. J. C. Bean, T. W. Lin, A. Sathyamurthy et al., “Genetic labeling reveals novel cellular targets of schizophrenia susceptibility gene: distribution of GABA and non-GABA ErbB4-positive cells in adult mouse brain,” *The Journal of Neuroscience*, vol. 34, no. 40, pp. 13549–13566, 2014.
27. H.J. Yau, H.-F. Wang, C. Lai, and F.C. Liu, “Neural development of the neuregulin receptor ErbB4 in the cerebral cortex and the hippocampus: preferential expression by interneurons tangentially migrating from the ganglionic eminences,” *Cerebral Cortex*, vol. 13, no. 3, pp. 252–264, 2003.
28. J. Neddens, K. N. Fish, L. Tricoire et al., “Conserved interneuron-specific ErbB4 expression in frontal cortex of rodents, monkeys, and humans: implications for schizophrenia,” *Biological Psychiatry*, vol. 70, no. 7, pp. 636–645, 2011.

29. N. Flames, J. E. Long, A. N. Garratt et al., “Short- and long-range attraction of cortical GABAergic interneurons by neuregulin-1,” *Neuron*, vol. 44, no. 2, pp. 251–561, 2004.
30. Del Pino, C. García-Frigola, N. Dehorter et al., “ErbB4 deletion from fast-spiking interneurons causes schizophrenia-like phenotypes,” *Neuron*, vol. 79, no. 6, pp. 1152–1168, 2013.
31. A. Newell, T. Karl, and X.F. Huang, “A neuregulin 1 transmembrane domain mutation causes imbalanced glutamatergic and dopaminergic receptor expression in mice,” *Neuroscience*, vol. 248, pp. 670–680, 2013.
32. M. E. Cahill, C. Remmers, K. A. Jones, Z. Xie, R. A. Sweet, and P. Penzes, “Neuregulin1 signaling promotes dendritic spine growth through kalirin,” *Journal of Neurochemistry*, vol. 126, no. 5, pp. 625–635, 2013.
33. Kushima, Y. Nakamura, B. Aleksic et al., “Resequencing and association analysis of the KALRN and EPHB1 genes and their contribution to schizophrenia susceptibility,” *Schizophrenia Bulletin*, vol. 38, no. 3, pp. 552–560, 2012.
34. D. H. R. Blackwood, A. Fordyce, M. T. Walker, D. M. St. Clair, D. J. Porteous, and W. J. Muir, “Schizophrenia and affective disorders— cosegregation with a translocation at chromosome 1q42 that directly disrupts brain-expressed genes: clinical and P300 findings in a family,” *The American Journal of Human Genetics*, vol. 69, no. 2, pp. 428–433, 2001.

35. K. Millar, J. C. Wilson-Annan, S. Anderson et al., “Disruption of two novel genes by a translocation co-segregating with schizophrenia,” *Human Molecular Genetics*, vol. 9, no. 9, pp. 1415–1423, 2000.
36. W. Hennah, T. Varilo, M. Kestilä et al., “Haplotype transmission analysis provides evidence of association for DISC1 to schizophrenia and suggests sex-dependent effects,” *Human Molecular Genetics*, vol. 12, no. 23, pp. 3151–3159, 2003.
37. M. Qu, F. Tang, W. Yue et al., “Positive association of the Disrupted-in-schizophrenia-1 gene (DISC1) with schizophrenia in the Chinese Han population,” *American Journal of Medical Genetics, Part B: Neuropsychiatric Genetics*, vol. 144, no. 3, pp. 266–270, 2007.
38. C. A. Hodgkinson, D. Goldman, J. Jaeger et al., “Disrupted in schizophrenia 1 (DISC1): association with schizophrenia, schizoaffective disorder, and bipolar disorder,” *American Journal of Human Genetics*, vol. 75, no. 5, pp. 862–872, 2004.
39. W. Song, W. Li, J. Feng, L. L. Heston, W. A. Scaringe, and S. S. Sommer, “Identification of high risk DISC1 structural variants with a 2% attributable risk for schizophrenia,” *Biochemical and Biophysical Research Communications*, vol. 367, no. 3, pp. 700–706, 2008.
40. N. J. Brandon and A. Sawa, “Linking neurodevelopmental and synaptic theories of mental illness through DISC1,” *Nature Reviews Neuroscience*, vol. 12, no. 12, pp. 707–722, 2011.

41. N. A. Sachs, A. Sawa, S. E. Holmes, C. A. Ross, L. E. DeLisi, and R. L. Margolis, "A frameshift mutation in disrupted in schizophrenia 1 in an American family with schizophrenia and schizoaffective disorder," *Molecular Psychiatry*, vol. 10, no. 8, pp. 758–764, 2005.
42. D.M. Yin, X.D. Sun, J. C. Bean et al., "Regulation of spine formation by ErbB4 in PV-positive interneurons," *The Journal of Neuroscience*, vol. 33, no. 49, pp. 19295–19303, 2013.
43. W. Li, Y. Zhou, J. D. Jentsch et al., "Specific developmental disruption of disrupted-in-schizophrenia-1 function results in schizophrenia-related phenotypes in mice," *Proceedings of the National Academy of Sciences of the United States of America*, vol. 104, no. 46, pp. 18280–18285, 2007.
44. M. V. Pletnikov, Y. Ayhan, O. Nikolskaia et al., "Inducible expression of mutant human DISC1 in mice is associated with brain and behavioral abnormalities reminiscent of schizophrenia," *Molecular Psychiatry*, vol. 13, no. 2, pp. 173–186, 2008.
45. S. J. Clapcote, T. V. Lipina, J. K. Millar et al., "Behavioral phenotypes of Disc1 missense mutations in mice," *Neuron*, vol. 54, no. 3, pp. 387–402, 2007.
46. A. Hayashi-Takagi, M. Takaki, N. Graziane et al., "Disrupted- in-schizophrenia 1 (DISC1) regulates spines of the glutamate synapse via Rac1," *Nature Neuroscience*, vol. 13, no. 3, pp. 327– 332, 2010.

47. Y. Z. Huang, S. Won, D. W. Ali et al., "Regulation of neuregulin signaling by PSD-95 interacting with ErbB4 at CNS synapses," *Neuron*, vol. 26, no. 2, pp. 443–455, 2000.
48. D. Wood, F. Bonath, S. Kumar, C. A. Ross, and V. T. Cunliffe, "Disrupted-in-schizophrenia 1 and neuregulin 1 are required for the specification of oligodendrocytes and neurones in the zebrafish brain," *Human Molecular Genetics*, vol. 18, no. 3, pp. 391–404, 2009.
49. S. Seshadri, A. Kamiya, Y. Yokota et al., "Disrupted-in-schizophrenia-1 expression is regulated by β -site amyloid precursor protein cleaving enzyme-1-neuregulin cascade," *Proceedings of the National Academy of Sciences of the United States of America*, vol. 107, no. 12, pp. 5622–5627, 2010.
50. A. Kamiya, K. I. Kubo, T. Tomoda et al., "A schizophrenia-associated mutation of DISC1 perturbs cerebral cortex development," *Nature Cell Biology*, vol. 7, no. 12, pp. 1167–1178, 2005.
51. K. Millar, B. S. Pickard, S. Mackie et al., "DISC1 and PDE4B are interacting genetic factors in schizophrenia that regulate cAMP signaling," *Science*, vol. 310, no. 5751, pp. 1187–1191, 2005.
52. J. E. Eykelenboom, G. J. Briggs, N. J. Bradshaw et al., "A t(1;11) translocation linked to schizophrenia and affective disorders gives rise to aberrant chimeric DISC1 transcripts that encode structurally altered, deleterious mitochondrial proteins," *Human Molecular Genetics*, vol. 21, no. 15, pp. 3374–3386, 2012.

53. V. Pletnikov, Y. Xu, M. V. Ovanesov, A. Kamiya, A. Sawa, and C. A. Ross, "PC12 cell model of inducible expression of mutant DISC1: new evidence for a dominant-negative mechanism of abnormal neuronal differentiation," *Neuroscience Research*, vol. 58, no. 3, pp. 234–244, 2007.
54. T. Hikida, H. Jaaro-Peled, S. Seshadri et al., "Dominant-negative DISC1 transgenic mice display schizophrenia-associated phenotypes detected by measures translatable to humans," *Proceedings of the National Academy of Sciences of the United States of America*, vol. 104, no. 36, pp. 14501–14506, 2007.
55. S. Seshadri, T. Faust, K. Ishizuka et al., "Interneuronal DISC1 regulates NRG1-ErbB4 signalling and excitatory-inhibitory synapse formation in the mature cortex," *Nature Communications*, vol. 6, Article ID 10118, 2015.
56. Y. Mao, X. Ge, C. L. Frank et al., "Disrupted in schizophrenia 1 regulates neuronal progenitor proliferation via modulation of GSK3 β / β -catenin signaling," *Cell*, vol. 136, no. 6, pp. 1017–1031, 2009.
57. D. Krivosheya, L. Tapia, J. N. Levinson et al., "ErbB4- neuregulin signaling modulates synapse development and dendritic arborization through distinct mechanisms," *The Journal of Biological Chemistry*, vol. 283, no. 47, pp. 32944–32956, 2008.
58. B. Chattopadhyaya, G. Di Cristo, H. Higashiyama et al., "Experience and activity-dependent maturation of perisomatic GABAergic innervation in primary visual

- cortex during a postnatal critical period,” *The Journal of Neuroscience*, vol. 24, no. 43, pp. 9598–9611, 2004.
59. J.J. Soghomonian and D. L. Martin, “Two isoforms of glutamate decarboxylase: why?” *Trends in Pharmacological Sciences*, vol. 19, no. 12, pp. 500–505, 1998.
60. R. Roskoski, “The ErbB/HER family of protein-tyrosine kinases and cancer,” *Pharmacological Research*, vol. 79, pp. 34–74, 2014.
61. A. Steinecke, C. Gampe, F. Nitzsche, and J. Bolz, “DISC1 knock- down impairs the tangential migration of cortical interneurons by affecting the actin cytoskeleton,” *Frontiers in Cellular Neuroscience*, vol. 8, article 190, 2014.
62. F. H. F. Lee, C. C. Zai, S. P. Cordes, J. C. Roder, and A. H. C. Wong, “Abnormal interneuron development in disrupted-in- schizophrenia-1 L100P mutant mice,” *Molecular Brain*, vol. 6, article 20, 2013.
63. A. Agarwal, M. Zhang, I. Trembak-Duff et al., “Dysregulated expression of neuregulin-1 by cortical pyramidal neurons disrupts synaptic plasticity,” *Cell Reports*, vol. 8, no. 4, pp. 1130–1145, 2014.

2.8 SUPPLEMENTARY FIGURE

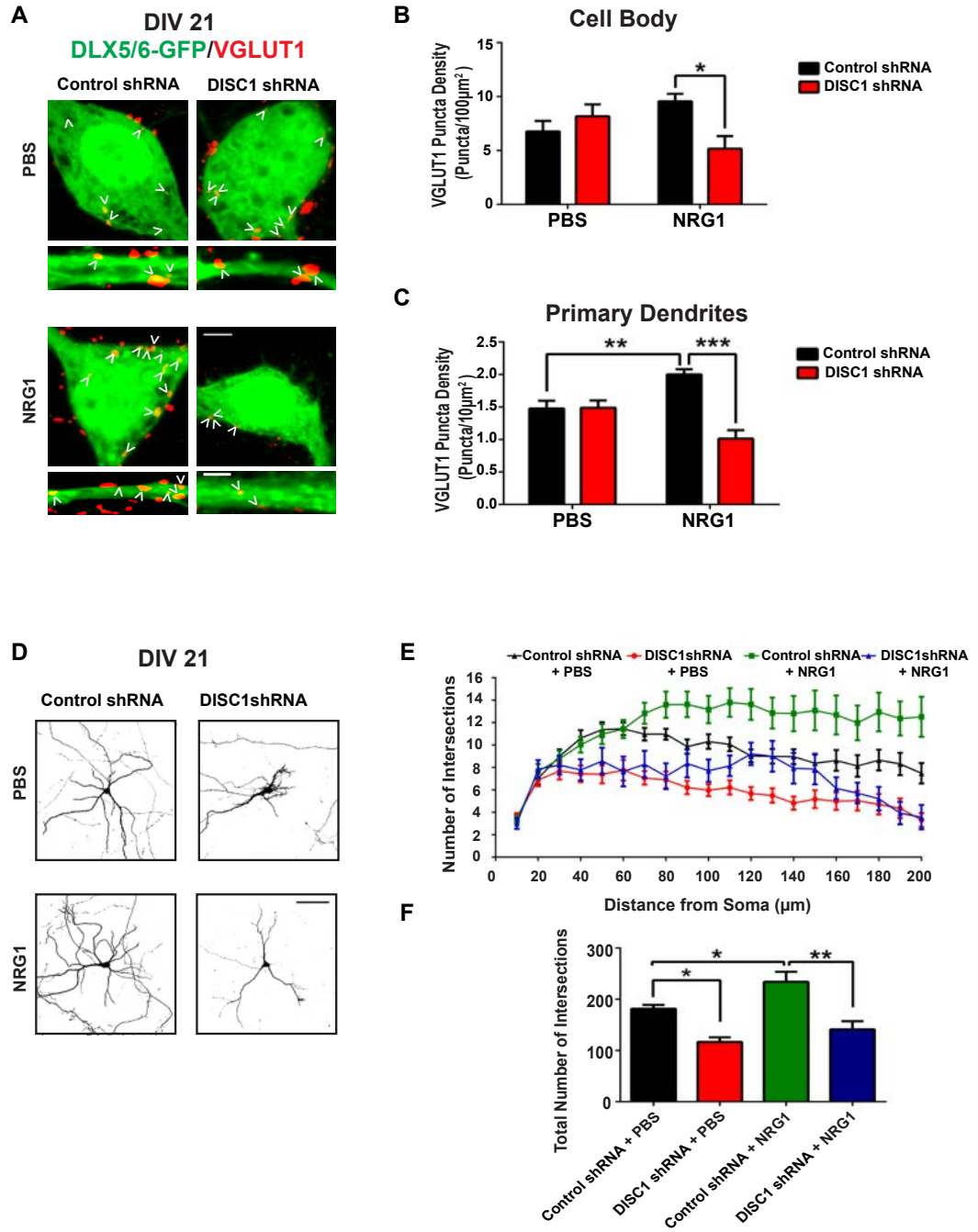


Figure S1. shRNA knockdown of DISC1 inhibits NRG1-mediated dendrite and excitatory synapse growth of cortical inhibitory neurons. (A) Representative images of immunofluorescent staining of VGLUT1 (red) in DIV21 cortical inhibitory neurons co-transfected with DLX5/6-GFP and control or DISC1 shRNA on DIV7. Cultures were treated with NRG1 β or PBS for 2 days. Cultures were also stained for GFP to enhance the GFP signal (green). Images were acquired at 63X. Scale bars= 5 μ m (cell body zoom image), 2 μ m (dendrite zoom image). Arrowheads indicate VGLUT1 puncta co-localized with DLX5/6-GFP. (B) In the cell body, expression of DISC1shRNA results in a decrease in VGLUT1 puncta density in cultures treated with NRG1. (C) In the primary dendrites, expression of DISC1 shRNA abolishes the NRG1 induced increase in VGLUT1 puncta density. Error bars represent standard error of the mean, n= 28-83 cells (2-3 primary dendrites/cell) per condition from 3 experiments, **p<0.01, ***p<0.001. Significance determined using a one-way analysis of variance (ANOVA) with Tukey's post hoc tests. (D) Representative images of DIV21 cortical inhibitory neurons co-transfected with DLX5/6-GFP and control shRNA or DISC1 shRNA on DIV7. Cells were treated with PBS (top panels) or NRG1 β (bottom panels) for 2 days. Cultures were stained for GFP to enhance the GFP signal. Images were acquired at 20X. Scale bar=100 μ m. (E) Dendrite growth was analyzed by sholl analysis using ImageJ. Briefly, concentric circles were made radiating from the soma at a constant increment of 10 μ m up to a maximum radius of 250 μ m and the number of dendritic intersections within each concentric circle was counted. (F) Expression of DISC1 shRNA causes a decrease in dendrite growth and abolishes the NRG1 induced increase in dendrite growth. Error bars represent standard error of the mean, n= 14-35 cells per condition from 3 independent experiments, *p<0.05, **p<0.01. Significance determined using a one-way analysis of variance (ANOVA) with Tukey's post hoc tests.

CHAPTER 3: *OTUD7A* REGULATES NEURODEVELOPMENTAL PHENOTYPES IN THE 15Q13.3 MICRODELETION SYNDROME

Mohammed Uddin,^{1,2,3,12} Brianna K. Unda,^{4,12} Vickie Kwan,⁴ Nicholas T. Holzapfel,⁴ Sean H. White,⁴ Leon Chalil,⁴ Marc Woodbury-Smith,^{1,5} Karen S. Ho,⁶ Erin Harward,⁶ Nadeem Murtaza,⁴ Biren Dave,⁴ Giovanna Pellecchia,^{1,2} Lia D'Abate,^{1,2,7} Thomas Nalpathamkalam,^{1,2} Sylvia Lamoureux,^{1,2} John Wei,^{1,2} Marsha Speevak,⁸ James Stavropoulos,⁹ Kristin J. Hope,⁴ Brad W. Doble,⁴ Jacob Nielsen,¹¹ E. Robert Wassman,⁶ Stephen W. Scherer,^{1,2,10,13,*} and Karun K. Singh^{4,13,*}

¹The Centre for Applied Genomics, The Hospital for Sick Children, Toronto, ON M5G 0A4, Canada; ²Program in Genetics and Genome Biology (GGB), The Hospital for Sick Children, Toronto, ON M5G 0A4, Canada; ³Mohammed Bin Rashid University of Medicine and Health Sciences, Dubai, UAE; ⁴Stem Cell and Cancer Research Institute, McMaster University, Hamilton, ON, Canada; Department of Biochemistry and Biomedical Sciences, McMaster University, Hamilton, ON L8N 3Z5, Canada; ⁵Institute of Neuroscience, Newcastle University, UK; ⁶Lineagen Inc., Salt Lake City, UT 84109, USA; ⁷Department of Molecular Genetics, University of Toronto, Toronto, ON M5S 1A8, Canada; ⁸Department of Laboratory Medicine and Pathobiology, University of Toronto, Toronto, ON L5M 2N1, Canada; ⁹Genome Diagnostics, Pediatric Laboratory Medicine, The Hospital for Sick Children, Toronto, ON M5G 0A4, Canada; ¹⁰McLaughlin Centre, University of Toronto, Toronto, ON M5G 0A4, Canada;

¹¹Synaptic Transmission, In Vitro, Neuroscience Research DK, H. Lundbeck A/S, Ottiliaavej 9, Valby 2500, Denmark

¹²These authors contributed equally to this work

¹³These authors contributed equally to this work

*Correspondence: stephen.scherer@sickkids.ca (S.W.S.), singhk2@mcmaster.ca (K.K.S.)

<https://doi.org/10.1016/j.ajhg.2018.01.006>.

© 2018 The Author(s). “This is an open access article under the CC BY-NC-ND license (<http://creativecommons.org/licenses/by-nc-nd/4.0/>).”

PREFACE

This manuscript was published in the *American Journal of Human Genetics* on February 1, 2018. It has been slightly modified to match the formatting of this thesis. Dr. Karun Singh, Dr. Stephen Scherer, Dr. Mohammed Uddin and Brianna Unda designed the study. Brianna Unda and Mohammed Uddin share co-first authorship and experiments were divided equally between them, with assistance. Dr. Mohammed Uddin performed all human genomics, whole genome sequencing, and bioinformatics data analysis, with assistance from Marc Woodbury-Smith, Giovanna Pellecchia, Lia D’Abate, Thomas Nalpathamkalam, Sylvia Lamoureux, John Wei, Marsha Speevak, and Dr. James Stavropoulos. Brianna Unda performed all mouse neuronal cultures, transfections, Golgi-staining, neuronal morphology analysis and biochemical experiments, with assistance from Vickie Kwan, Nadeem Murtaza, Biren Dave, Leon Chalil and Sean White. Vickie Kwan and Nicholas Holzapfel created Flag-tagged constructs. Dr. Karun Singh performed

in utero electroporation. Data were analyzed and figures were prepared by Brianna Unda and Mohammed Uddin, with assistance from Vickie Kwan. Dr. Jacob Nielsen provided Df(h15q13)/+ mice. Karen Ho and Erin Harward provided clinical genomic data. Brianna Unda, Dr. Mohammed Uddin, and Dr. Karun Singh wrote the manuscript. Dr. Karun, Singh, Dr. Stephen Scherer, Dr. Mohammed Uddin, Brianna Unda, Vickie Kwan, Dr. Bradley Doble, Dr. Kristin Hope. and Dr. Jacob Nielsen provided intellectual contribution and edited the manuscript.

ACKNOWLEDGEMENTS

This work was supported by grants to K.K.S. (Canadian Institutes of Health Research [CIHR], Natural Sciences and Engineering Research Council, Brain Canada Platform Support Grant, and the Ontario Brain Institute-POND study), S.W.S. (OB, CIHR, and Autism Speaks), K.J.H. (CIHR and the Ontario Institute of Cancer Research), and B.W.D. (CIHR).

3.1 ABSTRACT

Copy-number variations (CNVs) are strong risk factors for neurodevelopmental and psychiatric disorders. The 15q13.3 microdeletion syndrome region contains up to ten genes and is associated with numerous conditions, including autism spectrum disorder (ASD), epilepsy, schizophrenia, and intellectual disability; however, the mechanisms underlying the pathogenesis of 15q13.3 microdeletion syndrome remain unknown. We combined whole-genome sequencing, human brain gene expression (proteome and transcriptome), and a mouse model with a syntenic heterozygous deletion (*Df(h15q13)/+* mice) and determined that the microdeletion results in abnormal development of cortical dendritic spines and dendrite outgrowth. Analysis of large-scale genomic, transcriptomic, and proteomic data identified *OTUD7A* as a critical gene for brain function. *OTUD7A* was found to localize to dendritic and spine compartments in cortical neurons, and its reduced levels in *Df(h15q13)/+* cortical neurons contributed to the dendritic spine and dendrite outgrowth deficits. Our results reveal *OTUD7A* as a major regulatory gene for 15q13.3 microdeletion syndrome phenotypes that contribute to the disease mechanism through abnormal cortical neuron morphological development.

3.2 INTRODUCTION

Neurodevelopmental disorders include various conditions characterized by deficits or delays in typical developmental milestones that appear in childhood. Genetic studies indicate that copy-number variations (CNVs), comprising deletions or duplications of genomic DNA that may directly or indirectly affect the dosage of genes, can be

significant risk factors for these disorders. Certain genomic contexts are hotspots for recombination- and replication-based mechanisms that result in microdeletions or microduplications. While 5%–20% of developmentally delayed individuals carry a rare large pathogenic CNV,¹ the pathobiology is poorly understood. Furthermore, for most CNVs associated with neurodevelopmental disorders, the underlying genes that contribute to the clinical phenotypes remain unknown. The 22q11.2 and 16p11.2 microdeletions are two specific CNVs associated with schizophrenia (MIM: 181500) and autism spectrum disorder (ASD) (MIM: 209850), respectively, in which substantial progress has been made into the understanding of disease pathophysiology.^{2–9} In both, modeling microdeletions in animal models has accelerated the pace at which the underlying biological pathogenic mechanism(s) have been identified and has provided a means to test potential “driver genes” underlying CNV-associated phenotypes.^{10–14} Importantly, these studies have led to potential drug therapies that have been tested in preclinical mouse models,^{5,7,15} highlighting the power of this approach.

The 15q13.3 1.53 Mb microdeletion syndrome (MIM: 612001) locus (chr15:30,910,306–32,445,407 [hg19]) that resides within breakpoints BP4-BP5 on human chromosome 15 is a recurrent CNV that results in a highly heterogeneous set of phenotypes including intellectual disability (50%–60%), autism spectrum disorder (10%–20%), epilepsy (~30%) (MIM: 607208), and schizophrenia (10%–20%).^{16–23} Among the more than 200 individuals bearing 15q13.3 BP4-BP5 deletions who have been described in the clinical literature, 80% exhibited ascertainment-independent phenotypic manifestations; this implies that one or more genes in the CNV may contribute to disease manifestation,

including the incomplete penetrance and variable expressivity observed.²⁴ Individuals are typically heterozygous for the 15q13.3 microdeletion, which encompasses seven protein-coding genes, one microRNA, and two putative pseudogenes (*ARHGAP11BI* [MIM: 616310], *LOC100288637*, *FANI* [MIM: 613534], *MTMR10*, *TRPM1* [MIM: 603576], *LOC283710*, *microRNA-211*, *KLF13* [MIM: 605328], *OTUD7A* [MIM: 612024], and *CHRNA7* [MIM: 118511]). Recently, a heterozygous mouse model of the 15q13.3 microdeletion was generated (*Df(h15q13)/+* mice) that contains a deletion of the syntenic murine chromosome region (mouse chromosome 7qC) corresponding to the human CNV. Phenotypic manifestations of this heterozygous mouse model include schizophrenia- and epilepsy-related endophenotypes, notably long-term spatial memory deficits, increased sensitivity to stress, and reductions in auditory-evoked gamma power (similar to schizophrenia patients).²⁵ Many of these observed clinical phenotypes were replicated in another independent 15q13.3 heterozygous microdeletion mouse model.²⁶ In contrast to the heterozygous deletion, the homozygous deletion is extremely rare and only eight case subjects have been reported in the literature.^{24,27,28} All reported case subjects that carry the homozygous deletion manifested severe cognitive and physiological impairments including severe DD/ID, hypotonia, seizures, and visual impairment.²⁴ A recent study analyzed behavioral abnormalities of *Df(h15q13)^{-/-}* homozygous knock out (KO) mice²⁹ in which both copies of the genes within the locus are deleted.²⁷ While the majority of human case subjects are carriers of a heterozygous microdeletion, the homozygous KO mice displayed more pronounced phenotypes in seizure susceptibility, ASD behavior-related phenotypes, and auditory sensory processing, demonstrating a

gene- dosage dependency. While the underlying neurophysiological abnormalities remain unknown, recent studies using resting-state fMRI have revealed that *Df(h15q13)/+* mice display altered neuronal firing rates in the prefrontal cortex³⁰ and abnormal brain hyperconnectivity patterns;³¹ however, the underlying molecular and physiological brain abnormalities contributing to the mouse behavioral, imaging, and electrophysiological phenotypes remain unknown.

The complexities inherent in the identification of the critical driver gene(s) in a given CNV are significant and require evidence from multiple sources. With regard to the 15q13.3 microdeletion, *CHRNA7* (encoding a cholinergic receptor) has been proposed as a driver gene, in part because some patients have overlapping deletions that encompass *CHRNA7*.²⁰ Furthermore, *CHRNA7* agonists may improve cognition in humans with schizophrenia³² and abnormal fMRI-derived brain connectivity in *Df(h15q13)/+* mice.³¹ However, *Chrna7* KO mice display very mild defects in synaptic function and learning³³⁻³⁶ and have no consistent behavioral or neurophysiological phenotypes compared to *Df(h15q13)/+* mice.³⁷ Furthermore, among clinical case subjects, many of the deletions encompassing *CHRNA7* also overlap the adjacent gene *OTUD7A*.²⁰ One study reported 43 case subjects from the literature that had deletions encompassing both *CHRNA7* and the first exon of *OTUD7A*.²⁴ The Database of Genomic Variants (DGV) includes population control subjects that carry *CHRNA7* deletions, bringing into question the penetrance of haplo-insufficiency of *CHRNA7*.^{38,39} Another possible candidate is *FANI*, which encodes a DNA repair enzyme. Rare nonsynonymous variants have been found in

this gene among individuals with ASD or schizophrenia.⁴⁰ Consequently, other genes in the 15q13.3 microdeletion could contribute to disease pathogenesis.

Here, we used multiple *in silico*, *in vivo*, and *in vitro* strategies to dissect the cellular phenotypes and critical loci that contribute to the 15q13.3 microdeletion syndrome. By using the *Df(h15q13)/+* heterozygous mouse model, RNA sequencing, signaling pathway analysis, and neuronal morphology analysis, we discovered that developing cortical excitatory neurons have deficiencies in dendrite and synapse growth (Figure S2). We concurrently identified candidate gene(s) within this syndromic region contributing to these phenotypes by applying developmental human brain expression (transcriptome and proteome) data analysis together with whole-genome and -exome sequencing data from individuals with neurodevelopmental disorders and ASD.⁴¹ These analyses identified a strong candidate gene, *OTUD7A*, within the 15q13.3 microdeletion syndrome region, which encodes a putative deubiquitinating enzyme that localizes to dendritic spine compartments and has a protein-protein co-expression network that includes synaptic and dendritic signaling pathways. We biologically validated *OTUD7A* and found that re-expressing *OTUD7A* WT into cortical neurons from *Df(h15q13)/+* mice rescued the dendritic spine defects. However, a mutant *OTUD7A* harboring an ASD-linked *de novo* exonic mutation was unable to rescue these defects. Furthermore, we found that both *OTUD7A* and *CHRNA7* contribute to the dendrite outgrowth defects. Our data identify *OTUD7A* as a candidate gene that contributes to abnormalities in cortical neuron dendritic and spine development and a critical gene in the phenotypic manifestation of the 15q13.3 microdeletion syndrome.

3.3 MATERIAL AND METHODS

RNA Sequencing and Differential Expression Analysis

mRNA was extracted from E16, P21, and adult (P63) mouse cortical brain tissue using Trizol LS reagent (ThermoFisher Scientific). Two WT and two *Df(h15q13)/+* mice were used for each time point (12 mice total). All postnatal mice used for transcriptome analysis were male whereas sex was undetermined for embryonic mouse brain samples. Quality of total RNA samples was checked on an Agilent Bioanalyzer 2100 RNA Nano chip following Agilent Technologies' recommendation. We have measured the concentration by Qubit RNA HS Assay on a Qubit fluorometer (ThermoFisher). The library preparation for RNA was performed following the Illumina Stranded mRNA Library Preparation protocol. In brief, 500 ng of total RNA was used as the input material and enriched for poly(A) mRNA, fragmented into the 200- to 300-base range for 4 min at 94⁰C and converted to double stranded cDNA, end-repaired, and adenylated at the 3⁰ to create an overhang A to allow for ligation of Illumina adapters with an overhang T; library fragments were amplified under the following conditions: initial denaturation at 98⁰C for 10 s, followed by 10 cycles of 98⁰C for 10 s, 60⁰C for 30 s, and 72⁰C for 30 s, and finally an extension step for 5 minutes at 72⁰C; at the amplification step, each sample was amplified with different barcoded adapters to allow for multiplex sequencing. To check the size fragment, 1 mL of the final RNA libraries was loaded on a Bioanalyzer 2100 DNA High Sensitivity chip (Agilent Technologies); RNA libraries were quantified by qPCR using the Kapa Library Quantification Illumina/ABI Prism Kit protocol (KAPA Biosystems). Libraries were pooled in equimolar quantities and paired-end sequenced on

an Illumina HiSeq 2500 platform using a High Throughput Run Mode flowcell and the V4 sequencing chemistry following Illumina's recommended protocol to generate paired-end reads of 126 bases in length.

We used TopHat⁴² to align the read and conducted expression analysis for each gene through reads per kilobase of transcript per million mapped reads (rpkm) computation. To compute global differential expression (DE) analysis for each of the three time points—E16, P21, and adult (P63)—we conducted comprehensive DE analysis using a Bioconductor package named edgeR.⁴³ Differential expression was computed against control expression for each of the three time points separately and a gene was considered differentially expressed for a time point only if $p < 0.0001$ and $FDR < 0.05$.

Microarray and Sequencing Data

Microarray data were obtained for 38,325 ASD-affected and developmental delay (DD)-affected case subjects from four large sources (Table S3). The first dataset is comprised of 1,026 samples diagnosed primarily with ASD and genotyped with high-resolution microarrays (Illumina 1M). The other three other datasets comprised case subjects with developmental delay. The first of these includes 9,322 samples recruited from USA by a private company (Lineagen Inc.) and the data were generated using high-resolution Affymetrix Cytoscan HD in conjunction with the Chas algorithm. The second dataset comprised 10,619 DD-affected case subjects from two major clinics in Ontario, Canada. For the first and second datasets, ethical clearance was obtained from The Hospital for Sick Children's institutional ethical board. The third dataset is from a published dataset of

17,358 case subjects with DD in USA, primarily from a private diagnostic company which used the international standards for cytogenomic arrays (ISCA) for variant classification.⁴⁴ We have preprocessed 22,241 control samples from seven different sources that were recruited as population control subjects.⁴⁴⁻⁵⁰ For both case and control subjects, we focused on deletions with >50% reciprocal overlap with the 15q13.3 microdeletion region (BP4-BP5). Gene-specific deletions and atypical variants that were larger and overlapped with 15q13.3 were also kept for fine mapping. To identify *de novo* mutations within the 15q13.3 locus, we analyzed published whole-exome and -genome sequencing data from autism spectrum disorder cohorts⁵¹⁻⁵³ and a homogeneous population control.⁵⁴ Variants were validated using Sanger sequencing as described in Yuen et al.⁵³ Consent was obtained from all human participants, as approved by the Research Ethics Boards at The Hospital for Sick Children, McMaster University, and Memorial Hospital.

Critical Exon and Protein Expression Analysis

Whole-genome sequencing data from the 1000 Genomes Project was used to compute the burden of rare missense and loss-of-function mutations for each exon. Furthermore, exon-level expression data from RNA sequencing were obtained for developmental human brain tissues (prenatal and postnatal postmortem donors) from the BrainSpan project and ten other human tissues. The analysis to identify brain-specific critical exons has been described in Uddin et al.⁴¹ where 10% of genes within the genome were shown to be brain critical and this specific group of genes is significantly enriched for *de novo*

mutations in autism probands but not in unaffected siblings or in population control subjects. In brief, to classify critical exons, we computed the expression level from RNA-sequencing data from developmental human brain for each exon and classified high and low based on the 75th percentile of the entire dataset. An exon was classified as critical exon if it is highly expressed in a tissue and the burden of deleterious mutation is low. A critical exon was classified as brain specific if critical only for brain and not other tissues. We obtained a brain-specific protein module from Uddin et al.,¹ where a comprehensive weighted gene co-expression network analysis (WGCNA) was conducted on the high-resolution protein mass-spectrometry dataset from developmental human tissues (24 different human tissues, each pooled from 3 post-mortem donors which includes 17 adult and 7 prenatal samples). For the 15q13.3 microdeletion syndrome locus, *OTUD7A* is the only gene within the brain-specific protein module and we have extracted the first-degree neighbors from the module. An over-representation analysis was conducted with gene sets using a Fisher exact test and p value was corrected for multiple tests.

To produce gene level expression information, we normalized the entire protein expression level data from 24 different human tissues and quantified the 75th percentile of the expression value from the entire data. Expression for a gene was considered high if it was above the 75th percentile, and low otherwise. For gene-level RNA-seq expression data, we followed the same protocol as the protein expression data for consistency.

Geneset Enrichment Analysis and Visualization

We conducted a comprehensive geneset enrichment analysis on RNA-seq differentially expressed genes and for the first-degree neighbor proteins for OTUD7A that were extracted from the blue protein module. We manually curated 2,848 gene sets from the gene ontology (GO) (R package, v.2.8.0), pathways from the National Cancer Institute at the National Institutes of Health (NCI-NIH), Kyoto Encyclopedia of Genes and Genomes (KEGG) (May 30, 2013), and Reactome databases. Gene sets were considered significant after Benjamini-Hotchberg false discovery rate of 0.05. To visualize network datasets, we used Cytoscape plugins using v.3.2.0.

Animals

Df(h15q13)/+ mice were generated by Taconic Artemis as described in Fejgin et al.²⁵ Animals were bred, genotyped, and housed at the Central Animal Facility at McMaster University. All procedures received the approval of the Animal Research Ethics Board (AREB). Genotypes were identified during breeding by PCR of ear notches, and three WT females were bred with 1 *Df(h15q13)/+* male per breeding cage. The use of only WT females for breeding was performed to minimize effects of potential differences in the embryonic environment and/or mothering of the *Df(h15q13)/+* females compared to WT females. To obtain cortical cultures, WT females were timed-bred with *Df(h15q13)/+* males and males were removed when a plug was observed, indicating copulation. At E16, mothers were sacrificed and litters were collected. Animals of appropriate genotype were included, and any animals with unclear genotypes were excluded from experiments.

Cell Culture and Transfection

Primary cortical neurons were cultured as follows. Cortices were dissected out of WT and *Df(h15q13)/+* mouse embryonic brains at E16. Each brain was cultured individually. Dissociation was aided by incubation in 0.3 mg/mL Papain (Worthington Biochemical)/400 U/mL DNase I (Invitrogen) in 13 Hanks Buffered Saline Solution (HBSS) for 20 min at 37°C, followed by light trituration. Cells were seeded onto 0.1 mg/mL poly-D-lysine (BD Sciences)/3.3 mg/mL Laminin (Sigma)-coated coverslips (Matsunami) in 12-well plates in plating media containing Neurobasal medium, 10% fetal bovine serum, 1% penicillin/streptomycin, and 2 mM L-glutamine (Invitrogen). After 1.5 hr, media was changed to serum-free feeding media containing Neurobasal medium, 2% B27 supplement, 1% penicillin/streptomycin, and 2 mM L-glutamine. At DIV2-4, cultures were treated with 1 mM Cytosine b-D-arabinofuranoside hydrochloride (Ara-C) (Sigma) to inhibit glial cell proliferation. Cultures were maintained at 37°C, 5% CO₂. All media components were from GIBCO unless otherwise specified. Transfections were performed at DIV7 using Lipofectamine LTX and Plus reagents (Invitrogen) according to the manufacturer's instructions. HEK293FT cells (Invitrogen) were grown under standard cell culture conditions and transfected with plasmids using Lipofectamine 2000 according to the manufacturer's protocol (Invitrogen). HEK293FT cells were used for ease of plasmid expression and have not been tested for Mycoplasma contamination.

***In Utero* Electroporation**

Timed-pregnant WT female and *Df(h15q13)/+* male mice were anesthetized by isoflurane (gas). The uterine horns were exposed, and FLAG-pcDNA control or FLAG-OTUD7A WT plasmids with pCAG Venus constructs (4:1 ratio) mixed with Fast Green were injected into the lateral ventricles of E16 embryos. 5 current pulses (conditions: 950 ms pulse, 50 ms interval, 36V) were delivered across the head of the embryos. Litters were born and sacrificed by perfusion at P22. Mice were anesthetized by isoflurane gas followed by intraperitoneal injection of sodium pentobarbitol. This was followed by perfusion with lactate ringers solution and then 4% PFA. Following perfusion, brains were harvested and post-fixed in 4% PFA for 48 hr at 4⁰C. Mice were genotyped as described, and brains were sectioned using a vibratome (Leica) at 50 μ m thickness (coronal).

Antibodies and Constructs

The following primary antibodies were used in this study. Mouse anti-FLAG (Sigma F3165; IF 1:2,000; western blotting 1:2,000), rabbit anti-b-actin (Cell Signaling 4970; western blotting 1:2,000), and anti-rabbit PSD95 (Cell Signaling Technologies D27E11; IF 1:200). All secondary antibodies (anti-rabbit cy5, anti-mouse cy3; Jackson ImmunoResearch; IF 1:500, anti-rabbit- HRP, anti-mouse-HRP; GE Life Sciences; IB 1:5,000) were raised in donkey. pCAGIG-Venus was provided by Dr. Zhigang Xie (Boston University, MA). The FLAG-OTUD7A WT was amplified from a pCMV6_FLAG-WT-OTUD7A construct (Origene, RC213015,

GenBank: NM_130901) and cloned into the pcDNA3.3 vector between EcoRI and KpnI. pcDNA3.3_FLAG-OTUD7A p.Asn492_Lys494del plasmid was generated using In-Fusion cloning kit. FLAG-CHRNA7, FLAG-FAN1, and FLAG-KLF13 were amplified from a pCMV6_FLAG-CHRNA7 (Origene, RC221382, GenBank: NM_000746), pCMV6_FLAG-FAN1 (Origene, RC224249, GenBank: NM_014967), and pCMV6_FLAG-KLF13 (Origene, RC200805, GenBank: NM_015995) and cloned into the pcDNA3.3 vector using In-Fusion cloning kit.

Immunocytochemistry

On DIV14, cells on glass coverslips were fixed with 4% formaldehyde in PBS for 20 min at room temperature. Cells were washed in PBS, followed by blocking in blocking/permeabilization solution consisting of 10% Donkey Serum (Millipore) and 0.3% Triton X-100 (Fisher Scientific) in PBS for 1 hr at room temperature. Incubation in primary antibodies was performed at 4⁰C overnight. Cells were then washed in PBS, followed by incubation with secondary antibodies in 50% blocking/permeabilization solution at room temperature with gentle agitation for 1.5 hr. Cells were then washed in PBS and were mounted on VistaVision glass microscope slides (VWR) using Prolong Gold antifade reagent (Life Technologies). Images were acquired using a Zeiss LSM700 confocal microscope.

Golgi Staining

Golgi staining was performed on mouse brains from P28 male mice using a commercial kit and protocol (FD Rapid GolgiStain Kit, FD NeuroTechnologies, Inc.). Briefly, whole mouse brains were removed and washed with Milli-Q water. The brain was immersed in impregnation solution for 8 days. Following impregnation, brains were rinsed twice with water and incubated for 72 hr with Solution C. Brains were then removed and incubated in 30% sucrose/PBS for 24 hr in the dark. Using a vibratome (Leica), brain slices were cut at 150 μm thickness and mounted onto 3% gelatin-coated SuperFrost Plus microscope slides (ThermoFisher). Sections were incubated in staining solution for 10 min, washed with Milli-Q water, dehydrated with EtOH, and cleared with xylene (Sigma). Stained brain slices were imaged using Zeiss Axiocam ICm1 microscope camera. Z stacks were acquired at 1 μm intervals for sholl analysis and 0.28 mm intervals for spine analysis. Images were processed using ImageJ software (Sholl Analysis plugin).

Morphological Analyses

Images were processed and analyzed with ImageJ 1.44 software. Sholl analysis was performed using the Sholl analysis plugin in ImageJ. This plugin was used to make concentric circles increasing at a constant radius of 10 μm and to count the number of dendritic intersections. Neuron tracing was performed using the NeuronJ plugin for ImageJ 1.44. Spine density was calculated by visually counting all protrusions from a dendrite within a 15–25 μm distance starting at a secondary branch point. One to three dendritic segments were analyzed per neuron. Maximal spine head width (HW), neck width (NW), length (L), and neck length (NL) were measured for each dendritic

protrusion using the segmented line tool in ImageJ. Spines were defined as follows: stubby ($L < 1 \mu\text{m}$), mushroom ($1 \leq L \leq 5 \mu\text{m}$; $\text{HW} \leq 2 \times \text{NW}$), or thin ($1 \leq L \leq 5 \mu\text{m}$; $\text{WH} \leq 2 \times \text{NW}$). The proportion of each spine type was calculated by dividing the number of spines in each spine category (mushroom, thin, and stubby) by the total number of spines within the dendritic segment. For analyses on Golgi-stained brains, 40 neurons from 4 brains per condition were used for sholl analysis and 40 dendritic segments from 4 mouse brains per condition were used for spine analysis. For IUE experiments, 21–23 neurons from 3 brains per condition were used for sholl analysis, and 30 dendritic segments from 3 brains per condition were used for spine analysis. For in vitro analyses, 21–50 neurons were used from 3–4 biological replications (mouse litters) for sholl analysis, and 20–36 dendritic segments from 3–5 biological replications (mouse litters) for spine analysis.

Quantitative PCR

To measure postnatal developmental RNA expression of *OTUD7A* in the mouse brain, we obtained whole-brain samples of P0, P7, P14, P21, P28, and P63 WT C57BL/6 mice. Total RNA was extracted using TRIzol LS Reagent (Thermo Fisher Scientific), followed by cDNA synthesis using the qScript cDNA synthesis kit according to manufacturer instructions (Quanta Biosciences). Primers and probes were designed and selected using the Universal Probe Library (UPL) Profinder software for mouse (Roche). Quantitative PCR was performed using the Perfecta qPCR Supermix (Quanta Biosciences) and UPL

probe #50 (OTUD7A) or UPL probe #52 (GAPDH). Data represented as levels of OTUD7A normalized to GAPDH levels.

Western Blotting

Western blotting was performed using standard protocols. Briefly, HEK293FT cells were lysed in lysis buffer (150 mM NaCl, 1% Triton X-100, 50 mM Tris-Cl, and cOmplete mini protease inhibitor cocktail (Roche). 20–30 mg of sample was loaded into a 10% Tris-Glycine gel and transferred to a PVDF membrane (Bio-Rad). Membranes were blocked for 1 hr in 3% milk in 1x TBST, incubated with primary antibody overnight at 4°C, then with secondary antibody (donkey anti-mouse or anti-rabbit HRP, GE Healthcare) for 1 hr at room temperature before exposure using a ChemiDoc MP system (Bio-Rad).

Statistical Analysis

Data are expressed as mean \pm SEM. A minimum of three mice per condition or three mouse litters for *in vitro* culture experiments, was used for statistical analysis. Blinding was not performed. We used the Student's t test, one-way ANOVA with post hoc Tukey's test, and two-way ANOVA in GraphPad Prism 6 statistical software for statistical analyses. p values in the figure legends are from the specified tests, and $p < 0.05$ was considered statistically significant.

3.4 RESULTS

3.4.1 Df(h15q13)/+ Mice Show Defects in Forebrain Development Including Abnormalities in Dendritic Spines and Dendrite Growth

To study the 15q13.3 microdeletion (Figure 1), we utilized the heterozygous BP4-BP5 mouse model (*Df(h15q13)/+*).²⁵ We examined temporal gene expression (using RNA sequencing) in cortical brain tissue from *Df(h15q13)/+* and WT mice at three stages: prenatal (embryonic day 16; E16), early postnatal (postnatal day 21; P21), and adult (P63) (Figures S1A and S1B and Table S1). We identified 66 genes with significant ($p < 0.0001$ and $FDR < 0.05$) differential expression from the three developmental time points. *Mtmr10*, *Otud7a*, *Klf13*, *Fan1*, and *Chrna7* displayed significant differential expression (DE) in all periods (*Trpm1* is not expressed in the brain, and *miR211* was not detected because samples were not enriched for small RNAs during sample preparation) (Figure S1A), demonstrating that the heterozygosity of gene expression persists into adulthood. Interestingly, we found that differential gene expression was most pronounced (~2-fold) at postnatal time points, P21, and adulthood (when spine and synapse development is peaking). We conducted extensive gene enrichment analyses for all differentially expressed genes by using 2,848 gene sets with defined biological pathways in KEGG, GO, NCI-NIH, and Reactome databases. The most significant enrichment across all time points was observed for prenatal organ development ($p < 2.9 \times 10^{-05}$, significant after Benjamini-Hochberg correction) and forebrain development ($p < 6.8 \times 10^{-05}$) (Figure S1C and Table S2). The significant enrichment of the forebrain development pathway in the

WT versus *Df(h15q13)/+* comparison suggests that cortical development is disrupted by the microdeletion.

We next focused on postnatal cortical (forebrain) development in *Df(h15q13)/+* mice because of our transcriptional data and previous studies that identified abnormalities in excitatory neuron development.⁵⁵⁻⁵⁸ Therefore, we measured dendritic spine morphology and dendrite growth *in vivo* on Golgi-Cox-stained WT and *Df(h15q13)/+* mouse brains. We analyzed cortical neurons in layers 2/3 of the prefrontal cortex (PFC) of male P28 *Df(h15q13)/+* and age/sex-matched WT mice. We found that in *Df(h15q13)/+* prefrontal cortex, there was a small but significant ($p < 0.01$) reduction in spine density and mature mushroom-shaped spines (Figures 2A and 2B). *Df(h15q13)/+* mice also displayed a significant ($p < 0.05$) reduction in spine length and spine neck length (Figure S2A).

Dendritic arborization was measured using Sholl analysis⁵⁹ and revealed that *Df(h15q13)/+* mice showed decreased arborization in layer 2/3 PFC neurons compared to WT mice (Figures 2C and 2D). Since these findings were obtained *in vivo*, it is difficult to determine whether they are cell autonomous. Therefore, we cultured cortical neurons from littermate *Df(h15q13)/+* and WT mice, transfected with a Venus fluorescent reporter, and analyzed neurons at 14 days *in vitro* (DIV14). *Df(h15q13)/+* neurons also showed a significant reduction in the density of dendritic spines and spine length (Figures 2E, 2F, and S2B), as well as a decrease in mature mushroom-type spines ($p < 0.05$) and increase in immature stubby-type spines ($p < 0.01$) (Figure 2G), replicating many of the *in vivo* phenotypes. In addition, there was a significant decrease in dendritic arborization in *Df(h15q13)/+* neurons compared to WT littermates (Figures 2H and 2I). The spine and

dendrite phenotypes in Df(h15q13)/+ observed *in vitro* were stronger than *in vivo*, suggesting some level of compensation, similar to previous reports.^{3,60}

3.4.2 OTUD7A Is a Candidate Driver Gene in the 15q13.3 Microdeletion

We further assessed the pathogenicity of the 15q13.3 microdeletion by using large datasets to compile all available published and unpublished case subjects (Table S3). In addition, clinical microarray data from 38,325 case subjects with a range of neurodevelopmental disorders were examined to identify the frequency of 15q13.3 deletions (chr15: 30910306–32445407 [hg19], encapsulating BP4 and BP5). Stringent CNV calling parameters were applied (minimum of 5 probes, minimum of 2 algorithms, >30 kb in length) on the clinical microarray data, facilitating the discovery of 156 individuals with 15q13.3 microdeletions impacting the typical BP4-BP5. Among these microdeletions, 148 were detected in case subjects with broad developmental phenotypes and 8 in case subjects with a primary diagnosis of ASD (Figure S3A). In contrast, we identified only one BP4-BP5 deletion within a control population of 22,241 individuals (Figure S3A). The enrichment of 15q13.3 microdeletions within neurodevelopmental disorder-affected and ASD-affected case subjects (0.4% combined in NDD and ASD case subjects; 0.004% in control subjects) is highly significant ($p < 1.30 \times 10^{-29}$). Together, these data re-confirm that the 15q13.3 microdeletion is strongly associated with neurodevelopmental disorders.^{16,61} We then applied three approaches to narrow down the potential contributing gene(s) from the ten genes present in BP4-BP5. First, we determined whether there are smaller deletions within BP4-BP5 that are associated with

neurodevelopmental disorders. We delineated the minimal region (530 kb in size) of overlap from our clinical microarray sample and found that only two genes (*CHRNA7* and *OTUD7A*) are associated with an atypical smaller CNV. This has been reported previously, but it is particularly noteworthy that at least 43 overlapping deletions encompassing *CHRNA7* also impacted *OTUD7A*^{20,24} (Figure 1). Furthermore, since 52 microdeletions encompassing *CHRNA7* are found within our control samples (compared to zero smaller deletions in controls within *OTUD7A*), this also implicates other genes within the CNV. In further support of this, we identified a 5-year-old female, previously unreported in the literature, with global developmental delay who possessed a genetic deletion that spanned BP4-BP5 including *OTUD7A* but not *CHRNA7* (Figure S3B). Similarly, a duplication breakpoint that does not involve *CHRNA7* has also been recently reported in a female patient with atypical Rett syndrome who is negative for an *MECP2* mutation.⁶² Taken together, these data suggest that genes other than *CHRNA7*, such as *OTUD7A*, may contribute to the 15q13.3 microdeletion syndrome.

We next investigated DNA sequence-level mutations in the ten genes within the microdeletion among individuals with a neurodevelopmental disorder but who did not have a 15q13.3 microdeletion. We focused on *de novo* mutations, given their established role in pathogenicity.^{41,51–53,63–66} We investigated whole-genome sequencing data (n = 84 ASD quad families⁵³) and exome-sequencing data (n = 5,953 ASD trios^{51,52}) and discovered 8 *de novo* mutations impacting regions in the BP4-BP5 interval. Three of these mutations impacted

OTUD7A, one impacted *MTMR10*, one impacted *TRPM1* (Table 1, case 2, GenBank: NM_001252024.1; c.2382C>G [p.Phe794Leu]), and the remainder were intergenic *de novo* mutations. Among the *de novo OTUD7A* mutations specifically, the first is an exonic *de novo* 9 bp non-frame-shift deletion (Table 1, case 3, GenBank: NM_130901.2; c.1474_1482del [p.Asn492_Lys494del]), in an ASD-affected proband and their affected sibling (Figures 3A, S3D, and S3E, and Table 1). The second and third are both intronic, one a *de novo* indel (2 bp deletion) observed in an ASD-affected proband and the other an intronic *de novo* single-nucleotide mutation in an ASD-affected proband (Table 1). One of the intergenic *de novo* mutations was identified in two ASD-affected siblings between *OTUD7A* and *CHRNA7* (cases 5 and 6 in Table 1); genome-wide, no other pathogenic exonic mutations or CNVs were identified in either of these affected siblings.

Interestingly, the intergenic mutation between *OTUD7A* and *CHRNA7* occurs in the binding site of the transcription factor, enhancer of zeste 2 polycomb repressive complex subunit 2 (*EZH2*) (Figure S4). *EZH2* (MIM: 601573) has previously been implicated in dendrite growth,⁶⁷ which raises the hypothesis that *EZH2* regulates *OTUD7A* expression; however, further investigation is required to investigate the intergenic mutations. In contrast, no *de novo* mutations within *OTUD7A* were identified from whole-genome sequencing of 250 Dutch trio control samples⁵⁴ or exome sequencing of the unaffected siblings of ASD-affected probands (from a family dataset of 5,205 individuals).⁵² The identification of *de novo* mutations either within or near *OTUD7A* is further evidence in support of *OTUD7A* as a major critical gene in the 15q13.3 microdeletion syndrome.

In our final approach, we assessed the exons of human genes for relevancy in neurodevelopment according to their population-level deleterious mutational burden in concert with brain mRNA expression (from RNA-sequencing data), earmarking those exons with a low mutational burden and high mRNA expression only in the developing human brain as being “brain critical.”¹⁴¹ This analysis identified *FANI* and *OTUD7A* as genes bearing critical exons, with *OTUD7A* having a higher ratio of brain critical exons than *FANI* (Figure 3C). *FANI* was recently suggested to be a susceptibility gene in the 15q13.3 microdeletion based on the identification of an enrichment of small nucleotide variants (SNVs) in ASD and SCZ populations.⁴⁰ However, in our analysis, we did not identify *de novo* mutations in *FANI* or overlapping deletions containing this gene and therefore did not pursue it further. To complement the critical exon analysis, we also examined the tolerance of loss-of-function (pLI) mutations of each of the 15q13.3 genes (a measure of the probability that a given gene is extremely intolerant of loss-of-function variation) from the exome aggregation consortium (ExAC) database.⁶⁸ Comparison of the genes in the 15q13.3 microdeletion (no data were available for *CHRNA7*) revealed that *OTUD7A* possessed the most constrained gene scores (pLI = 0.97 and Z = 5.92) (Figure 3D), supporting its important evolutionary role in development.

To investigate the expression patterns of the genes within the BP4-BP5 deletion in the brain, we conducted qRT-PCR analysis of 8 genes (except *KLF13* and *miR-211*; *LOC100288637* was not detected) in 12 human tissues. For each gene, primers were designed targeting the exons that are common in all transcripts and our qRT-PCR analysis revealed that *OTUD7A* was the only gene that displayed a brain-specific mRNA

expression pattern compared to other tissues (Figures 3B and S3C). This is similar to the expression profile of *OTUD7A* in the GTeX database. Furthermore, the BrainSpan database for human developmental brain expression shows that many *OTUD7A* exons are expressed above the 75th percentile of the total brain expression dataset (Figure S3F). *KLF13* is notable because it has higher brain expression than *OTUD7A* in these databases; however, upon further examination it is largely driven by one exon (Figure S3F), and its expression is not brain specific, which is evident in the critical-exon analysis.

We also determined the protein co-expression network for *OTUD7A* in the brain using recently published human tissue protein-level data.⁶⁹ To identify a core set of proteins having an important role in brain development, we analyzed protein data from 24 human tissues (each pooled from 3 post-mortem samples) including 17 adult and 7 prenatal samples that were run through high-resolution Fourier transform mass spectrometers for fragmentation.⁶⁹ Weighted gene co-expression network analysis (WGCNA) analysis was used to identify 23 unbiased and independent protein modules. After rigorous gene set enrichment analysis (see STAR Methods), one of the modules was chosen for further analysis, as it was brain-specific and significantly associated with neurodevelopment and comprised of 2,484 proteins.⁷⁰ Strikingly, WGCNA analysis identified *OTUD7A* as being the only gene within 15q13.3 microdeletion that was part of the brain-specific protein module. This is because the other 15q13.3 genes' protein products did not have brain-specific expression. We identified 616 strongly connected (top 25th percentile) first-degree neighbor genes for *OTUD7A* within the brain-specific protein module. A

comprehensive enrichment analysis was conducted, which determined that these *OTUD7A* neighboring genes are highly enriched for targets of FMR1 (Fragile X Mental Retardation 1), many of which are known to play a role at the synapse, as well as genes harboring ASD *de novo* mutations (Figure 3F). We performed a comprehensive gene set enrichment analysis to decipher the pathways and biological relevance of *OTUD7A* neighbor genes. The three most significant associations were observed with synapse (GO:0045202) ($p < 1.1 \times 10^{-82}$), Benjamin-Hochberg corrected), synaptic component (GO:0044456) ($p < 9.92 \times 10^{-72}$), and neuron projection (GO: 0043005) ($p < 9.96 \times 10^{-71}$) (Table S4). These co-expression networks align with the potential involvement of *OTUD7A* in the spine and dendrite abnormalities observed in *Df(h15q13)/+* mice. Furthermore, the collective data indicate that *OTUD7A* is the only gene in the 15q13.3 microdeletion that has brain-specific expression, contains critical exons, and is interconnected with a brain-specific synaptic signaling network linked to ASD.

3.4.3 Expression and Localization of OTUD7A in Neurons

We utilized WT and *Df(h15q13)/+* mice to investigate the biological function of *Otud7a* in the brain and to test our hypothesis that *OTUD7A* is a critical gene in the 15q13.3 microdeletion. We first analyzed the expression of *Otud7a* mRNA in the developing WT mouse brain and observed an expression profile similar to the developing human brain, with an increase in expression during early postnatal stages when dendrite and spine development are important (Figure 3E) and similar to the RNA-sequencing data (Figure S1A). To determine the localization of *OTUD7A* in neurons, we transfected a FLAG-

tagged human OTUD7A (FLAG-OTUD7A WT) construct in cultured WT mouse cortical neurons and analyzed FLAG levels at DIV14, since no validated antibodies against OTUD7A are available. This experiment revealed that OTUD7A has a punctate localization pattern and is restricted to the soma and dendrites in Venus-transfected neurons (Venus is used for visualization) (Figure 3G). A very similar protein localization pattern was also independently reported by a companion study in this issue of *AJHG*.³⁷ Furthermore, we detected a fraction of FLAG-OTUD7A puncta in dendritic spines that co-localized with PSD95, a postsynaptic marker of mature excitatory synapses (Figures 3G and 3H). These data reveal that *Otud7a* is expressed in the brain and can localize to dendritic and synaptic compartments in cortical neurons.

3.4.4 Rescue of Spine and Dendrite Phenotypes in Df(h15q13)/+ Excitatory Neurons by OTUD7A

We hypothesized that the reduced expression of *Otud7a* in *Df(h15q13)/+* heterozygous neurons mediated the dendritic spine and dendrite growth phenotypes, and increasing *OTUD7A* expression in these neurons would rescue the deficit. To test this, we co-transfected Venus and FLAG-*OTUD7A* WT (or a control plasmid) into litter-mate WT or *Df(h15q13)/+* E16 mice using *in utero* electroporation to label layer 2/3 prefrontal cortical neurons. We examined dendritic spines and dendrite growth in brain slices at P22. We found that expression of *OTUD7A* WT in *Df(h15q13)/+* neurons completely rescued the deficit in spine density, the proportion of mushroom and stubby type spines, and spine length compared to WT conditions (Figures 4A–4E). We also found that expression of

OTUD7A WT in *Df(h15q13)/+* neurons rescued the deficit in dendrite branching, similar to WT conditions (Figures 4F and 4G). We then tested whether the rescue by *OTUD7A* is recapitulated *in vitro*. We cultured cortical neurons from littermate WT and *Df(h15q13)/+* mice at E16 and co-transfected FLAG-*OTUD7A* WT and Venus at DIV7. We evaluated FLAG/Venus double-positive neurons at DIV14 to visualize and quantify dendrites and spines expressing *OTUD7A* WT. We found that expression of *OTUD7A* WT in cultured *Df(h15q13)/+* cortical neurons rescued the reduction in spine density, spine length, and the proportion of mushroom and stubby spines but had no effect on the proportion of thin spines or spine head width, neck width, or neck length (Figures 5A–5E, S5B, and S5C). *OTUD7A* also rescued dendritic branching compared to WT controls as measured by Sholl analysis and the total number of dendritic intersections (Figures 5F and 5G). Together, these data indicate that *OTUD7A* contributes to spine and dendrite deficits caused by the 15q13.3 microdeletion.

3.4.5 An ASD-Associated De Novo Mutation in *OTUD7A* Impairs Dendrite and Spine Growth

We next examined whether the ASD-linked *de novo* mutation in *OTUD7A* (p.Asn492_Lys494del; case 3, Table 1) has a functional effect on dendritic and spine morphology. We generated a mutant *OTUD7A* (encoding p.Asn492_Lys494del) in the same FLAG-tagged plasmid as *OTUD7A* WT and found no overt difference in protein levels or localization between the WT and the mutant form of *OTUD7A* (Figures S5A, S6L, and S6M). Furthermore, *OTUD7A* p.Asn492_Lys494del failed to rescue the defects

in dendritic spine density, morphology, or spine length, spine neck length, spine head width, or neck width in *Df(h15q13)/+* neurons (Figures 5A–5E, S5B, and S5C). Compared to WT control neurons and *OTUD7A* WT, the expression of *OTUD7A* p.Asn492_Lys494del in *Df(h15q13)/+* cortical neurons failed to rescue dendritic arborization defects (Figures 5F and 5G). We also investigated whether *OTUD7A* p.Asn492_Lys494del has a dominant-negative effect when expressed in WT cortical neurons. We co-transfected Venus with *OTUD7A* WT or *OTUD7A* p.Asn492_Lys494del in cultured WT neurons and determined that expression of *OTUD7A* p.Asn492_Lys494del had a mild dominant-negative effect, significantly reducing dendritic spine length (Figures S6A and S6F) and arborization (Figures S6J and S6K) compared to the pcDNA control but had no effect on spine density, spine type, or length (Figures S6A–S6I). These experiments reveal that a *de novo* mutation in *OTUD7A* is sufficient to impair its function during dendritic spine and dendrite development.

3.4.6 *OTUD7A* Is the Predominant Gene Regulating Dendrite Spine Development

Finally, given that other genes in the 15q13.3 CNV have been implicated (*CHRNA7* and *FANI*), we tested the function of *OTUD7A* compared to other 15q13.3 genes. In addition to *CHRNA7* and *FANI*, *KLF13* was included in our analysis due to its high expression (Figure S3F). We created FLAG-tagged *CHRNA7*, *KLF13*, or *FANI* constructs to determine whether they could rescue the cellular phenotypes. Analysis of spine density and morphology showed that *OTUD7A* was the only gene tested that could rescue spine density, length, and the proportion of mushroom and stubby spines, whereas *CHRNA7*,

KLF13, or *FANI* were unable to (Figures 6A–6E). For dendrite outgrowth, we found that *KLF13* and *FANI* were unable to rescue the defect in dendrite growth, further suggesting that these genes have a minimal role in the 15q13.3 microdeletion syndrome (Figures 6F and 6G). Interestingly, expression of *CHRNA7* had a similar rescue effect as *OTUD7A* in dendrite outgrowth, suggesting that heterozygous loss of both genes contribute, possibly together, to the dendrite growth defects in *Df(h15q13)/+* mice. These data indicate that *OTUD7A* is the only gene in the BP4-BP5 interval regulating dendritic spine developmental phenotypes. A companion study by Yin et al. shows that *Otud7a* KO mice recapitulate many phenotypes of the 15q13.3 microdeletion syndrome including defective spine-synapse development, whereas a previous study from this laboratory showed no consistent behavioral phenotypes in a *Chrna7* KO mouse model.^{37,71} Our study, along with the companion study, provides evidence that *OTUD7A* is a critical gene in the 15q13.3 microdeletion syndrome.

3.5 DISCUSSION

Our data support an important and previously unidentified role for *OTUD7A* in the 15q13.3 microdeletion syndrome. Specifically, we identified that *OTUD7A* is a critical gene for brain development and an important contributing gene in the 15q13.3 microdeletion syndrome. We also biologically validated that *Otud7a* was the only gene in the interval that we tested that regulates the dendritic spine defects caused by the BP4-BP5 microdeletion in a validated mouse model. Our identification of *OTUD7A* as a critical component of brain protein-signaling networks that localizes to PSD95-positive

spine synapses and modulates spine morphology and dendrite growth leads us to conclude that *OTUD7A* is a critical driver gene of the 15q13.3 microdeletion.

Our findings are overall consistent with a companion study by Yin et al. showing that *Otud7a* localizes to dendritic spines and that *Otud7a* KO mice have deficits in cortical neuron dendritic spine density and glutamatergic transmission.³⁷ One difference is the lack of a dendrite outgrowth phenotype in *Otud7a* KO mice. However, given that Yin et al.³⁷ demonstrated that expression of *OTUD7A* increased dendrite branching, this suggests that *OTUD7A* expression is able to stimulate dendrite development, which is consistent with our rescue findings. Moreover, we found that *Otud7a* and *Chrna7* both contribute to dendrite growth defects in *Df(h15q13)/+* mice. Therefore, *CHRNA7* and *OTUD7A* could regulate dendrite growth together in excitatory cortical neurons or alternatively, *CHRNA7* and *OTUD7A* may regulate dendritic development at different times and/or through different cell types, since *CHRNA7* is also expressed in inhibitory neurons.⁷² Since *OTUD7A* was the only gene able to rescue spine deficits in *Df(h15q13)/+* neurons, this indicates a unique and important role for it at the synapse during development. Although we have observed a strong and cross-validated *OTUD7A* phenotype, our results indicate a multi-hit hypothesis where more than one gene contributes to the etiology of 15q13.3 microdeletion syndrome, which is in line with other CNVs. For example, *DGCR8* and *ZDHHC8* are proposed driver genes in the 22q11.2 microdeletion, *UBE3A* and *MAGEL2* for the 15q11-13 microdeletion region,^{73,74} and *GTF2I* and *FZD9* for the 7q11.23 region.⁷⁵⁻⁷⁷ For the 15q13.3 CNV, future experiments are needed using *OTUD7A* and

CHRNA7 single and double KO cellular models to compare to the 15q13.3 microdeletion to determine the unique and shared contribution of each gene to disease pathogenesis. It is also possible that while the heterozygous loss of the driver genes in the 15q13.3 region results in a core set of neurodevelopmental deficiencies, the heterogeneity of genetic background of the deletion carrier might contribute to the heterogeneous clinical presentation. Interestingly, such a mechanism has been shown to be at play in the 22q11.2 microdeletion syndrome,⁷⁸ suggesting that it could be the case for the 15q13.3 microdeletion.

OTUD7A is part of a family of deubiquitinases (DUBs) that are important for removing ubiquitin molecules from proteins that are targeted for degradation.^{79,80} While we did not investigate the mechanistic action of OTUD7A, its localization to the postsynaptic density suggests that it could regulate key proteins involved in synapse maturation. Given the limited information on the role of OTUD7A, its protein-interaction network in neurons needs to be identified. Interestingly, a recent study identified that biallelic variants in *OTUD6B*, a family member, causes a novel syndrome characterized by intellectual disability, dysmorphic features, and seizures,⁸¹ indicating that DUBs could play a broader role in NDDs. Important questions regarding *OTUD7A* remain, such as: what specific proteins does *OTUD7A* regulate and interact with at the synapse? Which stages of synapse development are impaired by a lack of *OTUD7A* and how does this impact synaptic physiology and the epilepsy phenotypes observed in this microdeletion? It should also be noted that the dysregulation of protein turnover and the ubiquitin pathway has been implicated in other neurodevelopmental disorder-related CNVs. For instance, at

the 15q11–13 locus, *UBE3A* has been reported to ubiquitinate key synaptic proteins.^{82,83} Furthermore, defects in the regulation of synaptic protein turnover (i.e., synaptic protein synthesis) have also been observed in the 16p11.2 deletion and single-gene disorders such as fragile X syndrome (FXS) and tuberous sclerosis complex (TSC).^{55,84} Thus, if *OTUD7A* is involved in protein turnover, particularly at the synapse, this would add to the growing evidence that this is a common pathological mechanism for neurodevelopmental disorders involving defective synaptic signaling.

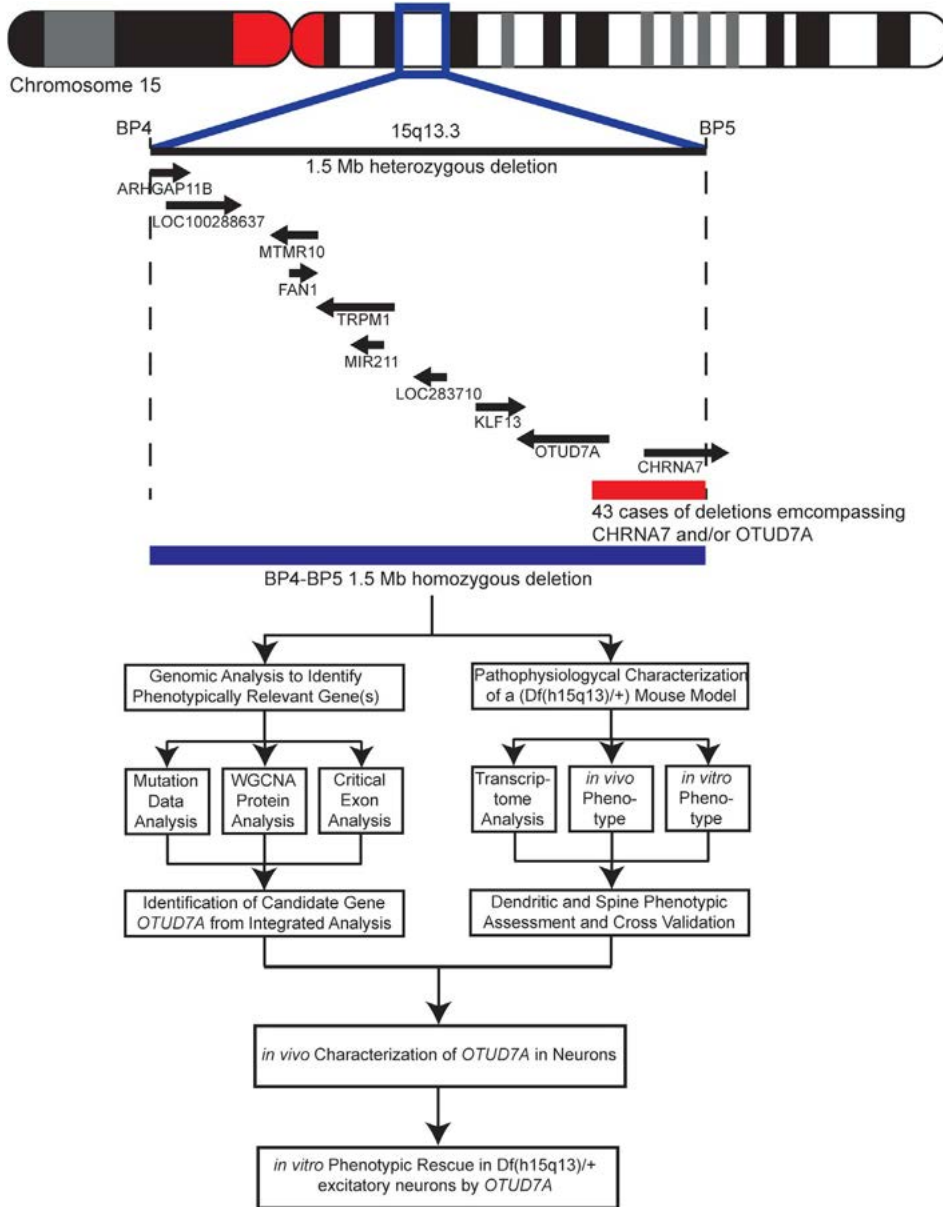


Figure 1. Overview of the 15q13.3 Microdeletion and *CHRNA7/OTUD7A* Overlapping Deletion

Schematic diagram showing the location of the human 15q13.3 locus and all ten genes within the 1.5 Mb BP4-BP5 deletion. Smaller deletions (red bar) are found within the BP4-BP5 region overlapping *CHRNA7* and/or *OTUD7A*, modified from Lowther et al.²⁴ The experimental work-flow of the current study is presented below the schematic.

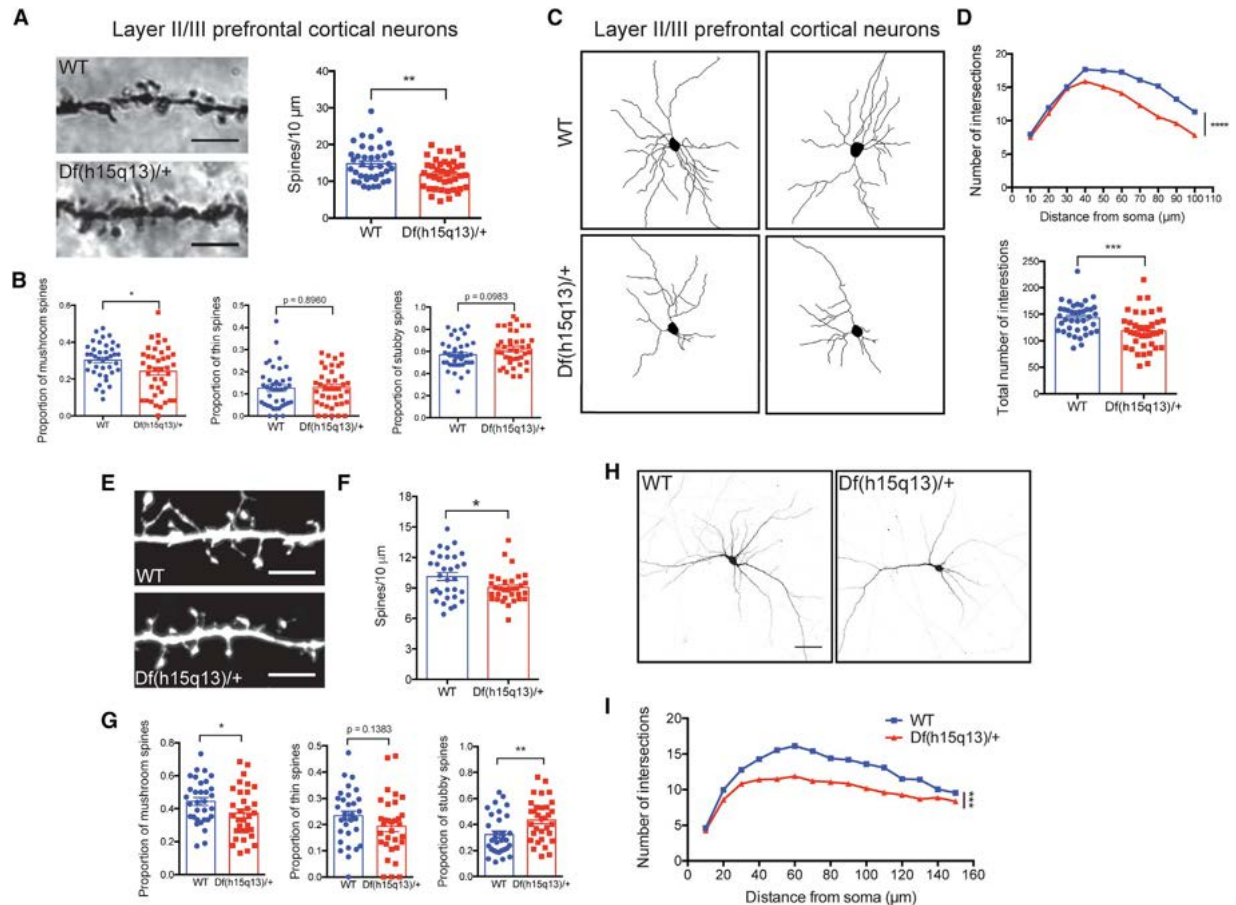


Figure 2. *Df(h15q13)/+* Mice Have Defects in Dendritic Spine Development and Neuronal Morphology

(A) Golgi-stained dendritic spine images (left) and spine density analysis (right).

Df(h15q13)/+ mice show a decrease in spine density in layer II/III PFC neurons. WT, n = 40 dendritic segments, 22 neurons; *Df(h15q13)/+*, n = 40 dendritic segments, 26 neurons, 4 mice per condition, Student's t test, ** $p < 0.01$, $t(78) = 2.846$. Scale bar = 5 μm .

(B) *Df(h15q13)/+* mice show a decrease in PFC mushroom spines (left). WT, n = 40 dendritic segments, 22 neurons; *Df(h15q13)/+*, n = 40 dendritic segments, 26 neurons, 4 mice per condition, Student's t test, * $p < 0.05$, $t(78) = 2.403$, $t(78) = 0.1312$, $t(78) = 1.673$.

(C) Traces of P28 WT and *Df(h15q13)/+* Golgi-stained layer II/III prefrontal cortical (PFC) neurons.

(D) Sholl analysis (left) and the total number of intersections (right). *Df(h15q13)/+* mice show a decrease in dendrite growth in layer II/III PFC neurons. n = 40 neurons, 4 mice per condition, two-way ANOVA followed by Tukey's post hoc test, ***p < 0.001, F(9, 780) = 109.2, t(78) = 3.449.

(E) Dendritic spine images from WT and *Df(h15q13)/+* cultured neurons (scale bar = 5 μ m).

(F) Spine density measurements in cultured neurons. Spine density is decreased in *Df(h15q13)/+* cultured cortical neurons. WT, n = 32 dendritic segments from 12 neurons; *Df(h15q13)/+*, n = 32 dendritic segments from 15 neurons, 3 cultures, Student's t test, *p < 0.05, t(62) = 2.311.

(G) Dendritic spine classification in WT and *Df(h15q13)/+* neurons. In *Df(h15q13)/+* cultured cortical neurons, the proportion of mushroom-type spines is decreased (left) and the proportion of stubby type spines is increased (right). WT, n = 32 dendritic segments from 12 neurons; *Df(h15q13)/+*, n = 32 dendritic segments from 15 neurons, 3 cultures, Student's t test, *p < 0.05, **p < 0.01, t(62) = 2.007, t(62) = 0.1383, t(62) = 2.875.

(H) DIV14 WT and *Df(h15q13)/+* cultured cortical neurons expressing Venus (scale bar = 50 μ m).

(I) Sholl analysis of cultured cortical neurons. Dendrite growth is decreased in *Df(h15q13)/+* neurons. n = 50 neurons, 3 cultures, two-way ANOVA followed by Sidak post hoc test, ***p < 0.001, F(14, 1470) = 85.55. Error bars represent SEM.

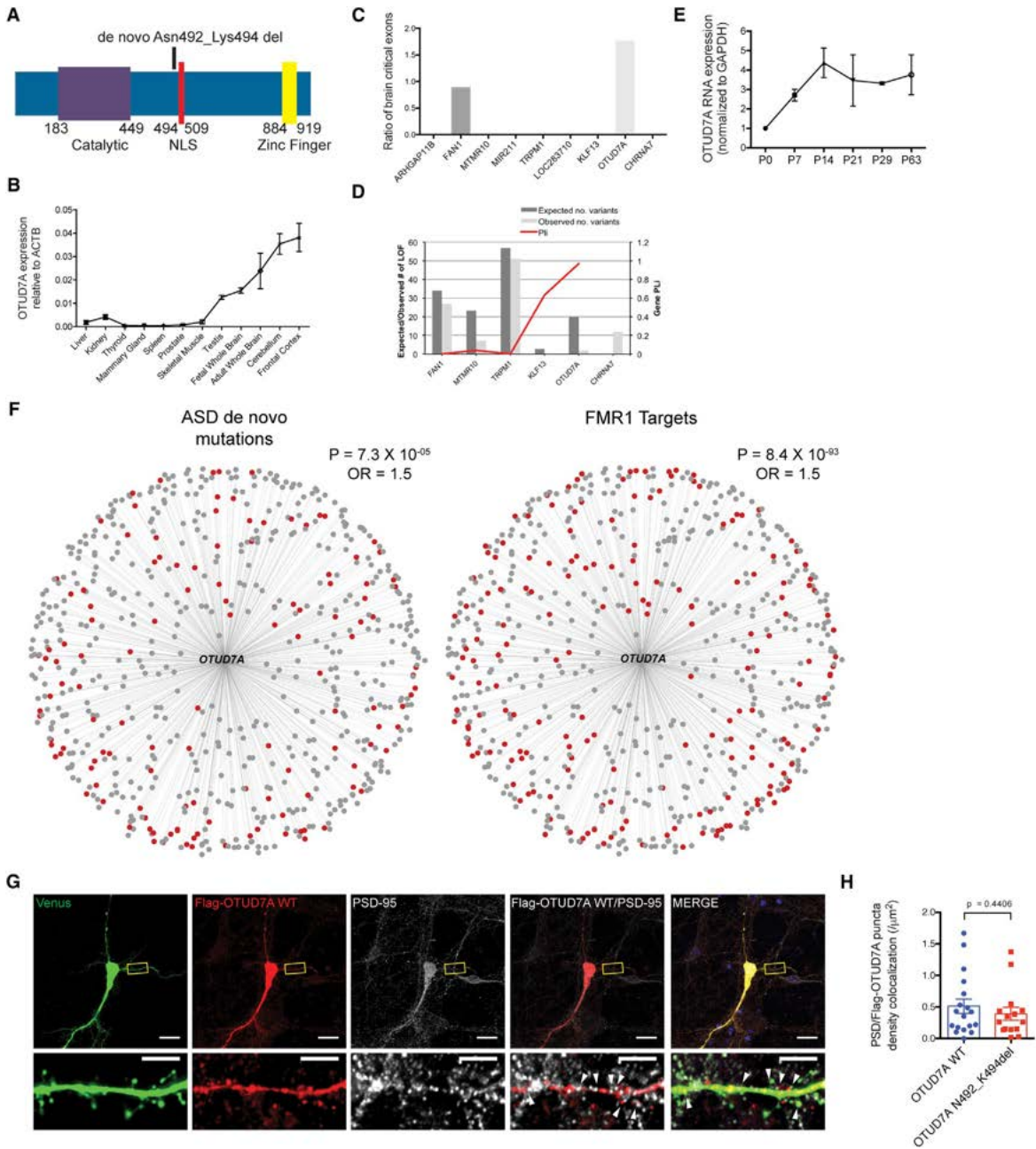


Figure 3. Identification of *OTUD7A* as a Driver Gene of the 15q13.3 Microdeletion

(A) Schematic of the human *OTUD7A* protein showing the exonic 9 bp mutation (*de novo* p.Asn492_Lys494 deletion in the protein) found in an ASD proband and affected sibling (proband is case 3 in Table 1). The mutation is located in the nuclear localization sequence (NLS) of *OTUD7A*.

(B) *OTUD7A* mRNA expression relative to ACTB in various human tissues. *OTUD7A* is enriched in the brain, with highest expression in the frontal cortex.

(C) Ratio of brain critical exons in nine genes within the 15q13.3 microdeletion region. *FANI* and *OTUD7A* contain brain critical exons, with *OTUD7A* showing a higher ratio than that of *FANI*.

(D) *OTUD7A* has the highest pLI (a score that indicates the probability that a gene is intolerant to a loss-of-function mutation) value compared to the other genes in the 15q13.3 critical region. The left y axis represents the number of observed LOF mutations within the ExAC population scale dataset and the right y axis shows the computed pLI score.

(E) *OTUD7A* mRNA expression in the mouse brain is low in early postnatal life, increases into adolescence, and remains stable into adulthood (n = 2 technical replicates).

(F) *OTUD7A* protein co-expression network module. Weighted gene correlation network analysis of *OTUD7A* from human proteome data shows that 616 genes are highly co-expressed with *OTUD7A* (top 25th percentile). 21% of genes highly co-expressed with *OTUD7A* harbor known ASD *de novo* mutations (left, red dots) and 30% of highly co-expressed genes are targets of FMR1 (right, red dots).

(G) DIV14 WT mouse cortical neurons co-expressing Venus and FLAG-*OTUD7A* WT and co-stained for FLAG and PSD95. *OTUD7A* is co-localized with PSD95 in dendrites and dendritic spines. Arrows indicate co-localized puncta located in dendritic spines (scale bars 20 μ m, top; 5 μ m bottom).

(H) Quantification of FLAG-*OTUD7A* and PSD95 puncta co-localization showed no changes between *OTUD7A* WT and *OTUD7A* p.Asn492_Lys494del overexpression (*OTUD7A* WT, n=18 neurons; *OTUD7A* p.Asn492_Lys494del, n=15 neurons, 2 cultures, Student's t test, $t(31) = 0.7813$). Error bars represent SEM.

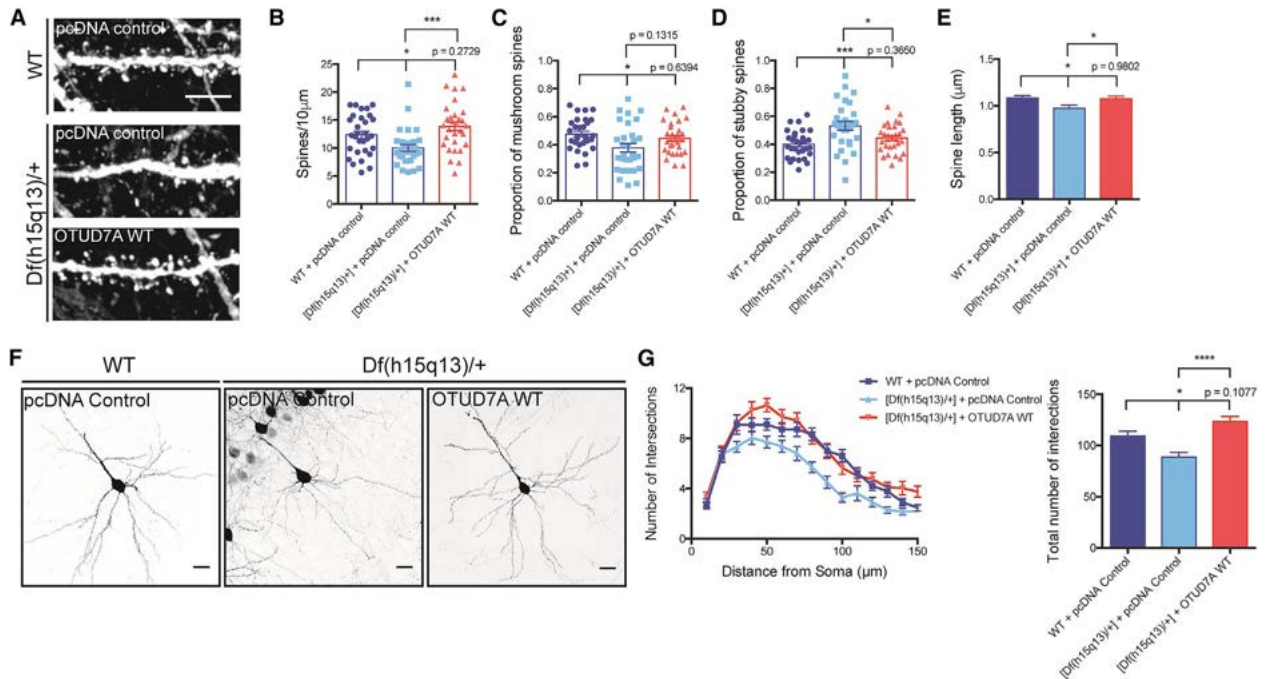


Figure 4. Reduced Expression of *OTUD7A* Contributes to Spine and Dendrite Defects in *Df(h15q13)/+* Mice

(A) Representative images of Venus-expressing dendritic spines from P22 WT or *Df(h15q13)/+* neurons co-expressing Venus and pcDNA control or FLAG-*OTUD7A* WT (scale bar = 5 μ m).

(B) Expression of *OTUD7A* WT rescues dendrite spine density defects in *Df(h15q13)/+* cortical neurons. WT + pcDNA control, n = 30 dendrite segments; [*Df(h15q13)/+*] + pcDNA, n = 30 dendrite segments; [*Df(h15q13)/+*] + *OTUD7A* WT, n = 30 dendrite segments; 3 cultures, one-way ANOVA followed by Tukey's post hoc test, *p < 0.05, ***p < 0.001, F(2, 87) = 8.049.

(C and D) *Df(h15q13)/+* neurons show a decrease in mushroom spines and an increase of stubby spines compared to WT neurons. Expression of *OTUD7A* WT in *Df(h15q13)/+* neurons decreases the proportion of stubby spines compared to *Df(h15q13)/+* neurons. WT + pcDNA control, n = 30 dendrite segments; [*Df(h15q13)/+*] + pcDNA control, n = 30 dendrite segments; [*Df(h15q13)/+*] + *OTUD7A* WT, n = 30 dendrite segments; 3 cultures, one-way ANOVA followed by Tukey's post hoc test, *p < 0.05, ***p < 0.001, F(2, 87) = 4.249, F(2, 87) = 8.636.

(E) *Df(h15q13)/+* neurons showed a decrease in spine length compared to WT neurons, and expression of *OTUD7A* WT in *Df(h15q13)/+* neurons increased spine length. WT + pcDNA control, n = 586 spines; [*Df(h15q13)/+*] + pcDNA control, n = 475 spines; [*Df(h15q13)/+*] + *OTUD7A* WT, n = 664 spines; 3 cultures, one-way ANOVA followed by Tukey's post hoc test, *p < 0.05, ***p < 0.001, F(2, 1722) = 3.956.

(F) Representative images of littermate P22 WT and *Df(h15q13)/+* neurons expressing Venus and pcDNA control or *OTUD7A* WT (scale bar = 50 μ m).

(G) Expression of *OTUD7A* WT rescues dendrite growth defects (number and total number of intersections) in *Df(h15q13)/+* cortical neurons. WT + pcDNA control, n = 28 neurons, [*Df(h15q13)/+*] + pcDNA control, n = 24; [*Df(h15q13)/+*] + *OTUD7A* WT, n = 28 neurons; 3 cultures, one-way ANOVA followed by Tukey's post hoc test, *p < 0.05, ****p < 0.0001, F(2, 61) = 13.53. Error bars represent SEM.

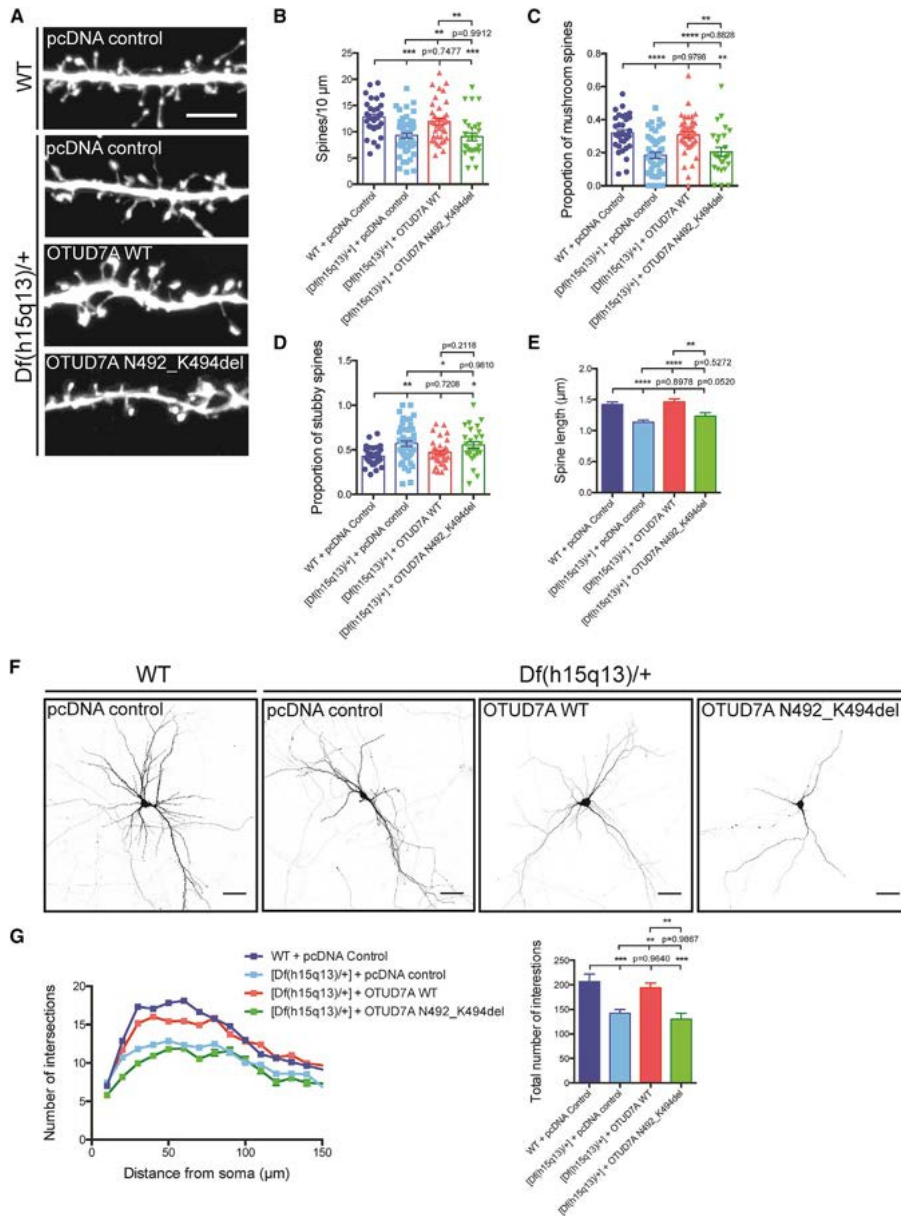


Figure 5. An Autism Spectrum Disorder-Linked *De Novo* Mutation in *OTUD7A* Disrupts Dendritic Spine Development and Neuronal Morphology

(A) Dendritic spines from DIV14 WT and *Df(h15q13)/+* cultured cortical neurons co-expressing Venus, and pcDNA control, FLAG-*OTUD7A* WT, or FLAG-*OTUD7A* p.As492_Lys494del (scale bar = 5 μ m).

(B) In *Df(h15q13)/+* neurons, expression of *OTUD7A* p.As492_Lys494del does not rescue the reduction of dendritic spine density. WT + pcDNA, n = 32 dendritic segments,

18 neurons; pcDNA control, n = 48 dendritic segments, 30 neurons; *OTUD7A* WT, n = 38 dendritic segments, 21 neurons; *OTUD7A* p.Asn492_Lys494del, n = 28 dendritic segments, 19 neurons, 5 cultures, one-way ANOVA followed by Tukey's post hoc test, **p < 0.01, ***p < 0.001, F(3, 142) = 9.422.

(C) Expression of *OTUD7A* p.Asn492_Lys494del does not increase the reduced proportion of mushroom spines in *Df(h15q13)/+* neurons. n = same as (B), one-way ANOVA followed by Tukey's post hoc test, **p < 0.01, ****p < 0.0001, F(3, 141) = 11.99.

(D) Expression of *OTUD7A* p.Asn492_Lys494del does not significantly decrease the increased proportion of stubby spines in *Df(h15q13)/+* neurons. n = same as (B), one-way ANOVA followed by Tukey's post hoc test, *p < 0.05, **p < 0.01, F(3, 141) = 5.751.

(E) Expression of *OTUD7A* p.Asn492_Lys494del is unable to increase the reduction in spine length in *Df(h15q13)/+* neurons. WT + pcDNA, n = 653 spines; [*Df(h15q13)/+*] + pcDNA control, n = 770 spines; [*Df(h15q13)/+*] + *OTUD7A* WT, n = 712 spines; [*Df(h15q13)/+*] + *OTUD7A* p.Asn492_Lys393del, n = 365 spines, 5 cultures, one-way ANOVA followed by Tukey's post hoc test, **p < 0.01, ****p < 0.0001, F(3, 2496) = 13.20.

(F) DIV14 WT and *Df(h15q13)/+* cortical neurons expressing Venus and pcDNA control, FLAG-*OTUD7A* WT, or FLAG-*OTUD7A* p.Asn492_Lys494del (scale bar = 50 μ m).

(G) In *Df(h15q13)/+* neurons, expression of *OTUD7A* p.Asn492_Lys494del does not rescue the reduction of dendrite growth. WT + pcDNA, n = 31 neurons; pcDNA control, n = 23 neurons; *OTUD7A* WT, n = 26 neurons; *OTUD7A* p.Asn492_Lys393del, n = 15 neurons, 5 cultures, one-way ANOVA followed by Tukey's post hoc test, **p < 0.01, ***p < 0.001, F(3, 133) = 9.613. Error bars represent SEM.

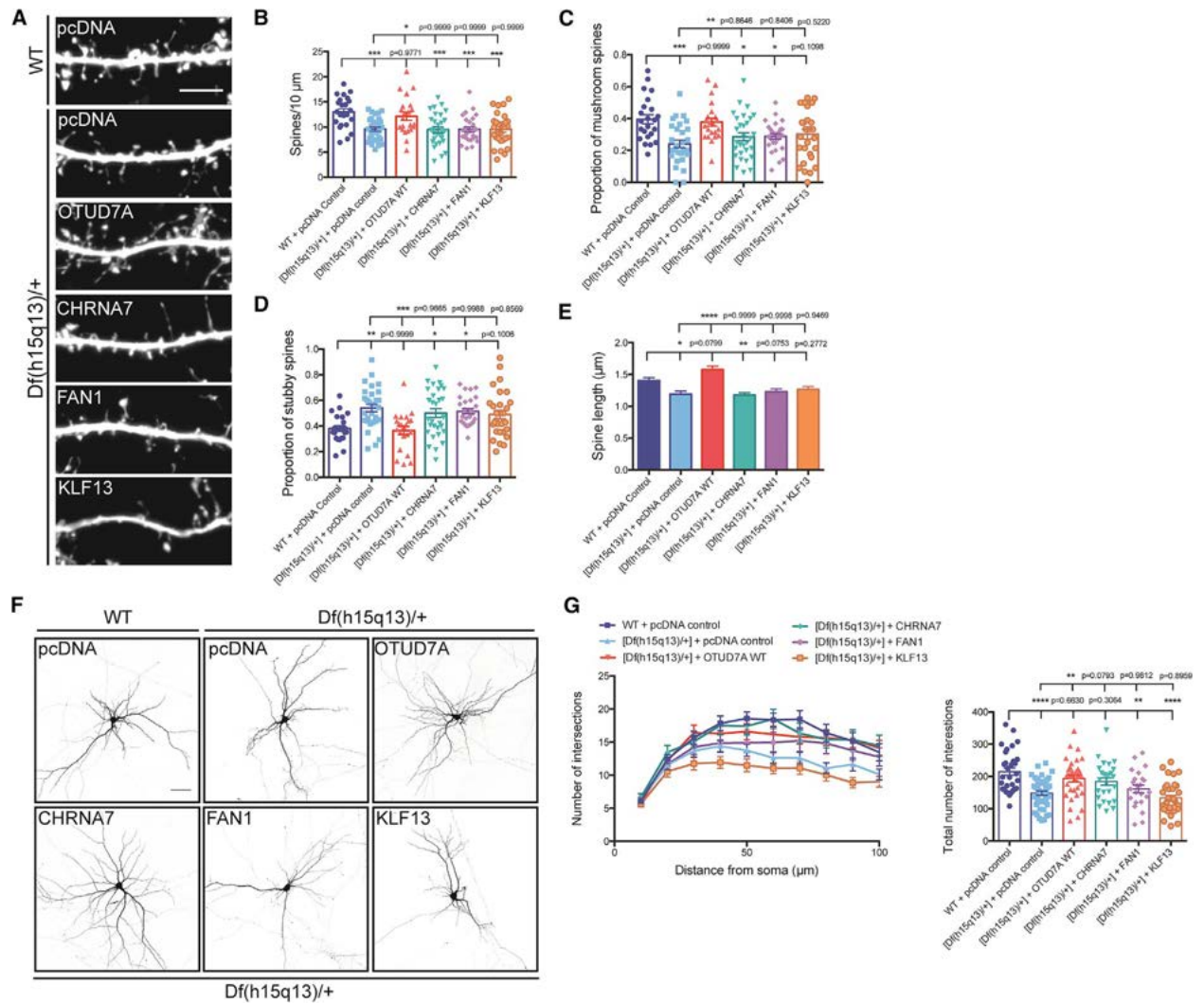


Figure 6. *OTUD7A* Is the Predominant Gene in the 15q13.3 Microdeletion Regulating Dendritic Spine Development

(A) Dendritic spines from DIV14 WT and *Df(h15q13)/+* cortical neurons co-expressing Venus and the indicated construct (scale bar 5 μ m).

(B–E) Expression of *CHRNA7*, *FAN1*, or *KLF13* in *Df(h15q13)/+* neurons did not rescue the defects in certain phenotypes.

(B) Dendritic spine density. WT + pcDNA control, n = 23 dendritic segments; [*Df(h15q13)/+*] + pcDNA control, n = 24 dendritic segments; [*Df(h15q13)/+*] + *OTUD7A* WT, n = 22 dendritic segments; [*Df(h15q13)/+*] + *CHRNA7*, n = 30 dendritic segments; [*Df(h15q13)/+*] + *FAN1*, n = 24 dendritic spines; [*Df(h15q13)/+*] + *KLF13*, n = 24 dendritic spines.

= 30 dendritic segments; 3 cultures, one-way ANOVA followed by Tukey's post hoc test, * $p < 0.05$, ** $p < 0.01$, *** $p < 0.001$, $F(5, 157) = 6.907$.

(C and D) Proportion of mushroom spines (C) and the proportion of stubby spines (D). WT + pcDNA control, $n = 23$ dendritic segments; [*Df(h15q13)/+*] + pcDNA control, $n = 24$ dendritic segments; [*Df(h15q13)/+*] + OTUD7A WT, $n = 22$ dendritic segments; [*Df(h15q13)/+*] + *CHRNA7*, $n = 30$ dendritic segments; [*Df(h15q13)/+*] + *FANI*, $n = 24$ dendritic spines; [*Df(h15q13)/+*] + *KLF13*, $n = 30$ dendritic segments; 3 cultures, one-way ANOVA followed by Tukey's post hoc test, * $p < 0.05$, ** $p < 0.01$, $F(5, 156) = 5.045$, $F(5, 157) = 5.666$.

(E) Spine length. WT + pcDNA control, $n = 484$ spines; [*Df(h15q13)/+*] + pcDNA control, $n = 379$ spines; [*Df(h15q13)/+*] + OTUD7A WT, $n = 444$ spines; [*Df(h15q13)/+*] + *CHRNA7*, $n = 454$ spines; [*Df(h15q13)/+*] + *FANI*, $n = 374$ spines; [*Df(h15q13)/+*] + *KLF13*, $n = 457$ spines; 3 cultures, one-way ANOVA followed by Tukey's post hoc test, * $p < 0.05$, ** $p < 0.01$, **** $p < 0.0001$, $F(5, 2728) = 10.64$.

(F) DIV14 WT and *Df(h15q13)/+* cortical neurons co-expressing Venus and the indicated construct (scale bar = 50 μm).

(G) Expression of OTUD7A WT or *CHRNA7* in *Df(h15q13)/+* cortical neurons rescues dendritic arborization defects, whereas *FANI* and *KLF13* did not. WT + pcDNA, $n = 30$ neurons, [*Df(h15q13)/+*] + pcDNA control, $n = 40$ neurons; [*Df(h15q13)/+*] + OTUD7A WT, $n = 35$ neurons; [*Df(h15q13)/+*] + *CHRNA7*, $n = 26$ neurons; [*Df(h15q13)/+*] + *FANI*, $n = 23$ neurons; [*Df(h15q13)/+*] + *KLF13*, $n = 33$ neurons, 3 cultures, one-way ANOVA followed by Tukey's post hoc test, * $p < 0.05$, $F(5, 181) = 6.873$. Error bars represent SEM.

Table 1. Individual ASD-Affected Case Subjects with De Novo Mutations Found near or within <i>OTUD7A</i>						
ASD Cases	Chromosome	Nucleotide-Level Change-HGV5 Format	Protein-Level Change	Seq-Type Variants	Gene/Nearby Genes	
Case 1	15	XM_005254506.1; c.936-17A>G	-	intronic	<i>MTMR10</i>	
Case 2	15	NM_001252024.1; c.2382C>G	p.Phe794Leu	missense	<i>TRPM1</i>	
Case 3	15	NM_130901.2; c.1474_1482del	p.Asn492_Lys494del	exonic-indel	<i>OTUD7A</i>	
Case 4	15	NC_000015.9; g.31557488A>C	-	intergenic	<i>KLF13</i>	
Case 5	15	NC_000015.9; g.32309599_32309610del	-	intergenic-indel	<i>OTUD7A, CHRNA7</i>	
Case 6	15	NC_000015.9; g.32309599_32309610del	-	intergenic-indel	<i>OTUD7A, CHRNA7</i>	
Case 7	15	XM_005254201.1; c.-223+11014A>G	-	intronic	<i>OTUD7A</i>	
Case 8	15	NM_130901.1; c.1150+935del	-	intronic-indel	<i>OTUD7A</i>	

Table 1. Individual ASD-Affected Case subjects with De Novo Mutations Found near or within *OTUD7A*

3.6 REFERENCES

1. Uddin, M., Pellecchia, G., Thiruvahindrapuram, B., D'Abate, L., Merico, D., Chan, A., Zarrei, M., Tammimies, K., Walker, S., Gazzellone, M.J., et al. (2016). Indexing effects of copy number variation on genes involved in developmental delay. *Sci. Rep.* 6, 28663.
2. Liu, H., Abecasis, G.R., Heath, S.C., Knowles, A., Demars, S., Chen, Y.J., Roos, J.L., Rapoport, J.L., Gogos, J.A., and Karayiorgou, M. (2002). Genetic variation in the 22q11 locus and susceptibility to schizophrenia. *Proc. Natl. Acad. Sci. USA* 99, 16859–16864.
3. Mukai, J., Dhillia, A., Drew, L.J., Stark, K.L., Cao, L., MacDermott, A.B., Karayiorgou, M., and Gogos, J.A. (2008). Palmitoylation-dependent neurodevelopmental deficits in a mouse model of 22q11 microdeletion. *Nat. Neurosci.* 11, 1302–1310.
4. Portmann, T., Yang, M., Mao, R., Panagiotakos, G., Ellegood, J., Dolen, G., Bader, P.L., Grueter, B.A., Goold, C., Fisher, E., et al. (2014). Behavioral abnormalities and circuit defects in the basal ganglia of a mouse model of 16p11.2 deletion syndrome. *Cell Rep.* 7, 1077–1092.
5. Blizinsky, K.D., Diaz-Castro, B., Forrest, M.P., Schürmann, B., Bach, A.P., Martin-de-Saavedra, M.D., Wang, L., Csernansky, J.G., Duan, J., and Penzes, P. (2016). Reversal of dendritic phenotypes in 16p11.2 microduplication mouse model neurons by pharmacological targeting of a network hub. *Proc. Natl. Acad. Sci. USA* 113, 8520–8525.
6. Migliavacca, E., Golzio, C., Männik, K., Blumenthal, I., Oh, E.C., Harewood, L., Kosmicki, J.A., Loviglio, M.N., Giannuzzi, G., Hippolyte, L., et al.;

- 16p11.2 European Consortium (2015). A potential contributory role for ciliary dysfunction in the 16p11.2 600 kb BP4-BP5 pathology. *Am. J. Hum. Genet.* 96, 784–796.
7. Pucilowska, J., Vithayathil, J., Tavares, E.J., Kelly, C., Karlo, J.C., and Landreth, G.E. (2015). The 16p11.2 deletion mouse model of autism exhibits altered cortical progenitor proliferation and brain cytoarchitecture linked to the ERK MAPK pathway. *J. Neurosci.* 35, 3190–3200.
8. Blumenthal, I., Ragavendran, A., Erdin, S., Klei, L., Sugathan, A., Guide, J.R., Manavalan, P., Zhou, J.Q., Wheeler, V.C., Levin, J.Z., et al. (2014). Transcriptional consequences of 16p11.2 deletion and duplication in mouse cortex and multiplex autism families. *Am. J. Hum. Genet.* 94, 870–883.
9. Golzio, C., Willer, J., Talkowski, M.E., Oh, E.C., Taniguchi, Y., Jacquemont, S., Reymond, A., Sun, M., Sawa, A., Gusella, J.F., et al. (2012). KCTD13 is a major driver of mirrored neuroanatomical phenotypes of the 16p11.2 copy number variant. *Nature* 485, 363–367.
10. Stark, K.L., Xu, B., Bagchi, A., Lai, W.S., Liu, H., Hsu, R., Wan, X., Pavlidis, P., Mills, A.A., Karayiorgou, M., and Gogos, J.A. (2008). Altered brain microRNA biogenesis contributes to phenotypic deficits in a 22q11-deletion mouse model. *Nat. Genet.* 40, 751–760.
11. Fénelon, K., Mukai, J., Xu, B., Hsu, P.K., Drew, L.J., Karayiorgou, M., Fischbach, G.D., Macdermott, A.B., and Gogos, J.A. (2011). Deficiency of *Dgcr8*, a gene disrupted by the 22q11.2 microdeletion, results in altered short-term plasticity in the prefrontal cortex. *Proc. Natl. Acad. Sci. USA* 108, 4447–4452.

12. Xu, B., Hsu, P.K., Stark, K.L., Karayiorgou, M., and Gogos, J.A. (2013). Derepression of a neuronal inhibitor due to miRNA dysregulation in a schizophrenia-related microdeletion. *Cell* 152, 262–275.
13. Sigurdsson, T., Stark, K.L., Karayiorgou, M., Gogos, J.A., and Gordon, J.A. (2010). Impaired hippocampal-prefrontal synchrony in a genetic mouse model of schizophrenia. *Nature* 464, 763–767.
14. Tian, D., Stoppel, L.J., Heynen, A.J., Lindemann, L., Jaeschke, G., Mills, A.A., and Bear, M.F. (2015). Contribution of mGluR5 to pathophysiology in a mouse model of human chromosome 16p11.2 microdeletion. *Nat. Neurosci.* 18, 182–184.
15. Tamura, M., Mukai, J., Gordon, J.A., and Gogos, J.A. (2016). Developmental inhibition of Gsk3 rescues behavioral and neurophysiological deficits in a mouse model of schizophrenia predisposition. *Neuron* 89, 1100–1109.
16. Sharp, A.J., Mefford, H.C., Li, K., Baker, C., Skinner, C., Stevenson, R.E., Schroer, R.J., Novara, F., De Gregori, M., Ciccone, R., et al. (2008). A recurrent 15q13.3 microdeletion syndrome associated with mental retardation and seizures. *Nat. Genet.* 40, 322–328.
17. Helbig, I., Mefford, H.C., Sharp, A.J., Guipponi, M., Fichera, M., Franke, A., Muhle, H., de Kovel, C., Baker, C., von Spiczak, S., et al. (2009). 15q13.3 microdeletions increase risk of idiopathic generalized epilepsy. *Nat. Genet.* 41, 160–162.
18. Antonacci, F., Dennis, M.Y., Huddleston, J., Sudmant, P.H., Steinberg, K.M., Rosenfeld, J.A., Miroballo, M., Graves, T.A., Vives, L., Malig, M., et al. (2014).

Palindromic GOLGA8 core duplicons promote chromosome 15q13.3 microdeletion and evolutionary instability. *Nat. Genet.* 46, 1293–1302.

19. Ziats, M.N., Goin-Kochel, R.P., Berry, L.N., Ali, M., Ge, J., Guffey, D., Rosenfeld, J.A., Bader, P., Gambello, M.J., Wolf, V., et al. (2016). The complex behavioral phenotype of 15q13.3 microdeletion syndrome. *Genet. Med.* 18, 1111–1118.
20. Shinawi, M., Schaaf, C.P., Bhatt, S.S., Xia, Z., Patel, A., Cheung, S.W., Lanpher, B., Nagl, S., Herding, H.S., Nevinny-Stickel, C., et al. (2009). A small recurrent deletion within 15q13.3 is associated with a range of neurodevelopmental phenotypes. *Nat. Genet.* 41, 1269–1271.
21. Stefansson, H., Rujescu, D., Cichon, S., Pietiläinen, O.P., Ingason, A., Steinberg, S., Fossdal, R., Sigurdsson, E., Sigmundsson, T., Buizer-Voskamp, J.E., et al.; GROUP (2008). Large recurrent microdeletions associated with schizophrenia. *Nature* 455, 232–236.
22. International Schizophrenia Consortium (2008). Rare chromosomal deletions and duplications increase risk of schizophrenia. *Nature* 455, 237–241.
23. Pagnamenta, A.T., Wing, K., Sadighi Akha, E., Knight, S.J., Bölte, S., Schmötzer, G., Duketis, E., Poustka, F., Klauck, S.M., Poustka, A., et al.; International Molecular Genetic Study of Autism Consortium (2009). A 15q13.3 microdeletion segregating with autism. *Eur. J. Hum. Genet.* 17, 687–692.
24. Lowther, C., Costain, G., Stavropoulos, D.J., Melvin, R., Silversides, C.K., Andrade, D.M., So, J., Faghfoury, H., Lionel, A.C., Marshall, C.R., et al. (2015).

Delineating the 15q13.3 microdeletion phenotype: a case series and comprehensive review of the literature. *Genet. Med.* 17, 149–157.

25. Fejgin, K., Nielsen, J., Birkenow, M.R., Bastlund, J.F., Nielsen, V., Lauridsen, J.B., Stefansson, H., Steinberg, S., Sorensen, H.B., Mortensen, T.E., et al. (2014). A mouse model that recapitulates cardinal features of the 15q13.3 microdeletion syndrome including schizophrenia- and epilepsy-related alterations. *Biol. Psychiatry* 76, 128–137.
26. Kogan, J.H., Gross, A.K., Featherstone, R.E., Shin, R., Chen, Q., Heusner, C.L., Adachi, M., Lin, A., Walton, N.M., Miyoshi, S., et al. (2015). Mouse model of chromosome 15q13.3 microdeletion syndrome demonstrates features related to autism spectrum disorder. *J. Neurosci.* 35, 16282–16294.
27. Masurel-Paulet, A., Drumare, I., Holder, M., Cuisset, J.M., Vallée, L., Defoort, S., Bourgois, B., Pernes, P., Cuvellier, J.C., Huet, F., et al. (2014). Further delineation of eye manifestations in homozygous 15q13.3 microdeletions including TRPM1: a differential diagnosis of ceroid lipofuscinosis. *Am. J. Med. Genet. A.* 164A, 1537–1544.
28. Spielmann, M., Reichelt, G., Hertzberg, C., Trimborn, M., Mundlos, S., Horn, D., and Klopocki, E. (2011). Homozygous deletion of chromosome 15q13.3 including CHRNA7 causes severe mental retardation, seizures, muscular hypotonia, and the loss of KLF13 and TRPM1 potentially cause macrocytosis and congenital retinal dysfunction in siblings. *Eur. J. Med. Genet.* 54, e441–e445.
29. Forsingdal, A., Fejgin, K., Nielsen, V., Werge, T., and Nielsen, J. (2016). 15q13.3 homozygous knockout mouse model display epilepsy-, autism- and schizophrenia-related phenotypes. *Transl. Psychiatry* 6, e860.

30. Nilsson, S.R., Celada, P., Fejgin, K., Thelin, J., Nielsen, J., Santana, N., Heath, C.J., Larsen, P.H., Nielsen, V., Kent, B.A., et al. (2016). A mouse model of the 15q13.3 microdeletion syndrome shows prefrontal neurophysiological dysfunctions and attentional impairment. *Psychopharmacology (Berl.)* 233, 2151–2163.
31. Gass, N., Weber-Fahr, W., Sartorius, A., Becker, R., Didriksen, M., Stensbøl, T.B., Bastlund, J.F., Meyer-Lindenberg, A., and Schwarz, A.J. (2016). An acetylcholine alpha7 positive allosteric modulator rescues a schizophrenia-associated brain endophenotype in the 15q13.3 microdeletion, encompassing CHRNA7. *Eur. Neuropsychopharmacol.* 26, 1150– 1160.
32. Freedman, R. (2014). $\alpha 7$ -nicotinic acetylcholine receptor agonists for cognitive enhancement in schizophrenia. *Annu. Rev. Med.* 65, 245–261.
33. Young, J.W., Meves, J.M., Tarantino, I.S., Caldwell, S., and Geyer, M.A. (2011). Delayed procedural learning in $\alpha 7$ -nicotinic acetylcholine receptor knockout mice. *Genes Brain Behav.* 10, 720–733.
34. Azzopardi, E., Typlt, M., Jenkins, B., and Schmid, S. (2013). Sensorimotor gating and spatial learning in $\alpha 7$ -nicotinic receptor knockout mice. *Genes Brain Behav.* 12, 414–423.
35. Lin, H., Hsu, F.C., Baumann, B.H., Coulter, D.A., and Lynch, D.R. (2014). Cortical synaptic NMDA receptor deficits in $\alpha 7$ nicotinic acetylcholine receptor gene deletion models: implications for neuropsychiatric diseases. *Neurobiol. Dis.* 63, 129–140.
36. Orr-Urtreger, A., Göldner, F.M., Saeki, M., Lorenzo, I., Goldberg, L., De Biasi, M., Dani, J.A., Patrick, J.W., and Beaudet, A.L. (1997). Mice deficient in the

alpha7 neuronal nicotinic acetylcholine receptor lack alpha-bungarotoxin binding sites and hippocampal fast nicotinic currents. *J. Neurosci.* 17, 9165–9171.

37. Yin, J., Wu, C., Chao, E.S., Soriano, S., Wang, L., Wang, W., Cummock, S.E., Tao, H., Pang, K., Liu, Z., et al. (2018). Otud7a knockout mice recapitulate many neurological features of 15q13.3 microdeletion syndrome. *Am. J. Hum. Genet.* 102, this issue, 296–308.
38. Redon, R., Ishikawa, S., Fitch, K.R., Feuk, L., Perry, G.H., Andrews, T.D., Fiegler, H., Shapero, M.H., Carson, A.R., Chen, W., et al. (2006). Global variation in copy number in the human genome. *Nature* 444, 444–454.
39. Locke, D.P., Sharp, A.J., McCarroll, S.A., McGrath, S.D., Newman, T.L., Cheng, Z., Schwartz, S., Albertson, D.G., Pinkel, D., Altshuler, D.M., and Eichler, E.E. (2006). Linkage disequilibrium and heritability of copy-number polymorphisms within duplicated regions of the human genome. *Am. J. Hum. Genet.* 79, 275–290.
40. Ionita-Laza, I., Xu, B., Makarov, V., Buxbaum, J.D., Roos, J.L., Gogos, J.A., and Karayiorgou, M. (2014). Scan statistic-based analysis of exome sequencing data identifies FAN1 at 15q13.3 as a susceptibility gene for schizophrenia and autism. *Proc. Natl. Acad. Sci. USA* 111, 343–348.
41. Uddin, M., Tammimies, K., Pellicchia, G., Alipanahi, B., Hu, P., Wang, Z., Pinto, D., Lau, L., Nalpathamkalam, T., Marshall, C.R., et al. (2014). Brain-expressed exons under purifying selection are enriched for de novo mutations in autism spectrum disorder. *Nat. Genet.* 46, 742–747.

42. Trapnell, C., Pachter, L., and Salzberg, S.L. (2009). TopHat: discovering splice junctions with RNA-Seq. *Bioinformatics* 25, 1105–1111.
43. Robinson, M.D., McCarthy, D.J., and Smyth, G.K. (2010). edgeR: a Bioconductor package for differential expression analysis of digital gene expression data. *Bioinformatics* 26, 139–140.
44. Coe, B.P., Witherspoon, K., Rosenfeld, J.A., van Bon, B.W., Vulto-van Silfhout, A.T., Bosco, P., Friend, K.L., Baker, C., Buono, S., Vissers, L.E., et al. (2014). Refining analyses of copy number variation identifies specific genes associated with developmental delay. *Nat. Genet.* 46, 1063–1071.
45. Bierut, L.J., Agrawal, A., Bucholz, K.K., Doheny, K.F., Laurie, C., Pugh, E., Fisher, S., Fox, L., Howells, W., Bertelsen, S., et al.; Gene, Environment Association Studies Consortium (2010). A genome-wide association study of alcohol dependence. *Proc. Natl. Acad. Sci. USA* 107, 5082–5087.
46. Coviello, A.D., Haring, R., Wellons, M., Vaidya, D., Lehtimäki, T., Keildson, S., Lunetta, K.L., He, C., Fornage, M., Lagou, V., et al. (2012). A genome-wide association meta-analysis of circulating sex hormone-binding globulin reveals multiple Loci implicated in sex steroid hormone regulation. *PLoS Genet.* 8, e1002805.
47. Bierut, L.J., Madden, P.A., Breslau, N., Johnson, E.O., Hatsukami, D., Pomerleau, O.F., Swan, G.E., Rutter, J., Bertelsen, S., Fox, L., et al. (2007). Novel genes identified in a high-density genome wide association study for nicotine dependence. *Hum. Mol. Genet.* 16, 24–35.

48. Verhoeven, V.J., Hysi, P.G., Wojciechowski, R., Fan, Q., Guggenheim, J.A., Höhn, R., MacGregor, S., Hewitt, A.W., Nag, A., Cheng, C.Y., et al.; Consortium for Refractive Error and Myopia (CREAM); Diabetes Control and Complications Trial/ Epidemiology of Diabetes Interventions and Complications (DCCT/EDIC) Research Group; Wellcome Trust Case Control Consortium 2 (WTCCC2); and Fuchs' Genetics Multi-Center Study Group (2013). Genome-wide meta-analyses of multiancestry cohorts identify multiple new susceptibility loci for refractive error and myopia. *Nat. Genet.* 45, 314–318.
49. Stewart, A.F., Dandona, S., Chen, L., Assogba, O., Belanger, M., Ewart, G., LaRose, R., Doelle, H., Williams, K., Wells, G.A., et al. (2009). Kinesin family member 6 variant Trp719Arg does not associate with angiographically defined coronary artery disease in the Ottawa Heart Genomics Study. *J. Am. Coll. Cardiol.* 53, 1471–1472.
50. Krawczak, M., Nikolaus, S., von Eberstein, H., Croucher, P.J., El Mokhtari, N.E., and Schreiber, S. (2006). PopGen: population-based recruitment of patients and controls for the analysis of complex genotype-phenotype relationships. *Community Genet.* 9, 55–61.
51. De Rubeis, S., He, X., Goldberg, A.P., Poultney, C.S., Samocha, K., Cicek, A.E., Kou, Y., Liu, L., Fromer, M., Walker, S., et al.; DDD Study; Homozygosity Mapping Collaborative for Autism; and UK10K Consortium (2014). Synaptic, transcriptional and chromatin genes disrupted in autism. *Nature* 515, 209–215.
52. Iossifov, I., O’Roak, B.J., Sanders, S.J., Ronemus, M., Krumm, N., Levy, D., Stessman, H.A., Witherspoon, K.T., Vives, L., Patterson, K.E., et al. (2014). The

contribution of de novo coding mutations to autism spectrum disorder. *Nature* 515, 216–221.

53. Yuen, R.K., Thiruvahindrapuram, B., Merico, D., Walker, S., Tammimies, K., Hoang, N., Chrysler, C., Nalpathamkalam, T., Pellecchia, G., Liu, Y., et al. (2015).

Whole-genome sequencing of quartet families with autism spectrum disorder. *Nat. Med.* 21, 185–191.

54. Genome of the Netherlands Consortium (2014). Whole- genome sequence variation, population structure and demographic history of the Dutch population. *Nat. Genet.* 46, 818–825.

55. Bourgeron, T. (2015). From the genetic architecture to synaptic plasticity in autism spectrum disorder. *Nat. Rev. Neurosci.* 16, 551–563.

56. Lee, E., Lee, J., and Kim, E. (2017). Excitation/inhibition imbalance in animal models of autism spectrum disorders. *Biol. Psychiatry* 81, 838–847.

57. de la Torre-Ubieta, L., Won, H., Stein, J.L., and Geschwind, D.H. (2016). Advancing the understanding of autism disease mechanisms through genetics. *Nat. Med.* 22, 345–361.

58. Chen, J.A., Peñagarikano, O., Belgard, T.G., Swarup, V., and Geschwind, D.H. (2015). The emerging picture of autism spectrum disorder: genetics and pathology. *Annu. Rev. Pathol.* 10, 111–144.

59. Kutzing, M.K., Langhammer, C.G., Luo, V., Lakdawala, H., and Firestein, B.L. (2010). Automated Sholl analysis of digitized neuronal morphology at multiple scales. *J. Vis. Exp.* 45, 2354.

60. Kwan, V., Meka, D.P., White, S.H., Hung, C.L., Holzapfel, N.T., Walker, S., Murtaza, N., Unda, B.K., Schwanke, B., Yuen, R.K.C., et al. (2016). DIXDC1 phosphorylation and control of dendritic morphology are impaired by rare genetic variants. *Cell Rep.* 17, 1892–1904.
61. Cooper, G.M., Coe, B.P., Girirajan, S., Rosenfeld, J.A., Vu, T.H., Baker, C., Williams, C., Stalker, H., Hamid, R., Hannig, V., et al. (2011). A copy number variation morbidity map of developmental delay. *Nat. Genet.* 43, 838–846.
62. Sajan, S.A., Jhangiani, S.N., Muzny, D.M., Gibbs, R.A., Lupski, J.R., Glaze, D.G., Kaufmann, W.E., Skinner, S.A., Annesse, F., Friez, M.J., et al. (2017). Enrichment of mutations in chromatin regulators in people with Rett syndrome lacking mutations in MECP2. *Genet. Med.* 19, 13–19.
63. O’Roak, B.J., Stessman, H.A., Boyle, E.A., Witherspoon, K.T., Martin, B., Lee, C., Vives, L., Baker, C., Hiatt, J.B., Nickerson, D.A., et al. (2014). Recurrent de novo mutations implicate novel genes underlying simplex autism risk. *Nat. Commun.* 5, 5595.
64. Helsmoortel, C., Vulto-van Silfhout, A.T., Coe, B.P., Vandeweyer, G., Rooms, L., van den Ende, J., Schuurs-Hoeijmakers, J.H., Marcelis, C.L., Willemsen, M.H., Vissers, L.E., et al. (2014). A SWI/SNF-related autism syndrome caused by de novo mutations in ADNP. *Nat. Genet.* 46, 380–384.
65. O’Roak, B.J., Vives, L., Fu, W., Egertson, J.D., Stanaway, I.B., Phelps, I.G., Carvill, G., Kumar, A., Lee, C., Ankenman, K., et al. (2012). Multiplex targeted sequencing identifies recurrently mutated genes in autism spectrum disorders. *Science* 338, 1619–1622.

66. O’Roak, B.J., Vives, L., Girirajan, S., Karakoc, E., Krumm, N., Coe, B.P., Levy, R., Ko, A., Lee, C., Smith, J.D., et al. (2012). Sporadic autism exomes reveal a highly interconnected protein network of de novo mutations. *Nature* 485, 246–250.
67. Qi, C., Liu, S., Qin, R., Zhang, Y., Wang, G., Shang, Y., Wang, Y., and Liang, J. (2014). Coordinated regulation of dendrite arborization by epigenetic factors CDYL and EZH2. *J. Neurosci.* 34, 4494–4508.
68. Lek, M., Karczewski, K.J., Minikel, E.V., Samocha, K.E., Banks, E., Fennell, T., O’Donnell-Luria, A.H., Ware, J.S., Hill, A.J., Cummings, B.B., et al.; Exome Aggregation Consortium (2016). Analysis of protein-coding genetic variation in 60,706 humans. *Nature* 536, 285–291.
69. Kim, M.S., Pinto, S.M., Getnet, D., Nirujogi, R.S., Manda, S.S., Chaerkady, R., Madugundu, A.K., Kelkar, D.S., Isserlin, R., Jain, S., et al. (2014). A draft map of the human proteome. *Nature* 509, 575–581.
70. Langfelder, P., and Horvath, S. (2008). WGCNA: an R package for weighted correlation network analysis. *BMC Bioinformatics* 9, 559.
71. Yin, J., Chen, W., Yang, H., Xue, M., and Schaaf, C.P. (2017). *Chrna7* deficient mice manifest no consistent neuropsychiatric and behavioral phenotypes. *Sci. Rep.* 7, 39941.
72. Adams, C.E., Yonchek, J.C., Schulz, K.M., Graw, S.L., Stitzel, J., Teschke, P.U., and Stevens, K.E. (2012). Reduced *Chrna7* expression in mice is associated with decreases in hippocampal markers of inhibitory function: implications for neuropsychiatric diseases. *Neuroscience* 207, 274–282.

73. Fountain, M.D., Tao, H., Chen, C.A., Yin, J., and Schaaf, C.P. (2017). *Magel2* knockout mice manifest altered social phenotypes and a deficit in preference for social novelty. *Genes Brain Behav.* 16, 592–600.
74. Schaaf, C.P., Gonzalez-Garay, M.L., Xia, F., Potocki, L., Gripp, K.W., Zhang, B., Peters, B.A., McElwain, M.A., Drmanac, R., Beaudet, A.L., et al. (2013). Truncating mutations of *MAGEL2* cause Prader-Willi phenotypes and autism. *Nat. Genet.* 45, 1405–1408.
75. Adamo, A., Atashpaz, S., Germain, P.L., Zanella, M., D’Agostino, G., Albertin, V., Chenoweth, J., Micale, L., Fusco, C., Unger, C., et al. (2015). 7q11.23 dosage-dependent dysregulation in human pluripotent stem cells affects transcriptional programs in disease-relevant lineages. *Nat. Genet.* 47, 132–141.
76. Sakurai, T., Dorr, N.P., Takahashi, N., McInnes, L.A., Elder, G.A., and Buxbaum, J.D. (2011). Haploinsufficiency of *Gtf2i*, a gene deleted in Williams Syndrome, leads to increases in social interactions. *Autism Res.* 4, 28–39.
77. Chailangkarn, T., Trujillo, C.A., Freitas, B.C., Hrvoj-Mihic, B., Herai, R.H., Yu, D.X., Brown, T.T., Marchetto, M.C., Bardy, C., McHenry, L., et al. (2016). A human neurodevelopmental model for Williams syndrome. *Nature* 536, 338–343.
78. Merico, D., Zarrei, M., Costain, G., Ogura, L., Alipanahi, B., Gazzellone, M.J., Butcher, N.J., Thiruvahindrapuram, B., Nalpathamkalam, T., Chow, E.W., et al. (2015). Whole-genome sequencing suggests schizophrenia risk mechanisms in humans with 22q11.2 deletion syndrome. *G3 (Bethesda)* 5, 2453–2461.

79. Mevissen, T.E.T., Kulathu, Y., Mulder, M.P.C., Geurink, P.P., Maslen, S.L., Gersch, M., Elliott, P.R., Burke, J.E., van Tol, B.D.M., Akutsu, M., et al. (2016). Molecular basis of Lys11-polyubiquitin specificity in the deubiquitinase Cezanne. *Nature* 538, 402–405.
80. Mevissen, T.E., Hospenthal, M.K., Geurink, P.P., Elliott, P.R., Akutsu, M., Arnaudo, N., Ekkebus, R., Kulathu, Y., Wauer, T., El Oualid, F., et al. (2013). OTU deubiquitinases reveal mechanisms of linkage specificity and enable ubiquitin chain restriction analysis. *Cell* 154, 169–184.
81. Santiago-Sim, T., Burrage, L.C., Ebstein, F., Tokita, M.J., Miller, M., Bi, W., Braxton, A.A., Rosenfeld, J.A., Shahrour, M., Lehmann, A., et al.; EuroEPINOMICS RES Consortium Autosomal Recessive working group, S. Hande Caglayan (2017). Biallelic variants in OTUD6B cause an intellectual disability syndrome associated with seizures and dysmorphic features. *Am. J. Hum. Genet.* 100, 676–688.
82. Greer, P.L., Hanayama, R., Bloodgood, B.L., Mardinly, A.R., Lipton, D.M., Flavell, S.W., Kim, T.K., Griffith, E.C., Waldon, Z., Maehr, R., et al. (2010). The Angelman Syndrome protein Ube3A regulates synapse development by ubiquitinating arc. *Cell* 140, 704–716.
83. Kühnle, S., Mothes, B., Matentzoglou, K., and Scheffner, M. (2013). Role of the ubiquitin ligase E6AP/UBE3A in controlling levels of the synaptic protein Arc. *Proc. Natl. Acad. Sci. USA* 110, 8888–8893.
84. Ebrahimi-Fakhari, D., and Sahin, M. (2015). Autism and the synapse: emerging mechanisms and mechanism-based therapies. *Curr. Opin. Neurol.* 28, 91–102.

85. Yuen, R.K.C., Merico, D., Bookman, M., Howe, J.L., Thiruvahindrapuram, B., Patel, R.V., Whitney, J., Deflaux, N., Bingham, J., Wang, Z., et al. (2017). Whole genome sequencing resource identifies 18 new candidate genes for autism spectrum disorder. *Nat. Neurosci.* 20, 602–611.

Accession Numbers

Whole-genome datasets generated during and analyzed during the current study are available at the Autism Speaks MSSNG repository.⁸⁵ Microarray data has been submitted to dbGAP under accession number phs001154.v1.p1.

Web Resources

Allen Brain Atlas, <http://www.brain-map.org/> Autism Speaks MSSNG Project,

<https://www.mss.ng>

Database of Genomic Variants (DGV), <http://dgv.tcag.ca/dgv/app/home>

dbGaP, <http://www.ncbi.nlm.nih.gov/gap> GenBank,

<https://www.ncbi.nlm.nih.gov/genbank/>

Human ProteomeMap, <http://www.humanproteomemap.org/> OMIM,

<http://www.omim.org/>

3.7 SUPPLEMENTAL DATA

OTUD7A Regulates Neurodevelopmental Phenotypes in the 15q13.3 Microdeletion Syndrome

Mohammed Uddin, Brianna K. Unda, Vickie Kwan, Nicholas T. Holzapfel, Sean H. White, Leon Chalil, Marc Woodbury-Smith, Karen S. Ho, Erin Harward, Nadeem Murtaza, Biren Dave, Giovanna Pellecchia, Lia D'Abate, Thomas Nalpathamkalam, Sylvia Lamoureux, John Wei, Marsha Speevak, James Stavropoulos, Kristin J. Hope, Brad W. Doble, Jacob Nielsen, E. Robert Wassman, Stephen W. Scherer, and Karun K. Singh

Supplemental Data include six figures and four tables. Table S1, S2 and S4 can be found with this article online at <https://doi.org/10.1016/j.ajhg.2018.01.006>.

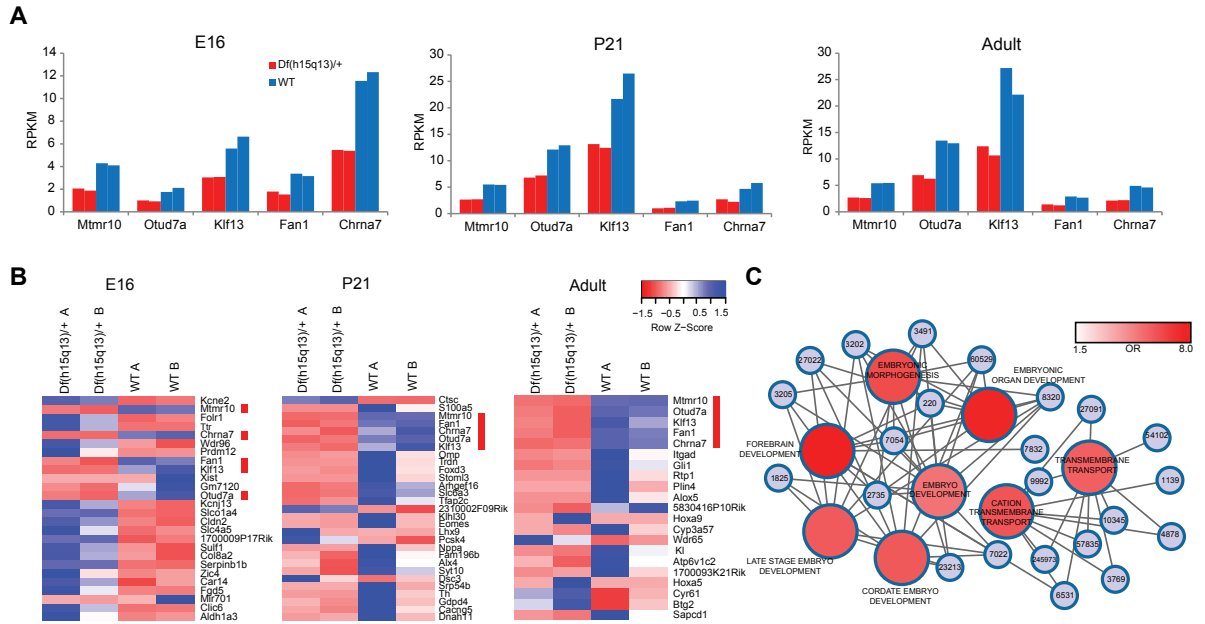


Figure S1 A 15q13.3 mouse model (*Df(h15q13)/+*) has defects in forebrain signaling pathways. (A) RNA sequencing analysis of cortical brain tissue from E16, P21, and adult WT and *Df(h15q13)/+* mice (n = 2 brains per condition). All 5 brain expressed genes within the deletion are downregulated by ~50%. **(B)** Differential expression analysis and **(C)** gene enrichment analysis revealed that forebrain development is the most significantly altered biological process across all ages.

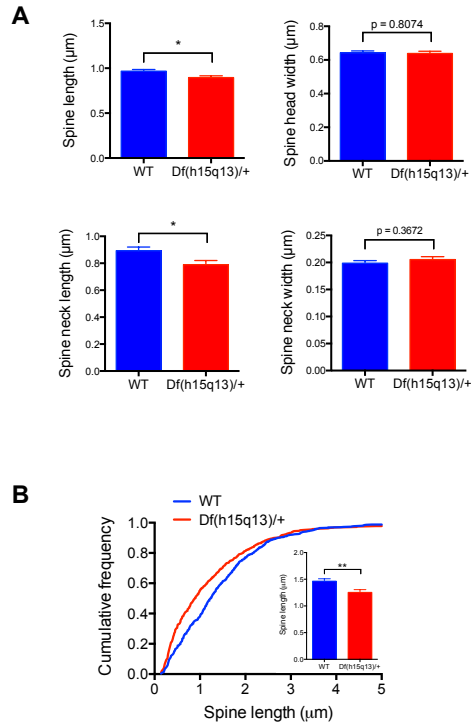


Figure S2 Df(h15q13)/+ mice have defects in dendritic spine development. (A)

Df(h15q13)/+ show a decrease in spine length (left), and neck length (right) (WT, n = 962 spines; Df(h15q13)/+, n = 775 spines, 4 mice per condition, student's t test, *p < 0.05, t(1735) = 2.566, t(544) = 0.2439, t(544) = 2.469, t(544) = 0.9025). 15q13.3 mouse model (Df(h15q13)/+) has defects in forebrain signaling pathways. **(B)** Analysis of dendritic spine length in WT and Df(h15q13)/+ neurons. Df(h15q13) cultured cortical neurons show a decrease in spine length. (WT, n = 645 spines; Df(h15q13)/+, n = 543 spines, 3 cultures, student's t test, **p < 0.01, t(1186) = 3.109). Error bars represent s.e.m.

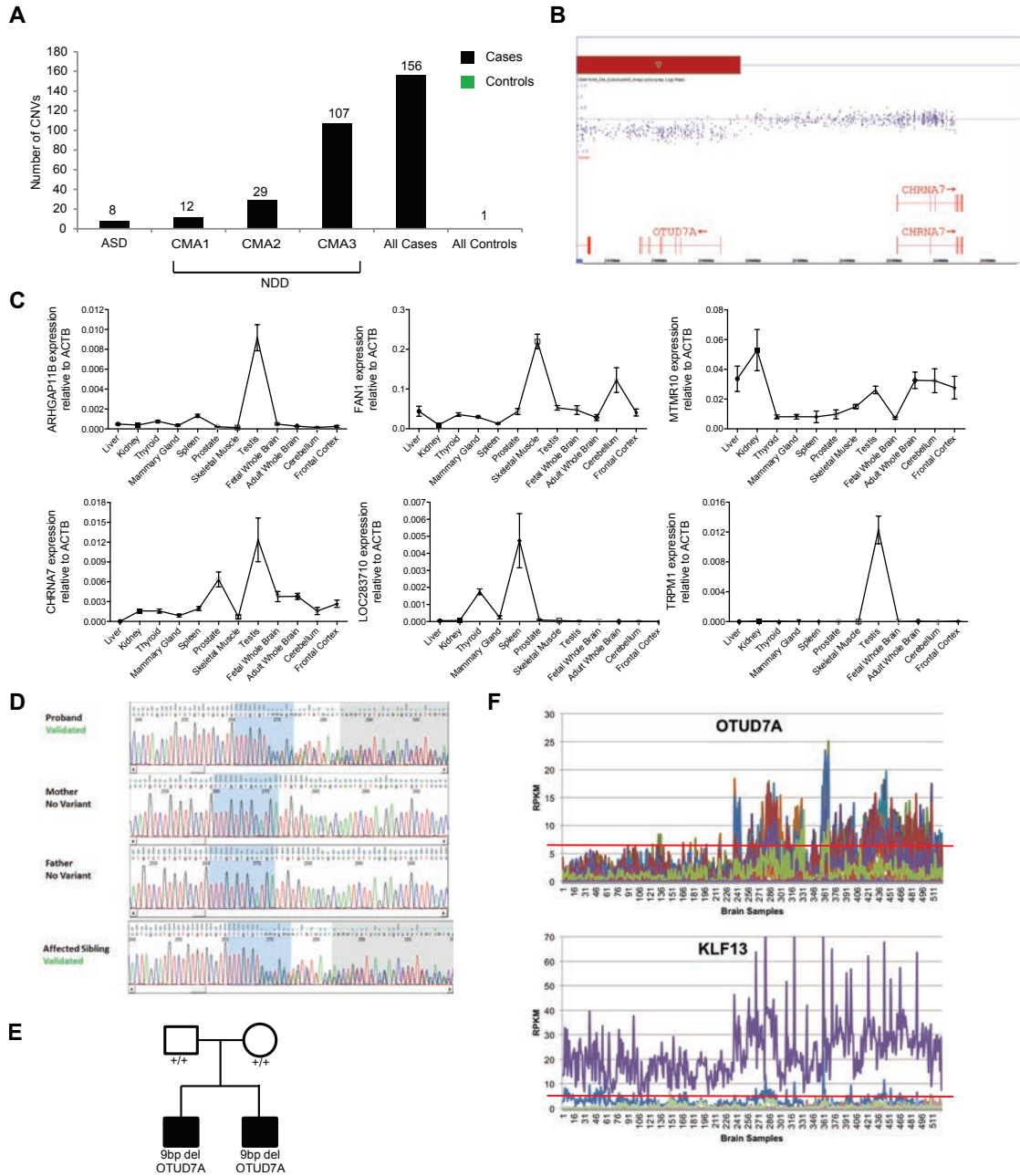


Figure S3 Analysis of overlapping deletions and gene expression in the human 15q13.3 region. (A) Number of typical 15q13.3 microdeletions identified within an autism spectrum disorder (ASD) cohort, three independent developmental delay (DD) cohorts (shown in black bars) and in controls (green bar). (B) An atypical deletion breakpoint showing the breakpoint (CNV call from CHAS algorithm) probe intensities (log₂ ratio) that clearly impacts *OTUD7A* and excludes *CHRNA7*. (C) Relative RNA expression (2^{-dCt}) from quantitative real-time PCR (qRT-PCR) relative to *ACTB* (replicated with another housekeeping gene *MED13*) shown for *ARHGAP11B*, *FANI*, *MTMR10*, *CHRNA7*, *LOC283710*, and *TRMP1* within 12 different human tissues. (D) Sanger sequencing chromatogram validating the *OTUD7A* *de novo* indel in Proband and affected sibling (Proband is case 3 in Table 1), which is not present in the mother and father. (E) Pedigree showing the unaffected father and mother and the two affected offspring diagnosed with ASD and harboring the *de novo* N492_K494 deletion in *OTUD7A*. (F) Spatio-temporal expression from 524 brain regions from Brain Span for *OTUD7A* and *KLF13*. The X-axis defines the brain region, and the Y-axis is the level of expression, and each colored line represents the level of expression for an individual exon. The red line defines the 75th percentile line of expression from the entire BrainSpan RNA-seq data. *KLF13* shows only one exon is highly expressed.

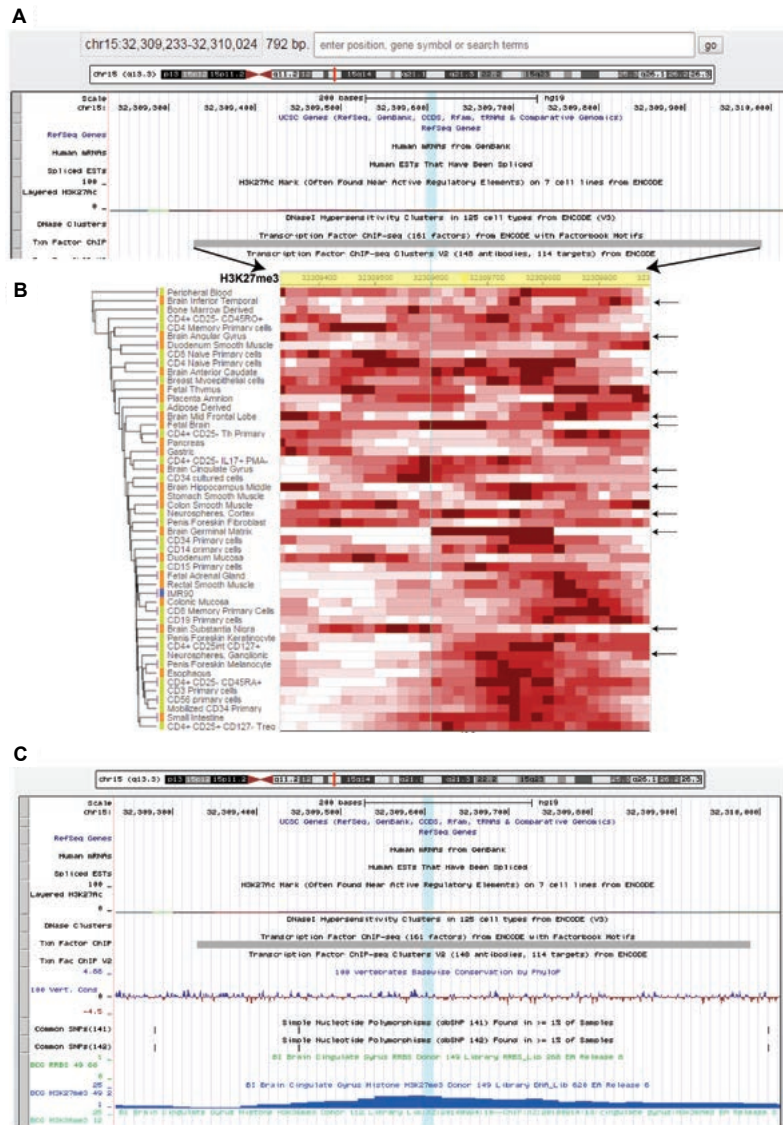


Figure S4 *In silico* analysis reveals a *de novo* ASD-linked mutation near *OTUD7A* occurs in the binding region of the transcription factor *EZH2*. (A) *De novo* mutation (chr15:32309598-32309610) impacts (blue vertical line) a known transcription factor *EZH2* (grey horizontal box) but the functional consequences is unknown. (B) Roadmap data on 50 different tissue types for the histone marker H3K27me3 and the color code represents the peak intensities (light to dark red) for different tissue types. (C) *De novo* mutation impacting a high peak from chip-seq experiment obtained from Cingulate Gyrus tissue type.

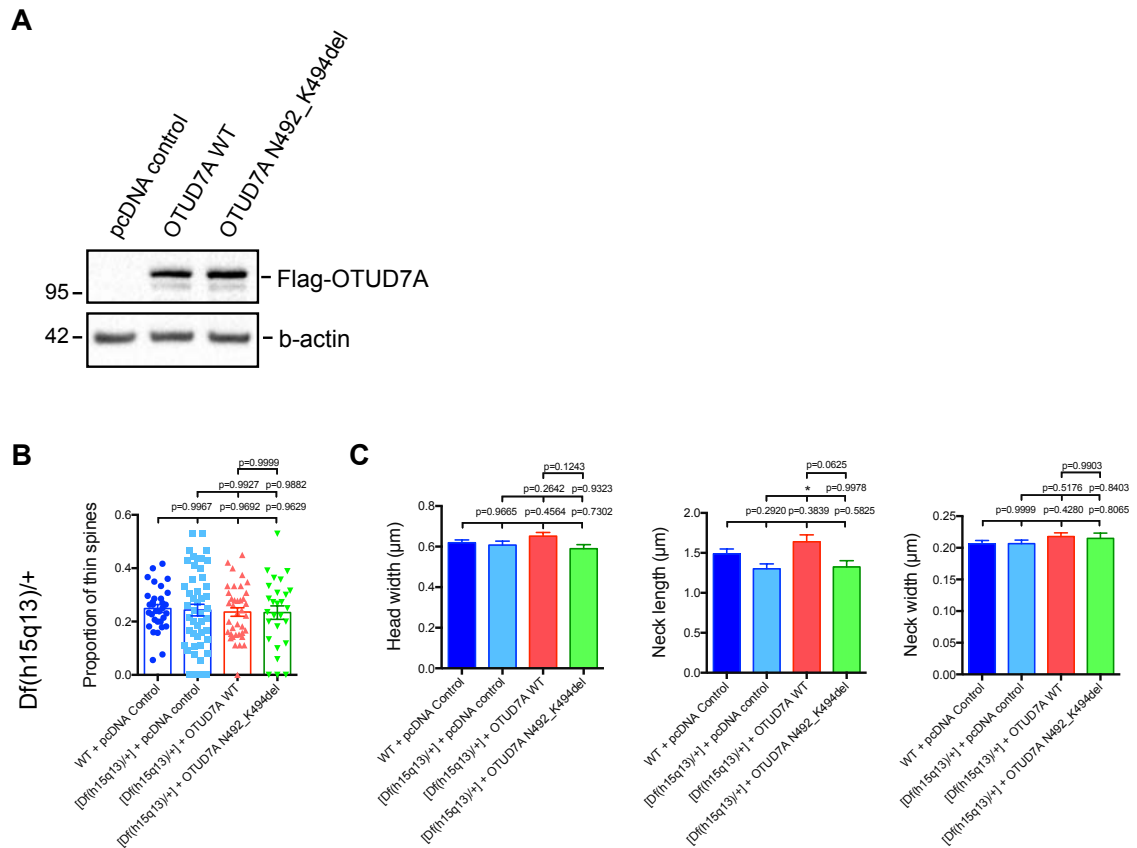


Figure S5 Dendritic spine analysis in Df(h15q13)/+ cultured neurons expressing OTUD7A WT or the de novo OTUD7A Asn492_Lys494del mutation. (

A) Overexpression of pcDNA control vector, FLAG-OTUD7A-WT, or FLAG-OTUD7A N492_K494del vectors in HEK293 cells show the presence of OTUD7A (isoform 1), detected by anti-Flag. **(B)** Overexpression of OTUD7A WT or OTUD7A N492_K494del in Df(h15q13)/+ neurons does not show changes in thin spines (WT + pcDNA, n = 32 dendritic segments, 18 neurons; pcDNA control, n = 48 dendritic segments, 30 neurons; OTUD7A WT, n = 38 dendritic segments, 21 neurons; OTUD7A N492_K494del, n = 28 dendritic segments, 20 neurons, 5 cultures, one-way ANOVA followed by Tukey's post hoc test, $F(3, 141) = 0.1061$). **(C)** Overexpression of OTUD7A WT in Df(h15q13)/+ neurons showed an increase in spine neck length. Overexpression of OTUD7A WT or

OTUD7A N492_K494del does not show any changes in spine head width or spine neck width (WT + pcDNA control, n = 244 spines; [Df(h15q13)/+] + pcDNA control, n = 180 spines; [Df(h15q13)/+] + OTUD7A WT, n = 247 spines; [Df(h15q13)/+] + OTUD7A N492_K494del, n = 112 spines, 5 cultures, one-way ANOVA followed by Tukey's post hoc test, **p < 0.01, F(3, 779) = 2.039, F(3, 768) = 4.209, F(3, 779) = 1.044). Error bars represent s.e.m.

Microarray Dataset	Phenotype Ascertainment	# of cases	15q13.3 microdeletion
ASD	Strictly Autism	1026	8
Clinical Microarray 1 (CMA 1)*	Broader neurodevelopmental disorders	9,322	12
Clinical Microarray 2 (CMA 2)*	Broader neurodevelopmental disorders	10,619	29
Clinical Microarray 3 (CMA 3)	Broader neurodevelopmental disorders	17358	107
All cases		38325	156
All controls		22,241	1

* New unpublished cohort analyzed for 15q13.3 microdeletion syndrome.

Table S3. Number of cases from each cohort, phenotypic ascertainment and the controls.

CHAPTER 4: PROXIMITY-LABELING PROTEOMICS OF THE 15Q13.3
MICRODELETION GENE *OTUD7A* IDENTIFIES SHARED
NEURODEVELOPMENTAL DISORDER SIGNALING NETWORKS THROUGH
ANK3

AUTHORS

Brianna K. Unda, Sehyoun Yoon, Savannah Kilpatrick, Sansi Xing, Nadeem Murtaza, Annie Cheng, Dr. Yu Lu, Dr. Peter Penzes, Dr. Karun Singh

PREFACE

This study was designed by Brianna Unda and Dr. Karun Singh. The majority of experiments were performed by Brianna Unda, with assistance from Dr. Sehyoun Yoon, Savannah Kilpatrick, Sansi Xing, Dr. Yu Lu, Nadeem Murtaza and Annie Cheng. Dr. Sehyoun Yoon performed SIM imaging and analysis. Liquid Chromatography and Tandem Mass Spectrometry (LC-MS/MS) for BioID2 was performed by Sansi Xing and Dr. Yu Lu. Annie Cheng performed lentiviral titering. Dr. Peter Penzes provided HA-AnkyrinG domain plasmids. Data were analyzed and figures prepared by Brianna Unda. Brianna Unda wrote the manuscript. This manuscript is currently in preparation to be submitted to *Nature Genetics*.

This work was supported by grants to K.K.S. from the Canadian Institutes of Health Research (CIHR) and the Ontario Brain Institute.

4.1 ABSTRACT

The 15q13.3 microdeletion region is a copy number variation (CNV) associated with multiple neurodevelopmental disorders (NDDs), including autism spectrum disorder (ASD), epilepsy, schizophrenia, and intellectual disability. Previous studies identified OTUD7A as an important gene within the deletion driving neurodevelopmental phenotypes. To study how OTUD7A may contribute to the heterogeneity of the 15q13.3 microdeletion syndrome and identify molecular mechanisms underlying this CNV, we used a proximity-based proteomics system, BioID2, to compare the protein-interaction networks of wildtype OTUD7A and two previously identified NDD-associated OTUD7A patient mutations. Strong OTUD7A protein interactors included a number of proteins localized to the axon initial segment and the post synaptic density, as well as known ASD-linked genes. The two OTUD7A mutations showed both shared and distinct changes in binding to target proteins compared to wildtype OTUD7A, highlighting the advantage of combining proximity labeling with patient mutations. One of the top OTUD7A protein interaction partners identified in our BioID2 screen was AnkyrinG (encoded by *Ank3*), a high-confidence bipolar disorder risk gene. Further biochemical experiments revealed that OTUD7A physically binds to the Ankyrin repeat domain (ANKRD) and spectrin binding domain of AnkyrinG, and that OTUD7A regulates levels of AnkyrinG in mouse cortical neurons. Using super-resolution imaging, we also found that the number of Ankyrin G nanodomains are decreased in Df(h15q13)/+ dendritic spines and dendrites. Over-expression of AnkyrinG in Df(h15q13)/+ cortical neurons was able to rescue neuronal morphology defects, and treatment with the selective GSK-3

inhibitor CHIR-99021 rescued neuronal activity phenotypes in Df(h15q13)/+ cortical neurons. This study presents a novel mechanism for the role of Otud7a in the 15q13.3 microdeletion syndrome. Additionally, we have shown that combining proximity-labelling proteomics and patient mutation analysis is a feasible, effective, and non-biased method for discovering downstream pathways and mechanisms of NDD risk genes for which there is little to no previously reported experimental data.

4.2 INTRODUCTION

The 15q13.3 1.53 Mb microdeletion syndrome (MIM: 612001) locus (chr15:30,910,306–32,445,407 [hg19]) that resides within breakpoints BP4-BP5 on human chromosome 15 is a recurrent CNV that results in a highly heterogeneous set of phenotypes including intellectual disability (50%–60%), autism spectrum disorder (10%–20%), epilepsy (30%) (MIM: 607208), and schizophrenia (10%–20%). Individuals are typically heterozygous for the 15q13.3 microdeletion, which encompasses seven protein-coding genes, one microRNA, and two pseudogenes (ARHGAP11B [MIM:616310], LOC100288637, FAN1 [MIM: 613534], MTMR10, TRPM1 [MIM: 603576], LOC283710, microRNA-211, KLF13, [MIM: 605328], OTUD7A [MIM: 612024], and CHRNA7 [MIM: 118511]) (Atonacci et al., 2014; Helbig et al., 2009; Sharp et al., 2008; International Schizophrenia Consortium, 2009; Pagnamenta et al., 2009; Shinawi et al., 2009; Stefansson et al., 2008; Ziats et al, 2016). Multiple genes within the deletion have been investigated as potential driver genes of the neurological phenotypes observed in the disorder. The majority of evidence has pointed to two of the genes, CHRNA7 and OTUD7A, as being particularly

important. CHRNA7 has been proposed as a driver gene, in part because some patients have overlapping deletions that encompass CHRNA7 (Shinawi et al., 2009). However, among clinical case subjects, many of the deletions encompassing CHRNA7 also overlap the adjacent gene OTUD7A (Lowther et al., 2014). Further implicating OTUD7A are two recent independent studies investigating the role of OTUD7A in the 15q13.3 microdeletion. A previous study from our lab combined bioinformatic analysis of human whole-genome sequencing (WGS) and whole-exome sequencing (WES) data with pathophysiological characterization of a heterozygous 15q13.3 microdeletion mouse model (Df(h15q13)/+), and identified OTUD7A as a strong candidate driver gene of the neurodevelopmental phenotypes observed in the 15q13.3 microdeletion (Uddin et al., 2018). Specifically, we identified 3 *de novo* variants in OTUD7A in ASD probands and affected siblings and discovered that OTUD7A contains “brain-critical” exons, suggesting that OTUD7A is likely important for brain function. We also showed that Df(h15q13)/+ cortical neurons have impaired dendrite and dendritic spine development, and that OTUD7A re-expression was sufficient to rescue neuronal morphology deficits (Uddin et al., 2018). A companion study determined that *Otud7a* KO mice recapitulate behavioural phenotypes observed in Df(h15q13)^{-/-} mice, including impaired ultrasonic vocalizations, seizure-like activity, and impaired pre-pulse inhibition (Yin et al., 2018). Both models displayed decreased dendritic spines and both studies showed that a subset of OTUD7A protein is localized to dendritic spines (Uddin et al., 2018; Yin et al., 2018). Although both of these studies strongly implicated the role of OTUD7A in the 15q13.3

microdeletion syndrome, neither study examined possible molecular mechanisms of OTUD7A's role in neurodevelopmental processes.

There are currently two studies that have reported *de novo* mutations in OTUD7A (Garret et al., 2020; Uddin et al., 2018). OTUD7AN492_494del is a previously published *de novo* non-frame shift deletion identified in an ASD proband and affected sibling through whole genome sequencing, resulting in the deletion of 9 base pairs that is predicted to delete amino acids 492-494 of OTUD7A, just upstream of the nuclear localization sequence (NLS). We previously found that this mutation impairs the ability of OTUD7A to regulate dendrite and dendritic spine formation (Uddin et al., 2018). The second mutation, OTUD7AL233F, is a recently published inherited homozygous point mutation in the catalytic domain of OTUD7A which results in a substitution of Leucine 233 to Phenylalanine (Garret et al., 2020). This patient is a two-year-old boy with severe global developmental delay, language impairments and epileptic encephalopathy. Fibroblasts from the OTUD7AL233F patient showed proteasome dysfunction, identified by an increase in K-48 linked ubiquitinated proteins as well as decreased expression of PA28 complexes, an activator of the 20S proteasome (Garret et al., 2020). However, how these mutations affect OTUD7A molecular function and protein interactions remains unknown. The OTUD7A protein (also known as Cezanne 2, for cellular zinc finger anti-NF- κ B 2) is a member of the ovarian tumor (OTU) family of cysteine protease deubiquitinases (Evans et al., 2003; Mevissen et al., 2013). Ubiquitination is a post-translational modification (PTM) which targets proteins for proteasomal degradation, lysosomal degradation, intracellular trafficking or signaling. Substrate proteins are reversibly tagged with

ubiquitin molecules through a series of enzymatic reactions by ubiquitin-activating enzyme (E1), ubiquitin-conjugating enzyme (E2), ubiquitin ligase (E3); deubiquitinases fall into this pathway by removing ubiquitin molecules from target proteins (Mabb & Ehlers, 2010). The most widely studied function of ubiquitination is protein turnover via the ubiquitin-proteasome system (UPS), which is a critical process for neural cells, regulating learning and memory, and synaptic plasticity (Mabb & Ehlers, 2010; Widagdo et al., 2017). *In Vitro* ubiquitination assay studies have found that OTUD7A shows linkage specificity towards Lysine 11 polyubiquitin chains (Mevisen et al., 2013). Despite the scarcity of literature analyzing the functions of this linkage type, some studies suggest that it may be involved in processes such as proteasomal degradation, cell cycle regulation, endoplasmic reticulum associated degradation (ERAD) and mitophagy (Akutsu et al., 2016). OTUD7A is thought to play a role in cancer and immunology, whereby it negatively regulates the NF- κ B signaling pathway through deubiquitination and inhibition of TRAF6 (Xu et al., 2014). However, no studies have examined the molecular function of OTUD7A in the brain.

Proximity-labeling proteomics has become an important non-biased method for investigating protein-protein interactions and is particularly useful in discovery-based studies where little is known about the protein in question. BioID is a proximity-labeling based proteomics system that has been widely used in various cell lines to identify protein-protein interactions and to map the spatial organization of cellular compartments (Kim et al., 2016; Liu et al., 2018; Roux et al., 2012; Youn et al., 2018). This system uses a mutated “promiscuous” version of a bacterial biotin ligase (BirA*), with the ability to

biotinylate proteins within close proximity (Roux et al., 2012). Although BioID has been widely used to map the proteomes of various cells lines, only three studies have utilized this system in neurons or the brain. Two studies delivered BioID-tagged synaptic proteins virally *in vivo* using adeno-associated virus (AAV); one mapped excitatory and inhibitory synaptic proteomes in the mouse brain while the other characterized the protein interaction network of a novel regulator of the cytoskeleton at the synapse (Spence et al., 2019 ;Uezu et al., 2016). The most recent study used AAV packaged BioID constructs to map the axon-initial segment (AIS) proteome in cultured mouse cortical neurons (Hamdan et al., 2020). This method has recently been improved (BioID2), which uses a smaller biotin ligase derived from *A. aeolicus*, which was shown to retain the same enzymatic activity of BioID, but has improved fusion-protein subcellular localization and reduced the amount of biotin supplementation needed (Kim et al., 2016). Here, we used a lentiviral delivery system to deliver BioID2-tagged OTUD7A to mouse cortical neurons *in vitro* to identify a novel OTUD7A protein interaction network (PIN) and to investigate the impact of NDD-associated patient mutations OTUD7AN492_K494del and OTUD7AL233F on the OTUD7A PIN. The OTUD7A PIN included proteins localized to the axon initial segment (AIS), postsynaptic membrane as well as proteins encoded by high confidence ASD-risk genes. Additionally, the two patient mutations showed both shared and distinct changes to protein interactions and functional networks. Namely, the most impaired network of proteins in the OTUD7AN492_K494del mutation sample was localized to the postsynaptic membrane, whereas AIS proteins were most affected by the OTUD7AL233F mutation. We focused

on validation of the one of the highest-confidence BioID2 hits, AnkyrinG. *ANK3* is a high confidence bipolar gene which encodes AnkyrinG, a scaffold protein that anchors plasma membrane associated proteins to the actin/spectrin cytoskeleton (Hedstrom et al., 2008, Leussis et al, 2012). It has 3 main brain-expressed isoforms due to alternative splicing which differ in size: 190kDa, 270kDa and 480kDa. The 270 and 480 kDa isoforms show restricted localization to the axon initial segment, whereas the 190kDa isoform is localized to both the AIS and the PSD (Smith & Penzes, 2018; Smith et al., 2014). We discovered that OTUD7A and AnkyrinG-190 share a protein-protein interaction network and that OTUD7A binds the Ankyrin repeat domain (ANKRD) and spectrin binding domains of AnkyrinG. Through SIM imaging we show that AnkyrinG levels are decreased in dendrites and dendritic spines of *Df(h15q13)/+* neurons. Finally, we show that exogenous expression of AnkyrinG or chemical inhibition of GSK-3 through treatment with CHIR-99021 rescues synaptic and functional deficits in *Df(h15q13)/+* neurons. Our data uncover a novel OTUD7A molecular pathway intersecting with known neurodevelopmental pathways that is impacted by NDD-associated patient mutations. Additionally, neurodevelopmental phenotypes relevant to the 15q13.3 microdeletion syndrome can be ameliorated through targeting of this pathway.

4.3 MATERIALS AND METHODS

Animals

Df(h15q13)/+ mice were generated by Taconic Artemis as described in Fejgin et al.

Animals were bred, genotyped, and housed at the Central Animal Facility at McMaster

University. All procedures received the approval of the Animal Research Ethics Board (AREB). Genotypes were identified during breeding by PCR of ear notches, and two WT females were bred with 1 Df(h15q13)/+ male per breeding cage. The use of only WT females for breeding was performed to minimize effects of potential differences in the embryonic environment and/or mothering of the Df(h15q13)/+ females compared to WT females. To obtain cortical cultures, WT females were timed-bred with Df(h15q13)/+ males and males were removed when a plug was observed, indicating copulation. At E16, mothers were sacrificed, and litters were collected. Animals of appropriate genotype were included, and any animals with unclear genotypes were excluded from experiments. The mouse line C57BL/6J-Otud7A^{3XFLAG} (3XFLAG-Otud7a) was made at The Centre for Phenogenomics by electroporating Cas9 ribonucleoprotein complexes with a guide RNA with the spacer sequence GCTAGAGACCATCCATCTGC and a single-strand oligonucleotide encoding a 3XFLAG tag and GGSG flexible linker inserted immediately after the start codon. Also identified was an upstream intronic variant 1-bp delG Chr7:63650782 (GRCm38). For BioID2 studies, timed-pregnant CD1 mice were ordered from Charles River and were euthanized for embryo collection at E16.

Cell Culture

Primary cortical neurons were cultured as follows. Cortices were dissected out of WT and Df(h15q13)/+ mouse embryonic brains at E16. The last 1-2mm of their tails were used for genotyping. Dissociation of cortices was aided by incubation in 0.3 mg/mL Papain (Worthington Biochemical)/400 U/mL DNase I (Invitrogen) in Hanks Buffered Saline

Solution (HBSS) for 20 min at 37 °C, followed by light trituration. Cells were seeded onto 0.1 mg/mL poly-D-lysine (BD Sciences)/3.3 mg/mL Laminin (Sigma)-coated coverslips in plating media containing Neurobasal medium, 10% fetal bovine serum, 1% penicillin/streptomycin, and 2 mM GIBCO Glutamax supplement. After 1.5 hr, media was changed to serum-free feeding media containing Neurobasal medium, 2% B27 supplement, 1% penicillin/streptomycin, and 2 mM L-glutamine. For immunocytochemistry experiments, cultures were treated with 1 mM Cytosine b-D-arabino-furanoside hydrochloride (Ara-C) (Sigma) at DIV 4 to inhibit glial cell proliferation. Cultures were maintained at 37 °C, 5% CO₂. All media components were from GIBCO unless otherwise specified.

HEK293 FT cells were maintained in DMEM with 4.5g/L glucose, 10% Fetal bovine serum, 2mM GIBCO Glutamax supplement, 1mM Sodium pyruvate and 1X MEM Non-essential amino acids. Lenti-X 293T cells were maintained in the same base media with 20% Fetal Bovine serum.

Multielectrode Arrays

48-well Cytoview MEA plates (Axion Biosystems, M768-tMEA-48B) were coated with 0.1% Polyethylenimine (PEI) 24 hours prior to plating. Primary mouse cortical cultures were dissected at E16 and plated onto PEI-coated 48-well Cytoview MEA plates at a density of 3×10^4 cells/ well in plating media containing Neurobasal medium, 10% fetal bovine serum, 1% penicillin/streptomycin, and 2 mM GIBCO Glutamax supplement. After 1.5 hr, media was changed to serum-free feeding media containing Neurobasal

medium, 2% B27 supplement, 1% penicillin/streptomycin, and 2 mM L-glutamine. Half of the culture media was replaced every 2 days. To record extracellular spontaneous activity, MEA plates were placed in the MaestroPro MEA system (Axion Biosystems) at 37 °C for 5 minutes to acclimate, followed by a 10 minute recording period. Spike data were analyzed with the AxIS Navigator software (Axion Biosystems) at a sampling rate of 12.5 kHz with a 4kHz Kaiser Window low pass filter and a 200Hz IIR High Pass filter. Analyzed data were exported to CSV files and statistical analysis was performed in GraphPad Prism 6 software. Wells that had zero active electrodes throughout the duration of the experiment were excluded for statistical analysis. Raster plots were generated with the Neural Metric Tool (Axion Biosystems).

Cell Treatments

Primary mouse cortical neurons in 48-well Cytoview MEA plates were treated with either 1 μ M CHIR-99021 (Sigma) or vehicle (DMSO) starting at DIV 6. Every other day, half the culture media was exchanged with fresh culture media plus CHIR-99021 or DMSO.

Transfection

Primary neurons were transfected at DIV 7 using Lipofectamine LTX with Plus reagent (Invitrogen) according to the manufacturer's instructions. Approximately 9×10^5 cells per well were transfected with 1 μ g DNA with 2 μ L Lipofectamine LTX and 1 μ L Plus reagent. HEK293FT cells were grown under standard cell culture conditions and transfected with plasmids using Lipofectamine 2000 according to the manufacturer's

protocol (Invitrogen) at approximately 80-90% confluency. HEK293FT cells were used for ease of plasmid expression and have not been tested for Mycoplasma contamination.

Antibodies and Constructs

The following antibodies were used in this study. Mouse anti-FLAG (Sigma F1804; Western Blot 1:1000, IF 1:1000), Mouse anti-HA (Santa Cruz Biotechnology F-7; Western Blot 1:500), Rabbit anti-AnkyrinG (Synaptic Systems 386 003; Western blot 1:4000, IF 1:1000), Mouse anti-AnkyrinG (Neuromab N106/36; IF 1:200) Mouse anti-BetaActin (Sigma A5316; Western blot 1:5000), Rabbit anti-BetaActin (Cell Signaling Technologies #4907; Western blot 1:1000), Rabbit anti-GFP (Santa Cruz Biotechnology sc-8334; Western blot 1:1000), anti-TurboGFP (Thermo Fisher Scientific PA5-22688; Western blot 1:1000; IF 1:1000), Rabbit anti-mCherry (Abcam ab167453; IF 1:500), Chicken anti-GFP (Aves Labs AB_2307313; IF 1:1000), Rabbit anti-AlphaTubulin (Cell signaling 2144S; Western blot 1:1000). Fluorophore-conjugated secondary antibodies were raised in donkey and used at a concentration of 1:1000. Alexa Fluor 647-Streptavidin (Jackson ImmunoResearch; IF 1:1000) was used to detect biotin in IF experiments. Pierce™ High Sensitivity Streptavidin-HRP (Thermo Fisher scientific; western blot 1:30 000) was used to detect biotin in western blots.

To create the BioID2 fusion constructs, we obtained an expression plasmid containing a C-terminal 3Xflag tagged BioID2 sequence with a 198bp (13X “GGGS” repeat) linker sequence upstream of BioID2 (Genscript). For lentiviral expression, 13X linker-BioID2-3XFLAG was amplified and cloned into the lentiviral backbone pLV-hSYN-RFP

(Addgene Plasmid #22909) using InFusion cloning. For ease of visualization and to create a bicistronic construct, TurboGFP-P2A was amplified from pCW57-GFP-2A-MCS (Addgene plasmid #71783) and cloned into the pLV-hSYN-RFP backbone between the BamHI and PmeI restriction sites, replacing RFP. InFusion cloning was used to insert individual transgenes between the P2A and the 13Xlinker-BioID2 sequences.

The pcDNA-OTUD7AL233F-FLAG construct was made by incorporating a C>T mutation at bp 697 of the human OTUD7DA cDNA sequence into the PCR primers prior to amplification. The pcDNAOTUD7AC210S mutation was made similarly by incorporating a C>G mutation at bp 629 of the human OTUD7DA cDNA sequence into the PCR primers prior to amplification. The PCR product was subcloned into the pcDNA3.3 backbone using the InFusion cloning system between the EcoRI and MluI restriction sites. mCherry-tagged constructs were created by amplification of WT OTUD7A, OTUD7AN492_494del or OTUD7AL233F from the pcDNA3.3 backbone and amplification of mCherry from Lenti U6-sgRNA EF1a-mCherry (Dr. Jeremy Day, UAB, Alabama), followed by InFusion of PCR products into the pcDNA3.3 backbone between the EcoRI and KpnI restriction sites.

AnkyrinG-190-GFP (plasmid #31059) and AnkyrinB-2XHA (plasmid #31057) were bought from Addgene. The 3XHA-AnkyrinG domain constructs were gifts from Dr. Peter Penzes (Northwestern University). pCAGIG-Venus was provided by Dr. Zhigang Xie (Boston University, MA).

Lentivirus Production

Lenti-X 293T cells were transfected with transfer plasmid containing overexpression construct, along with the packaging plasmid psPAX2 (Addgene Plasmid #12260) and the VSV-G envelope plasmid PMD2.G (Addgene Plasmid #12259). 48 hours after transfection, viral supernatant was collected and ultracentrifuged at 25 000 RPM for 2 hours at 4°C. To titer the lentivirus, primary mouse cortical neurons were transduced at DIV 3 at three different concentrations, followed by flow cytometry at DIV 5 to calculate the percentage of GFP+ cells. Titers were calculated using the following equation:

$$\text{Fraction GFP+} \times \text{dilution} \times \text{cell\#} / \text{volume (mL)} = \text{transducing units (TU) / mL.}$$

Functional titers were calculated as the average titer obtained from the three dilutions and ranged from 10^7 – 10^8 TU/mL.

***In vitro* Biotinylation**

Cultured mouse primary cortical neurons (approximately 7.2×10^6 neurons per virus) were transduced with lentiviral BioID2 constructs at a MOI of 0.7. Neurons were transduced at DIV 14 and biotin was added at DIV 17 at a final concentration of 50µM. Cells were lysed in RIPA buffer, sonicated, and biotinylated proteins were pulled down with streptavidin-sepharose beads (GE ref# 17-5113-01). Bead-protein conjugates were resuspended in ammonium bicarbonate and on-bead trypsin digestion was performed overnight at 37 °C. Beads were washed with ammonium bicarbonate and supernatants containing digested peptides were speed vac dried before preparation for LC-MS.

Liquid Chromatography and Tandem Mass Spectrometry (LC-MS/MS) for BioID2

BioID2 samples were resuspended with 20 μ l 0.1% formic acid, 1 ml out of 20 ml was injected for LC-MS/MS analysis. Liquid chromatography was conducted using a home-made trap-column (5 cm x 200 mm inner diameter) and a home-made analytical column (50 cm x 50 mm inner diameter) packed with Reprosil-Pur 120 C18-AQ 5 μ m particles (Dr. Maisch), running a 3hour reversed-phase gradient at 70nl/min on a Thermo Fisher Ultimate 3000 RSLCNano UPLC system coupled to a Thermo QExactive HF quadrupole-Orbitrap mass spectrometer. A parent ion scan was performed using a resolving power of 120,000 and then up to the 30 most intense peaks were selected for MS/MS (minimum ion counts of 1000 for activation), using higher energy collision induced dissociation (HCD) fragmentation. Dynamic exclusion was activated such that MS/MS of the same m/z (within a range of 10ppm; exclusion list size=500) detected twice within 5s were excluded from analysis for 50s.

Mass Spectrometric Data Analysis

Mass spectrometric raw files from the Thermo QExactive HF quadrupole-Orbitrap were searched using Proteome Discoverer, against the UniProt Mouse database (Version 2017-06-07), in addition to a list of common contaminants maintained by MaxQuant (Tyanova et al., 2016). The database parameters were set to search for tryptic cleavages, allowing up to 2 missed cleavage site per peptide, with a parent MS tolerance of 10 ppm for precursors with charges of 2+ to 4+ and a fragment ion tolerance of ± 0.02 amu. Variable modifications were selected for oxidized methionine. The results from each search were statistically validated within Proteome Discoverer, with 1 unique peptide and a FDR

cutoff at 0.01 required for protein identification. SAINTexpress was used to calculate the probability of each potential proximal-protein from background (control BioID2) using default parameters (Choi et al., 2011; Teo et al., 2014). Specificity plot and Dotplot were generated from SAINTexpress data using ProHits-Viz (Knight et al., 2017).

Protein Network Analysis

Protein networks were constructed in Cytoscape using the STRING protein interaction database for *mus musculus*. Proteins with a SAINT score of greater than or equal to 0.6 were included. The size of each node represents the fold change between the PSMs for each protein in the experimental BioID2 sample vs the control BioID2 sample. Gene Ontology enrichment tests were performed on geneontology.org (Mi et al., 2013) using a mouse cortex transcriptome reference list (<https://portal.brain-map.org/atlasses-and-data/rnaseq>). Only the most specific GO terms in a family were reported to avoid redundancy and GO terms that were not relevant to the cell type (neurons) were not reported. GO terms with FDR <0.05 were considered significant.

Immunoprecipitation and Immunoblotting

For immunoprecipitation, cells or brain tissue were lysed in lysis buffer (50mM Tris-HCl, 150mM NaCl and 1% NP-40) with cOmplete mini protease inhibitor cocktail (Roche) and centrifuged at 12 000g for 10 minutes at 4 °C. Protein G Dynabeads (Invitrogen) were incubated with primary antibody for 2 hours at room temperature on a rotator, followed

by incubation with lysate overnight at 4 degrees on a rotator. Immunoprecipitants were eluted in 2X lamelli sample buffer with beta mercaptoethanol for 10 minutes at 95 °C. For western blotting, cells or tissue were lysed in lysis buffer or RPIA buffer (50mM Tris-HCl, 150mM NaCl, 0.5% sodium deoxycholate, 0.1% SDS, and 1% NP-40). Samples were loaded into Tris-Glycine gels and transferred to a PVDF membrane (Bio-Rad). Membranes were blocked for 1 hr in 5% milk in 1X TBST, incubated with primary antibody overnight at 4 degrees C, then with secondary antibody (donkey anti-mouse or antirabbit HRP, GE Healthcare) for 1 hr at room temperature before exposure using a ChemiDoc MP system (Bio-Rad).

Immunocytochemistry

Cells on glass coverslips were fixed with 4% paraformaldehyde in PBS for 20 min at room temperature. Cells were washed in PBS three times, followed by blocking in blocking/permeabilization solution consisting of 10% Donkey Serum (Millipore) or 1% BSA and 0.3% Triton X-100 (Fisher Scientific) in PBS for 1 hr at room temperature. Incubation in primary antibodies was performed at 4 °C overnight. Cells were then washed in PBS three times, followed by incubation with secondary antibodies in 50% blocking/permeabilization solution at room temperature for 1.5 hr. Cells were then washed in PBS and were mounted on VistaVision glass microscope slides (VWR) using Prolong Gold antifade reagent (Life Technologies). Confocal images were acquired using a Zeiss LSM700 confocal microscope.

SIM imaging and analysis

Imaging and reconstruction parameters were empirically determined with the assistance of the expertise in the Nikon Imaging Center at Northwestern. The acquisition was set to 10MHz, 14 bit with EM gain, and no binning. Auto exposure was kept between 100-300ms, and the EM gain multiplier restrained below 300. Conversion gain was held at 1x. Laser power was adjusted to keep LUTs within the first quarter of the scale (<4000). Reconstruction parameters (0.96, 1.19, and 0.17) were kept consistent across experiments and imaging sessions. The resolution of images was taken with 2048 x 2048 pixels in the area of 66.56 x 66.56 μm . For each spine analyzed, the single-plane in which the spine head was in focus, based on the cell fill, was chosen for analysis. Using ImageJ software, each spine head was outlined manually in the channel of the cell fill to detect the area. A specific dendritic region (WT: 59.03 \pm 4.96 μm ; Df(h15q13)/+: 67.40 \pm 4.33 μm) was selected, and puncta counts were made for the measurement of ankyrin-G puncta; puncta smaller than 0.065 μm^2 were excluded from the analysis. Visual assessment of fluorescence intensity was used to delineate separate or connected puncta. Puncta were considered separate if a region of decreased intensity was readily visible. The number of puncta within the spine head was quantified manually and recorded. For the dendritic analysis, the first branched apical dendrite from a pyramidal neuron was outlined automatically by thresholding 10,000 in a 16-bit image. In the chosen region of interest (ROI) of the dendritic shaft without spines, ankyrin-G puncta were analyzed with the option of analyze particles automatically by ImageJ; also, puncta smaller than 0.065 μm^2 were excluded. All images were processed with converting mask and watershed with a binary option.

Morphological Analyses

Confocal images were taken at a resolution of 2048 x 2048 pixels in an area of 145.16 x 145.16 μm and were processed and analyzed with ImageJ 1.44 software. Sholl analysis was performed using the Sholl analysis plugin in ImageJ. This plugin was used to make concentric circles increasing at a constant radius of 10 μm and to count the number of dendritic intersections. Spine density was calculated by visually counting all protrusions from a dendrite within a 15–25 μm distance starting at a secondary branch point. One to three dendritic segments were analyzed per neuron. Maximal spine head width (HW), neck width (NW), length (L), and neck length (NL) were measured for each dendritic protrusion using the segmented line tool in ImageJ. Spines were defined as follows: stubby ($L < 1 \mu\text{m}$), mushroom ($1 \leq L \leq 5 \mu\text{m}$; $\text{HW} \geq 2 \times \text{NW}$), or thin ($1 \leq L \leq 5 \mu\text{m}$; $\text{HW} \leq 2 \times \text{NW}$). The density of each spine type was calculated by dividing the number of spines in each spine category (mushroom, thin, and stubby) by the total number of spines within the dendritic segment.

Statistical Analysis

Data are expressed as mean \pm SEM. Blinding was performed for SIM imaging experiments. Normality tests were performed using the D'Agostino & Pearson test, Shapiro-Wilk test and Kolmogorov-Smirnov test. For normally distributed datasets, we used the Student's t test, one-sample t test, one-way ANOVA with Dunnett's post-hoc test, two-way ANOVA with Dunnett's post-hoc test, and Repeated Measures two-way ANOVA with Tukey's post-hoc test in GraphPad Prism 9 statistical software for

statistical analyses. For non-normally distributed data, we used non-parametric statistical tests (Mann-Whitney test or Kruskal-Wallis test). p values in the figure legends are from the specified tests, and $p < 0.05$ was considered statistically significant. For SAINT analysis, a cutoff SAINT score of 0.6 was used for significance. For Gene Ontology PANTHER over-representation tests, an FDR < 0.05 was considered significant.

4.3 RESULTS

4.3.1 Df(h15q13)/+ cortical neurons show decreased spontaneous firing and bursting patterns

We previously determined that Df(h15q13)/+ cortical neurons display a decrease in dendritic spine density and a shift in spine morphology to a lower proportion of mushroom spines and a higher proportion of stubby type spines. This suggested that Df(h15q13)/+ neurons may be more immature than those of WT mice. However, we did not examine whether or not this was associated with a functional difference. To investigate this, we used a multi-electrode array (MEA) system to record spontaneous neuronal activity over time from WT and Df(h15q13)/+ neurons. We measured spikes (action potentials) from cultured cortical neurons plated on 48-well plates, with each well containing 16 electrodes (Fig 1a), and analyzed firing rate, bursting activity and network bursting. Firing rate is a measure of neuronal activity or functionality, whereas bursting, defined as discrete periods of rapid action potential firing followed by a quiescent period, is correlated with neuronal excitability. Network bursts are synchronized population-level bursting patterns between neurons, and changes in network bursts are indicative of

changes in synaptic connectivity. Recordings were taken starting at DIV 7 every 3-4 days until DIV 31. At DIV 7, Df(h15q13)/+ neurons show a significant decrease in active electrodes, which disappears from DIV 14 onward, suggesting an early defect in activity (Fig 1b). Df(h15q13)/+ neurons showed a significant decrease in firing rate from DIV 14 onwards (Fig 1c). Df(h15q13)/+ cortical neurons also showed a significant decrease in the frequency of bursts (Fig 1d) and networks bursts (Fig 1e) from DIV 21 onward. These results suggest that Df(h15q13)/+ neurons develop lower levels of spontaneous activity, as well as lower levels of coordinated activity between neurons within a well, and that these phenotypes persist late into neuronal maturity.

4.3.2 Df(h15q13)/+ dendritic spine phenotypes, but not dendrite complexity phenotypes, can be rescued by expression of an epilepsy-associated OTUD7A patient mutation

The first case of a homozygous missense variant (NM_130901.2:c.697C>T, p.(Leu233Phe)) in *OTUD7A* was recently reported in a two year old male presenting with severe global developmental delay, language impairment and epileptic encephalopathy (Garret et al., 2020). This mutation was inherited from each of his parents, who are both heterozygous for the mutation and who also display mild learning difficulties (Fig 1g) (Garret et al., 2020). The heterozygous mutation is also present in the brother of the proband, who presented with non-specific learning difficulties (Fig 1g) (Garret et al., 2020). The mutation results in a substitution of leucine 233 to phenylalanine within a conserved region of the catalytic domain of the *OTUD7A* protein, suggesting that it may potentially affect protein function (Fig 1f).

We first examined protein levels of the OTUD7AL233F mutation by expressing a human OTUD7AL233F construct in HEK293 cells. We compared protein levels via western blot to that of WT OTUD7A as well as three mutations. The OTUD7AN492_K494del mutation is a previously identified ASD patient mutation located just upstream of the nuclear localization sequence of OTUD7A. The OTUD7AC210S mutation affects the catalytic cysteine of OTUD7A, and was previously shown to abolish its ability to deubiquitinate a known target substrate¹⁷. There was a small but significant decrease in OTUD7AN492_K494del levels and a large significant decrease (~75%) in levels of OTUD7AL233F compared to WT OTUD7A (Supplementary Fig 1a). We initially hypothesized that this decrease in levels may be due to a defect in auto-deubiquitination, since this mutation is located in its catalytic domain. However, OTUD7AC210S levels were not significantly different compared to WT OTUD7A (Supplementary Fig 1a), suggesting that the decrease in OTUD7AL233F levels may not be due to changes in its deubiquitinase activity.

We previously discovered that Df(h15q13)/+ neurons display decreased dendrite complexity as well as a more immature dendritic spine phenotype. Expression of WT OTUD7A was sufficient to rescue both of these phenotypes, whereas expression of OTUD7AN492_K494del was not (Uddin et al., 2018). To determine the impact of the OTUD7AL233F mutation on dendrite and dendritic spine formation and maturity, we co-expressed Venus + WT OTUD7A-mCherry, Venus + OTUD7AL233F-mCherry or Venus + mCherry in WT and Df(h15q13)/+ neurons. Fluorescence intensity of WTOTUD7A and OTUD7AL233F mCherry tagged constructs was not significantly different

(Supplementary Fig 1b,c). Sholl analysis revealed that WT OTUD7A expression in Df(h15q13)/+ neurons rescued dendritic complexity, most notably in the area of the dendritic tree more distal to the soma (Fig 1h, I,j). Expression of OTUD7AL233F in Df(h15q13)/+ did not rescue dendrite complexity, suggesting that the OTUD7AL233F mutation affects the ability of OTUD7A to regulate dendrite complexity (Fig 1h, I,j). Df(h15q13)/+ neurons showed an overall decrease in spine density compared to WT neurons (Fig 1k,l), corroborating our previous finding that spine formation is impacted in Df(h15q13)/+ neurons (Uddin et al., 2018). When stratified by spine morphological type, only mushroom spine density was significantly decreased in Df(h15q13)/+ neurons (Fig 1k,n,o). Df(h15q13)/+ also displayed a shift in the proportion of mushroom and stubby type spines, with a decrease in mushroom type spines and an increase in stubby type spines, suggesting that remodeling of existing spines is also affected. Expression of both WT OTUD7A and OTUD7AL233F were able to rescue the decrease in mushroom spine density, as well as restoring the WT proportions of mushroom, thin, filopodia and stubby type spines (Fig 1k,m). Taken together the data indicate that the OTUD7AL233F mutation impacts the ability of OTUD7A to regulate neurite arborization but does not impact its ability to regulate dendritic spine formation or maturation.

4.3.3 Establishing a neuron-specific in vitro BioID2 proximity-labelling proteomics system

OTUD7A protein binding partners have never been assessed in neurons or the brain. Therefore, elucidating the OTUD7A protein interactome in neurons can tell us where

OTUD7A is localized in neurons and may shed light on the molecular mechanisms through which OTUD7A affects neuronal morphology. Additionally, we sought to determine how patient mutations affect the OTUD7A protein interaction network in cortical neurons. We decided to use a global, unbiased approach to uncover OTUD7A protein interactors, the BioID system. BioID utilizes a mutated bacterial biotin ligase (BirA*), which abolishes the stringent target specificity of the ligase by reducing its affinity for activated biotin. This leads to premature release of activated biotin, allowing proteins within a small radius to be biotinylated. When fused to a bait protein of interest, proximal proteins will be biotinylated and these proteins can then be purified using streptavidin-coated beads, which have a high affinity for biotin (Kim et al., 2016; Roux et al., 2012).

The first consideration in establishing our neuronal BioID2 system was to determine the appropriate expression method in cortical neurons. Primary cortical neurons are extremely difficult to transfect, and chemical transfection methods produce low transfection efficiencies along with the added drawback of cytotoxic effects (Kim & Eberwine, 2010). Because the end point of this experiment required entire wells of cells to be harvested, a large proportion of cells needed to express our BioID2 fusion protein to reduce background and obtain a sufficient number of biotinylated proteins to proceed to mass spectrometry. Lentivirus can be titered to obtain the desired transduction efficiency, and post-mitotic cells such as neurons can be transduced with high efficiency with very little cell death. Therefore, we decided to use a lentiviral backbone to infect primary mouse cortical neurons *in vitro* to overexpress an OTUD7A-BioID2 fusion protein. We

chose a lentiviral backbone containing the human synapsin 1 promoter (hSYN) to drive neuronal-specific expression of our BioID2 fusion protein (Nathanson et al., 2009). We also cloned TurboGFP into this backbone, to be used as a fluorescent reporter for transduction efficiency, followed by a self-cleaving P2A sequence to allow for bicistronic expression. Downstream of the P2A sequence, we cloned in the human OTUD7A cDNA sequence, followed by a flexible 13X GGGGS linker and then a 3XFLAG tagged BioID2 sequence, to create pLV-hSYN-TurboGFP-P2A-OTUD7A-BioID2-3XFLAG. To compare the protein interaction networks of WT OTUD7A and patient mutations, we also cloned OTUD7AN492_K494del and OTUD7AL233F into this back bone to create pLV-hSYN-TurboGFP-P2A-OTUD7AN492_K494del-BioID2-3XFLAG and pLV-hSYN-TurboGFP-P2A-OTUD7AL233F-BioID2-3XFLAG, respectively (Supplementary Fig 2a).

Previous BioID studies have used a construct expressing the BioID protein alone as a background control (Roux et al., 2012; Uezu et al., 2016). Expression of BioID alone results in non-specific proximity-dependent biotinylation, thereby providing a baseline list of proteins to compare to the BioID fusion protein interaction list. We cloned the BioID2 sequence into our lentiviral backbone to create pLV-TurboGFP-BioID2-3XFLAG. However, this does not control for potential effects of overexpressing the protein of interest in the cells. Therefore, we opted to create an additional control which contains an additional P2A sequence between OTUD7A and BioID2, to allow for separate expression of three genes: TurboGFP, OTUD7A and BioID2 (pLV-hSYN-TurboGFP-P2A-OTUD7A-P2A-BioID2-3XFLAG).

Bi-cistronic expression of the reporter gene (TurboGFP) and the BioID2-3XFlag or BioID2-3XFlag tagged OTUD7A was confirmed through western blotting of lysates from HEK 293 cells transfected with each of the constructs (Supplementary Fig 2b).

Expression of the BioID2-3XFlag also resulted in a very faint band at approximately 70kDa, indicating a slight inefficiency of P2A cleavage (Supplementary Fig 2b). In line with this, previous studies have reported an approximately 90% cleavage efficiency (Kim et al., 2011)

We proceeded to produce lentivirus using a second-generation packaging system in Lenti-X HEK 293 cells. In order to confirm neuronal expression and proximity-dependent biotinylation, primary mouse cortical neurons were transduced at DIV 14 at an equal multiplicity of infection (MOI) of 0.7. Cells were treated with 50 μ M Biotin at DIV 17 and lysed for western blotting at DIV 18. Interestingly, BioID2-3XFlag expression was much higher when expressed from the BioID2 control compared to the OTUD7A-P2A-BioID23XFLAG control (Supplementary Fig 3a). One possible reason for this could be due to the fact that the BioID2 control has one P2A sequence whereas the other overexpression control contains two P2A sequences. A study which systematically tested the effect of various 2A sequences on protein expression showed that having multiple P2A sequences in one construct can affect expression of each protein depending on its position in the construct (Liu et al., 2017). This difference was also reflected in the streptavidin blot, which showed more biotinylated proteins in the BioID2-3XFLAG control sample compared to the WTOTUD7A-P2A-BioID2-3XFlag control sample. However, enhanced protein biotinylation was observed in both the BioID2-3XFlag and

WTOTUD7A-P2A-BioID2-3XFlag control transduced neuron samples compared to the OTUD7A-BioID2-3XFlag samples, confirming proper function of the BioID2 system (Supplementary Fig 3a) (Roux et al., 2012). Confocal imaging of transduced cortical neurons revealed a punctate localization pattern for OTUD7A-BioID2-3XFlag protein in the neurites (Supplementary Fig 3c), similar to previous overexpression of a FLAG-tagged OTUD7A construct indicating that the addition of the BioID2 tag does not disrupt the localization of OTUD7A (Uddin et al., 2018). Streptavidin signal co-localized with FLAG signal, further confirming proper proximity-dependent biotinylation (Supplementary Fig 3b,c). As expected, the BioID2-3XFlag control showed more diffuse expression as well as a diffuse pattern of biotinylation (Supplementary Fig 3c), indicating non-specific biotinylation.

To validate that our BioID2 system can accurately identify known protein interactions, we decided to test it using a widely studied synaptic protein with many known protein interactors. PSD95 is a synaptic scaffold protein which is localized to dendritic spines at the post-synaptic density and interacts with a variety of receptors, scaffold proteins and cytosolic proteins (Kim et al., 2004). The BioID system has been used previously to identify protein interactors of PSD95 in the mouse brain, in which BioID-tagged PSD95 was delivered virally *in vivo* using adeno-associated virus (AAV) (Uezu et al., 2016). We cloned the mouse PSD95 cDNA sequence into our lentiviral backbone to create pLV-hSYN-TurboGFP-P2A-PSD95-BioID2-3XFLAG. Primary mouse cortical neurons were transduced at DIV 14 at an MOI of 0.7 and cells were treated with biotin at DIV 17. The next day, cells were either fixed for immunostaining or lysed for mass spectrometry

preparation (Fig 2a). Once appropriate protein expression and localization were confirmed (Supplementary Fig 3b,c), we proceeded with the PSD95-BioID2 experiment, using the BioID2 construct as a control. Due to the very specific localization of PSD95-BioID2 versus the non-specific cytosolic localization of BioID2, we hypothesized that this control would be appropriate to reduce the potential false negatives that might occur if our protein of interest was also a cytosolic protein. Following streptavidin pulldown of biotinylated proteins and identification of digested peptides via LC-MS, we obtained a list of proteins from the PSD95-BioID2 condition as well as the control BioID2 condition. To compare the hits from the PSD95-BioID2 and BioID2 control runs, as well as assign significance values to the hits, we decided to use the Significance Analysis of Interactome (SAINT) tool. SAINT was specifically designed to assign confidence scores to protein-protein interaction data generated using label-free affinity purification–mass spectrometry, and converts the label quantification for a prey protein into the probability of a true interaction between the bait and prey through modeling of probability distributions (Choi et al., 2011; Teo et al., 2014). SAINT scores range from 0-1, with 0 indicating a very unlikely interaction and 1 indicating a highly likely interaction. In a previous study, when comparing a dataset from affinity purification (AP)-mass spectrometry to known interactions for a bait, lowering the cutoff to 0.8 did not qualitatively change the level of overlap between the experimental data and the interaction database data, suggesting that a cutoff of 0.8 can reliably predict biologically relevant protein-protein interactions (Choi et al., 2011). We performed SAINT analysis from the ~ 1700-2500 identified proteins from the PSD95-BioID2 and BioID2 lists and

obtained a list of high confidence PSD95 interactors. To determine if our list of top hits comprise a high percentage of known PSD95 interactors, we compared our list to two different datasets: the BioGRID protein interaction database as well as a list of PSD95 interactors from an AAV PSD95-BioID2 study in mouse brain (Supplementary Fig4b) (Uezu et al., 2016). We progressively lowered the SAINT score to determine the lowest cutoff that produces an increase in overlap with the other lists without greatly increasing the number of unique proteins in our list (which could potentially be false positives, or newly identified PSD proteins). When we set the cutoff to 0.9, 38 were shared with the BioGRID list, 52 were shared with the AAV-PSD95 list, and 19 proteins (25%) were unique to our list. Lowering the cutoff to 0.8 did not appreciably increase the number of unique proteins but did increase the number of shared proteins, with 84 total proteins, 40 proteins shared with the BioGRID list, 54 shared with the AAV-PSD95 list and 23 (27%) being unique to our list. Similarly, lowering the SAINT score to 0.65 resulted in a list of 107 total proteins, 44 of which were shared with the BioGRID list, 59 shared with the AAV-PSD95 list and 39 (36%) being unique to our list. However, lowering the cutoff down to 0.4 resulted in only two additional shared proteins, for a total of 170 proteins, with 44 shared with the BioGRID list, 61 being shared with the AAV-PSD95 list and 101 proteins (63%) being unique to our list. It's very unlikely that more than half of our list would comprise newly identified interactors; therefore, it is more probable that many of these represent false positives. Therefore, we concluded that a SAINT score of 0.8 would result in the most accurate list of hits, and lowering to ~0.65 could potentially increase the number of real hits, but with the chance of also including some false positives. Analysis

of functional pathways using the Reactome database showed that PSD95-BioID2 hits were enriched in pathways involved in protein-protein interactions at synapses, receptor activation and trafficking and synaptic adhesion (Supplementary Fig 4c). Enriched gene ontology (GO) molecular function terms included scaffold protein binding, ion channel activity and cell adhesion (Supplementary Fig 4d). Given that our data showed a high degree of overlap with two different PSD95 interaction lists, and showed functional associations previously identified for PSD95, we moved forward with our *in vitro* culture BioID2 approach to uncover novel OTUD7A interactors.

4.3.4 Elucidation of a neuron-specific OTUD7A protein interaction network using proximity labelling proteomics

To elucidate the OTUD7A protein-protein interaction network, we applied the workflow from the PSD95-BioID2 experiment (Supplementary Fig 4a). Following protein identification, SAINT analysis was performed, using the OTUD7A-P2A-BioID2 condition as the control, due to our previous observation of higher BioID2-3XFLAG expression (Supplementary Fig3a,c). The raw spectral counts for the BioID2 control also showed that more proteins were pulled down in the BioID2 control compared to the other samples (~2200 vs ~1800), but also that the spectral counts themselves were much higher for highly abundant cytosolic proteins, which reflects a higher expression of the diffusely expressed BioID2 protein. This is especially concerning when comparing to proteins such as OTUD7A, which is localized at least partially in the cytosol and does not show a very

specialized localization when over-expressed; therefore, the expression between OTUD7A-BioID2 and the control must be as similar as possible to be able to make meaningful comparisons.

Following SAINT analysis, we identified 11 high confidence hits (SAINT score >0.8): Mical3, Kcnq2, Fam131b, Kcnb1, Palm2, Mllt4, Bai3, Itsn1, Zfyve20, Ank3 and Otud7a (Supplementary Fig 5). In order to create the most comprehensive functional protein network map possible from our dataset, we decided to include all protein hits with a SAINT score of 0.6 and above for functional network analysis, which yielded a list of 44 proteins (Table 1). We identified a highly connected interactome of postsynaptic density (PSD) and axon initial segment (AIS) proteins that were impacted by patient mutations (Fig 2a). The presence of such a large number of AIS proteins prompted us to compare our dataset to a recently published study which used BioID to map the axon initial segment (AIS), which is a dense specialized area of the axon proximal to the cell body, important for regulating neuronal excitability (Hamdan et al., 2020). Remarkably, 12 of their top AIS proteins were also present in the OTUD7A PIN, which included previously known and newly identified AIS proteins (Table 2). To determine whether the OTUD7A interactome includes known NDD-associated genes, we compared the OTUD7A PIN with the gene list from the SFARI database of high-confidence ASD risk genes. We identified 10 high-confidence category 1, 2 or syndromic SFARI genes in our list (Fig 2b, Table 3), suggesting that OTUD7A may be a part of known ASD-associated pathways.

4.3.5 Shared and Distinct Effects of de novo patient mutations on the OTUD7A PIN and functional networks

Both patient mutations showed a general decrease in the number of hits meeting our significance cutoff, with 26 in the OTUD7AN492_K494del list and 18 in the OTUD7AL233F mutation (Table 1, Fig 2a, 3a). There was a large degree of overlap between the mutation PINs and the WT OTUD7A PINs, with 14 proteins shared between all three conditions and only 1 protein unique to each of the mutations (Fig 2c). To identify functional networks enriched in the WT OTUD7A and patient mutation PINs, we used the PANTHER overrepresentation test to statistically determine which functional pathways are enriched in these datasets above a set cortical transcriptome background. Significant GO cellular component terms enriched in the WT OTUD7A list included proteins localized to the postsynaptic density, AIS, glutamate receptor complexes, voltage-gated potassium channel complexes, and the spectrin cytoskeleton, representing a high degree of membrane or cytoskeleton associated cellular compartments (Fig 2d). Thus, it is likely that OTUD7A is localized throughout the neuron in association with the plasma membrane and/or cytoskeleton, corroborating previous imaging data of an over-expressed OTUD7A construct (Yin et al., 2018). Significant biological processes included intracellular signal transduction, cytoskeleton organization, Golgi organization, neuron projection development and maintenance of synapse structure, suggesting that OTUD7A may impact diverse cellular processes throughout the neuron (Fig 2e). Both mutations showed decreased enrichment in the majority of significant GO terms.

However, AIS and spectrin-associated protein networks were uniquely impacted in the OTUD7AL233F PIN, with no changes to this network in the OTUD7AN492_K494del PIN (Fig 2d). In contrast, the regulation of golgi organization biological network was uniquely impacted in the OTUD7AN492_K494del PIN. The data indicate that mutations identified in NDD patients with different clinical presentation show shared and distinct changes in protein-protein interactions in neurons. Additionally, the data suggest that OTUD7A may play a role at the postsynaptic density and the AIS, and that OTUD7A may be uniquely impacted in each of these processes by distinct patient mutations. To directly compare the impact of the patient mutations on protein interactions, we calculated the fold change of the abundance of each protein in the list for each mutation compared to its abundance in the WT OTUD7A list (Fig 3b,c). OTUD7AN492_K494 showed a significant decrease in the abundance of five proteins (encoded by *SHANK2*, *KCNB1*, *MLLT4*, *SPTAN1* and *ANK3*), with *SHANK2* showing the greatest decrease compared to WT OTUD7A (50%) (Fig 4b). A GO over-representation test revealed that these proteins are significantly enriched in the postsynaptic membrane cellular component (Fig 3d). Protein abundances in the OTUD7AL233F sample were decreased by as much as 80% for some proteins, indicating a severe impact on protein binding (Fig 3c). It is important to note that the abundance of OTUD7A itself was significantly decreased, by about 30%, which could be due to decreased expression of the OTUD7A-BioID2 construct itself and/or reduced binding of the fusion protein to endogenous mouse OTUD7A. OTUD7AL233F showed a significant decrease in binding to 15 proteins, encoded by *MICAL3*, *KCNQ2*, *SPTAN1*, *FAM131B*, *SPTBN1*, *LPHN3*, *ANK3*, *ANK2*,

BAI3, *PALM2*, *MLLT4*, *FAM171B*, *CDC42BPA*, *PLPPR4*, *LRRC7*, and *OTUD7A* (Figure 3c). Interestingly, 10 out of these 15 proteins are known or putative AIS proteins, and a GO overrepresentation test showed that the most enriched cellular components were the AIS, followed by the spectrin-associated cytoskeleton (Fig 3d). We did not observe this pattern with the OTUD7AN492_K494 mutation, which suggests that the OTUD7AL233F mutation may significantly impact either localization of OTUD7A at the AIS or the direct binding of proteins at the AIS.

4.3.6 OTUD7A binds the ANKRD and spectrin-binding domains of ANKG and shares a common protein interaction network

To pinpoint NDD-relevant OTUD7A interactors, we compared the list of SFARI genes present in the WT OTUD7A PIN to the proteins significantly decreased in each of the patient mutation PINs. Interestingly, they converged on one protein, AnkyrinG (*ANK3*), which was shared between all three lists (Fig 3e). Therefore, we hypothesized that the interaction between AnkyrinG and OTUD7A may be an important regulator of processes relevant to neural development and NDDs. AnkyrinG is considered to be a master regulator of the AIS, coordinating the precise organization of ion channels and structural proteins (Smith & Penzes, 2018; Yang et al., 2019) Additionally, genetic variants in *ANK3* have been associated with bipolar, schizophrenia, and ASD (Bi et al., 2012; Leussis et al., 2012; Yuan et al., 2012).

We next performed a reverse BioID2 experiment by expressing an AnkyrinG-BioID2 fusion protein in mouse cortical neurons. We hypothesized that, if AnkyrinG is an OTUD7A binding partner, then AnkyrinG-BioID2 should biotinylate endogenous OTUD7A itself and/or a shared OTUD7A binding protein network. There are 3 major isoforms of AnkyrinG in the brain, with the 270kDa and 480kDa isoforms being almost completely restricted to the AIS. The smallest isoform, at 190kDa, is the only isoform that has been identified in dendritic spines (Smith et al., 2014). For this reason, as well as size restrictions of our lentiviral system, we decided to use the 190kDa isoform for our BioID2 experiment. Following validation of construct expression (Supplementary fig 6a,b), we obtained a list of 13 proteins with SAINT scores between 0.6 and 1. Eight of those proteins were shared with the OTUD7A-BioID2 protein interactome: Mical3, Ank3, Tnks1bp1, Ank2, Sptbn1, Sptan1, Kcnq2, and Palm2 (Fig 4a,c). The AnkG-190 PIN and OTUD7A PIN were both enriched in spectrin/actin cytoskeleton proteins, axonal proteins and AIS proteins (Fig 4b). We confirmed physical binding between OTUD7A and AnkyrinG-190 through over-expression in HEK293 cells (Fig 4d). We further confirmed endogenous OTUD7A and ANKG-190 binding through co-immunoprecipitation in P20 3XFlag-Otud7a mouse cortex (Fig 4e). This mouse line expresses endogenous N-terminal 3X FLAG tagged OTUD7A (Supplementary figure 7a), with OTUD7A expression peaking at P21 in the cortex (Supplementary Figure 7b). We next mapped the interaction domain of the OTUD7A/AnkyrinG interaction by overexpressing various HA-tagged AnkyrinG domains with OTUD7A-FLAG in HEK293 cells and performing co-immunoprecipitation. We determined that OTUD7A binds to the N-terminal ankyrin

repeat domain (ANKRD), as well as the spectrin binding domain, but not the C-terminal regulatory domain (Fig 4f,g). Interestingly, a previous study showed that both the ANKRD and spectrin binding domains are ubiquitinated, but that the regulatory domain is not (Yoon et al., 2020). Given OTUD7A's molecular function as a deubiquitinase, it's possible that OTUD7A may deubiquitinate ANKG's ANKRD and/or spectrin binding domain.

4.3.7 AnkyrinG protein levels and localization are altered in Df(h15q13)/+ cortical neurons

To determine how OTUD7A may regulate AnkyrinG in the mouse brain, we analyzed AnkyrinG levels in WT and Df(h15q13)/+ mouse cortical neurons via western blotting. There was a small (~20%) but significant decrease in AnkyrinG-190 levels, but no significant change in the 270kDa or 480kDa isoforms (Fig 5a,b). We also observed a significant decrease in AnkyrinG-190 levels in P14 Df(h15q13)/+ mouse cortex (Fig 4c,d). To determine how OTUD7A patient mutations affect AnkyrinG levels, we transduced Df(h15q13)/+ cortical neurons with lentiviral constructs expressing FLAG-tagged WT OTUD7A, OTUD7AN492_K494del or OTUD7AL233F and probed lysates for AnkyrinG. WT OTUD7A-FLAG, as well as both patient mutations, significantly increased levels of AnkG-270, with the WT OTUD7A-FLAG and OTUD7AN492_K494del-FLAG showing a 6-fold and 6.5-fold increase in AnkG-270 respectively, and the OTUL233F-FLAG mutation showing the lowest fold-change (FC)

of 4.3 (Fig 5f). Levels of AnkG-190 were significantly increased in neurons expressing WT OTUD7A-FLAG but were not significantly increased in neurons expressing OTUD7AN492_K494del-FLAG or OTUD7AL233F-FLAG (Fig 5g). We observed that expression of OTUD7AN492_K494del-FLAG was significantly higher than WT OTUD7A-FLAG (after normalizing for transduction efficiency), whereas levels of OTUD7AL233F-FLAG were not statistically different from WT OTUD7A-FLAG levels (Fig 5h). These data suggest that OTUD7A can regulate AnkyrinG levels in cortical neurons.

A previous study using structured illumination microscopy (SIM) imaging showed that AnkyrinG forms condense clusters (nanodomains) that are organized perisynaptically and in the spine neck (Smith et al., 2014). We decided to use SIM to analyze the precise spatial organization of AnkyrinG in the dendrites and dendritic spines of WT and Df(h15q13)/+ mouse cortical neurons (Fig 6a). Analysis of dendritic spines revealed that spine head size and mushroom spine density are decreased in Df(h15q13)/+ neurons, corroborating previous confocal microscopy morphological data from our lab (Fig 6b,c). We found that the ratio of dendritic spines expressing Ankyrin-G is decreased in Df(h15q13)/+ neurons (Fig 6d). Additionally, the number of Ankyrin-G puncta was decreased in Df(h15q13)/+ dendrites whereas the size of Ankyrin-G puncta was unchanged (Fig 6e).

4.3.8 Exogenous expression of AnkyrinG rescues synaptic phenotypes in Df(h15q13)/+ cortical neurons

Given our finding that levels of AnkyrinG-190 are lower in Df(h15q13)/+ dendrites and dendritic spines, we hypothesized that exogenous expression of AnkyrinG-190 would be able to rescue synaptic deficits in Df(h15q13)/+ neurons. Morphological analysis of DIV 14 Df(h15q13)/+ neurons expressing GFP-tagged AnkyrinG-190 showed a significant increase in dendritic tree complexity to a similar level as WT dendritic tree complexity (Fig 7a,b). Overexpression of AnkyrinG-190 in a WT background did not affect dendritic tree complexity (Fig 7a,b). Expression of AnkyrinG-190 in Df(h15q13)/+ cortical neurons also caused a significant increase in spine density, back to WT levels (Fig 7c,d). More detailed analysis of spine morphology showed that mushroom spine density was also rescued by AnkyrinG-190 expression (Fig 7f). However, stubby spine density was also significantly increased in Df(h15q13)/+ neurons (Fig 7g), suggesting that AnkyrinG-190 overexpression may be increasing spine formation non-specifically without changing spine maturation. Corroborating this, aberrant spine type proportions in Df(h15q13)/+ neurons were not rescued by AnkyrinG-190 expression (Fig 7e). Overexpression of AnkyrinG-190 in a WT background did not significantly change any of the dendritic spine parameters analyzed. Taken together, this data indicate that the effects of reduced Ankyrin G levels may be important in early processes in neuronal development, including dendritic tree formation and complexity, as well as dendritic spine formation.

4.3.9 Targeted GSK-3 inhibition with CHIR-99021 rescues neuronal bursting deficits in Df(h15q13)/+ cortical neurons

Previous studies have implicated functional interactions between AnkyrinG and the Wnt pathway. Specifically, the mood stabilizing drug lithium, which is a GSK-3 inhibitor, is able to rescue behavioural defects in Ankyrin 3 mouse models (Leussis et al., 2013; Zhu et al., 2017) Additionally, AnkyrinG has been found to regulate Wnt signaling by altering the subcellular localization of Beta-catenin, as well as by regulating phosphorylation of GSK-3 Beta (Durak et al., 2015 ; Garza et al., 2018). We hypothesized that, since Ankyrin G levels are decreased in Df(h15q13)/+ mice, inhibition of GSK-3 beta may be able to rescue synaptic deficits in this model. We used the specific GSK-3 inhibitor CHIR-99021 to treat WT and Df(h15q13)/+ mouse cortical neurons on a multi-electrode array and record neural activity over time (Fig 7h). Long-term treatment of Df(h15q13)/+ neurons with CHIR-99021 resulted in a rescue of burst frequency and network burst frequency back to WT levels, whereas CHIR-99021 had no significant effect on WT neurons (Fig 7 i,j). Interestingly, CHIR-99021 treatment caused a significant decrease in network burst duration in both WT and Df(h15q13)/+ that started just before the rescue in network burst frequency (Fig 7 k), suggesting that CHIR-99021 treatment may result in a neuronal activity pattern constituted by frequent short coordinated firing patterns.

4.4 DISCUSSION

Our study expands upon previous work which identified OTUD7A as a driver gene regulating neurodevelopmental and behavioural phenotypes in the NDD-linked 15q13.3 microdeletion (Uddin et al., 2018; Yin et al., 2018). However, the molecular mechanisms regulating the neurological phenotypes observed in individuals with this microdeletion have not been previously examined. In the present study, we used a proximity labeling proteomics method to identify a novel neuronal OTUD7A protein interactome which converged on known synaptic and NDD-associated networks. Furthermore, we validated physical binding and functional interaction with a high confidence OTUD7A protein interactor, AnkyrinG, and rescued neuronal activity deficits in a 15q13.3 microdeletion mouse model by pharmacologically targeting an AnkyrinG related pathway.

4.4.1 Persistent deficits in neural network activity in a 15q13.3 microdeletion mouse model

Previous functional studies in Df(h15q13)/+ mice have been limited to electroencephalogram (EEG) analyses using implanted multichannel electrodes in live mice. One study found that Df(h15q13)/+ mice showed decreased baseline activity of fast-spiking interneurons as well as decreased interneuron and pyramidal neuron sensitivity to an auditory stimulus (Nilsson et al., 2016). In the present study, we characterized neuronal function in the Df(h15q13)/+ mouse model using multi-electrode array (MEA) technology to analyze spontaneous neuronal activity across time in cultured cortical neurons. We discovered that Df(h15q13)/+ cortical neurons have a decreased

action potential firing rate, as well as decreased bursting and network bursting, suggesting that both neuronal activity and synaptic connectivity are affected. This is consistent with our previous report that Df(h15q13)/+ cortical neurons show an immature neuronal morphology, with less neurite complexity and decreased dendritic spines (Uddin et al., 2018), which may be associated with the decreases in activity and synaptic function. Additionally, a previous study using OTUD7A KO mice reported a decrease in spine density as well as a decrease in mEPSC frequency, suggesting that loss of OTUD7A is sufficient to cause a reduction in neuronal function (Yin et al., 2018). Additionally, multiple studies have examined neuronal activity in neurological disease models using MEAs. (Cao et al., 2012; Liu., X.S et al., 2018; Woodward et al, 2014) Additionally, patients with schizophrenia, ASD and intellectual disability have all shown decreased neural synchrony in EEG studies, which are thought to be related to cognitive deficits that are common to all three disorders (Ulhaas & Singer, 2006; Ulhaas & Singer., 2010)

4.4.2 Shared and distinct effects of patient mutations on synaptic connectivity

The first patient identified with a homozygous point mutation in OTUD7A (OTUD7A^{L233F/L233F}) was recently reported, presenting with severe global developmental delay, language impairment and epileptic encephalopathy (Garret et al., 2020). The mutation, which results in a substitution of leucine 233 to phenylalanine, is located in the catalytic domain of OTUD7A, which suggested that it would likely have an impact on protein function. We performed rescue experiments in Df(h15q13)/+ cortical neurons by

overexpressing WT OTUD7A or OTUD7AL233F and assessed neurite complexity and dendritic spine density and morphology. The OTUD7AL233F mutation was able to rescue dendritic spine deficits but not neurite complexity deficits, suggesting that this mutation may specifically affect OTUD7A protein function in processes regulating neurite formation or branching. Interestingly, previous rescue experiments using an ASD-associated non-frame shift deletion in OTUD7A (OTUD7AN492_K494del) found that it was not able to rescue neurite complexity or dendritic spine defects in Df(h15q13)/+ cortical neurons, demonstrating that different mutations in OTUD7A have both shared and distinct effects on neuronal morphology (Uddin et al., 2018). The data suggest that the heterogeneity of the 15q13.3 microdeletion clinical presentation may be partially mediated by the different roles of OTUD7A in neuronal development.

4.4.3 Identification of a novel neuronal OTUD7A protein interaction network that is impacted by patient mutations

To further understand how OTUD7A regulates neural development, and how patient mutations affect these processes, we used an unbiased proximity- labeling proteomics method, BioID2. Conventional methods of assessing binding between proteins, such as co-immunoprecipitation, require prior hypothesis-based targets, and only one or a few proteins can be tested at a time. Additionally, co-immunoprecipitation is only useful for identifying strong interactions and various lysis and wash conditions can easily disrupt protein-protein interactions in the samples. IP mass spec utilizes mass spectrometry to

identify proteins purified in an IP; however, this method still has the drawback of potentially missing weak and/or transient reactions (Morris et al., 2014). BioID has the advantage of being able to capture weak and transient interactions in their native environment (Roux et al., 2012). BioID2 is a subsequent improvement to this system, which decreased the amount of biotin supplementation needed and a flexible linker was introduced to increase the biotinylation range to 35nm (Kim et al., 2016). We developed a lentiviral BioID2 system to overexpress BioID2 fusion proteins in mature primary mouse cortical neurons. Although an endogenous BioID2-tagging system would theoretically provide the most accurate depiction of native protein-protein interactions, low expression levels of the protein could result in low yields of biotinylated proteins, making it hard to overcome background biotinylation in the cells. An extremely large number of cells would be needed to overcome this; as such, endogenous BioID has only been performed in cell lines, which can be expanded to obtain the desired number of cells (Kim et al., 2016; Liu et al., 2018; Roux et al., 2012; Youn et al., 2018). *In Vivo* proximity based proteomics using a viral expression system has been used in mice to test the widely studied synaptic protein, PSD95, and showed that there is a great deal of overlap between known PSD95 interactors and hits obtained through PSD95-BioID (Uezu et al., 2016). We also tested our system using PSD95-BioID2 and found that there was a large amount of overlap between our hits and previously identified PSD95 interactors contained in the BioGRID database of curated protein-protein interactions and in an *in vivo* PSD95-BioID study. Our results show that lentiviral delivery of BioID2 tagged proteins is a valid way to elucidate protein interaction networks in mature cultured neurons.

We used this system to identify interaction partners of WT OTUD7A, a previously published ASD-associated mutation, as well as the recently published epilepsy-associated mutation. Ten high-confidence SFARI genes were identified in the OTUD7A interactome, suggesting that OTUD7A may interact with and known ASD-associated pathways. The OTUD7A protein interactome was enriched for postsynaptic proteins, which corroborates previous imaging and morphological findings (Uddin et al., 2018; Yin et al., 2018). Surprisingly, the OTU7DA interactome was also enriched for AIS proteins, and this network of proteins was affected by the epilepsy-associated OTUD7DA mutation. The AIS is an important neuronal component which integrates synaptic inputs and generates action potentials and maintains neuronal polarity by maintaining the differential distribution of cellular components between the axonal and dendritic compartments. It is comprised of a highly ordered protein dense structure composed of ion channels and plasma membrane proteins which anchor ion channels in the AIS, making it an important regulator of neuronal excitability (Leterrier, 2018). AIS structure and/or function have never been examined in 15q13.3 microdeletion or OTUD7A models, so this result was unexpected and novel, and further study is required to determine the role of OTUD7A at the AIS. While both patient mutations affected postsynaptic protein binding to OTUD7A, the epilepsy-associated mutation uniquely affected AIS and spectrin-cytoskeleton protein binding. The shared and distinct changes in binding observed in the two mutations may also explain the shared and distinct effects of each mutation on neuronal morphology, with both mutations impacting neurite complexity, but only the ASD-associated mutation affecting dendritic spines (Uddin et al., 2018).

4.4.4 OTUD7A and AnkyrinG protein interaction networks converge on a network of spectrin cytoskeleton and axonal proteins

We identified AnkyrinG (*ANK3*) as a high-confidence OTUD7A protein interactor that is implicated in NDDs. *ANK3*, which encodes AnkyrinG, is a widely studied bipolar risk gene, as well as a category 1 ASD-associated SFARI gene. Ankyrin G is frequently referred to as the master regulator of the AIS, as depletion of AnkyrinG results in drastic changes in AIS protein composition (Hedstrom et al., 2008; Smith & Penzes, 2018). Remarkably, axons of AnkyrinG depleted neurons develop dendritic properties and express dendrite specific markers such as MAP2, highlighting the essential role of AnkyrinG in maintaining neuronal polarity (Hedstrom et al., 2008). AnkyrinG has multiple brain-expressed isoforms; of these, the 480 and 270 kDa isoforms are largely restricted to the AIS (Smith & Penzes, 2018). All three isoforms contain an N-terminal membrane-binding ankyrin repeat domain (ANKRD), a spectrin binding domain and a C-terminal regulatory domain. However, the 270 and 480 kDa isoforms contain a serine-rich domain that restricts it to the AIS, which is lacking in the 190kDa isoform (Smith & Penzes, 2018). Instead, the 190kDa isoform has been shown to be localized throughout the neuron and enriched in dendritic spines, where it regulates of dendritic spine morphology and dendrite complexity (Smith et al., 2014). Using a reverse BioID2 experiment, we discovered that OTUD7A and AnkyrinG-190 shared a protein interaction network, which were similarly enriched with spectrin/actin cytoskeleton, axonal, and AIS

proteins. The dispersed cellular compartments that comprised the top AnkyrinG-190 hits reflects the heterogenous localization of this isoform, compared to the AIS-restricted 270/480kDa isoforms. OTUD7A itself was not pulled down by AnkyrinG-BioID2 to a detectable level, which may be due to the fact that endogenous levels of OTUD7A are quite low, especially when compared to endogenous levels of AnkyrinG, which would make it easier to identify AnkyrinG in the OTUD7A-BioID2 pulldown, but not vice versa. The AnkyrinG-190 isoform is localized to dendritic spines, but rather than directly interacting with the PSD, it is localized to the perisynaptic region as well as in the spine neck, where it acts as a diffusion barrier between the spine head and dendritic shaft (Smith et al., 2014). The perisynaptic region consists of metabotropic glutamate receptors (mGluRs), dopamine D1 receptors, endocytic machinery as well as the spectrin-actin cytoskeleton (Smith & Penzes, 2018). The spectrin-actin cytoskeleton is a highly structured set of membrane associated actin filaments and spectrin tetramers, which are important for maintaining domain organization and membrane protein localization. The AIS, dendrites and dendritic spine necks are enriched with the spectrin-actin cytoskeleton (Unsain et al., 2018). We found that the OTUD7A and AnkyrinG protein interactomes were enriched for spectrin-associated cytoskeleton proteins, suggesting that they may interact at the spectrin/actin cytoskeleton in the neurites and/or dendritic spines the presynaptic region of dendritic spines and/or the spine neck.

Through co-immunoprecipitation experiments, we found that endogenous OTUD7A binds AnkyrinG-190 in P20 mouse cortex. Through domain mapping, we found that OTUD7A specifically binds the ankyrin repeat domain (ANKRD) and spectrin binding

domains of AnkyrinG, but not the C-terminal regulatory domain. The ANKRD of AnkyrinG maintains the organization of various membrane proteins, including ion channels, adhesions molecules and cytoskeletal proteins. The spectrin binding domain binds the spectrin-actin cytoskeleton, whereas the c-terminal domain extends intracellularly where it may interact with cytosolic proteins. The spectrin-binding domain was recently found to be necessary for AnkyrinG-190 targeting to dendritic spines (Smith et al., 2014). The data corroborate our BioID2 data and suggest that OTUD7A may bind to AnkyrinG at the plasma membrane and/ or the spectrin cytoskeleton, possibly in dendritic spines. Given that OTUD7A and AnkyrinG-190 protein interactomes were both enriched for AIS proteins, it is possible that OTUD7A may also exist in a complex with AnkyrinG at the AIS. Further studies are necessary to determine whether OTUD7A is localized to the AIS and to validate its binding to other AIS and axonal proteins. Additionally, a recent study found that AnkyrinG is targeted for ubiquitination at the ANKRD and spectrin binding domains, but not at the C-terminal regulatory domain (Yoon et al., 2020). Therefore, binding of OTUD7A at these ubiquitinated domains in AnkyrinG suggest that OTUD7A may de-ubiquitinate AnkyrinG at one or both of these domains. However, further studies are required to investigate the role of OTUD7A catalytic activity on AnkyrinG levels and function.

4.4.5 AnkyrinG reduction underlies synaptic deficits in 15q13.3 microdeletion mouse neurons

We discovered that AnkyrinG-190 levels are decreased in Df(h15q13)/+ cortex, and are increased in cells overexpressing WT OTUD7A, while neither OTUD7A mutant was able to increase levels of AnkyrinG-190. A previous study using SIM imaging showed that AnkyrinG forms condense clusters (nanodomains) that are organized perisynaptically and in the spine neck (Smith et al., 2014). Super-resolution imaging of cortical neurons from Df(h15q13)/+ mice revealed that the size of mushroom spine heads was decreased, and that there was a decrease in the number of AnkyrinG nanodomains in mushroom spine heads. A previous study using super-resolution imaging found that the number of AnkyrinG nanodomains positively correlates with spine head size and PSD size, suggesting that it may modulate the PSD and contribute to the abnormal spine morphology observed in Df(h15q13)/+ cortical neurons (Smith et al., 2014). Further studies are necessary to determine whether OTUD7A regulates AnkyrinG levels through its deubiquitinase activity. AnkyrinG contains multiple ubiquitination sites and is known to be regulated by the ubiquitin proteasome system (UPS). Additionally, a recent paper showed that AnkyrinG binds to and is regulated by another DUB (Usp9x) in the brain (Yoon et al., 2020).

A previous report showed that when all three isoforms of AnkyrinG were knocked down in cortical neurons, only the 190kDa was able to rescue dendritic spine morphology defects, highlighting the specific importance of this isoform in dendritic spines (Smith et al., 2014). We determined that exogenous expression of AnkyrinG-190 in Df(h15q13)/+ cortical neurons was sufficient to rescue dendrite complexity deficits in Df(h15q13)/+ neurons, whereas overexpression of AnkyrinG in WT neurons had no effect, suggesting

that reduced AnkyrinG levels resulting from OTUD7A haploinsufficiency may underlie morphological deficits in the Df(h15q13)/+ model. Spine density was also rescued with exogenous AnkyrinG expression; however, when we analyzed specific spine classes, we found that while mushroom spine density was rescued, stubby spine density was also increased above WT levels, as stubby spine density is unchanged in Df(h15q13)/+ neurons compared to WT. This suggests that while reduced AnkyrinG levels may underlie spine formation deficits in Df(h15q13)/+ neurons, it may not be the regulatory mechanism governing the changes in spine morphology and maintenance. In support of this, expression of Ankyrin G did not restore the proportions of each spine type to WT levels.

4.4.6 GSK-3 inhibition rescues persistent neural activity deficits in a 15q13.3.

microdeletion mouse model

Lithium is a widely used bipolar drug and has also been used to rescue behavioural deficits in mice with forebrain specific AnkyrinG knockout (Zhu et al., 2019). Although the exact mechanism of action of lithium is unknown, there is evidence that it directly inhibits GSK-3 through regulation of phosphorylation of Ser9 (Stambolic & Woodgett, 1994). Both lithium and the specific GSK-3 inhibitor CHIR-99021 have been shown to reverse microtubule instability observed in cells with ANK3 repression by regulating GSK3-mediated phosphorylation and inhibition of the microtubule stabilizing protein CRMP2 (Garza et al., 2018). Here, we showed that modulating a known AnkyrinG-

associated pathway rescues functional defects in mature Df(h15q13)/+ cortical neurons. Specifically, we found that chronic treatment of the specific GSK-3 inhibitor CHIR-99021 increases bursting and network bursting and bursting activity in Df(h15q13)/+ neurons back to WT levels. Interestingly, a proteomic study showed that the 190 kDa isoform of AnkyrinG becomes enriched at the PSD following treatment with lithium (Nanavati et al., 2011). Given our finding of decreased AnkyrinG in spine heads coupled with decreased dendritic spine density and altered morphology, it's possible that increased Ankyrin G in the PSD is one mechanism through which CHIR-99021 rescued functional phenotypes in Df(h15q13)/+ neurons. Overall the data show that increasing AnkyrinG levels directly or by modulating a pathway downstream of AnkyrinG is sufficient to rescue morphological and functional deficits in the Df(h15q13)/+ mouse model.

4.5 SIGNIFICANCE

This study provides the first look at the molecular mechanisms of OTUD7A in the 15q13.3 microdeletion syndrome and suggests that OTUD7A haploinsufficiency may contribute to the heterogeneity of the syndrome. We have identified the novel interaction between OTUD7A and AnkyrinG in cortical neurons and show that targeting an AnkyrinG-associated pathway rescues 15q13.3 microdeletion functional phenotypes. We demonstrate that using BioID2 in primary mouse cortical neurons is a feasible and effective method to investigate patient mutations and to identify downstream druggable target pathways. This work provides a template for early investigation of other NDD-

associated genes for which there is little to no available mechanistic data, and also lays the groundwork for further investigation of therapeutic intervention for individuals with the 15q13.3 microdeletion syndrome.

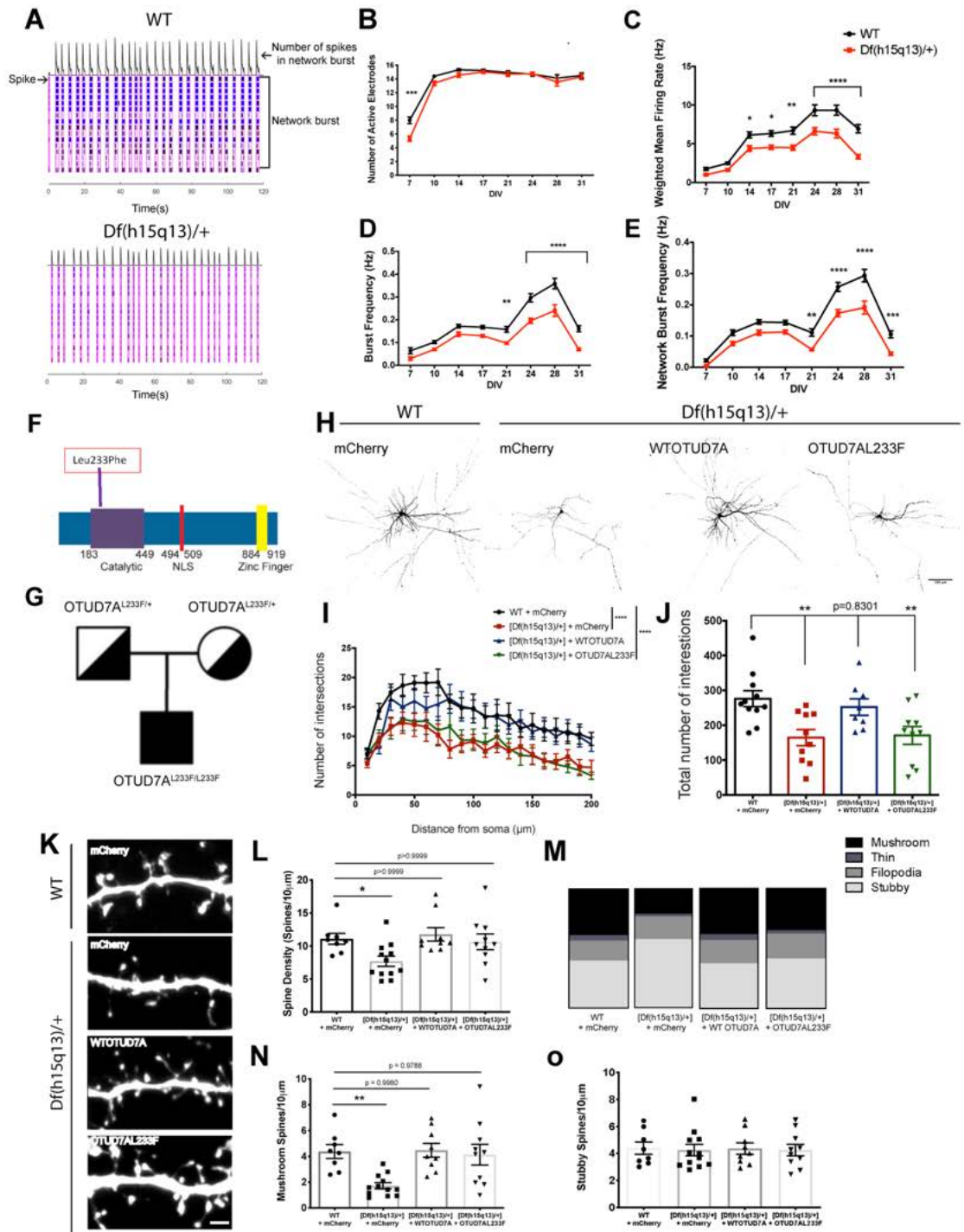


Figure 1. Persistent synaptic deficits in Df(h15q13)/+ cortical neurons. (A) Raster plot showing neural spikes over time from DIV 24 WT and Df(h15q13)/+ mouse cortical neurons on 48-well multi-electrode array (MEA) plate. (B) The number of active electrodes is decreased in Df(h15q13)/+ mouse cortical neurons at DIV 7 (*** $p < 0.001$, multiple Mann-Whitney tests). Weighted mean firing rate (C), burst frequency (D), and network burst frequency (E) are decreased in Df(h15q13)/+ across time; $n = 77$ wells WT, 65 wells Df(h15q13)/+ from 3 mouse cortical cultures on 3 MEA plates. * $p < 0.05$, ** $p < 0.01$, *** $p < 0.001$, **** $p < 0.0001$; Repeated Measures 2-Way ANOVA with Tukey's post-hoc test. (F) Schematic of human OTUD7A protein showing the location of the OTUD7AL233F patient mutation. (G) Family pedigree showing the male proband with homozygous OTUD7AL233F point mutation and his parents with heterozygous OTUD7AL233F point mutation. (H) Representative images from DIV 14 WT and Df(h15q13)/+ mouse cortical neurons co-transfected with Venus and mCherry or mCherry-tagged WT OTUD7A or OTUD7AL233F; 20X objective, scale bar 100 μm . (I) and (J) Sholl analysis shows a decrease in neurite complexity in Df(h15q13)/+ neurons compared to WT neurons. Expression of WT OTUD7A increases neurite complexity to WT levels whereas expression of OTUD7AL233F does not; $n = 8-11$ neurons from 3 mouse cultures. ** $p < 0.01$; 2-Way ANOVA with Dunnett's post-hoc test. (K) Representative images of dendritic segments from DIV 14 WT and Df(h15q13)/+ mouse cortical neurons co-transfected with Venus and mCherry or mCherry-tagged WT OTUD7A or OTUD7AL233F; 63X objective, scale bar 2 μm . (L) Dendritic spine density is decreased in Df(h15q13)/+ neurons and expression of WT OTUD7A or OTUD7AL233F increases spine density to WT levels (* $p < 0.05$, Kruskal Wallis test with Dunn's post-hoc test). (M) Expression of WT OTUD7A or OTUD7AL233F rescues altered dendritic spine proportions. (N) Mushroom spine density is decreased in Df(h15q13)/+ neurons and expression of WT OTUD7A or OTUD7AL233F increases mushroom spine density to WT levels. (O) Stubby spine density; $n = 23-32$ dendritic segments from 8-12 neurons from 3 mouse cultures. ** $p < 0.01$; One-Way ANOVA with Dunnett's post-hoc test.

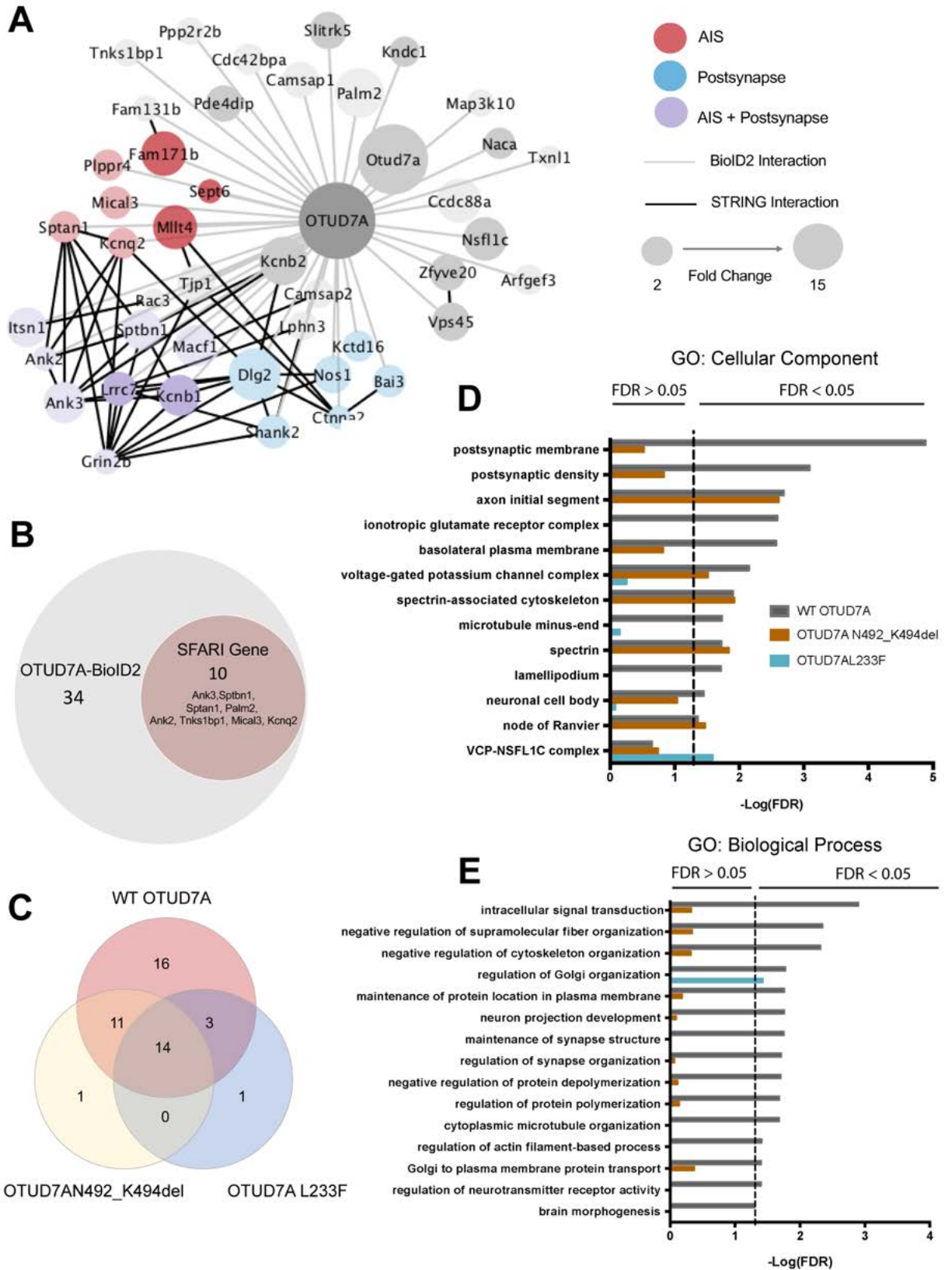


Figure 2. The OTUD7A protein-interaction network is enriched for postsynaptic and axon initial segment proteins (A) STRING analysis of functional interactions for WT OTUD7A-BioID2 proteins with SAINT scores ≥ 0.6 . Node size represents fold change in abundance compared to the OTUD7A-P2A-BioID2 control. Node colours represent AIS (including those shared with AIS-BioID2 study by Hamdan et al., 2020) : red, postsynapse: blue, and proteins that are both AIS and postsynaptic: purple. Faded nodes represent proteins that did not meet statistical significance in OTUD7AN492K_k494del and/or OTUD7AL233F BioID2 runs. Data shown are from 3 biological replicates. (B) Diagram showing 10 SFARI genes shared with OTUD7A-BioID2 hits. (C) Venn diagram of BioID2 hits with SAINT score ≥ 0.6 from WT OTUD7A-BioID2, OTUD7AN492_K494del-BioID2 and OTUD7AL233F-BioID2. (D) GO: Cellular component and (E) GO: Biological Process enrichment analysis for OTUD7A-BioID2, OTUD7AN492_K494del-BioID2 and OTUD7AL233F-BioID2 hits. Dotted line indicates FDR $p=0.05$.

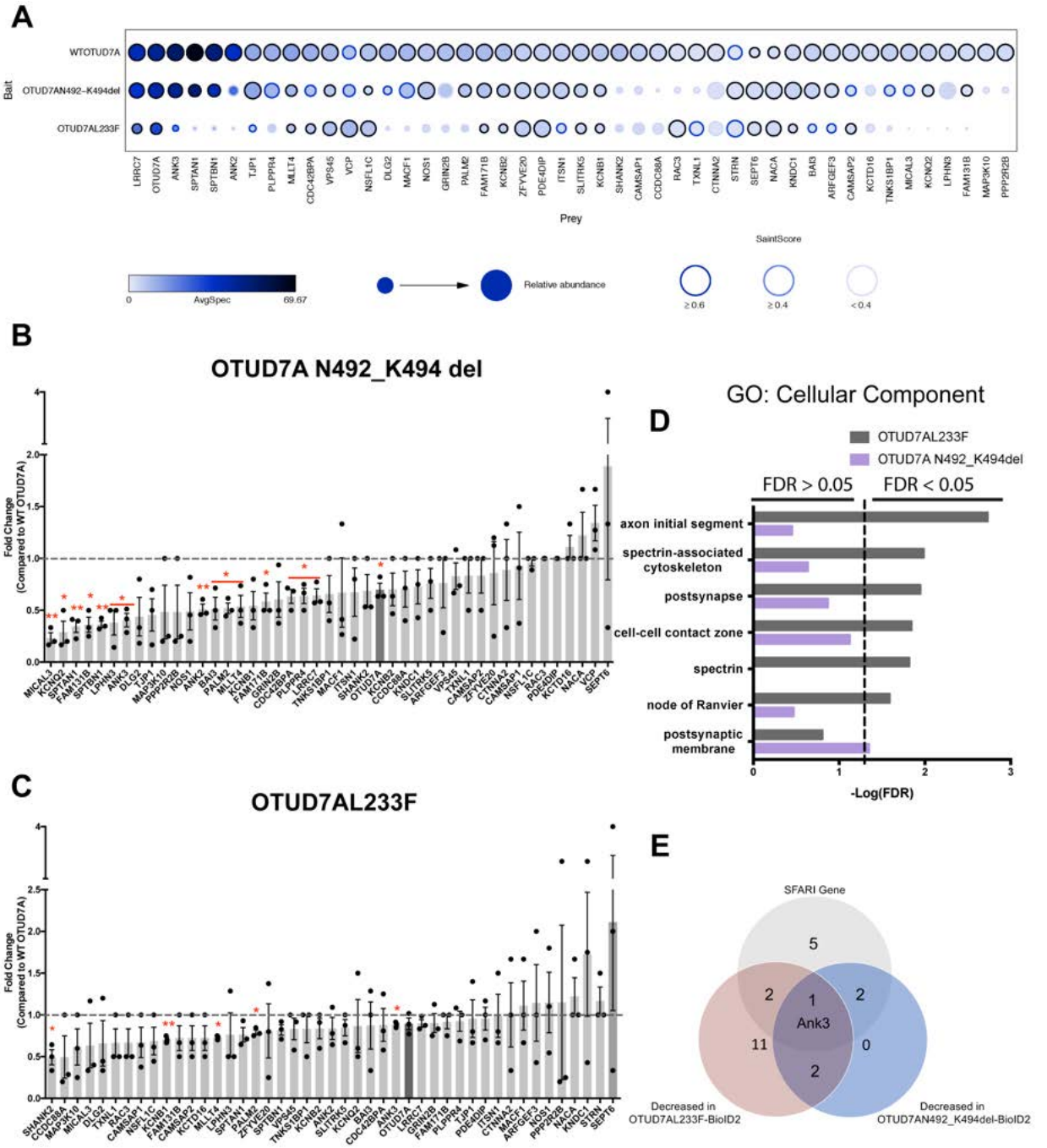


Figure 3. Effects of patient mutations on the OTUD7A protein interaction network

(A) Dotplot showing average spectral counts, relative abundance and SAINTScore of WT OTUD7A, OTUD7AN492_K494del, and OTUD7AL233F BioID2 proteins. (B) Fold change in abundance of each protein from OTUD7AN492_K494del-BioID2 (C) and OTUD7AL233F compared to its abundance in WT OTUD7A-BioID2 condition. OTUD7A shown in dark grey. * $p < 0.05$, ** $p < 0.01$, one-sample t-test compared to hypothetical mean of 1. (D) GO: Cellular component enrichment analysis for proteins with significantly decreased abundance in OTUD7AL233F-BioID and OTUD7AN492_K494del-BioID2 samples. Dotted line indicates FDR $p = 0.05$. (E) Venn diagram of proteins with significantly decreased abundance in OTUD7AL233F-BioID2 sample, significantly decreased abundance in OTUD7AN492_K494del-BioID2 sample, and SFARI genes.

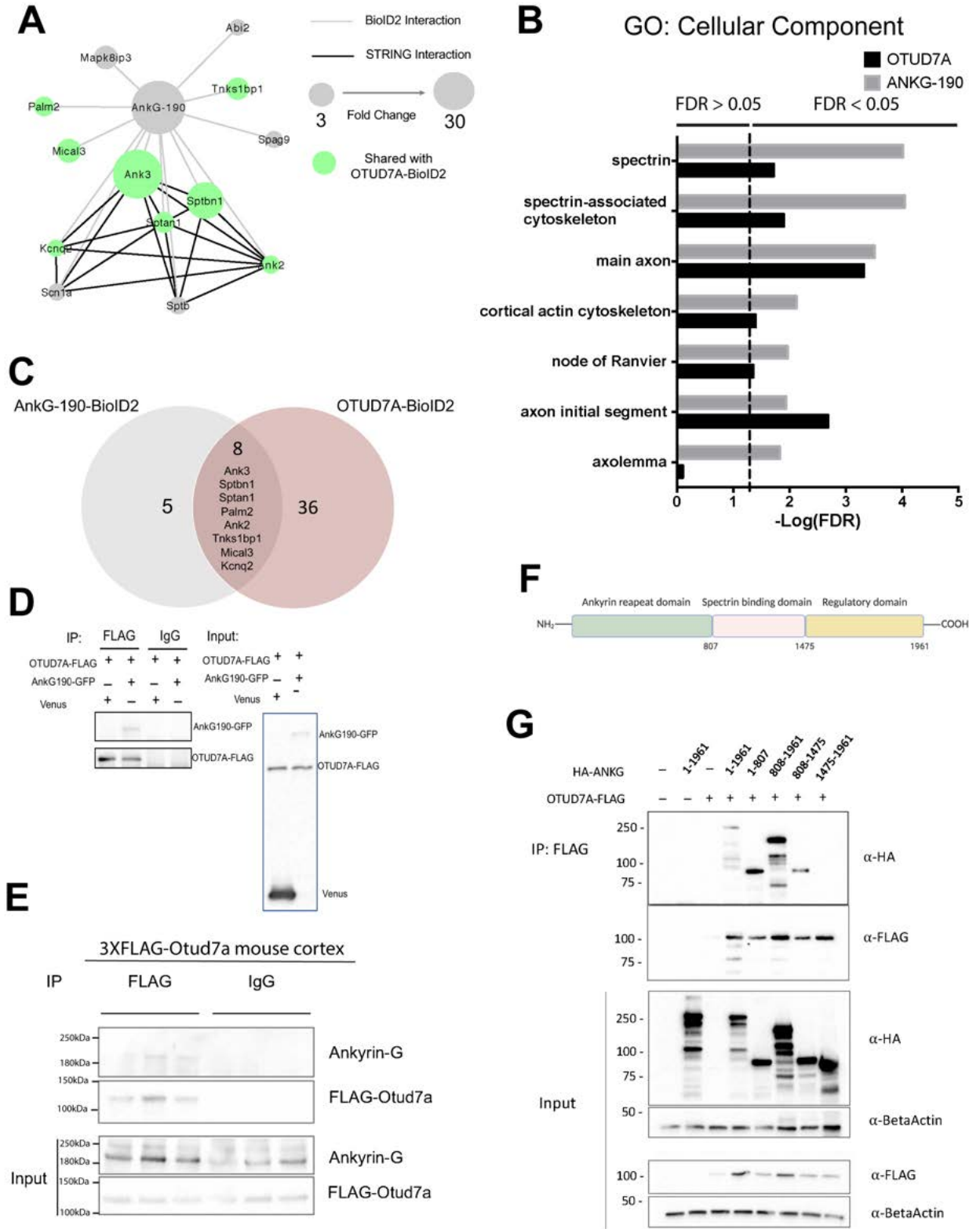


Figure 4. AnkyrinG binds OTUD7A and shares a protein interaction network (A) STRING analysis of functional networks interactions for Ankyrin-G-190-BioID2 (from 3 replicates). Nodes coloured in green represent proteins shared with the OTUD7A-BioID2 list. (B) GO: Cellular component terms enriched in AnkG-190-BioID2 list compared to WT OTUD7A-BioID2 list. (C) Venn diagram showing shared and distinct proteins from ANKG-190-BioID2 and OTUD7A-BioID2 samples. (D) Co-immunoprecipitation of OTUD7A-FLAG with AnkG-190-EGFP from co-transfected HEK293FT cells. (E) Endogenous co-immunoprecipitation of FLAG-OTUD7A with AnkyrinG-190 from mouse cortex from P20 FLAG-Otud7a mice. (F) Schematic of AnkyrinG-190 showing protein domains. (G) Domain mapping of AnkyrinG-OTUD7A interaction from co-transfected HEK293FT cells expressing HA-AnkyrinG domains and OTUD7A-FLAG.

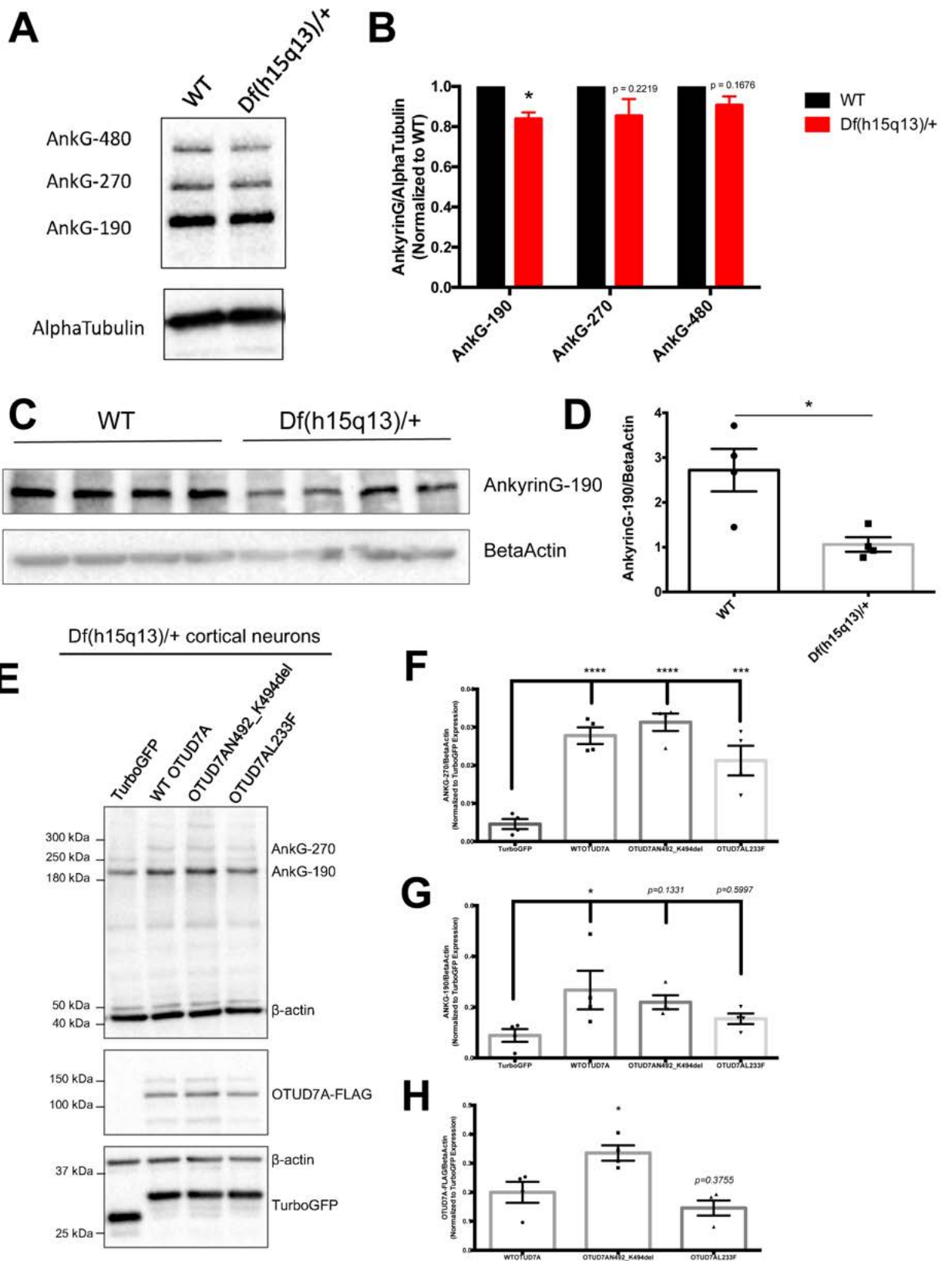


Figure 5. AnkyrinG levels are decreased in Df(h15q13)/+ neurons and are modulated by OTUD7A (A) Representative western blot and (B) protein levels of AnkyrinG isoforms in DIV 16 primary cortical neurons from WT and Df(h15q13)/+ mice.; n= 3 mouse cultures. *p<0.05; one-sample t-test. (C) Representative western blot and (D) Protein levels of AnkyrinG-190 in P14 cortex from WT and Df(h15q13)/+ mice; n=4 cortices. *p<0.05; student's t-test. (E) Representative western blot and (F) levels of AnkyrinG-270 (G) AnkyrinG-190 and (H) OTUDA-FLAG in Df(h15q13)/+ primary cortical neurons transduced with TurboGFP, WT OTUD7A or OTUD7A patient mutations; n= 3 transductions in 3 mouse cultures. *p<0.05, ***p<0.001, ****p<0.0001; One-way ANOVA with Dunnett's post-hoc test.

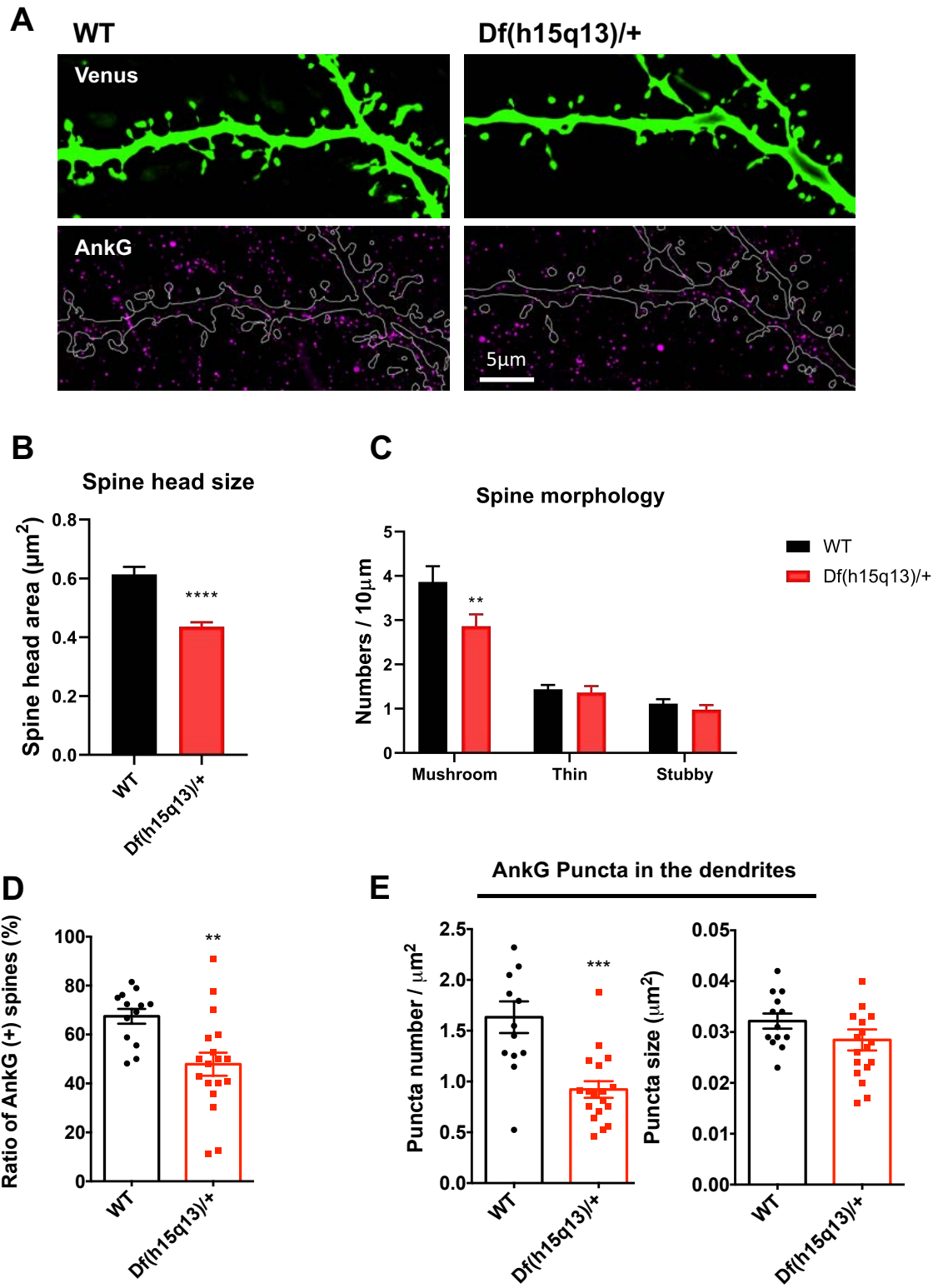


Figure 6. AnkyrinG nanodomains are decreased in the dendrites and dendric spines of Df(h15q13)/+ cortical neurons (A) Representative super-resolution images from DIV 17 WT and Df(h15q13)/+ cortical neurons; Scale bar 5 μ m. (B) Spine head size is decreased in Df(h15q13)/+ cortical neurons. (C) Mushroom spine density is decreased in Df(h15q13)/+ cortical neurons. (D) The ratio of AnkG (+) mushroom spines is decreased in Df(h15q13)/+ cortical neurons. (E) AnkG puncta number is decreased in dendritic shafts of neurons from Df(h15q13)/+ mice. AnkG puncta size is unchanged; n= 13- 18 neurons from one mouse culture. **p<0.01, ***p<0.001, ****p<0.0001; two-tailed unpaired t-test.

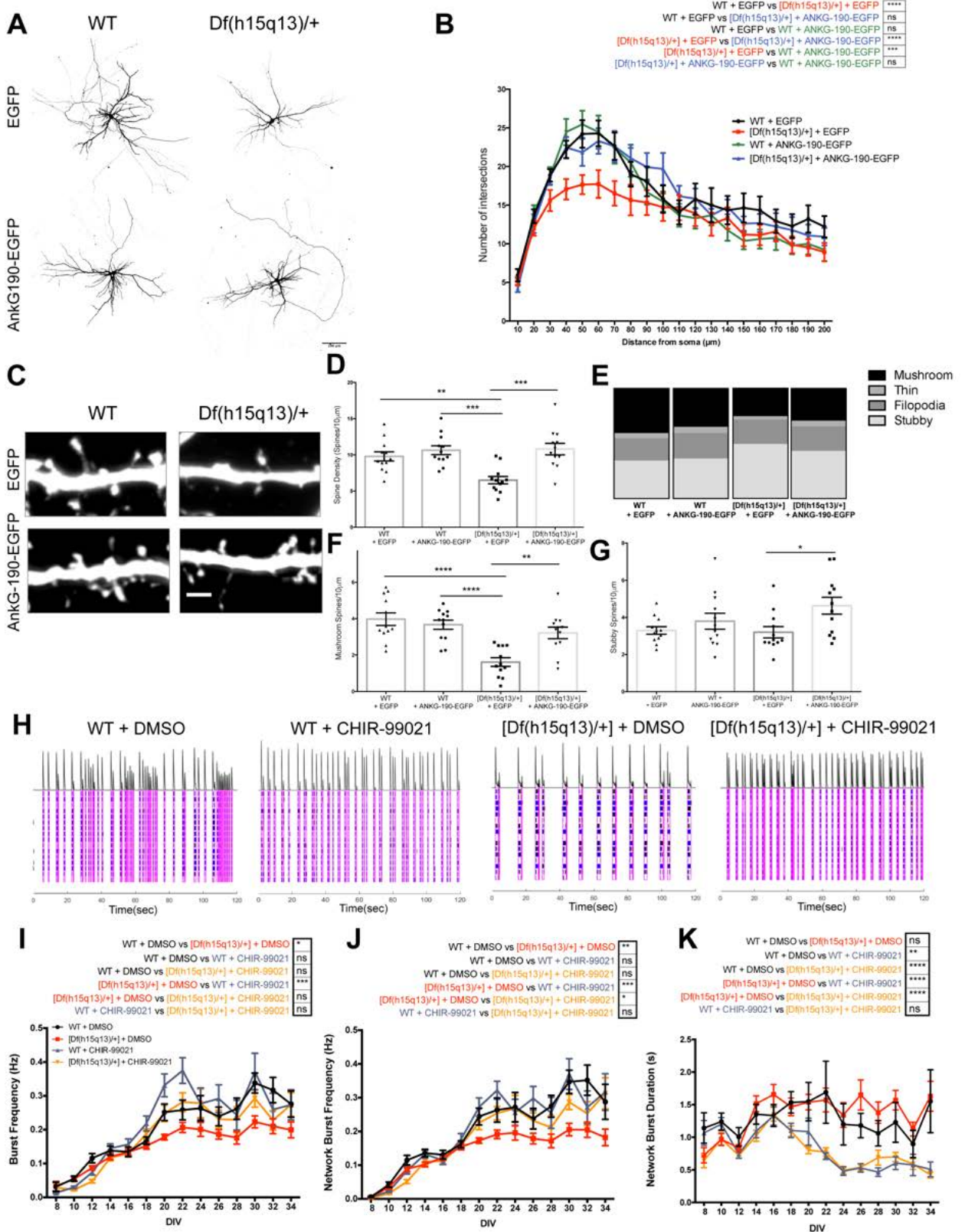


Figure 7. Rescue of synaptic phenotypes through exogenous AnkyrinG expression or targeted inhibition of GSK-3. (A) Representative images from DIV 14 WT and Df(h15q13)/+ cortical neurons co-transfected with mCherry and EGFP or AnkG-190-EGFP; 20X Objective, scale bar 100 μ m. (B) Sholl analysis shows a decrease in neurite complexity in Df(h15q13)/+ neurons compared to WT neurons. Expression of AnkG-190-EGFP increases neurite complexity to WT levels; n= 13- 15 neurons from 3 mouse cultures. ***p<0.001, ****p<0.0001; 2-Way ANOVA with Tukey's post-hoc test. (C) Representative images of dendritic segments from DIV 14 WT and Df(h15q13)/+ cortical neurons co-transfected with mCherry and EGFP or AnkG-190-EGFP; 63X Objective, scale bar 2 μ m. (D) Expression of AnkG-190-EGFP in Df(h15q13)/+ cortical neurons increases spine density to WT levels. (E) Proportions of dendritic spine types. (F) Expression of AnkG-190-EGFP increases mushroom spine density to WT levels. (G) Expression of AnkG-190-EGFP increases stubby spine density; n= 12 neurons per condition from 3 mouse cultures. *p<0.05, **p<0.01, ***p<0.001, ****p<0.0001; One-Way ANOVA with Dunnett's post-hoc test. (H) Raster plot showing neural spikes over time from DIV 30 WT and Df(h15q13)/+ mouse cortical neurons on 48-well multi-electrode array (MEA) plate treated with CHIR-99021 or DMSO vehicle control. (I) Burst Frequency (J) CHIR-99021 increases network burst frequency and decreases Network Burst duration (K) in Df(h15q13)/+ neurons. n= 21 wells WT + DMSO, 42 wells [Df(h15q13)/+] + DMSO, 24 wells WT + CHIR-99021, 40 wells [Df(h15q13)/+] + CHIR-99021 on 3 MEA plates from 3 mouse cultures, *p<0.05, **p<0.01, ***p<0.001 ****p<0.0001; Repeated Measures 2-Way ANOVA with Tukey's post-hoc test.

WT OTUD7A		OTUD7AN492_K494del		OTUD7AL233F	
Uniprot ID	Gene Name	Uniprot ID	Gene Name	Uniprot ID	Gene Name
Q80Y56	ZFYVE20	Q0KK55	KNDC1	Q8R554	OTUD7A
Q8CJ19	MICAL3	Q9Z351	KCNO2	Q01853	VCP
Q80ZF8	BAI3	Q8R554	ANK3	Q80TE7	LRRC7
G5E8K5	ANK3	Q8R554	OTUD7A	A6H8H5	KCNB2
Q8R554	OTUD7A	Q3UGY8	ARFGEF3	Q80Y56	ZFYVE20
Q8BR92	PALM2	Q8BR92	PALM2	P97390	VPS45
Q03717	KCNB1	Q9Z0R4	ITSN1	Q9CZ44	NSFL1C
Q9Z351	KCNO2	Q03717	KCNB1	Q80YT7	PDE4DIP
Q9Z0R4	ITSN1	Q9Z0J4	NOS1	P70670	NACA
Q9QZO1	MLLT4	Q9QZO1	MLLT4	Q9R1T4	SEPT6
Q3TY60	FAM131B	Q62261	SPTBN1	Q810B7	SLITRK5
Q80TS3	LPHN3	Q80TE7	LRRC7	P60764	RAC3
Q7TME0	PLPPR4	A6H8H5	KCNB2	Q03717	KCNB1
Q91XM9	DLG2	P39447	TJP1	Q14CH0	FAM171B
Q80TE7	LRRC7	Q14CH0	FAM171B	Q9QZO1	MLLT4
Q9Z0J4	NOS1	Q80YT7	PDE4DIP	Q8C1B1	CAMSAP2
Q62261	SPTBN1	P16546	SPTAN1	Q0KK55	KNDC1
Q8C8R3	ANK2	Q810B7	SLITRK5	Q3UU96	CDC42BPA
A6H8H5	KCNB2	Q80Y56	ZFYVE20		
P39447	TJP1	P97390	VPS45		
Q80Z38	SHANK2	Q9CZ44	NSFL1C		
P97390	VPS45	Q80ZF8	BAI3		
Q9CZ44	NSFL1C	P70670	NACA		
Q5SNZ0	CCDC88A	Q9R1T4	SEPT6		
Q3UU96	CDC42BPA	Q3TY60	FAM131B		
Q14CH0	FAM171B	O55106	STRN		
Q80YT7	PDE4DIP				
P16546	SPTAN1				
Q810B7	SLITRK5				
Q0KK55	KNDC1				
Q66L42	MAP3K10				
Q6ZWR4	PPP2R2B				
Q3UGY8	ARFGEF3				
Q8C1B1	CAMSAP2				
Q8CDN6	TXNL1				
P60764	RAC3				
P58871	TNKS1BP1				
P70670	NACA				
Q9QXZ0	MACF1				
A2AHC3	CAMSAP1				
Q9R1T4	SEPT6				
Q61301	CTNNA2				
Q01097	GRIN2B				
Q5DTY9	KCTD16				

Table 1. Proteins with SAINT scores ≥ 0.6 in the WT OTUD7A, OTUD7AN492_K494del, and OTUD7AL233F BioID2 datasets

**Proteins shared between OTUD7A-BioID2 and Hamdan et al., 2020
AIS-BioID**

FAM171B

MLLT4

SEPT6

LRRC7

MICAL3

ANK3

ANK2

SPTBN1

SPTAN1

PLPPR4

MACF1

ITSN1

Table 2. List of proteins shared between OTUD7A-BioID2 list of proteins with SAINT scores ≥ 0.6 and proteins identified in the Hamdan et al., 2020 AIS-BioID2 study

SFARI genes in OTUD7A-BioID2 dataset	Category
ANK3	1
KCNB1	1
GRIN2B	1
SHANK2	1
KCNQ2	2
DLG2	2
ITSN1	2
SLITRK5	2
CTNNA2	S

Table 3. Category 1, 2 and S (syndromic) SFARI genes shared with WT OTUD7A-BioID2 list of proteins with SAINT scores ≥ 0.6

4.6 SUPPLEMENTARY FIGURES

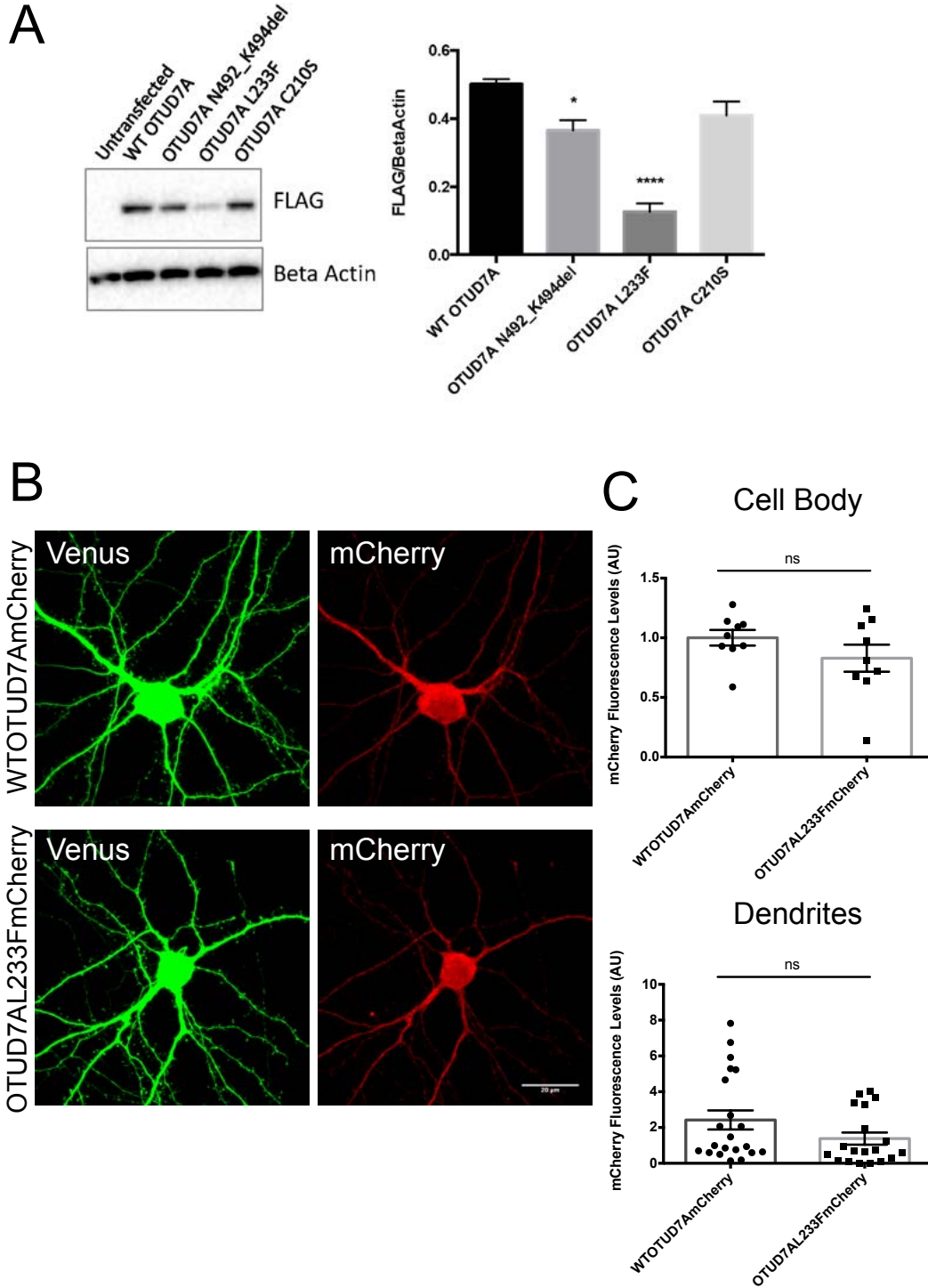


Figure S1. Analysis of overexpressed tagged OTUD7A constructs. (A) HEK293FT cells were transfected with OTUD7A-FLAG constructs and lysates were probed with antibodies against FLAG and BetaActin. OTUD7AN492_K494del and OTUD7AL233F show decreased expression compared to WT OTUD7A. n= 3 transfections. *p<0.05, ****p<0.0001; One Way ANOVA with Dunnett's post-hoc test. (B) Comparison of OTUD7A-mCherry tagged expression levels in primary mouse cortical neurons. Neurons were co-transfected at DIV 7, fixed at DIV14, and stained with anti-mCherry antibody. No significant differences in expression were observed in the cell body or dendrites. n= 9 neurons, 19-21 dendritic segments; student's t-test.

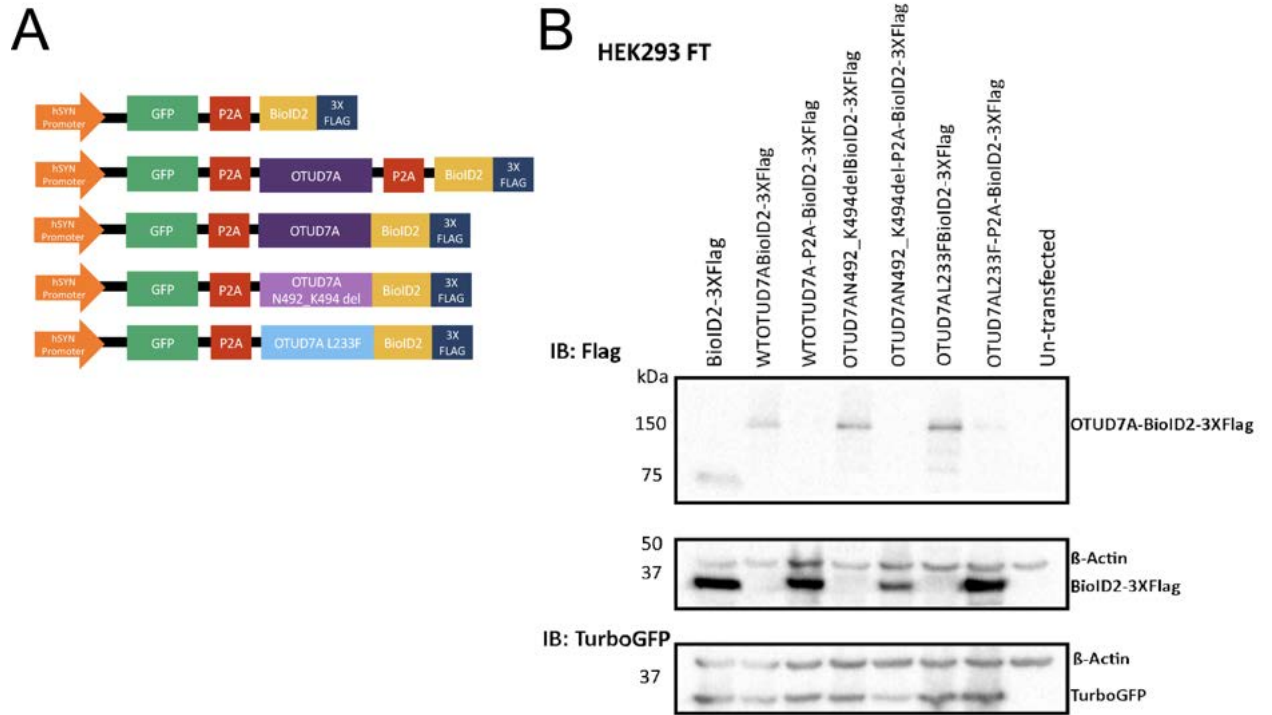


Figure S2. Validation of BioID2 constructs in HEK 293 cells. (A) Schematic of OTUD7A BioID2 constructs. (B) Western blot on protein lysates from HEK293 cells transfected with each of the indicated plasmids.

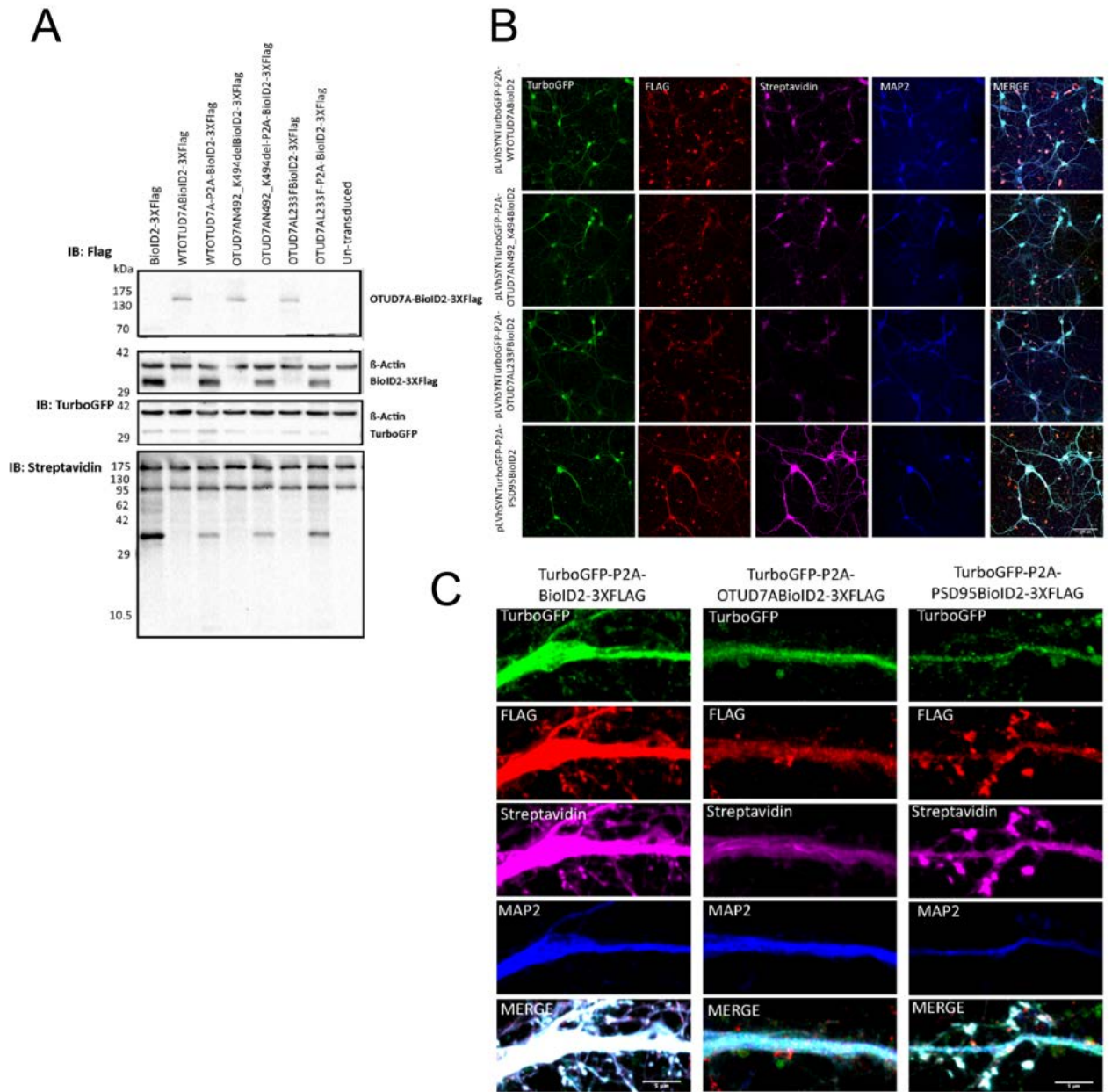


Figure S3. Validation of transduced lentiviral BioID2 construct expression and localization in neurons. Expression of BioID2 Constructs in mouse primary cortical neurons. (A) Western blot using protein lysates from Primary cortical neurons were transduced at DIV 5, followed by 50uM biotin treatment at DIV 8. Cells were then lysed and lysates were probed with antibodies against, Flag, Beta-Actin, TurboGFP and HRP-conjugated streptavidin antibody (Right). (B) and (C) Primary cortical neurons were transduced at DIV 14, followed by 50uM biotin treatment at DIV 17. Cells were fixed at DIV 18 and stained with antibodies against TurboGFP, FLAG, Streptavidin and MAP2. B) Objective 20X, Scale Bar: 100µm; C) Objective 63X, Scale Bar: 5µm.

Figure S4. PSD95-BioID2 identified known PSD95 interactors. (A) BioID2 workflow schematic. Created in Biorender.com (B) STRING analysis of functional interactions for PSD95-BioID2, showing PSD95 hits common shared with an *in vivo* PSD95-BioID study (Uezu et al., 2016) as well as with the BioGRID database for protein-protein interactions for PSD95. Sizes of circles represent SAINT score. (C) Top 10 Reactome pathways for PSD95-BioID2 hits. (D) Diagram showing PSD95-BioID2 hits falling into top GO: Molecular Function categories. Data shown are from 3 biological replicates.

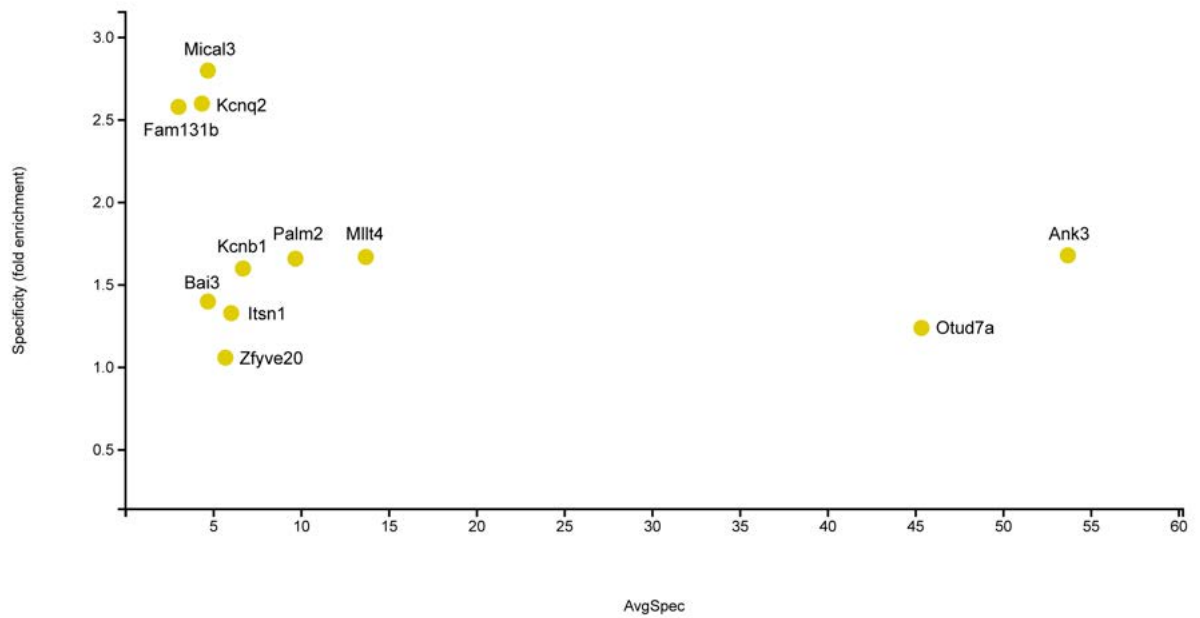


Figure S5. Top OTUD7A-BioID2 hits. (A) Specificity plot for OTUD7A-BioID2 top hits (Saint score 0.8-1) showing average spectral counts as a function of fold change compared to the OTUD7A-P2A-BioID2 control.

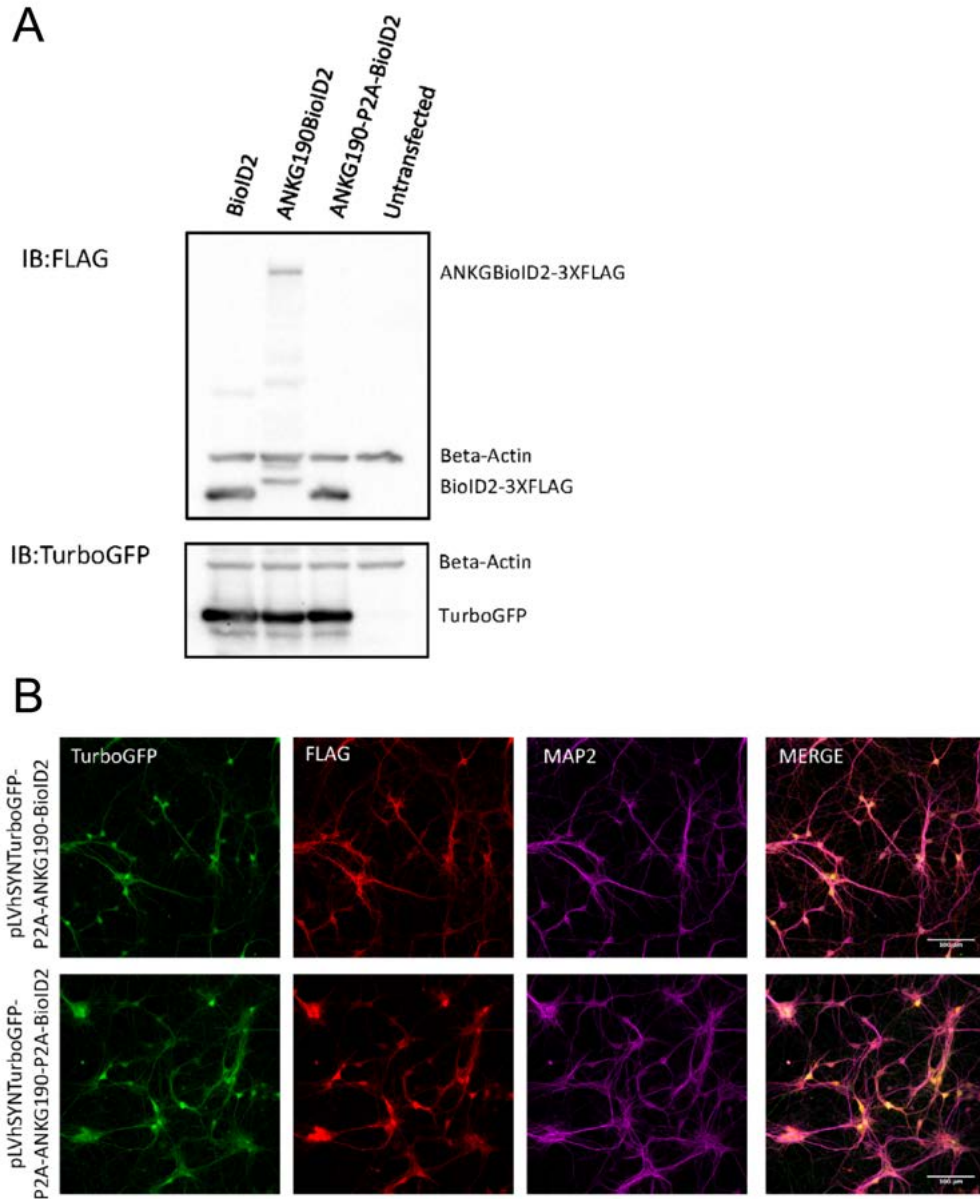


Figure S6. Validation of AnkyrinG-190-BioID2 construct expression. (A) Western blot on protein lysates from HEK293 cells transfected with each of the indicated plasmids. (B) Primary cortical neurons were transduced with the indicated constructs at DIV 5 and fixed at DIV 9. Fixed cells were stained with antibodies against TurboGFP, FLAG and MAP2. Objective 20X, Scale Bar: 100 μ m.

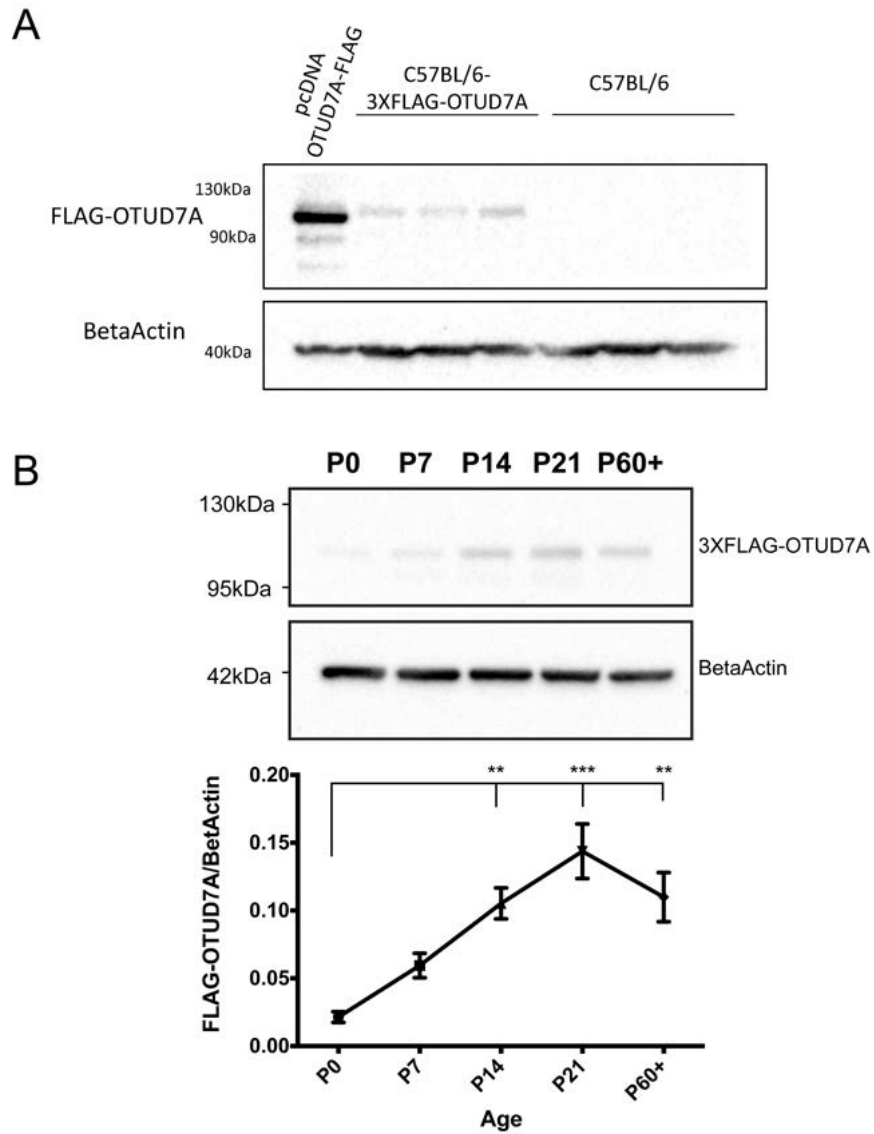


Figure S7. Endogenous OTUD7A protein expression in 3XFLAG-Otud7a mouse cortex across development. (A) Western blot on lysates from P20 3XFLAG-Otud7a and C57BL/6J mouse cortex and HEK293FT cells transfected with pcDNA-OTUD7A-FLAG. (B) Representative western blot from 3XFLAG-Otud7a mouse cortex harvested at the indicated ages. FLAG-Otud7a levels are significantly increased at P14, P21 and P60 compared to P0. N= 3 cortices per age, **p<0.01, ***p<0.001, One-Way ANOVA with Dunnett's post-hoc test.

CHAPTER 5: DISCUSSION AND FUTURE DIRECTIONS

5.1 Convergence of two Schizophrenia-linked pathways in cortical inhibitory neuron development

One of the leading hypotheses in NDD etiology is that there is an imbalance in the excitation to inhibition (E/I) ratio. Therefore, understanding the mechanisms that regulate excitatory and inhibitory development are paramount to understanding how NDDs develop. In Chapter 2 of this thesis, my aim was to investigate the physical and functional interaction between the schizophrenia (SZ)-risk genes DISC1, NRG1 and ErbB4 in cortical inhibitory neurons and to determine if the DISC1 dominant negative (DISC1-DN) mutation impacts this interaction. We discovered that the DISC1 dominant negative mutation cell-autonomously reduces excitatory synaptic contacts made onto inhibitory neurons and abolishes the NRG1-induced increase in excitatory contacts onto inhibitory neurons. There was a similar effect on inhibitory neuron dendritic tree complexity. Since the publication of our study, others have further investigated the role of DISC1 in inhibitory neuron development. For example, investigation of a heterozygous DISC1 locus impairment model (DISC1-LI), in which the majority of DISC1 isoforms are abolished, showed dysregulation of fast-spiking parvalbumin positive (PV) interneurons (INs) (Delevich et al., 2020). Specifically, they found reduced miniature inhibitory postsynaptic currents (mIPSCs) onto L2/3 pyramidal neurons in the medial prefrontal cortex (mPFC) from both juvenile and adult mice which was mediated by reduced GABA

release from PV+ INs onto L2/3 Pyramidal neurons. Interestingly, miniature excitatory postsynaptic currents (mEPSCs) recorded from L2/3 pyramidal neurons were unchanged in the DISC-LI model, suggesting that the effects of reduced DISC1 expression in this model mainly affect inhibitory transmission. Further, they found that feedforward inhibition was reduced in the mPFC which was not caused by reduced excitatory drive from inputs onto PV+ INs from the thalamus (Delevich et al., 2020). Overall this study suggests that heterozygous loss of DISC1 severely impairs PV interneurons in early development and this extends into adulthood. In another study, DOX-inducible DISC-DN mice were used to express DISC1-DN during embryonic development specifically in NPCs (Nes-DN-DISC1). Remarkably, increased anxiety-like behaviours and chronic stress-induced depression were observed in 2 month old mice, implicating a critical period for proper DISC1 function (Deng et al., 2017). Although there were no changes in overall cortical cell density, the distribution of GABA-ergic inhibitory neuron subtypes were altered in the cortex. Interestingly, they found a decrease in progenitor proliferation in the medial ganglion eminence (MGE), which is the main site of inhibitory neuron precursor proliferation, suggesting that early changes in inhibitory neuron development may lead to behavioural changes in adult mice with the DISC1-DN mutation (Deng et al., 2017). Overall, newer studies investigating the role of DISC1 in inhibitory neuron development corroborate our findings of aberrant inhibitory neuron development in neurons with DISC1 knockdown or expression of DISC1-DN.

Although previous studies identified a functional relationship between DISC1 and NRG1-ErbB4 signaling, they did not investigate whether ErbB4 and DISC1 physically interact in

inhibitory neurons (Seshadri et al., 2015). To answer this question, we analyzed endogenous ErbB4-DISC1 binding in GAD67-GFP positive inhibitory neurons using the proximity ligation assay (PLA). We discovered the novel physical interaction between DISC1 and ErbB4 in cortical inhibitory neurons, which was increased upon NRG1-treatment. This finding showed that DISC1 and ErbB4 exist in a complex in inhibitory neurons, and that this binding is increased upon activation of ErbB4 by NRG1. However, we did not investigate the direct downstream molecular consequence of this binding. It has been previously shown that ErbB4 is expressed in inhibitory neurons at both inhibitory and excitatory postsynaptic sites, where it co-localizes with VGAT and VGLUT1, respectively (Krivosheya et al., 2008). Therefore, it's possible that binding of ErbB4 to DISC1 following NRG1 stimulation brings DISC1 into contact with postsynaptic sites. This is supported by our finding that NRG1 stimulation increases co-localization of VGLUT1 and DISC1 in inhibitory neurons. Additionally, newer techniques such as proximity-labeling proteomics coupled with cell-type specific expression constructs can be used to further explore the DISC1 and/or ErbB4 interactome in inhibitory neurons and uncover other interacting pathways, as well as impacts of the DISC1 dominant negative mutation.

Recent studies using human iPSC models have replicated findings from DISC1 mouse models and have identified new DISC1 interactions and mechanisms (Srikanth et al., 2015; Srikanth et al., 2018; Ye et al., 2017). Remarkably, a recent study using brain organoids derived from isogenic human iPSC lines with a DISC1 mutation showed altered organoid morphology and decreased expression of inhibitory genes such as

CALB2 (calretinin), GAD1, GAD2 and VGAT, as well as altered expression of NRG1 (Srikanth et al., 2018). Interestingly, NRG1 expression was significantly increased in Day 19 brain organoids but was significantly decreased in 2-D monolayer cultures from DISC1 mutant cells, highlighting the importance of using a 3-D system for studying brain development (Srikanth et al., 2018).

Studying the molecular mechanisms of known SZ risk genes can help inform pre-clinical studies, by helping to delineate the mechanism of action of new or repurposed drugs to treat individuals with schizophrenia. The NRG1-ErbB4 pathway has long been touted as a potential druggable pathway in SZ treatment, largely due to human studies showing increased NRG1-ErbB4 expression in SZ patient brains and NRG1 overexpression mouse models showing a SZ-related behavioural phenotype (Joshi et al., 2014; Mei & Nave, 2014; Papaleo et al., 2016). A recent pre-clinical study applied a drug repurposing strategy by screening a compound library of approved drugs that cause changes in NRG1-ERBB4 signaling and identified the drug spironolactone. They found that Nrg1 transgenic mice showed improvements in positive symptoms and working memory as well as increased spontaneous inhibitory postsynaptic currents following treatment with spironolactone (Wehr et al., 2017). A human clinical trial is currently underway to test the effects of spironolactone on cognition in SZ patients (Hasan et al. 2020).

Overall, the work presented in Chapter 2 identified the convergence of two high-confidence SZ-risk genes in cortical inhibitory neuron development, and recent research has corroborated and extended our findings. These results extend our understanding of molecular mechanisms governing cortical inhibitory neuron development and reveal how

different risk genes interact at the molecular level to produce phenotypes relevant to SZ pathophysiology.

5.2 Identifying Synaptic Phenotypes in a mouse model of the 15q13.3 Microdeletion

CNVs represent a significant proportion of risk for NDDs, including ASD, ID, DD, SZ and epilepsy, with inherited and *de novo* CNVs estimated to cause 15% of cases of NDDs (Wilfert et al., 2017). In Chapter 3 of my thesis, my aims were to (1) characterize cellular phenotypes in a heterozygous 15q13.3 microdeletion mouse model (Df(h15q13)/+) and to (2) identify disease-driving genes using a more unbiased genomic approach. The experiments in this study were divided equally between myself and Dr. Mohammed Uddin from Dr. Stephen Scherer's lab (SickKids Hospital, Toronto, CA), based on each of our labs' expertise. Dr. Stephen Scherer is a pioneer in the field of ASD genetics, sequencing and bioinformatics, whereas our lab has expertise in cellular and molecular biology. For the first part of this aim, we started with an unbiased omics approach to determine broad pathways that are affected in the Df(h15q13)/+ mouse model by performing RNA sequencing of WT and Df(h15q13)/+ mouse cortex at three developmental time points (E16, P21, Adult). We found that differential gene expression was most pronounced at postnatal timepoints, and that the differentially expressed genes (DEGs) were significantly enriched in forebrain development and cation transmembrane transport. One of the caveats of this experiment was that only two mice per genotype were used for each time point, leading to high levels of variability which can explain the low number of DEGs meeting statistical significance (21-29 per timepoint, 66 genes in

total). Therefore, a similar temporal RNA sequencing study with a larger sample size can be completed in the future to obtain a more comprehensive dataset of DEGs. A recent study performed RNA sequencing on samples from Df(h15q13)/+ cortex and found that DEGs were enriched in astrocytes, implicating glial cell alterations in the 15q13.3 microdeletion (Al-Absi, et al., 2020).

We focused on investigating cellular morphological phenotypes in cortical pyramidal neurons and found that dendritic tree complexity was reduced in Df(h15q13)/+ neurons *in vitro* as well as in Layer 2/3 cortical pyramidal neurons in brain slices of P28 mice. We also found that dendritic spine formation was decreased and that there was a shift in morphological classes of spines, with a decrease in mushroom spines and an increase in stubby spines. These results suggested that Df(h15q13)/+ neurons show an overall immature neuronal morphological phenotype. A recent study from another group also corroborated these findings in the Df(h15q13)/+ model (Al-absi, et al.). Dendritic spines go through an initial period of dendritic spine formation and growth, followed by a period of synaptic pruning, and the precise timing of these events are tied to critical periods during neural development. One report analyzed dendritic density across time from P14 to adulthood in a mouse model heterozygous for the ASD risk gene SYNGAP1 and discovered accelerated spine formation and premature pruning in cortical neurons (Aceti et al., 2014). Therefore, analysis of a snapshot of dendritic spine development does not encompass the dynamic nature of dendritic spine development. Thus, it is important to analyze the trajectory of synaptic phenotypes across development, which is an avenue for future research.

To follow up on our discovery of synaptic changes in Df(h15q13)/+ microdeletion cortical neurons, we examined whether these changes correlate with functional changes in neural activity. These results are presented in Chapter 4 of this thesis. We used multi-electrode arrays (MEAs) to measure spontaneous population level neuronal activity in WT and Df(h15q13)/+ cortical neuron cultures across time. We observed significant decreases in neuronal activity, excitability and synaptic connectivity. Interestingly, the timing of the start of these functional phenotypes align with the peak of OTUD7A expression in the mouse brain, as well as with the decreased dendritic tree complexity and dendritic spines in cortical cultures, which we observed at DIV 14 *in vitro*. Patch clamp electrophysiology is the gold standard for measuring neuronal activity, and changes in neuronal activity in individual cells with or without the presence of network activity can be parsed and evaluated to determine whether pre-or postsynaptic events are the likely cause of these changes. In the study by Yin et al. (2018), patch-clamp electrophysiology recordings revealed that OTUD7A KO mice shows a decreased in miniature excitatory postsynaptic current (mEPSC) frequency, which is typically correlated with a decrease in presynaptic release or numbers of functional synapses. However, because mEPSCs are recorded without the presence of network activity (in the presence of a sodium channel blocker), these results cannot be directly compared to our MEA results from the Df(h15q13)/+ neurons. Therefore, further experiments using patch-clamp electrophysiology remain to be performed to assess in more detail the functional consequences of the 15q13.3 microdeletion.

5.3 A multimodal approach to Pinpointing disease-driving genes in the 15q13.3

Microdeletion

One of the main challenges in studying CNVs is understanding how individual genes contribute to the development and heterogeneity of NDDs. Therefore, we devised a concurrent approach in which we characterized cellular and synaptic phenotypes in Df(h15q13)/+ mice while Dr. Uddin (SickKids Hospital, Toronto, CA) utilized human whole exome sequencing (WES) data and bioinformatic methods to pinpoint phenotypically relevant genes. Our analyses converged in order to test the role of putative driver genes in cellular phenotypes relevant to the Df(h15q13)/+ model. While other CNV studies have typically utilized one method or the other (cellular biology or genomics), our collaboration with Dr. Stephen Scherer's lab allowed us to develop a streamlined workflow to identify and test putative disease-driving genes relevant to the 15q13.3 microdeletion.

To identify disease-driving genes, we applied three complementary approaches: (1) identification of smaller nested deletions, (2) analysis of WGS and WES to identify *de novo* mutations in individual genes and (3) assessment of brain-critical exons. Only one gene, *OTUD7A*, stood out in all three of these approaches. Notably, analysis of control and ASD microarray data showed that, whereas *CHRNA7* was encompassed in nested deletions in both case and control samples, deletions encompassing *OTUD7A* were only present in case samples, suggesting that it may be more relevant to clinical outcomes. Further, we identified three *de novo* mutations in *OTUD7A*, including one exonic 9bp

non-frameshift deletion in an ASD proband and affected sibling (OTUD7A N492_K494del). Additionally, OTUD7A was the only microdeletion gene with brain-specific expression as well as a low population level mutational burden, earmarking it as critical for brain function (Uddin et al., 2014). This was the first evidence of a potential role for OTUD7A in the 15q13.3 microdeletion, and there was no prior literature on the role of OTUD7A in the brain. Although OTUD7A is expressed in the brain, no studies had examined its localization in neurons. We analyzed subcellular localization of OTUD7A in cortical neurons with an overexpressed FLAG tagged OTUD7A construct and found that while it was expressed throughout the neuron, it showed co-localization with PSD95 at dendritic spines. Our results were also corroborated by a companion study that was co-published with our study in AJHG (Yin et al., 2018). This suggested that OTUD7A may play a role at the postsynaptic density in dendritic spines. However, we were limited to over-expression of OTUD7A instead of analyzing endogenous expression due to a lack of available antibodies showing specificity to OTUD7A in mouse cortical samples. Mislocalization can occur with overexpression of tagged proteins, and the levels of overexpression cannot be effectively controlled with transfection methods (Gibson et al., 2013). Therefore, it will be important to examine endogenous localization of OTUD7A in neurons.

With our newfound knowledge of clearly defined cellular phenotypes in our Df(h15q13)/+ microdeletion mouse model, we decided to investigate if OTUD7A plays a role in regulating these phenotypes. Remarkably, re-expression of individual 15q13.3 genes (OTUD7A, KLF13, FAN1 or CHRNA7) showed that OTUD7A was the only gene

that was sufficient to rescue dendritic spine phenotypes. However, expression of CHRNA7 or OTUD7A was sufficient to rescue dendritic tree complexity phenotypes. This provided the first evidence of shared and distinct roles of CHRNA7 and OTUD7A in neurological phenotypes relevant to the 15q13.3 microdeletion. Interestingly, we found that CHRNA7 and OTUD7A have inverse developmental expression timelines, with CHRNA7 decreasing from infancy to adulthood and OTUD7A increasing from infancy to adulthood. Therefore, it's possible that CHRNA7 and OTUD7A play a role in neurodevelopmental processes at different developmental stages. This can be further investigated by creating an inducible system to knockdown expression of CHRNA7 or OTUD7A at various developmental timepoint and to elucidate the role of each gene during distinct developmental critical periods.

One of the theories in CNV research is that the effects of gene dosage alterations of multiple genes in a CNV, when added together, give rise to the clinical phenotype. In fact, many studies have reported multiple disease-driving genes within a CNV; for example, ZDHHC8 and Dgcr8 have both been shown to play important roles in the 22q11.2 microdeletion (Forstner et al., 2013; Mukai et al., 2008). In our study, we did not examine the potential of combined effects between combinations of genes in the 15q13.3 microdeletion region. In order to investigate this, rescue experiments can be performed with co-transfection of two or more genes in various combinations.

Alternatively, CRISPR-Cas9 can be used to knockout various combinations of genes and phenotypes can be compared to those seen in the Df(h15q13)/+ mouse model. One of the limitations of using over-expression for rescue experiments is the lack of control of gene

expression levels (Gibson et al., 2013). CRISPR activation (CRISPRa) is a modified CRISPR CAS9 system that uses an enzymatically inactive (dead) CAS9 protein (dCAS9) coupled with transcriptional activators to promote targeted activation of genes.

Conversely, CRISPR repression (CRISPRi) uses a transcriptional repressor to downregulate gene expression (Gilbert et al., 2014). In a proof of principle study, Dr. Kristen Brennand's lab discovered that using various guide RNAs (gRNAs) and/or multiplexing combinations of gRNAs for various NDD-linked genes results in varying levels of gene expression, allowing for the potential of fine-tuning gene expression to the desired level (Ho et al. 2017). This is especially useful in rescue experiments in heterozygous models, where a two-fold increase in gene expression is generally desired.

A landmark paper published in 2019 showed that *in vivo* activation using CRISPRa rescued obesity phenotypes in a *Sim1* haploinsufficiency model, marking the first use of CRISPRa to rescue clinically relevant phenotypes *in vivo* (Matharu et al., 2019). These exciting results suggest that CRISPRs technology can be extended to NDD-linked CNV haploinsufficiency models, to identify disease-driving genes. Multiplexing of CRISPRa target genes can also shed light on potential additive effects of multiple genes in CNVs. Additionally, it provides evidence of the potential for future gene therapy approaches for rescuing clinically relevant phenotypes in individuals with CNV related disorders.

A companion study was co-published with our study in *AJHG* in 2018 (Yin et al., 2018) which examined cellular and behavioural deficits in a novel *Otud7a* mouse model.

Otud7a KO mice recapitulated the decrease in dendritic spine density observed in the *Df(h15q13)/+* model (Yin et al., 2018). They subjected *Otud7a* HET and KO mice to a

battery of ASD, SZ and epilepsy related behavioural tests. While HET mice displayed mild to no changes in behavioural phenotypes, *Otud7a* KO mice recapitulated behavioural phenotypes observed in homozygous *Df(h15q13)*⁻ mice, including impaired acoustic startle, ultrasonic vocalizations and increased seizure susceptibility (Forsingdal et al., 2014; Yin et al., 2018). The lack of significant behavioural changes in *Otud7a* HET mice suggests that haploinsufficiency of *Otud7a* alone may not be sufficient to recapitulate clinically relevant phenotypes in the 15q13.3 microdeletion syndrome. However, because they did not investigate cellular phenotypes in *Otud7a* HET mice, it is unknown whether haploinsufficiency of *Otud7a* alone is sufficient to produce cellular and synaptic phenotypes that we observed in *Df(h15q13)*⁺ mice.

5.4 Pleiotropy as a mechanism of CNV Expression in the 15q13.3 Microdeletion

One of the theories in CNV research is the idea that the effects of one or a few genes in a CNV underlie the heterogeneity of clinical phenotypes, rather than the additive effect of all genes in the CNV. Pleiotropy is also thought to underlie the observation that mutations in the same gene can lead to heterogenous clinical outcomes. This is thought to be carried out at the molecular level, where individual genes converge on multiple signaling pathways. In chapter 4 of this thesis, I detailed experiments which uncovered pleiotropic effects of the 15q13.3 microdeletion syndrome gene *OTUD7A* through the use of proximity-labeling proteomics and mutation analysis.

5.4.1 A novel OTUD7A protein interactome at the postsynaptic density and the axon initial segment

We used the proximity proteomics labeling technique BioID2 to investigate the protein-interaction network (PIN) of OTUD7A in mature cortical neurons. We discovered that OTUD7A interacts with proteins involved in major neurodevelopmental processes such as intracellular signal transduction, cytoskeleton organization, neuron projection development and maintenance of synapse structure. Additionally, OTUD7A interacts with proteins that were localized to the postsynaptic density (PSD), axon initial segment (AIS) and the spectrin cytoskeleton. Consistent with OTUD7A imaging experiments (Chapter 3), this suggests that OTUD7A has broad localization throughout the neuron but is also localized to more specific compartments such as the PSD. The enrichment of AIS and spectrin cytoskeleton proteins is novel and suggests that OTUD7A may play a role in neuronal compartments that are enriched with the spectrin-actin cytoskeleton, such as the perisynaptic compartment of dendritic spines, the axon and the AIS. Overall, the data suggest that OTUD7A may play a role in a heterogenous set of neuronal processes, which may have distinct roles in pathophysiology of different NDDs. These data also provided the first evidence of putative localization of OTUD7A at the axon and the AIS.

From the work outlined in Chapter 3 of this thesis, we have evidence to suggest that OTUD7A regulates dendritic spines, corroborating its binding to PSD proteins. However, we have not examined axonal or AIS phenotypes in the Df(h15q13)/+ microdeletion model. The AIS serves a critical role in regulation of the intrinsic electrical properties of neurons and is the site of action potential initiation. Our findings from MEA recordings of

spontaneous firing from Df(h15q13)/+ cortical neurons can also potentially be explained by changes in the AIS, as spontaneous recordings are influenced by intrinsic excitability, which is regulated by the AIS (Lezmy et al., 2017; Meza et al., 2018). The study by Yin et al., (2018) found that mEPSC frequency was decreased in Otud7a KO mice whereas an in vitro ANK3 study found decreased mEPSC amplitude, suggesting that synaptic connectivity is altered in both models, which could potentially be partially mediated by changes at the AIS (Smith et al., 2014). Previous studies have observed differences in the length, location and integrity of the AIS in NDD models (Hsu et al., 2014; Wimmer et al., 2010). Therefore, investigation of AIS deficits in the 15q13.3 microdeletion remains an important area of study in the future.

5.4.2 Studying NDD-associated mutations to understand clinical heterogeneity

We utilized the BioID2 system to examine the effects of two distinct mutations on the OTUD7A PIN. The OTUD7AN492_494del was identified in an ASD proband and affected sibling, whereas the OTUD7AL233F mutation was identified in a child with infantile seizures and learning difficulties (Uddin et al., 2018; Garret et al., 2020). However, due to the age of the child at clinical diagnosis (~2 years of age), we cannot preclude the possibility that this child may develop other NDDs later in life. We found that although both OTUD7A mutation PINs showed decreased enrichment of similar pathways such as ionotropic glutamate receptor complexes, they also showed specific differences. Proteins that were significantly reduced in the epilepsy mutation PIN were enriched in AIS, spectrin cytoskeletal and postsynaptic compartments, whereas

enrichment was observed only in the postsynaptic compartments in the ASD mutation PIN. These results can also provide a molecular basis for the observed differences in these mutations on synaptic pathology in the Df(h15q13)/+ mouse model. It is possible that each of these mutations may be localized to distinct neuron compartments and/or affect distinct molecular processes in neuronal development, leading to distinct synaptic defects. The effect of each of these mutations on the AIS can be investigated in future rescue experiments in 15q13.3 microdeletion models. Additionally, the results from studying patient mutation protein interaction networks may provide a way of potentially molecular categorizing various patient mutations. Notably, a large proportion of epilepsy risk genes are involved in the axon/AIS whereas ASD is enriched with risk genes related to synaptic connectivity, which is reflected in the differential effects of the ASD and epilepsy associated mutations on the OTUD7A protein interactome in this study (Lima et al., 2019; Wimmer et al., 2010). Overall, this work provides evidence that using proximity labeling techniques such as BioID2 to study and compare NDD-associated patient mutations can provide novel information on how different mutations in the same gene can lead to shared and distinct NDD-related phenotypes.

5.4.3 Convergence of OTUD7A with known NDD-associated pathways

We discovered that the OTUD7A PIN contains proteins that are encoded by high confidence ASD risk genes, providing evidence that OTUD7A converges on known NDD-associated pathways. This finding also corroborated our previous analysis of human proteomic data that showed that OTUD7A protein co-expression network was enriched

for proteins encoded by genes harboring known ASD de novo mutations (Chapter 3). We used this information, along with BioID2 significance scores and the impact of patient mutations and found that these analyses converged on one protein interactor, AnkyrinG (encoded by ANK3) highlighting it as a top candidate for further study. Ankyrin G has multiple brain-expressed isoforms; of these, the 480 and 270 kDa isoforms are largely restricted to the AIS whereas the 190kDa isoform is enriched in dendritic spines (Smith et al., 2014). AnkyrinG plays important roles at both the AIS and in dendritic spines, and shows a strong association with bipolar and ASD, which led us to examine this functional and physical interaction further. We found that OTUD7A and AnkyrinG share a protein interaction network localized to the spectrin cytoskeleton, the axon and the AIS. We determined that OTUD7A binds to the ANKRD and spectrin binding domains of AnkyrinG and that AnkyrinG levels are decreased in Df(h15q13)/+ neurons, which can be regulated by OTUD7A expression. We also found that AnkyrinG nanodomains in spine heads and in dendritic shafts are decreased in Df(h15q13)/+ neurons, and that re-expression of the AnkyrinG 190 isoform in Df(h15q13)/+ neurons rescued dendrite and dendritic spines defects. These results provide evidence that decreased AnkyrinG levels in dendritic spines and dendrites may underline neuron morphological phenotypes in the 15q13.3 microdeletion.

Previous studies have implicated a functional interaction between AnkyrinG and the WNT pathway proteins GSK-3B and beta-catenin (Garza et al., 2018; Leussis et al., 2013; Gottschalk et al., 2017; Zhu et al., 2017). Briefly, the canonical WNT pathway is activated when Wnt binds to its receptor complex, causing a series of events that disrupts

the APC/Axin/GSK-3 destruction complex that is required for the phosphorylation and subsequent destruction of beta-catenin. This allows beta-catenin to translocate to the nucleus, where it acts as a transcriptional co-activator for target genes (Clevers, 2006). It is important to note that there are multiple “non-canonical” forms of WNT signaling which are beta-catenin independent. Several potent and specific synthetic inhibitors of GSK-3 exist, including CHIR-99021 and SB-216763. Lithium, a widely used bipolar drug, is a naturally occurring GSK-3 inhibitor which has been shown to rescue anxiety-like phenotypes in *ANK3* repression mouse models (Leussis et al., 2013; Zhu et al., 2017). Interestingly, it has also been shown to rescue aberrations in *ANK3* related molecular pathways such as axonal transport and microtubule dynamics (Garza et al., 2018). Notably, there is also new evidence to suggest that lithium rescues AnkyrinG knockdown-induced spine and dendrite defects by increasing AnkyrinG mobility in dendritic spines (Piguel et al., 2019). However, it is important to note that lithium has various other cellular targets, and it is unclear as to whether lithium exerts its therapeutic effects via GSK-3 inhibition. However, studies showing similar phenotypic rescue using lithium or a selective GSK-3 inhibitor such as CHIR-99021 suggest that lithium at least partially exerts its effect through GSK-3 inhibition (Garza et al., 2018; Pan et al., 2011). In the experiments described in Chapter 4, we discovered that chronic treatment of *Df(h15q13)/+* neurons with CHIR-99021 increases bursting and network bursting, restoring them to WT levels. Interestingly, CHIR-99021 treatment also resulted in a significant decrease in network burst duration in both genotypes, suggesting that CHIR-99021 may result in a fast-spiking phenotype, with frequent short bursts.

A recent study found that alterations in cytoskeletal dynamics in cells with *ANK3* repression were rescued with treatment with lithium or CHIR-99021 (Garza et al., 2018). Interestingly, they found that cells with *ANK3* repression had lower levels of inhibitory phosphorylation of GSK-3B than control cells. One of the actions of lithium is inhibitory phosphorylation of GSK-3B, providing a mechanism for the lithium rescue in an *ANK3* repression model. Given our finding of decreased AnkyrinG levels in D(h15q13)/+ mouse neurons, it is possible that a similar mechanism exists in this model, which is an important area for investigation. Interestingly, a recent study performed RNA sequencing of human patient iPSC-derived neurons from 15q13.3 microdeletion patients and found that the Wnt signaling pathway was significantly enriched in 15q13.3 microdeletion patient induced neurons (Zhang et al. 2020). Our findings implicate OTUD7A in a known NDD-associated pathway which can be targeted to rescue phenotypes in a 15q13.3 microdeletion model. An important next question is whether there is a critical developmental window for the effects of GSK-3 inhibition in the 15q13.3 microdeletion, which we did not investigate in our study.

Overall, the data presented in Chapters 3 and 4 of this thesis provide novel cellular and molecular insights into the pathophysiology and molecular mechanisms underlying the 15q13.3 microdeletion syndrome. Namely, we identified alterations in neuronal morphology and function in a heterozygous 15q13.3 mouse model and pin-pointed OTUD7A as an important driver gene in this deletion that regulates neurodevelopmental phenotypes. Furthermore, we elucidated novel protein interaction networks in OTUD7A which converged on known NDD-associated pathways which could be targeted to rescue

functional phenotypes in a 15q13.3 microdeletion mouse model. This work also provides a framework with which to study the downstream molecular pathways regulated by novel disease-driving genes in CNVs.

5.5 Future Directions

5.5.1 A multi-model approach to studying CNVs

One of the limitations of the studies outlined in Chapters 3 and 4 is that only one model of the 15q13.3 microdeletion was used. Mouse models represent only one important method for investigating NDDs and findings from mice may not always translate to the human clinical condition. To overcome these limitations, our lab is in the process of characterizing human patient induced pluripotent stem cell (iPSC)-derived induced neurons (iNs) from ASD cohorts with the 15q.13. microdeletion and familial controls. We also have access to patient iPSC-derived iNs from the patient with the OTUD7A^{L233F} mutation, providing an exciting opportunity to directly study the impact of a *de novo* OTUD7A mutation in patient cells.

As mentioned in Chapter 3, we were limited to analyzing the expression of over-expressed FLAG tagged OTUD7A due to a lack of available specific antibodies. To overcome this limitation, we obtained to a 3XFLAG-tagged OTUD7A mouse line and have so far validated OTUD7A developmental expression in the brain as well as binding with AnkyrinG. However, there are still many experiments that remain to be completed using this mouse model. One of the main areas lacking in our current understanding of OTUD7A is its endogenous subcellular localization and cell-type specific expression. Our

previous work was limited to excitatory pyramidal neurons and did not examine the role of inhibitory neurons or glial cells. Interestingly, defects in inhibitory neurons have been consistently reported in models of the 15q13.3 microdeletion (Al-Absi et al., 2020; Gordon et al., 2019; Steullet et al., 2017). Therefore, it will be important to determine whether OTUD7A is expressed in inhibitory neurons and whether it plays a role in this neuronal population.

The study by Yin et al. (2018) reported on the behavioural and synaptic characterization of a novel OTUD7A KO model. Our lab recently obtained this mouse model and will be assaying neuronal function with the use of MEAs, which can be compared to our results from Df(h15q13)/+ mice. Additionally, the OTUD7A KO mouse provides a tool to assay the levels and subcellular localization of OTUD7A BioID2 hits in the absence of only OTUD7A, instead of the full deletion. Comparison of the OTUD7A KO mouse model to the 15q13.3 microdeletion mouse model will be useful for parsing the OTUD7A-relevant molecular phenotypes in the 15q13.3 microdeletion. Global proteomic strategies can also be utilized to compare the proteomes of OTUD7A KO and Df(h15q13)/+ mice as well as human 15q13.3 and OTUD7A mutant patient lines to further distinguish OTUD7A-specific molecular mechanisms.

5.5.2 Convergence of the ubiquitin proteasome system (UPS) with synaptic and NDD-related Pathways

Exploring the mechanistic action of OTUD7A on its PIN is an important next area of investigation. Although *in vitro* DUB assays have confirmed that OTUD7A shows

catalytic DUB activity toward ubiquitin chains, further studies are required to determine whether OTUD7A regulates neurodevelopmental processes via its catalytic DUB activity. The ubiquitin system serves two main functions with distinct mechanisms: (1) control of protein turnover by targeting substrates for proteasomal degradation via the ubiquitin proteasome system (UPS) and (2) regulating cell signaling networks and protein interactions (Clague et al., 2019). This system is ubiquitously important for cellular maintenance, and in neural cells it has also been shown to regulate complex processes such as learning and memory, and synaptic plasticity and activity (Mabb & Ehlers, 2010). Interestingly, pioneering work on cultured neurons showed that neuronal activity can also regulate ubiquitination and degradation in the postsynaptic proteome (Ehlers 2003, Bingol & Schuman 2006, Djakovic et al 2009).

Substrate proteins are covalently tagged with ubiquitin molecules at lysine residues through a series of enzymatic reactions by ubiquitin-activating enzymes (E1), ubiquitin-conjugating enzymes (E2), and E3 ubiquitin ligases (Louros & Osterweil, 2016).

Ubiquitin tags are composed of one or more ubiquitin molecules, forming a “ubiquitin code” of chains of various length and conformation, each signaling a different cascade of downstream events. DUBs converge on this pathway by removing ubiquitin molecules from substrate proteins, thereby preventing proteasomal degradation or modifying downstream signaling pathways. There are seven internal lysine residues of ubiquitin that can be ubiquitinated to form various chains (Lys29, Lys33, Lys6, Lys11, Lys27, Lys48, and Lys63). Lys48 is the most widely studied of the linkage types, and proteins tagged with this ubiquitin chain are typically targeted for degradation through the UPS (Swatek

& Komander, 2016). The UPS is a critical cellular mechanism that facilitates degradation of misfolded proteins and regulates protein turnover. While it has mainly been implicated in neurodegenerative disorders such as Alzheimer's Disease, where accumulation of misfolded proteins is a known pathological mechanism of disease, recent studies have also shown that this pathway may contribute to NDDs (Cheon & Chahrour, 2019, 2018; Louros et al., 2016; Ross & Poirier, 2004).

OTUD7A, also known as CEZANNE2, is one of 99 currently identified DUBs grouped into categories based on sequence similarity of their catalytic domains. Specifically, OTUD7A is a member of the ovarian tumor (OTU) family of deubiquitinases with sequence similarity to A20, a well-studied negative regulator of NFKappa-B signaling (Evans et al., 2003, Mevissen et al., 2013). While its paralog, OTUD7B (CEZANNE), has been the subject of many studies examining its role in cellular mechanisms such as DNA damage, cancer, and inflammation, OTUD7A has received much less attention (Bonacci et al., 2018; Chiu et al., 2018; Hu et al., 2016). However, there is evidence to suggest that OTUD7A plays a role in similar mechanisms such as negative regulation of NFKappaB signaling and tumor suppressor activity (Xu et al., 2014). DUBs from different families show target specificity through distinct mechanisms, either through substrate specificity at binding domains other than the catalytic domain or specificity for particular ubiquitin chains (Clague et al., 2019). Remarkably, OTUD7A and OTUD7B are the only known DUBs showing linkage specificity to Lys 11 ubiquitin chains, but can also target heterotypic chains containing Lys11/Ly43 or Lys11/Lys63 branched chains (Mevissen et al., 2013, Wu et al., 2019, Mevissen et al., 2016). Lys11 chains typically do not target

substrates to the UPS but are instead involved in signaling pathways such as cell cycle regulation, endoplasmic reticulum associated degradation and mitophagy (Akutsu et al., 2016). However, heterotypic chains containing both Lys11/48 can target proteins for the UPS. Interestingly, a recent study showed that OTUD7A and OTUD7B interact with and modify Lys11/Lys63 heterotypic chains in order to regulate DNA damage (Wu et al., 2019). This suggests that OTUD7A may regulate a wide range of cellular activities based on substrate linkage type.

Many studies have implicated a role for the ubiquitin system at synapses. One of the most extensively studied mechanisms of the UPS at synapses is the regulation of AMPA and NMDA receptor turnover at the postsynaptic density (Mabb & Ehlers, 2010; Widagdo et al., 2017). Regulation of the number and localization of these receptors is critical for proper neuronal function and synaptic plasticity. A recent study suggests that one of the actions of DUBs at synapses may be to oppose the actions of E3 ubiquitin ligases on postsynaptic receptors to control synaptic strength (Scudder et al., 2014). Another recent study showed that PSD95 is a direct target of K63 ubiquitination, resulting in targeting of PSD95 to synapses and regulation of synaptic plasticity (Ma et al., 2017). They identified TRAF6 as an E3 ubiquitin ligase for PSD95 and CYLD as a K63 specific DUB that cleaved K63 chains from TRAF6. Interestingly, TRAF6 is a known protein interactor of OTUD7A which suggests that OTUD7A may also converge on this pathway (Xu et al., 2014).

Several NDD-risk genes associated with ASD and ID have been identified that encode proteins that are either components of or are targeted by the UPS. The most notable is

UBE3A, which encodes an E3 ubiquitin ligase. *De novo* maternal deletions of the 15q11-q13 locus containing UBE3A result in the NDD Angelman syndrome and identification of specific UBE3A loss of function mutations in Angelman syndrome patients support a causative role for UBE3A in Angelman syndrome (Margolis et al., 2015). Studies have shown that UBE3A regulates protein turnover of the immediate early gene Arc, which affects AMPA receptor surface expression at synapses (Greer et al., 2010). UBE3A mouse models display alterations in E/I balance as well as NDD-related behavioural phenotypes and seizure susceptibility, defining a role for the UPS in behavioural phenotypes relevant to NDDs (Khatri & Man, 2019). Although the literature on NDD-associated DUBs is sparse, several have been identified, although the mechanistic role of these DUBs in NDD pathophysiology remains unclear. For example, mutations in the genes USP7 have been identified in individuals with ASD, ID and seizures (Fountain et al., 2019). A recent study identified the ASD-linked gene USP9X as a DUB targeting AnkyrinG and regulating spine dynamics and levels of other ANKRD containing proteins in the brain (Yoon et al., 2020). Additionally, pathogenic variants were identified in another OTU family DUB (OTUD6B) in 12 individuals with ID and seizures (Santiago-Sim, 2017). Interestingly, peripheral blood cells from these patients displayed reduced proteasome activity (Santiago-Sim, 2017). These results are similar to proteasome deficits observed in fibroblasts from the OTUD7AL233F mutation (Garret et al., 2020). Our work has identified novel roles of the DUB OTUD7A in 15q13.3 microdeletion pathophysiology, as well as identification of synaptic and AIS related protein interactors. It will be important to determine whether OTUD7A's DUB activity is important for

regulating neuronal morphology and function. We determined that a patient mutation affecting the catalytic domain of OTUD7A affects proteins localized at the axon and PSD, suggesting that altered DUB activity may be important for binding to these proteins. However, this needs to be functionally confirmed through ubiquitin co-immunoprecipitation assays with these particular proteins. Additionally, an integrated approach can be used to efficiently narrow down proteins that are likely deubiquitinated by OTUD7A. Global ubiquitin proteomics can be used to obtain a global map of ubiquitinated proteins altered by loss of OTUD7A, which can be compared to OTUD7A BioID2 hits to determine which are likely to be direct targets of OTUD7A catalytic function (Qian et al., 2019).

The concept of targeting the UPS as a therapeutic approach to disease is not new; the first proteasome inhibitor for refractory multiple myeloma was approved by the FDA in 2003, and since then other proteasome targeting drugs have shown promise for other cancers. However, because of the broad impact of proteasomal alteration, side effects to these medications are common (Schmidt & Finley 2014). Therefore, more specific targeting of the UPS is favourable for therapeutic use for disease treatment. DUBs are an attractive candidate due to their substrate specificity and roles that are involved in fine tuning of cellular responses. In fact, drugs that target DUBs, including USP7 and USP9X, are currently being investigated as potential therapeutics for cancers (Yuan et al., 2018; Zhang et al., 2020). Given the emerging role of the UPS in NDDs, targeting of DUBs is an exciting new area to be explored for future drug development for NDDs.

5.6 Significance

Neurodevelopmental disorders remain one of the leading causes of disability in the world. There is currently a lack of understanding of the etiology of these disorders, which is driven by a lack of understanding of the molecular mechanisms regulating their pathophysiology. High throughput sequencing studies have identified hundreds of genetic variants that are linked to NDDs and have laid the groundwork for functional studies. However, they have also uncovered layers of complexity that have proven challenging to understand. One of the main challenges is understanding how NDD risk genes overlap and interact at the level of molecular signaling pathways and how this contributes to clinical phenotypic heterogeneity. As outlined in this thesis, we addressed this challenge using a variety of bioinformatic, cellular, and molecular methods and identified interactions between risk genes associated with SZ, ASD, and epilepsy at the level of molecular signaling pathways to regulate important processes for neural development. This work adds to our understanding of the role of signaling pathway interactions in the clinical heterogeneity of neurodevelopmental disorders.

REFERENCES

- Abraham, J. R., Szoko, N., Barnard, J., Rubin, R. A., Schlatzer, D., Lundberg, K., ...
Natowicz, M. R. (2019). Proteomic Investigations of Autism Brain Identify Known
and Novel Pathogenetic Processes. *Scientific Reports*, 9(1), 1–11.
<https://doi.org/10.1038/s41598-019-49533-y>
- Abrahams, B.S., Arking, D.E., Campbell, D.B., Mefford, H.C., Morrow, E.M.,
Weiss, L.A., Menashe, I., Wadkins, T., Banerjee-Basu, S., and Packer, A. (2013).
SFARI Gene 2.0: a community-driven knowledgebase for the autism spectrum
disorders (ASDs). *Mol Autism*, 4, 36.
- Aceti, M., Creson, T. K., Vaissiere, T., Rojas, C., Huang, W.C., Wang, Y.X., ...
Rumbaugh, G. (2014). Syngap1 Haploinsufficiency Damages a Postnatal Critical
period of Pyramidal Cell Structural Maturation Linked to Cortical Circuit Assembly.
Biological Psychiatry, 77(9), 805–815.
<https://doi.org/10.1016/j.biopsych.2014.08.001>
- Akutsu, M., Dikic, I., & Bremm, A. (2016). Ubiquitin chain diversity at a glance. *Journal
of Cell Science*, 129(5), 875–880. <https://doi.org/10.1242/jcs.183954>
- Al-Absi, A.-R., Qvist, P., Glerup, S., Sanchez, C., & Nyengaard, J. R. (2020).
Df(h15q13)/+ Mouse Model Reveals Loss of Astrocytes and Synaptic-Related
Changes of the Excitatory and Inhibitory Circuits in the Medial Prefrontal Cortex.
Cerebral Cortex, 1–13. <https://doi.org/10.1093/cercor/bhaa313>

- Antoine, M. W., Langberg, T., Schnepel, P., & Feldman, D. E. (2019). Increased Excitation-Inhibition Ratio Stabilizes Synapse and Circuit Excitability in Four Autism Mouse Models. *Neuron*, 101(4), 648-661.e4.
<https://doi.org/10.1016/j.neuron.2018.12.026>
- Antonacci, F., Dennis, M. Y., Huddleston, J., Sudmant, P. H., Steinberg, K. M., Rosenfeld, J. a, ... Eichler, E. E. (2014). Palindromic GOLGA8 core duplicons promote chromosome 15q13.3 microdeletion and evolutionary instability. *Nature Genetics*, (October), 1–11. <https://doi.org/10.1038/ng.3120>
- Arim, R. G., Kohen, D. E., Garner, R. E., Lach, L. M., Brehaut, J. C., MacKenzie, M. J., & Rosenbaum, P. L. (2015). Psychosocial functioning in children with neurodevelopmental disorders and externalizing behavior problems. *Disability and Rehabilitation*, 37(4), 345–354. <https://doi.org/10.3109/09638288.2014.919361>
- Arrington JV, Hsu CC, Elder SG, Andy TW. Recent advances in phosphoproteomics and application to neurological diseases. *Analyst. Royal Society of Chemistry*, 142:4373–87
- Behar, T. N., Smith, S. V., Kennedy, R. T., Mckenzi, J. M., Maric, I., & Barker, J. L. (2001). GABAB receptors mediate motility signals for migrating embryonic cortical cells. *Cerebral Cortex*, 11(8), 744–753. <https://doi.org/10.1093/cercor/11.8.744>
- Bhakar, A.L., Dolen, G., and Bear, M.F. (2012). The pathophysiology of fragile X (and

what it teaches us about synapses). *Annual review of neuroscience* 35, 417-443.

Bi, C., Wu, J., Jiang, T., Liu, Q., Cai, W., Yu, P., Cai, T., Zhao, M., Jiang, Y., & Sun, Z. S. (2012). Mutations of ANK3 identified by exome sequencing are associated with Autism susceptibility. *Human Mutation*, 33(12), 1635–1638.
<https://doi.org/10.1002/humu.22174>

Bingol, B., & Schuman, E. M. (2006). Activity-dependent dynamics and sequestration of proteasomes in dendritic spines. *Nature*, 441(7097), 1144–1148.
<https://doi.org/10.1038/nature04769>

Birnbaum, R., & Weinberger, D. R. (2017). Genetic insights into the neurodevelopmental origins of schizophrenia. *Nature Reviews Neuroscience*, 18(12), 727–740.
<https://doi.org/10.1038/nrn.2017.125>

Bonacci, T., Suzuki, A., Grant, G. D., Stanley, N., Cook, J. G., Brown, N. G., & Emanuele, M. J. (2018). Cezanne/ OTUD 7B is a cell cycle-regulated deubiquitinase that antagonizes the degradation of APC /C substrates. *The EMBO Journal*, 37(16), 1–17. <https://doi.org/10.15252/embj.201798701>

Bourne, J. N., & Harris, K. M. (2008). Balancing structure and function at hippocampal dendritic spines. *Annual Review of Neuroscience*, 31, 47–67.
<https://doi.org/10.1146/annurev.neuro.31.060407.125646>

- Buonanno A. (2010). The neuregulin signaling pathway and schizophrenia: From genes to synapses and neural circuits. *Brain Res Bull.*;83(3-4):122-131. doi: 10.1016/j.brainresbull.2010.07.012; 10.1016/j.brainresbull.2010.07.012
- Branon TC, Bosch JA, Sanchez AD, Udeshi ND, Svinkina T, Carr SA, et al. (2018). Efficient proximity labeling in living cells and organisms with TurboID. *Nat Biotechnol*, 36, 880–98.
- Brandon NJ, Sawa A. (2011). Linking neurodevelopmental and synaptic theories of mental illness through DISC1. *Nat Rev Neurosci.*;12(12):707-722. doi: 10.1038/nrn3120; 10.1038/nrn3120.
- Brentani, H., Paula, C.S., Bordini, D., Rolim, D., Sato, F., Portolese, J., Pacifico, M.C., & McCracken, J.T. (2013). Autism spectrum disorders: an overview on diagnosis and treatment. *Revista brasileira de psiquiatria* (35) Suppl 1, S62-72.
- Broadbelt K, Byne W, Jones LB. (2002). Evidence for a decrease in basilar dendrites of pyramidal cells in schizophrenic medial prefrontal cortex. *Schizophr Res.*;58(1):75-81.
- Bush, W.S., and Moore, J.H. (2012). Chapter 11: Genome-wide association studies. *PLoS computational biology* 8, e1002822.
- Cao, Z., Hulsizer, S., Tassone, F., Tang, H. T., Hagerman, R. J., Rogawski, M. A., ... Pessah, I. N. (2012). Clustered burst firing in FMR1 premutation hippocampal

neurons: Amelioration with allopregnanolone. *Human Molecular Genetics*, 21(13), 2923–2935. <https://doi.org/10.1093/hmg/dds118>

Cannon M, Caspi A, Moffitt TE, et al. (2002) Evidence for early-childhood, pan-developmental impairment specific to schizophreniform disorder: Results from a longitudinal birth cohort. *Arch Gen Psychiatry*;59(5):449-456.

Cetica, V., Chiari, S., Mei, D., Parrini, E., Grisotto, L., Marini, C., ... Guerrini, R. (2017). Clinical and genetic factors predicting Dravet syndrome in infants with SCN1A mutations. *Neurology*, 88(11), 1037–1044. <https://doi.org/10.1212/WNL.0000000000003716>

Chao, H. P., Chen, Y., Takata, Y., Tomida, M. W., Lin, K., Kirk, J. S., ... Shen, J. (2019). Systematic evaluation of RNA-Seq preparation protocol performance. *BMC Genomics*, 20(1), 1–20. <https://doi.org/10.1186/s12864-019-5953-1>

Chen C, Perrimon N. (2017). Proximity-dependent labeling methods for proteomic profiling in living cells. *WIREs Dev Biol*. 2017;6:1–10.

Chen, X., Winters, C., Azzam, R., Li, X., Galbraith, J. A., Leapman, R. D., & Reese, T. S. (2008). Organization of the core structure of the postsynaptic density. *PNAS*, 105(11), 4453-4458. Retrieved from www.pnas.org/cgi/content/full/

- Cheon, S., Dean, M., & Chahrour, M. (2019). The ubiquitin proteasome pathway in neuropsychiatric disorders. *Neurobiology of Learning and Memory*, 165(November 2017), 106791. <https://doi.org/10.1016/j.nlm.2018.01.012>
- Chisholm, K., Lin, A., Abu-Akel, A., & Wood, S. J. (2015). The association between autism and schizophrenia spectrum disorders: A review of eight alternate models of co-occurrence. *Neuroscience and Biobehavioral Reviews*, 55, 173–183. <https://doi.org/10.1016/j.neubiorev.2015.04.012>
- Chiu, H. W., Lin, H. Y., Tseng, I. J., & Lin, Y. F. (2018). OTUD7B upregulation predicts a poor response to paclitaxel in patients with triple-negative breast cancer. *Oncotarget*, 9(1), 553–565. <https://doi.org/10.18632/oncotarget.23074>
- Choi, H., Larsen, B., Lin, Z. Y., Breitkreutz, A., Mellacheruvu, D., Fermin, D., ... Nesvizhskii, A. I. (2011). SAINT: Probabilistic scoring of affinity purification-mass spectrometry data. *Nature Methods*, 8(1), 70–73. <https://doi.org/10.1038/nmeth.1541>
- Chubb, J. E., Bradshaw, N. J., Soares, D. C., Porteous, D. J., & Millar, J. K. (2008). The DISC locus in psychiatric illness. *Molecular Psychiatry*, 13(1), 36–64. <https://doi.org/10.1038/sj.mp.4002106>
- Clague, M. J., Urbé, S., & Komander, D. (2019). Breaking the chains: deubiquitylating enzyme specificity begets function. *Nature Reviews Molecular Cell Biology*, 20(6), 338–352. <https://doi.org/10.1038/s41580-019-0099-1>

- Clement, J. P., Ozkan, E. D., Aceti, M., Miller, C. a., & Rumbaugh, G. (2013). SYNGAP1 Links the Maturation Rate of Excitatory Synapses to the Duration of Critical-Period Synaptic Plasticity. *Journal of Neuroscience*, 33(25), 10447–10452. <https://doi.org/10.1523/JNEUROSCI.0765-13.2013>
- Clevers, H. (2006). Wnt/ β -Catenin Signaling in Development and Disease. *Cell*, 127(3), 469–480. <https://doi.org/10.1016/j.cell.2006.10.018>
- Connolly, M. B. (2016). Dravet Syndrome: Diagnosis and Long-Term Course. *Canadian Journal of Neurological Sciences*, 43(S3), S3–S8. <https://doi.org/10.1017/cjn.2016.243>
- Crawley, J. N. (2012). Translational animal models of autism and neurodevelopmental disorders. *Dialogues in Clinical Neuroscience*, 14(3), 293–305. <https://doi.org/10.31887/dcns.2012.14.3/jcrawley>
- Culotta, L., & Penzes, P. (2020). Exploring the mechanisms underlying excitation/inhibition imbalance in human iPSC-derived models of ASD. *Molecular Autism*, 11(1), 1–11. <https://doi.org/10.1186/s13229-020-00339-0>
- Delevich, K., Jaaro-Peled, H., Penzo, M., Sawa, A., & Li, B. (2020). Parvalbumin interneuron dysfunction in a thalamo-prefrontal cortical circuit in disc1 locus impairment mice. *ENeuro*, 7(2). <https://doi.org/10.1523/ENEURO.0496-19.2020>

- Deng, D., Jian, C., Lei, L., Zhou, Y., McSweeney, C., Dong, F., ... Mao, Y. (2017). A prenatal interruption of DISC1 function in the brain exhibits a lasting impact on adult behaviors, brain metabolism, and interneuron development. *Oncotarget*, 8(49), 84798–84817. <https://doi.org/10.18632/oncotarget.21381>
- Deribe YL, Pawson T, Dikic I. (2010). Post-translational modifications in signal integration. *Nat Struct Mol Biol*. Nature Publishing Group.;17:666–72.
- Djakovic, S. N., Schwarz, L. A., Barylko, B., DeMartino, G. N., & Patrick, G. N. (2009). Regulation of the proteasome by neuronal activity and calcium/calmodulin-dependent protein kinase II. *Journal of Biological Chemistry*, 284(39), 26655–26665. <https://doi.org/10.1074/jbc.M109.021956>
- Durak, O., De Anda, F. C., Singh, K. K., Leussis, M. P., Petryshen, T. L., Sklar, P., & Tsai, L. H. (2015). Ankyrin-G regulates neurogenesis and Wnt signaling by altering the subcellular localization of β -catenin. *Molecular Psychiatry*, 20(3), 388–397. <https://doi.org/10.1038/mp.2014.42>
- Ehlers, M. D. (2003). Activity level controls postsynaptic composition and signaling via the ubiquitin-proteasome system. *Nature Neuroscience*, 6(3), 231–242. <https://doi.org/10.1038/nn1013>
- Evans, P. C., Smith, T. S., Lai, M.-J., Williams, M. G., Burke, D. F., Heyninck, K., ... Kilshaw, P. J. (2003). A novel type of deubiquitinating enzyme. *The Journal of*

Biological Chemistry, 278(25), 23180–23186.

<https://doi.org/10.1074/jbc.M301863200>

Fazal FM, Han S, Parker KR, Kaewsapsak P, Xu J, Boettiger AN, et al. (2019). Atlas of subcellular RNA localization revealed by APEX-seq. *Cell*. Elsevier Inc.;178(2):473–90.

Fazzari P, Paternain AV, Valiente M, et al. (2010). Control of cortical GABA circuitry development by Nrg1 and ErbB4 signalling. *Nature*.;464(7293):1376-1380. doi: 10.1038/nature08928; 10.1038/nature08928.

Fejgin, K., Nielsen, J., Birknow, M. R., Bastlund, J. F., Nielsen, V., Lauridsen, J. B., ... Didriksen, M. (2014). A mouse model that recapitulates cardinal features of the 15q13.3 microdeletion syndrome including schizophrenia- and epilepsy-related alterations. *Biological Psychiatry*, 76(2), 128–137.
<https://doi.org/10.1016/j.biopsych.2013.08.014>

Föcking, M., Dicker, P., Lopez, L. M., Hryniewiecka, M., Wynne, K., English, J. A., ... Cotter, D. R. (2016). Proteomic analysis of the postsynaptic density implicates synaptic function and energy pathways in bipolar disorder. *Translational Psychiatry*, 6(11). <https://doi.org/10.1038/tp.2016.224>

Folstein., S., & Rutter., M. (1977). Infantile autism: a genetic study of 21 twin pairs. *Journal of child psychology and psychiatry, and allied disciplines* (18), 297-321.

- Forsingdal, A., Fejgin, K., Nielsen, V., Werge, T., & Nielsen, J. (2016). 15q13.3 Homozygous Knockout Mouse Model Display Epilepsy-, Autism-and Schizophrenia- Related Phenotypes. *Translational Psychiatry*, 6(7), e860-9. <https://doi.org/10.1038/tp.2016.125>
- Forstner, A. J., Degenhardt, F., Schratt, G., & Nöthen, M. M. (2013). MicroRNAs as the cause of schizophrenia in 22q11.2 deletion carriers, and possible implications for idiopathic disease: A mini-review. *Frontiers in Molecular Neuroscience*, 6(DEC), 1–10. <https://doi.org/10.3389/fnmol.2013.00047>
- Fountain, M.D., Oleson, D.S., Rech, M.E. et al.(2019). Pathogenic variants in USP7 cause a neurodevelopmental disorder with speech delays, altered behavior, and neurologic anomalies. *Genet Med*, 1797–1807. <https://doi.org/10.1038/s41436-019-0433-1>
- Freeman, J. L., Perry, G. H., Feuk, L., Redon, R., Mccarroll, S. A., Altshuler, D. M., ... Lee, C. (2007). Copy number variation: New insights in genome diversity. *Genome Res* (16), 949-961 <https://doi.org/10.1101/gr.3677206>
- Gao, R., & Penzes, P. (2015). Common Mechanisms of Excitatory and Inhibitory Imbalance in Schizophrenia and Autism Spectrum Disorders. *Current Molecular Medicine*, 15(2), 146–167. <https://doi.org/10.2174/1566524015666150303003028>
- Garey, L. J., Ong, W. Y., Patel, T. S., Kanani, M., Davis, A., Mortimer, A. M., ... Hirsch, S. R. (1998). Reduced dendritic spine density on cerebral cortical pyramidal neurons

in schizophrenia. *Journal of Neurology Neurosurgery and Psychiatry*, 65(4), 446–453. <https://doi.org/10.1136/jnnp.65.4.446>

Garret, P., Ebstein, F., Delplancq, G., Dozieres-Puyravel, B., Boughalem, A., Auvin, S., ... Vitobello, A. (2020). Report of the first patient with a homozygous OTUD7A variant responsible for epileptic encephalopathy and related proteasome dysfunction. *Clinical Genetics*, 97(4), 567–575. <https://doi.org/10.1111/cge.13709>

Garza, J. C., Qi, X., Gjeluci, K., Leussis, M. P., Basu, H., Reis, S. A., ... Petryshen, T. L. (2018). Disruption of the psychiatric risk gene Ankyrin 3 enhances microtubule dynamics through GSK3/CRMP2 signaling. *Translational Psychiatry*, 8(1). <https://doi.org/10.1038/s41398-018-0182-y>

Gaugler, T., Klei, L., Sanders, S. J., Bodea, C. a, Goldberg, A. P., Lee, A. B., ... Buxbaum, J. D. (2014). Most genetic risk for autism resides with common variation. *Nature Genetics*, 46(8), 881–885. <https://doi.org/10.1038/ng.3039>

Geschwind, D.H., and Levitt, P. (2007). Autism spectrum disorders: developmental disconnection syndromes. *Current opinion in neurobiology* 17, 103-111.

Gdalyahu, A., Lazaro, M., Penagarikano, O., Golshani, P., Trachtenberg, J. T., & Gescwind, D. H. (2015). The Autism Related Protein Contactin-Associated Protein-Like 2 (CNTNAP2) Stabilizes New Spines: An In Vivo Mouse Study. *PloS One*, 10(5). <https://doi.org/10.1371/journal.pone.0125633>

- Gibson, T. J., Seiler, M., & Veitia, R. A. (2013). The transience of transient overexpression. *Nature Methods*, 10(8), 715–721.
<https://doi.org/10.1038/nmeth.2534>
- Gilbert, L. A., Horlbeck, M. A., Adamson, B., Villalta, J. E., Chen, Y., Whitehead, E. H., ... Weissman, J. S. (2014). Genome-Scale CRISPR-Mediated Control of Gene Repression and Activation. *Cell*, 159(3), 647–661.
<https://doi.org/10.1016/j.cell.2014.09.029>
- Gillberg, C., & Billstedt, E. (2000). Autism and Asperger syndrome: coexistence with other clinical disorders. *Acta Psychiatrica Scandinavica*, 102(5), 321–330.
<https://doi.org/10.1034/j.1600-0447.2000.102005321.x>
- Gilman, S. R., Chang, J., Xu, B., Bawa, T. S., Gogos, J. a, Karayiorgou, M., & Vitkup, D. (2012). Diverse types of genetic variation converge on functional gene networks involved in schizophrenia. *Nature Neuroscience*, 15(12), 1723–1728.
<https://doi.org/10.1038/nn.3261>
- Goeree, R., Farahati, F., Burke, N., Blackhouse, G., O'Reilly, D., Pyne, J., & Tarride, J.-E. (2005). The economic burden of schizophrenia in Canada in 2004. *Current Medical Research and Opinion*, 21(12), 2017–2028.
<https://doi.org/10.1185/030079905X75087>

- Gogtay, N., Vyas, N. S., Testa, R., Wood, S. J., & Pantelis, C. (2011). Age of Onset of Schizophrenia: Perspectives From Structural Neuroimaging Studies. *Schizophrenia Bulletin*, 3(37), 504–513. <https://doi.org/10.1093/schbul/sbr030>
- Gordon, A., Forsingdal, A., Klewe, I. V., Nielsen, J., Didriksen, M., Werge, T., & Geschwind, D. H. (2019). Transcriptomic networks implicate neuronal energetic abnormalities in three mouse models harboring autism and schizophrenia-associated mutations. *Molecular Psychiatry*. <https://doi.org/10.1038/s41380-019-0576-0>
- Gottschalk, M.G., Leussis, M. P., Ruland, T., Gjeluci, K., Petryshen, T. L., & Bahn, S. (2017). Lithium reverses behavioral and axonal transport-related changes associated with ANK3 bipolar disorder gene disruption. *European Neuropsychopharmacology*, 27(3), 274–288. <https://doi.org/10.1016/j.euroneuro.2017.01.001>
- Greer, P. L., Hanayama, R., Bloodgood, B. L., Mardinly, A. R., Lipton, D. M., Flavell, S. W., ... Greenberg, M. E. (2010). The Angelman Syndrome Protein Ube3A Regulates Synapse Development by Ubiquitinating Arc. *Cell*, 140(5), 704–716. <https://doi.org/10.1016/j.cell.2010.01.026>
- Grutzner C, Wibrall M, Sun L, et al. (2013). Deficits in high- (>60 hz) gamma-band oscillations during visual processing in schizophrenia. *Front Hum Neurosci.*;7:88. doi: 10.3389/fnhum.2013.00088; 10.3389/fnhum.2013.00088.
- Gu, W., Zhang, F., & Lupski, J. R. (2008). Mechanisms for human genomic rearrangements. *PathoGenetics*, 1(4) <https://doi.org/10.1186/1755-8417-1-4>

- Guo, H., Wang, T., Wu, H., Long, M., Coe, B. P., Li, H., ... Xia, K. (2018). Inherited and multiple de novo mutations in autism/developmental delay risk genes suggest a multifactorial model. *Molecular Autism*, 9(1), 64. <https://doi.org/10.1186/s13229-018-0247-z>
- Hallmayer, J., Cleveland, S., Torres, A., Phillips, J., Cohen, B., Torigoe, T., Miller, J., Fedele, A., Collins, J., Smith, K., et al. (2011). Genetic heritability and shared environmental factors among twin pairs with autism. *Archives of general psychiatry* 68, 1095-1102.
- Hamdan, H., Lim, B. C., Torii, T., Joshi, A., Konning, M., Smith, C., ... Rasband, M. N. (2020). Mapping axon initial segment structure and function by multiplexed proximity biotinylation. *Nature Communications*, 11(1). <https://doi.org/10.1038/s41467-019-13658-5>
- Han S, Li J, Ting AY. (2018). ScienceDirect Proximity labeling : spatially resolved proteomic mapping for neurobiology. *Curr Opin Neurobiol*. Elsevier Ltd.;50:17–23.
- Hasan, A., Roeh, A., Leucht, S., Langguth, B., Hansbauer, M., Oviedo-Salcedo, T., ... Falkai, P. (2020). Add-on spironolactone as antagonist of the NRG1-ERBB4 signaling pathway for the treatment of schizophrenia: Study design and methodology of a multicenter randomized, placebo-controlled trial. *Contemporary Clinical Trials Communications*, 17. <https://doi.org/10.1016/j.conctc.2020.100537>

Hasin, Y., Seldin, M., & Lusk, A. (2017). Multi-omics approaches to disease. *Genome Biology*, 18(1), 1–15. <https://doi.org/10.1186/s13059-017-1215-1>

Hedstrom, K. L., Ogawa, Y., & Rasband, M. N. (2008). AnkyrinG is required for maintenance of the axon initial segment and neuronal polarity. *Journal of Cell Biology*, 183(4), 635–640. <https://doi.org/10.1083/jcb.200806112>

Helbig, I., Mefford, H. C., Sharp, A. J., Guipponi, M., Fichera, M., Franke, A., ... Sander, T. (2009). 15q13.3 Microdeletions Increase Risk of Idiopathic Generalized Epilepsy. *Nature Genetics*, 41(2), 160–162. <https://doi.org/10.1038/ng.292>

Hiroi, N., Takahashi, T., Hishimoto, A., Izumi, T., Boku, S., & Hiramoto, T. (2013). Copy number variation at 22q11.2: from rare variants to common mechanisms of developmental neuropsychiatric disorders. *Molecular Psychiatry*, 18, 1153–1165. <https://doi.org/10.1038/mp.2013.92>.

Ho, S. M., Hartley, B. J., Flaherty, E., Rajarajan, P., Abdelaal, R., Obiorah, I., ... Brennand, K. J. (2017). Evaluating Synthetic Activation and Repression of Neuropsychiatric-Related Genes in hiPSC-Derived NPCs, Neurons, and Astrocytes. *Stem Cell Reports*, 9(2), 615–628. <https://doi.org/10.1016/j.stemcr.2017.06.012>

Hoffman, G. E., Hartley, B. J., Flaherty, E., Ladran, I., Gochman, P., Ruderfer, D. M., ... Brennand, K. J. (2017). Transcriptional signatures of schizophrenia in hiPSC-derived NPCs and neurons are concordant with post-mortem adult brains. *Nature Communications*, 8(1). <https://doi.org/10.1038/s41467-017-02330-5>

- Homayoun, H., & Moghaddam, B. (2007). NMDA receptor hypofunction produces opposite effects on prefrontal cortex interneurons and pyramidal neurons. *The Journal of Neuroscience*, 27(43), 11496–11500.
<https://doi.org/10.1523/JNEUROSCI.2213-07.2007>
- Hor, K., & Taylor, M. (2010). Suicide and schizophrenia: a systematic review of rates and risk factors. *J Psychopharmacol*, (4 Suppl):81-90.
<https://doi.org/10.1177/1359786810385490>
- Hsu, W. C. J., Nilsson, C. L., & Laezza, F. (2014). Role of the axonal initial segment in psychiatric disorders: Function, dysfunction, and intervention. *Frontiers in Psychiatry*, 5(AUG), 1–11. <https://doi.org/10.3389/fpsy.2014.00109>
- Hu, H., Wang, H., Xiao, Y., Jin, J., Chang, J. H., Zou, Q., ... Sun, S. C. (2016). Otud7b facilitates T cell activation and inflammatory responses by regulating Zap70 ubiquitination. *Journal of Experimental Medicine*, 213(3), 399–414.
<https://doi.org/10.1084/jem.20151426>
- Hulbert, S. W., & Jiang, Y. H. (2016). Monogenic mouse models of autism spectrum disorders: Common mechanisms and missing links. *Neuroscience*, 321, 3–23.
<https://doi.org/10.1016/j.neuroscience.2015.12.040>
- Hwang, J., & Espenshade, P. J. (2016). Proximity-dependent biotin labeling in yeast using the engineered ascorbate peroxidase APEX2. *Biochem J*, 473(16), 2463–2469.
<https://doi.org/10.1042/BCJ20160106>

International Schizophrenia Consortium. (2008). Rare chromosomal deletions and duplications increase risk of schizophrenia. *Nature*, 455(7210), 237–241.

<https://doi.org/10.1038/nature07239>

Joshi, D., Fullerton, J. M., & Weickert, C. S. (2014). Elevated ErbB4 mRNA is related to interneuron deficit in prefrontal cortex in schizophrenia. *Journal of Psychiatric Research*, 53, 125–132. <https://doi.org/10.1016/j.jpsychires.2014.02.014>

Kaizuka, T., & Takumi, T. (2018). Postsynaptic density proteins and their involvement in neurodevelopmental disorders. *Journal of Biochemistry*, 163(6), 447–455.

<https://doi.org/10.1093/jb/mvy022>

Kalus, P., Bondzio, C. A. J., Federspiel, A., Müller, T. J., & Zuschratter, W. (2002). Cell-type specific alterations of cortical interneurons in schizophrenic patients.

Neuroreport, 13(5), 713–717.

Kazdoba, T. M., Leach, P. T., Silverman, J. L., & Crawley, J. N. (2014). Modeling fragile X syndrome in the Fmr1 knockout mouse. *Intractable and Rare Diseases Research*,

3(4), 118–133. <https://doi.org/10.5582/irdr.2014.01024>

Kaminsky, E. B., Kaul, V., Paschall, J., Church, D. M., Bunke, B., Kunig, D., ... Sarah, T. (2011). An evidence-based approach to establish the functional and clinical significance of CNVs in intellectual and developmental disabilities. *Genetics in Medicine : Official Journal of the American College of Medical Genetics*, 13(9),

777–784. <https://doi.org/10.1097/GIM.0b013e31822c79f9>.An

- Kelley AR, Bach SBH, Perry G. (2019). Analysis of post-translational modifications in Alzheimer's disease by mass spectrometry. *Biochim Biophys Acta - Mol Basis Dis.* Elsevier. 1865;2019:2040–7.
- Khatri, N., & Man, H. Y. (2019). The autism and Angelman syndrome protein Ube3A/E6AP: The gene, E3 ligase ubiquitination targets and neurobiological functions. *Frontiers in Molecular Neuroscience*, 12(April), 1–12.
<https://doi.org/10.3389/fnmol.2019.00109>
- Kim, D. I., Jensen, S. C., Noble, K. A., Kc, B., Roux, K. H., Motamedchaboki, K., & Roux, K. J. (2016). An improved smaller biotin ligase for BioID proximity labeling. *Molecular Biology of the Cell*, 27(8), 1188–1196. <https://doi.org/10.1091/mbc.E15-12-0844>
- Kim, E., & Sheng, M. (2004). PDZ domain proteins of synapses. *Nature Reviews Neuroscience*, 5(10), 771–781. <https://doi.org/10.1038/nrn1517>
- Kim, J. H., Lee, S. R., Li, L. H., Park, H. J., Park, J. H., Lee, K. Y., ... Choi, S. Y. (2011). High cleavage efficiency of a 2A peptide derived from porcine teschovirus-1 in human cell lines, zebrafish and mice. *PLoS ONE*, 6(4), 1–8.
<https://doi.org/10.1371/journal.pone.0018556>
- Kim, T. K., & Eberwine, J. H. (2010). Mammalian cell transfection: The present and the future. *Analytical and Bioanalytical Chemistry*, 397(8), 3173–3178.
<https://doi.org/10.1007/s00216-010-3821-6>

- Knight, J. D. R., Choi, H., Gupta, G. D., Pelletier, L., Raught, B., Nesvizhskii, A. I., & Gingras, A. C. (2017). ProHits-viz: A suite of web tools for visualizing interaction proteomics data. *Nature Methods*, *14*(7), 645–646.
<https://doi.org/10.1038/nmeth.4330>
- Konopaske, G. T., Lange, N., Coyle, J. T., & Benes, F. M. (2014). Prefrontal cortical dendritic spine pathology in schizophrenia and bipolar disorder. *JAMA Psychiatry*, *71*(12), 1323–1331. <https://doi.org/10.1001/jamapsychiatry.2014.1582>
- Krivosheya, D., Tapia, L., Levinson, J. N., Huang, K., Kang, Y., Hines, R., ... El-Husseini, A. (2008). ErbB4-neuregulin signaling modulates synapse development and dendritic arborization through distinct mechanisms. *The Journal of Biological Chemistry*, *283*(47), 32944–32956. <https://doi.org/10.1074/jbc.M800073200>
- Lazaro, M. T., Taxidis, J., Shuman, T., Bachmutsky, I., Ikrar, T., Santos, R., ... Golshani, P. (2019). Reduced Prefrontal Synaptic Connectivity and Disturbed Oscillatory Population Dynamics in the CNTNAP2 Model of Autism. *Cell Reports*, *27*(9), 2567-2578.e6. <https://doi.org/10.1016/j.celrep.2019.05.006>
- LeBlanc, J.J., and Fagiolini, M. (2011). Autism: a "critical period" disorder? *Neural Plasticity*, 2011, 921680.
- Lee, E., Lee, J., & Kim, E. (2017). Excitation/Inhibition Imbalance in Animal Models of Autism Spectrum Disorders. *Biological Psychiatry*, *81*(10), 838–847.
<https://doi.org/10.1016/j.biopsych.2016.05.011>

- Lee, F. H. F., Zai, C. C., Cordes, S. P., Roder, J. C., & Wong, A. H. C. (2013). Abnormal interneuron development in disrupted-in-schizophrenia-1 L100P mutant mice. *Molecular Brain*, 6, 20. <https://doi.org/10.1186/1756-6606-6-20>
- Le Magueresse, C., & Monyer, H. (2013). GABAergic interneurons shape the functional maturation of the cortex. *Neuron*, 77(3), 388–405. <https://doi.org/10.1016/j.neuron.2013.01.011>
- Le Roux, N., Amar, M., Baux, G., & Fossier, P. (2006). Homeostatic control of the excitation-inhibition balance in cortical layer 5 pyramidal neurons. *European Journal of Neuroscience*, 24(12), 3507–3518. <https://doi.org/10.1111/j.1460-9568.2006.05203.x>
- Leterrier, C. (2018). The axon initial segment: An updated viewpoint. *Journal of Neuroscience*, 38(9), 2135–2145. <https://doi.org/10.1523/JNEUROSCI.1922-17.2018>
- Leussis, M. P., Berry-Scott, E. M., Saito, M., Jhuang, H., De Haan, G., Alkan, O., ... Petryshen, T. L. (2013). The ANK3 bipolar disorder gene regulates psychiatric-related behaviors that are modulated by lithium and stress. *Biological Psychiatry*, 73(7), 683–690. <https://doi.org/10.1016/j.biopsych.2012.10.016>
- Leussis, M. P., Madison, J. M., & Petryshen, T. L. (2012). Ankyrin 3: genetic association with bipolar disorder and relevance to disease pathophysiology. *Biology of Mood & Anxiety Disorders*, 2(1), 18. <https://doi.org/10.1186/2045-5380-2-18>

- Lewis, T. L., Courchet, J., & Polleux, F. (2013). Cellular and molecular mechanisms underlying axon formation, growth, and branching. *Journal of Cell Biology*, 202(6), 837–848. <https://doi.org/10.1083/jcb.201305098>
- Lezmy, J., Lipinsky, M., Khrapunsky, Y., Patrich, E., Shalom, L., Peretz, A., ... Attali, B. (2017). M-current inhibition rapidly induces a unique CK2-dependent plasticity of the axon initial segment. *PNAS*, 114(47), E10234–E10243. <https://doi.org/10.1073/pnas.1708700114>
- Li, Y., Zhu, Y., Nguchu, B. A., Wang, Y., Wang, H., Qiu, B., & Wang, X. (2020). Dynamic Functional Connectivity Reveals Abnormal Variability and Hyper-connected Pattern in Autism Spectrum Disorder. *Autism Research*, 13(2), 230–243. <https://doi.org/10.1002/aur.2212>
- Lichtenstein, P., Carlström, E., Råstam, M., Gillberg, C., & Anckarsäter, H. (2010). The genetics of autism spectrum disorders and related neuropsychiatric disorders in childhood. *The American Journal of Psychiatry*, 167(11), 1357–1363. <https://doi.org/10.1176/appi.ajp.2010.10020223>
- Lim, L., Mi, D., Llorca, A., & Marín, O. (2018). Development and Functional Diversification of Cortical Interneurons. *Neuron*, 100(2), 294–313. <https://doi.org/10.1016/j.neuron.2018.10.009>

- Lima Caldeira, G., Peça, J., & Carvalho, A. L. (2019). New insights on synaptic dysfunction in neuropsychiatric disorders. *Current Opinion in Neurobiology*, 57(February), 62–70. <https://doi.org/10.1016/j.conb.2019.01.004>
- Liu, X. S., Wu, H., Krzisch, M., Wu, X., Graef, J., Muffat, J., ... Jaenisch, R. (2018). Rescue of Fragile X Syndrome Neurons by DNA Methylation Editing of the FMR1 Gene. *Cell*, 172(5), 979-992.e6. <https://doi.org/10.1016/j.cell.2018.01.012>
- Liu X, Salokas K, Tamene F, Jiu Y, Weldatsadik RG, Öhman T, et al. (2018). An AP-MS- and BioID-compatible MAC-tag enables comprehensive mapping of protein interactions and subcellular localizations. *Nat Commun*. Springer US.;9.
- Loh, K. H., Stawski, P. S., Draycott, A. S., Udeshi, N. D., Lehrman, E. K., Wilton, D. K., ... Ting, A. Y. (2016). Proteomic Analysis of Unbounded Cellular Compartments: Synaptic Clefts. *Cell*, 166(5), 1295-1307.e21. <https://doi.org/10.1016/j.cell.2016.07.041>
- Lomholt, L. H., Andersen, D. V., Sejrsgaard-Jacobsen, C., Øzdemir, C. M., Graff, C., Schjerning, O., ... Nielsen, R. E. (2019). Mortality rate trends in patients diagnosed with schizophrenia or bipolar disorder: a nationwide study with 20 years of follow-up. *International Journal of Bipolar Disorders*. <https://doi.org/10.1186/s40345-018-0140-x>

Louros, S. R., & Osterweil, E. K. (2016). Perturbed proteostasis in autism spectrum disorders. *Journal of Neurochemistry*, 139(6), 1081–1092.

<https://doi.org/10.1111/jnc.13723>

Lowther, C., Costain, G., Stavropoulos, D. J., Melvin, R., Silversides, C. K., Andrade, D. M., ... Bassett, A. S. (2014). Delineating the 15q13.3 microdeletion phenotype: a case series and comprehensive review of the literature. *Genetics in Medicine : Official Journal of the American College of Medical Genetics*, (February), 1–9.

<https://doi.org/10.1038/gim.2014.83>

Luoni, A., Massart, R., Nieratschker, V., Nemoda, Z., Blasi, G., Gilles, M., ... Riva, M. A. (2016). Ankyrin-3 as a molecular marker of early-life stress and vulnerability to psychiatric disorders. *Translational Psychiatry*, 6(11), e943-9.

<https://doi.org/10.1038/tp.2016.211>

Ma, Q., Ruan, H., Peng, L., Zhang, M., Gack, M. U., & Yao, W. D. (2017). Proteasome-independent polyubiquitin linkage regulates synapse scaffolding, efficacy, and plasticity. *PNAS*, 114(41), E8760–E8769. <https://doi.org/10.1073/pnas.1620153114>

Mabb, A. M., & Ehlers, M. D. (2010). Ubiquitination in postsynaptic function and plasticity. *Annual Review of Cell and Developmental Biology*, 26, 179–210.

<https://doi.org/10.1146/annurev-cellbio-100109-104129>

Maenner, M. J., Shaw, K. A., Baio, J., Washington, A., Patrick, M., DiRienzo, M., ...

Dietz, P. M. (2020). Prevalence of autism spectrum disorder among children aged 8

Years-Autism and developmental disabilities monitoring network, 11 Sites, United States, 2016. *MMWR Surveillance Summaries*, 69(4), 1–12.

<https://doi.org/10.15585/MMWR.SS6904A1>

Margolis, S. S., Sell, G. L., Zbinden, M. A., & Bird, L. M. (2015). Angelman Syndrome.

Neurotherapeutics, 12(3), 641–650. <https://doi.org/10.1007/s13311-015-0361-y>

Matharu, N., Rattanasopha, S., Tamura, S., Maliskova, L., Wang, Y., Bernard, A., ...

Ahituv, N. (2019). CRISPR-mediated activation of a promoter or enhancer rescues obesity caused by haploinsufficiency. *Science*, 363(6424).

<https://doi.org/10.1126/science.aau0629>

Matic K, Eninger T, Bardoni B, Davidovic L, Macek B. (2014) Quantitative

phosphoproteomics of murine Fmr1 -KO cell lines provides new insights into

FMRP-dependent signal transduction mechanisms. *J Proteome Res.* 13(10), 4388–97.

May, D. G., Scott, K. L., Campos, A. R., & Roux, K. J. (2020). Comparative Application

of BioID and TurboID for Protein-Proximity Biotinylation. *Cells*, 9(5).

<https://doi.org/10.3390/cells9051070>

McFadden, K., & Minshew, N. J. (2013). Evidence for dysregulation of axonal growth

and guidance in the etiology of ASD. *Frontiers in Human Neuroscience*, 7(OCT), 1–

10. <https://doi.org/10.3389/fnhum.2013.00671>

McPheeters, M. L., Warren, Z., Sathe, N., Bruzek, J. L., Krishnaswami, S., Jerome, R. N., & Veenstra-Vanderweele, J. (2011). A systematic review of medical treatments for children with autism spectrum disorders. *Pediatrics*, 127(5), e1312–e1321.

<https://doi.org/10.1542/peds.2011-0427>

Mehla J, Caufield JH, Sakhawalker N, Uetz P. (2017). A comparison of two hybrid approaches for detecting protein- protein interactions. *Methods Enzym*, 333–58.

Mei, L., & Nave, K.-A. (2014). Neuregulin-ERBB signaling in the nervous system and neuropsychiatric diseases. *Neuron*, 83(1), 27–49.

<https://doi.org/10.1016/j.neuron.2014.06.007>

Mei L, Xiong WC. (2008). Neuregulin 1 in neural development, synaptic plasticity and schizophrenia. *Nat Rev Neurosci.*;9(6):437-452. doi: 10.1038/nrn2392;

10.1038/nrn2392.

Mevissen, T. E. T., Hospenthal, M. K., Geurink, P. P., Elliott, P. R., Akutsu, M., Arnaudo, N., ... Komander, D. (2013). OTU deubiquitinases reveal mechanisms of linkage specificity and enable ubiquitin chain restriction analysis. *Cell*, 154(1), 169–

184. <https://doi.org/10.1016/j.cell.2013.05.046>

Mevissen, T. E. T., Kulathu, Y., Mulder, M. P. C., Geurink, P. P., Maslen, S. L., Gersch, M., ... Komander, D. (2016). Molecular basis of Lys11-polyubiquitin specificity in the deubiquitinase Cezanne. *Nature*, 538(7625), 402–405.

<https://doi.org/10.1038/nature19836>

- Meza, R. C., López-Jury, L., Canavier, C. C., & Henny, P. (2018). Role of the axon initial segment in the control of spontaneous frequency of nigral dopaminergic neurons in vivo. *Journal of Neuroscience*, 38(3), 733–744.
<https://doi.org/10.1523/JNEUROSCI.1432-17.2017>
- Mi, H., Muruganujan, A., Casagrande, J. T., & Thomas, P. D. (2013). Large-scale gene function analysis with the panther classification system. *Nature Protocols*, 8(8), 1551–1566. <https://doi.org/10.1038/nprot.2013.092>
- Mitchell, A.J., Vancampfort, D., Sweers, K., van Winkel, R., Yu, W., & De Hert, M. (2013). Prevalence of metabolic syndrome and metabolic abnormalities in schizophrenia and related disorders--a systematic review and meta-analysis. *Schizophr Bull*, 39(2):306-318. doi: 10.1093/schbul/sbr148; 10.1093/schbul/sbr148.
- Millar, J. K., Wilson-annan, J. C., Anderson, S., Christie, S., Martin, S., Semple, C. A. M., ... Porteous, D. J. (2000). Disruption of two novel genes by a translocation co-segregating with schizophrenia. *Hum Mol Genet*, 9(9), 1415–1424.
- Miles, J. H. (2011). Autism spectrum disorders--a genetics review. *Genetics in Medicine : Official Journal of the American College of Medical Genetics*, 13(4), 278–294.
<https://doi.org/10.1097/GIM.0b013e3181ff67ba>
- Moreira, D. P., Griesi-Oliveira, K., Bossolani-Martins, A. L., Lourenço, N. C. V., Takahashi, V. N. O., da Rocha, K. M., ... Passos-Bueno, M. R. (2014). Investigation of 15q11-q13, 16p11.2 and 22q13 CNVs in Autism Spectrum Disorder Brazilian

Individuals with and without Epilepsy. *PloS One*, 9(9), e107705.

<https://doi.org/10.1371/journal.pone.0107705>

Morris JH, Knudsen GM, Verschueren E, Johnson JR, Cimermancic P, Greninger AL, et al. (2014). Affinity purification–mass spectrometry and network analysis to understand protein-protein interactions. *Nat Protoc.*;9:2539–54.

Morris, C. A., Mervis, C. B., Paciorkowski, A. P., Abdul-Rahman, O., Dugan, S. L., Rope, A. F., ... Osborne, L. R. (2015). 7q11.23 Duplication syndrome: Physical characteristics and natural history. *American Journal of Medical Genetics, Part A*, 167(12), 2916–2935. <https://doi.org/10.1002/ajmg.a.37340>

Nakazawa, K., & Sapkota, K. (2020). The origin of NMDA receptor hypofunction in schizophrenia. *Pharmacology and Therapeutics*, 205, 107426.

<https://doi.org/10.1016/j.pharmthera.2019.107426>

Nakazawa, K., Zsiros, V., Jiang, Z., Nakao, K., Kolata, S., Zhang, S., & Belforte, J. E. (2012). GABAergic interneuron origin of schizophrenia pathophysiology.

Neuropharmacology, 62(3), 1574–1583.

<https://doi.org/10.1016/j.neuropharm.2011.01.022>

Nestler, E. J.; Hyman, S. E. (2010). Animal Models of Neuropsychiatric Disorders.

Nature Neuroscience, 23(1), 1–7. <https://doi.org/10.1038/nn.2647>.Animal

Niarchou, M., Chawner, S.J.R.A., Doherty, J.L. et al. Psychiatric disorders in children with 16p11.2 deletion and duplication. (2019). *Transl Psychiatry* 9, 8.

<https://doi.org/10.1038/s41398-018-0339-8>

Nilsson, S. R. O., Celada, P., Fejgin, K., Thelin, J., Nielsen, J., Santana, N., ... Didriksen, M. (2016). A mouse model of the 15q13.3 microdeletion syndrome shows prefrontal neurophysiological dysfunctions and attentional impairment. *Psychopharmacology*, 233(11), 2151–2163. <https://doi.org/10.1007/s00213-016-4265-2>

O'Connor, E. C., Bariselli, S., & Bellone, C. (2014). Synaptic basis of social dysfunction: a focus on postsynaptic proteins linking group-I mGluRs with AMPARs and NMDARs. *The European Journal of Neuroscience*, 39(7), 1114–1129.

<https://doi.org/10.1111/ejn.12510>

O'Roak, B.J., Vives, L., Girirajan, S., Karakoc, E., Krumm, N., Coe, B.P., Levy, R., Ko, A., Lee, C., Smith, J.D., et al. (2012). Sporadic autism exomes reveal a highly interconnected protein network of de novo mutations. *Nature*, 485, 246-250.

Pagnamenta, A. T., Wing, K., Sadighi Akha, E., Knight, S. J. L., Bölte, S., Schmötzer, G., ... Monaco, A. P. (2009). A 15q13.3 microdeletion segregating with autism. *EJHG*, 17(5), 687–692. <https://doi.org/10.1038/ejhg.2008.228>

Papaleo, F., Yang, F., Paterson, C., Palumbo, S., Carr, G. V., Wang, Y., ... Law, A. J. (2016). Behavioral, neurophysiological, and synaptic impairment in a transgenic

neuregulin1 (NRG1-IV) murine schizophrenia model. *Journal of Neuroscience*, 36(17), 4859–4875. <https://doi.org/10.1523/JNEUROSCI.4632-15.2016>

Patterson, T.L., & Leeuwenkamp, O.R. (2008). Adjunctive psychosocial therapies for the treatment of schizophrenia. *Schizophr Res*, 100(1-3):108-119. doi: 10.1016/j.schres.2007.12.468; 10.1016/j.schres.2007.12.468.

Peñagarikano, O., Abrahams, B. S., Herman, E. I., Winden, K. D., Gdalyahu, A., Dong, H., ... Geschwind, D. H. (2011). Absence of CNTNAP2 leads to epilepsy, neuronal migration abnormalities, and core autism-related deficits. *Cell*, 147(1), 235–246. <https://doi.org/10.1016/j.cell.2011.08.040>

Penzes, P., Cahill, M. E., Jones, K. a, VanLeeuwen, J.-E., & Woolfrey, K. M. (2011). Dendritic spine pathology in neuropsychiatric disorders. *Nature Neuroscience*, 14(3), 285–293. <https://doi.org/10.1038/nn.2741>

Phillips, M., & Pozzo-Miller, L. (2014). Dendritic spine dysgenesis in autism related disorders. *Neuroscience Letters*, 601, 30–40. <https://doi.org/10.1016/j.neulet.2015.01.011>

Pinto, D., Delaby, E., Merico, D., Barbosa, M., Merikangas, A., Klei, L., Thiruvahindrapuram, B., Xu, X., Ziman, R., Wang, Z., et al. (2014). Convergence of genes and cellular pathways dysregulated in autism spectrum disorders. *American Journal of Human Genetics* 94, 677-694.

- Pucilowska, J., Vithayathil, J., Tavares, E. J., Kelly, C., Karlo, J. C., & Landreth, G. E. (2015). The 16p11.2 Deletion Mouse Model of Autism Exhibits Altered Cortical Progenitor Proliferation and Brain Cytoarchitecture Linked to the ERK MAPK Pathway. *Journal of Neuroscience*, 35(7), 3190–3200. <https://doi.org/10.1523/JNEUROSCI.4864-13.2015>
- Qian, S., Zhan, X., Lu, M., Li, N., Long, Y., Li, X., ... Zhan, X. (2019). Quantitative analysis of ubiquitinated proteins in human pituitary and pituitary adenoma tissues. *Frontiers in Endocrinology*, 10(MAY). <https://doi.org/10.3389/fendo.2019.00328>
- Qiao, Y., Chansonette Badduke, |, Flamingo Tang, |, Cowieson, D., Martell, S., Lewis, S. M. E., ... Rajcan-Separovic, E. (2017). Whole exome sequencing of families with 1q21.1 microdeletion or microduplication. *American Journal of Medical Genetics, Part A*, 173A, 1782–1791. <https://doi.org/10.1002/ajmg.a.38247>.
- Ong SE, Blagoev B, Kratchmarova I, Kristensen DB, Steen H, Pandey A, et al. (2002). Stable isotope labeling by amino acids in cell culture, SILAC, as a simple and accurate approach to expression proteomics. *Mol Cell Proteomics*.;1:376–86.
- Pan, J. Q., Lewis, M. C., Ketterman, J. K., Clore, E. L., Riley, M., Richards, K. R., ... Haggarty, S. J. (2011). AKT kinase activity is required for lithium to modulate mood-related behaviors in mice. *Neuropsychopharmacology*, 36(7), 1397–1411. <https://doi.org/10.1038/npp.2011.24>

- Patel, V. J., Thalassinou, K., Slade, S. E., Connolly, J. B., Crombie, A., Murrell, J. C., & Scrivens, J. H. (2009). A comparison of labeling and label-free mass spectrometry-based proteomics approaches. *Journal of Proteome Research*, 8(7), 3752–3759. <https://doi.org/10.1021/pr900080y>
- Piguel, N. H., Yoon, S., DeSimone, F. I., Sanders, S. S., Gao, R., Horan, K. E., ... Penzes, P. (2019). Ankyrin-G-190 palmitoylation mediates dendrite and spine morphogenesis and is altered in response to lithium. *BioRxiv*, 620708. Retrieved from <https://doi.org/10.1101/620708>
- Rao, V. R., & Lowenstein, D. H. (2015). Epilepsy. *Current Biology*, 25(17), R742–R746. <https://doi.org/10.1016/j.cub.2015.07.072>
- Reichenberg A, Caspi A, Harrington H, et al.(2010) Static and dynamic cognitive deficits in childhood preceding adult schizophrenia: A 30-year study. *Am J Psychiatry*.;167(2):160-169. doi: 10.1176/appi.ajp.2009.09040574; 10.1176/appi.ajp.2009.09040574.
- Reim D, Distler U, Halbedl S, Verpelli C, Sala C, Bockmann J, et al. (2017). Proteomic analysis of post-synaptic density fractions from Shank3 mutant mice reveals brain region specific changes relevant to autism spectrum disorder. *Front Mol Neurosci*.;10:1–10.

- Remington, G., Foussias, G., Fervaha, G., Agid, O., Takeuchi, H., Lee, J., ... Hahn, M. (2016). Treating Negative Symptoms in Schizophrenia: an Update. *Curr Treat Options Psych*, 3, 133–150. <https://doi.org/10.1007/s40501-016-0075-8>
- Rhee HW, Zou P, Udeshi ND, et al.: Proteomic mapping of mitochondria in living cells via spatially restricted enzymatic tagging. *Science*. 2013; 339(6125): 1328–31.
- Rosoklija, G., Toomayan, G., Ellis, S. P., Keilp, J., Mann, J. J., Latov, N., ... Dwork, A. J. (2000). Structural abnormalities of subicular dendrites in subjects with schizophrenia and mood disorders: Preliminary findings. *Archives of General Psychiatry*, 57(4), 349–356. <https://doi.org/10.1001/archpsyc.57.4.349>
- Ross, C. A., & Poirier, M. A. (2004). Protein aggregation and neurodegenerative disease. *Nature Medicine*, 10(7), S10. <https://doi.org/10.1038/nm1066>
- Rossignol, D. A., & Frye, R. E. (2012). Mitochondrial dysfunction in autism spectrum disorders: a systematic review and meta-analysis. *Molecular Psychiatry*, 17, 290–314. <https://doi.org/10.1038/mp.2010.136>
- Roux KJ, Kim DI, Raida M, Burke B. (2012). A promiscuous biotin ligase fusion protein identifies proximal and interacting proteins in mammalian cells. *J Cell Biol*, 196:801–10.
- Ruzzo, E. K., Pérez-Cano, L., Jung, J. Y., Wang, L. kai, Kashef-Haghighi, D., Hartl, C., ... Wall, D. P. (2019). Inherited and De Novo Genetic Risk for Autism Impacts

Shared Networks. *Cell*, 178(4), 850-866.e26.

<https://doi.org/10.1016/j.cell.2019.07.015>

Sakai, J. (2016). How synaptic pruning shapes neural wiring during development and, possibly, in disease. *PNAS*, 117(28). <https://doi.org/10.1073/pnas.2010281117>

Sandin, S., Lichtenstein, P., Kuja-Halkola, R., Larsson, H., Hultman, C.M., and Reichenberg, A. (2014). The familial risk of autism. *JAMA* 311, 1770-1777.

Sano, T., Vajda, C., & Cantor, C.R. (1998). Genetic engineering of streptavidin, a versatile affinity tag. *J Chromatogr B Biomed Sci Appl*, 715(1):85-91. doi: 10.1016/s0378-4347(98)00316-8.

Santiago-Sim, T., Burrage, L. C., Ebstein, F., Tokita, M. J., Miller, M., Bi, W., ... Walkiewicz, M. A. (2017). Biallelic Variants in OTUD6B Cause an Intellectual Disability Syndrome Associated with Seizures and Dysmorphic Features. *American Journal of Human Genetics*, 100(4), 676–688.
<https://doi.org/10.1016/j.ajhg.2017.03.001>

Schmidt, M., & Finley, D. (2014). Regulation of proteasome activity in health and disease. *Biochimica et Biophysica Acta - Molecular Cell Research*, 1843(1), 13–25.
<https://doi.org/10.1016/j.bbamcr.2013.08.012>

- Schopp, I. M., & Béthune, J. (2018). Split-bioid — proteomic analysis of context-specific protein complexes in their native cellular environment. *Journal of Visualized Experiments*, 2018(134), 1–11. <https://doi.org/10.3791/57479>
- Schork, A. J., Won, H., Appadurai, V., Nudel, R., Gandal, M., Delaneau, O., ... Werge, T. (2019). A genome-wide association study of shared risk across psychiatric disorders implicates gene regulation during fetal neurodevelopment. *Nature Neuroscience*, 22(3), 353–361. <https://doi.org/10.1038/s41593-018-0320-0>
- Scudder, S. L., Goo, M. S., Cartier, A. E., Molteni, A., Schwarz, L. A., Wright, R., & Patrick, G. N. (2014). Synaptic strength is bidirectionally controlled by opposing activity-dependent regulation of nedd4-1 and USP8. *Journal of Neuroscience*, 34(50), 16637–16649. <https://doi.org/10.1523/JNEUROSCI.2452-14.2014>
- Selimbeyoglu, A., Kim, C. K., Inoue, M., Lee, S. Y., Hong, A. S. O., Kauvar, I., ... Deisseroth, K. (2017). Modulation of prefrontal cortex excitation/inhibition balance rescues social behavior in CNTNAP2-deficient mice. *Science Translational Medicine*, 9(401). <https://doi.org/10.1126/scitranslmed.aah6733>
- Seshadri, S., Faust, T., Ishizuka, K., Delevich, K., Chung, Y., Kim, S. H., ... Sawa, a. (2015). Interneuronal DISC1 regulates NRG1-ErbB4 signalling and excitatory-inhibitory synapse formation in the mature cortex. *Nat Commun*, 6(May), 10118. <https://doi.org/10.1038/ncomms10118>

Sharp, A. J., Mefford, H. C., Li, K., Baker, C., Skinner, C., Stevenson, R. E., ... Eichler, E. E. (2008). A recurrent 15q13.3 microdeletion syndrome associated with mental retardation and seizures. *Nature Genetics*, 40(3), 322–328.

<https://doi.org/10.1038/ng.93>

Shinawi, M., Schaaf, C. P., Bhatt, S. S., Xia, Z., Patel, A., Cheung, S. W., ... Stankiewicz, P. (2009). A small recurrent deletion within 15q13.3 is associated with a range of neurodevelopmental phenotypes. *Nature Genetics*, 41(12), 1269–1271.

<https://doi.org/10.1038/ng.481>

Silva JC, Gorenstein MV, Li GZ, Vissers JPC, Geromanos SJ. (2006). Absolute quantification of proteins by LCMSE: a virtue of parallel MS acquisition. *Mol Cell Proteomics*.;5:144–56.

Singh, S., Kumar, A., Agarwal, S., Phadke, S.R. & Jaiswal, Y. (2014). Genetic insight of schizophrenia: Past and future perspectives. *Gene*, 535(2):97-100. doi:

10.1016/j.gene.2013.09.110; 10.1016/j.gene.2013.09.110.

Silverman, J. L., Yang, M., Lord, C., & Crawley, J. N. (2010). Behavioural phenotyping assays for mouse models of autism. *Nature Reviews Neuroscience*, 11(7), 490–502.

<https://doi.org/10.1038/nrn2851>

Smith, K. R., Kopeikina, K. J., Fawcett-Patel, J. M., Leaderbrand, K., Gao, R., Schürmann, B., ... Penzes, P. (2014). Psychiatric Risk Factor ANK3/Ankyrin-G

Nanodomains Regulate the Structure and Function of Glutamatergic Synapses.

Neuron, 84(2), 399–415. <https://doi.org/10.1016/j.neuron.2014.10.010>

Smith, K. R., & Penzes, P. (2018). Ankyrins: Roles in synaptic biology and pathology.

Molecular and Cellular Neuroscience, 91(April), 131–139.

<https://doi.org/10.1016/j.mcn.2018.04.010>

Spence EF, Dube S, Uezu A, Locke M, Soderblom EJ, Soderling SH. (2019). In vivo proximity proteomics of nascent synapses reveals a novel regulator of cytoskeleton-mediated synaptic maturation. *Nat Commun*. Springer US.;10:1–16.

Srikanth, P., Han, K., Callahan, D. G., Makovkina, E., Muratore, C. R., Lalli, M. A., ...

Young-Pearse, T. L. (2015). Genomic DISC1 Disruption in hiPSCs Alters Wnt Signaling and Neural Cell Fate. *Cell Reports*, 12(9), 1414–1429.

<https://doi.org/10.1016/j.celrep.2015.07.061>

Srikanth, P., Lagomarsino, V. N., Muratore, C. R., Ryu, S. C., He, A., Taylor, W. M., ...

Young-Pearse, T. L. (2018). Shared effects of DISC1 disruption and elevated WNT signaling in human cerebral organoids. *Translational Psychiatry*, 8(1).

<https://doi.org/10.1038/s41398-018-0122-x>

Stambolic, V., & Woodgett, J. R. (1994). Mitogen inactivation of glycogen synthase

kinase-3 β in intact cells via serine 9 phosphorylation. *Biochemical Journal*, 303(3),

701–704. <https://doi.org/10.1042/bj3030701>

- Stämpfli, P., Sommer, S., Manoliu, A., Burrer, A., Schmidt, A., Herdener, M., ... Kirschner, M. (2019). Subtle white matter alterations in schizophrenia identified with a new measure of fiber density. *Scientific Reports*, 9(1), 1–11. <https://doi.org/10.1038/s41598-019-40070-2>
- Star, E. N., Kwiatkowski, D. J., & Murthy, V. N. (2002). Rapid turnover of actin in dendritic spines and its regulation by activity. *Nature Neuroscience*, 5(3), 239–246. <https://doi.org/10.1038/nn811>
- Steen RG, Mull C, McClure R, Hamer RM, Lieberman JA. (2006). Brain volume in first-episode schizophrenia: Systematic review and meta-analysis of magnetic resonance imaging studies. *Br J Psychiatry*.;188:510-518. doi: 10.1192/bjp.188.6.510.
- Stein, J. L., Parikshak, N. N., & Geschwind, D. H. (2013, January 23). Rare Inherited Variation in Autism: Beginning to See the Forest and a Few Trees. *Neuron*. <https://doi.org/10.1016/j.neuron.2013.01.010>
- Stefansson, H., Rujescu, D., Cichon, S., Pietiläinen, O. P. H., Ingason, A., Steinberg, S., ... Stefansson, K. (2008). Large recurrent microdeletions associated with schizophrenia. *Nature*, 455(7210), 232–236. <https://doi.org/10.1038/nature07229>
- Stessman, H. A. F., Turner, T. N., & Eichler, E. E. (2016). Molecular subtyping and improved treatment of neurodevelopmental disease. *Genome Medicine*, 8(1), 1–9. <https://doi.org/10.1186/s13073-016-0278-z>

- Steullet, P., Cabungcal, J. H., Coyle, J., Didriksen, M., Gill, K., Grace, A. A., ... Do, K. Q. (2017). Oxidative stress-driven parvalbumin interneuron impairment as a common mechanism in models of schizophrenia. *Molecular Psychiatry*, 22(7), 936–943. <https://doi.org/10.1038/mp.2017.47>
- Stranger, B. E., Forrest, M. S., Dunning, M., Ingle, C. E., Beazley, C., Thorne, N., ... Dermitzakis, E. T. (2007). Relative Impact of Nucleotide and Copy Number Variation on Gene Expression Phenotypes. *Science*, 315(5813), 848–853. <https://doi.org/10.1126/science.1135710>
- Subramanian, L., Calcagnotto, M. E., & Paredes, M. F. (2020). Cortical Malformations: Lessons in Human Brain Development. *Frontiers in Cellular Neuroscience*, 13(January), 1–17. <https://doi.org/10.3389/fncel.2019.00576>
- Subramanian, A., Tamayo, P., Mootha, V. K., Mukherjee, S., Ebert, B. L., Gillette, M. A., ... Mesirov, J. P. (2005). Gene set enrichment analysis: A knowledge-based approach for interpreting genome-wide expression profiles. *PNAS*, 102(43), 15545–15550. <https://doi.org/10.1073/pnas.0506580102>
- Sun L, Castellanos N, Grutzner C, et al. (2013). Evidence for dysregulated high-frequency oscillations during sensory processing in medication-naive, first episode schizophrenia. *Schizophr Res.*;150(2-3):519-525. doi: 10.1016/j.schres.2013.08.023; 10.1016/j.schres.2013.08.023.

- Swartz, M.S., Perkins, D.O., Stroup TS, Davis, S.M., Capuano, G., Rosenheck, R.A., et al. (2007). Effects of antipsychotic medications on psychosocial functioning in patients with chronic schizophrenia: Findings from the NIMH CATIE study. *Am J Psychiatry*, 164(3):428-436. doi: 10.1176/appi.ajp.164.3.428.
- Swatek, K. N., & Komander, D. (2016). Ubiquitin modifications. *Cell Research*, 26(4), 399–422. <https://doi.org/10.1038/cr.2016.39>
- Sweet, R. A., Henteleff, R. A., Zhang, W., Sampson, A. R., & Lewis, D. A. (2009). Reduced dendritic spine density in auditory cortex of subjects with schizophrenia. *Neuropsychopharmacology*, 34(2), 374–389. <https://doi.org/10.1038/npp.2008.67>
- Syrbe, S., Harms, F. L., Parrini, E., Montomoli, M., Mütze, U., Helbig, K. L., ... Guerrini, R. (2017). Delineating SPTAN1 associated phenotypes: From isolated epilepsy to encephalopathy with progressive brain atrophy. *Brain*, 140(9), 2322–2336. <https://doi.org/10.1093/brain/awx195>
- Tam, V., Patel, N., Turcotte, M., Bossé, Y., Paré, G., & Meyre, D. (2019). Benefits and limitations of genome-wide association studies. *Nature Reviews Genetics*, 20(8), 467–484. <https://doi.org/10.1038/s41576-019-0127-1>
- Tau, G. Z., & Peterson, B. S. (2010). Normal development of brain circuits. *Neuropsychopharmacology*, 35(1), 147–168. <https://doi.org/10.1038/npp.2009.115>

- Teo, G., Liu, G., Zhang, J., Nesvizhskii, A. I., Gingras, A. C., & Choi, H. (2014). SAINTexpress: Improvements and additional features in Significance Analysis of INTeractome software. *Journal of Proteomics*, *100*, 37–43. <https://doi.org/10.1016/j.jprot.2013.10.023>
- Thibert, R. L., Larson, A. M., Hsieh, D. T., Raby, A. R., & Thiele, E. A. (2013, April 1). Neurologic manifestations of Angelman syndrome. *Pediatric Neurology*. *48*(4), 271-279, <https://doi.org/10.1016/j.pediatrneurol.2012.09.015>.
- Tiihonen, J., Taipale, H., Mehtälä, J., Vattulainen, P., Correll, C. U., & Tanskanen, A. (2019). Association of Antipsychotic Polypharmacy vs Monotherapy with Psychiatric Rehospitalization among Adults with Schizophrenia. *JAMA Psychiatry*, *76*(5), 499–507. <https://doi.org/10.1001/jamapsychiatry.2018.4320>
- Trost, B., Walker, S., Wang, Z., Thiruvahindrapuram, B., MacDonald, J. R., Sung, W. W. L., ... Scherer, S. W. (2018). A Comprehensive Workflow for Read Depth-Based Identification of Copy-Number Variation from Whole-Genome Sequence Data. *American Journal of Human Genetics*, *102*(1), 142–155. <https://doi.org/10.1016/j.ajhg.2017.12.007>
- Tuchman, R., & Rapin, I. (2002). Epilepsy in autism. *Lancet Neurology*, *1*(6), 352–358. [https://doi.org/10.1016/S1474-4422\(02\)00160-6](https://doi.org/10.1016/S1474-4422(02)00160-6)

Turner, T. N., Coe, B. P., Dickel, D. E., Hoekzema, K., Nelson, B. J., Zody, M. C., ...

Eichler, E. E. (2017). Genomic Patterns of De Novo Mutation in Simplex Autism. *Cell*, 171(3), 710-722.e12. <https://doi.org/10.1016/j.cell.2017.08.047>

Tyanova, S., Temu, T., & Cox, J. (2016). The MaxQuant computational platform for mass spectrometry-based shotgun proteomics. *Nature Protocols*, 11(12), 2301–2319. <https://doi.org/10.1038/nprot.2016.136>

Uezu, A., Kanak, D. J., Bradshaw, T. W. A., Soderblom, E. J., Catavero, C. M., Burette, A. C., ... Soderling, S. H. (2016). Identification of an elaborate complex mediating postsynaptic inhibition. *Science*, 353(6304), 1123–1129. <https://doi.org/10.1126/science.aag0821>

Uddin, M., Tammimies, K., Pellecchia, G., Alipanahi, B., Hu, P., Wang, Z., ... Scherer, S. W. (2014). Brain-expressed exons under purifying selection are enriched for de novo mutations in autism spectrum disorder. *Nature Genetics*, 46(7), 742–747. <https://doi.org/10.1038/ng.2980>

Uddin, M., Unda, B. K., Kwan, V., Holzapfel, N. T., White, S. H., Chalil, L., ... Singh, K. K. (2018). OTUD7A Regulates Neurodevelopmental Phenotypes in the 15q13.3 Microdeletion Syndrome. *American Journal of Human Genetics*, 102(2), 278–295. <https://doi.org/10.1016/j.ajhg.2018.01.006>

Uhlhaas, P. J., & Singer, W. (2006). Neural Synchrony in Brain Disorders: Relevance for Cognitive Dysfunctions and Pathophysiology. *Neuron*, 52(1), 155–168.

<https://doi.org/10.1016/j.neuron.2006.09.020>

Uhlhaas, P. J., & Singer, W. (2010). Abnormal neural oscillations and synchrony in schizophrenia. *Nature Reviews. Neuroscience*, 11(2), 100–113.

<https://doi.org/10.1038/nrn2774>

Ummethum, H., & Hamperl, S. (2020). Proximity Labeling Techniques to Study Chromatin. *Frontiers in Genetics*, 11(May), 1–13.

<https://doi.org/10.3389/fgene.2020.00450>

Unsain, N., Stefani, F. D., & Cáceres, A. (2018). The actin/spectrin membrane-associated periodic skeleton in neurons. *Frontiers in Synaptic Neuroscience*, 10(MAY), 1–8.

<https://doi.org/10.3389/fnsyn.2018.00010>

van Os, J., & Kapur, S. (2009). Schizophrenia. *Lancet*, 374(9690):635-645. doi:

10.1016/S0140-6736(09)60995-8; 10.1016/S0140-6736(09)60995-8.

Varghese, M., Keshav, N., Jacot-Descombes, S., Warda, T., Wicinski, B., Dickstein, D. L., ... Hof, P. R. (2017). Autism spectrum disorder: neuropathology and animal

models. *Acta Neuropathologica*, 134(4), 537–566. <https://doi.org/10.1007/s00401-017-1736-4>

- Vicari, S., Napoli, E., Cordeddu, V., Menghini, D., Alesi, V., Loddo, S., ... Tartaglia, M. (2019, June 8). Copy number variants in autism spectrum disorders. *Progress in Neuro-Psychopharmacology and Biological Psychiatry*. Elsevier Inc.
<https://doi.org/10.1016/j.pnpbp.2019.02.012>
- Virués-Ortega, J. (2010). Applied behavior analytic intervention for autism in early childhood: Meta-analysis, meta-regression and dose-response meta-analysis of multiple outcomes. *Clinical Psychology Review*, 30(4), 387–399.
<https://doi.org/10.1016/j.cpr.2010.01.008>
- Wang, P., Zhao, D., Lachman, H. M., & Zheng, D. (2018). Enriched expression of genes associated with autism spectrum disorders in human inhibitory neurons. *Translational Psychiatry*, 8(1). <https://doi.org/10.1038/s41398-017-0058-6>
- Wassman, E. R., Ho, K. S., Bertrand, D., Davis, K. W., Martin, M. M., Page, S., ... Hensel, C. H. (2019). Critical exon indexing improves clinical interpretation of copy number variants in neurodevelopmental disorders. *Neurology Genetics*, 5(6), e378.
<https://doi.org/10.1212/nxg.0000000000000378>
- Wehr, M. C., Hinrichs, W., Brzózka, M. M., Unterbarnscheidt, T., Herholt, A., Wintgens, J. P., ... Rossner, M. J. (2017). Spironolactone is an antagonist of NRG 1- ERBB 4 signaling and schizophrenia-relevant endophenotypes in mice. *EMBO Molecular Medicine*, 9(10), 1448–1462. <https://doi.org/10.15252/emmm.201707691>

- Weibrecht, I., Leuchowius, K. J., Clausson, C. M., Conze, T., Jarvius, M., Howell, W. M., ... Söderberg, O. (2010). Proximity ligation assays: A recent addition to the proteomics toolbox. *Expert Review of Proteomics*, 7(3), 401–409.
<https://doi.org/10.1586/epr.10.10>
- Widagdo, J., Guntupalli, S., Jang, S. E., & Anggono, V. (2017). Regulation of AMPA receptor trafficking by protein ubiquitination. *Frontiers in Molecular Neuroscience*, 10(October), 1–10. <https://doi.org/10.3389/fnmol.2017.00347>
- Wilfert, A. B., Sulovari, A., Turner, T. N., Coe, B. P., & Eichler, E. E. (2017). Recurrent de novo mutations in neurodevelopmental disorders: properties and clinical implications. *Genome Med.* <https://doi.org/10.1186/s13073-017-0498-x>
- Wimmer, V. C., Reid, C. A., So, E. Y., Berkovic, S. F., & Petrou, S. (2010). Axon initial segment dysfunction in epilepsy. *J Physiol*, 11, 1829–1840.
<https://doi.org/10.1113/jphysiol.2010.188417>
- Wonders, C. P., & Anderson, S. a. (2006). The origin and specification of cortical interneurons. *Nature Reviews Neuroscience*, 7(9), 687–696.
<https://doi.org/10.1038/nrn1954>
- Woodard, C. M., Campos, B. A., Kuo, S. H., Nirenberg, M. J., Nestor, M. W., Zimmer, M., ... Noggle, S. A. (2014). iPSC-derived dopamine neurons reveal differences between monozygotic twins discordant for parkinson's disease. *Cell Reports*, 9(4), 1173–1182. <https://doi.org/10.1016/j.celrep.2014.10.023>

- Wu, X., Liu, S., Sagum, C., Chen, J., Singh, R., Chaturvedi, A., ... Wang, B. (2019). Crosstalk between Lys63- and Lys11-polyubiquitin signaling at DNA damage sites is driven by Cezanne. *Genes & Development*, 33(23–24), 1702–1717. <https://doi.org/10.1101/gad.332395.119>
- Wu YE, Parikshak NN, Belgard TG, Geschwind DH. (2016). Genome-wide, integrative analysis implicates microRNA dysregulation in autism spectrum disorder. *Nat Neurosci*, 19, 1463–76.
- Xu, Z., Pei, L., Wang, L., Zhang, F., Hu, X., & Gui, Y. (2014). Snail1-dependent transcriptional repression of Cezanne2 in hepatocellular carcinoma. *Oncogene*, 33(22), 2836–2845. <https://doi.org/10.1038/onc.2013.243>
- Yaeger, C. E., Ringach, D. L., & Trachtenberg, J. T. (2019). Neuromodulatory control of localized dendritic spiking in critical period cortex. *Nature*, 567(7746), 100–104. <https://doi.org/10.1038/s41586-019-0963-3>
- Yang, R., Walder-Christensen, K. K., Lalani, S., Yan, H., García-Prieto, I. D., Álvarez, S., ... Bennett, V. (2019). Neurodevelopmental mutation of giant ankyrin-G disrupts a core mechanism for axon initial segment assembly. *PNAS*, 116(39), 19717–19726. <https://doi.org/10.1073/pnas.1909989116>
- Ye, F., Kang, E., Yu, C., Qian, X., Jacob, F., Yu, C., ... Zhang, M. (2017). DISC1 Regulates Neurogenesis via Modulating Kinetochore Attachment of Ndel1/Nde1

during Mitosis. *Neuron*, 96(5), 1041-1054.e5.

<https://doi.org/10.1016/j.neuron.2017.10.010>

Yin, J., Chen, W., Chao, E. S., Soriano, S., Wang, L., Wang, W., ... Schaaf, C. P. (2018).

Otud7a Knockout Mice Recapitulate Many Neurological Features of 15q13.3

Microdeletion Syndrome. *American Journal of Human Genetics*, 102(2), 296–308.

<https://doi.org/10.1016/j.ajhg.2018.01.005>

Yoon, S., Parnell, E., Kasherman, M., Forrest, M. P., Myczek, K., Premarathne, S., ...

Penzes, P. (2020). Usp9X Controls Ankyrin-Repeat Domain Protein Homeostasis

during Dendritic Spine Development. *Neuron*, 105(3), 506-521.e7.

<https://doi.org/10.1016/j.neuron.2019.11.003>

Youn, J. Y., Dunham, W. H., Hong, S. J., Knight, J. D. R., Bashkurov, M., Chen, G. I., ...

Gingras, A. C. (2018). High-Density Proximity Mapping Reveals the Subcellular

Organization of mRNA-Associated Granules and Bodies. *Molecular Cell*, 69(3),

517-532.e11. <https://doi.org/10.1016/j.molcel.2017.12.020>

Young CE, Arima K, Xie J, et al. (1998) SNAP-25 deficit and hippocampal connectivity

in schizophrenia. *Cereb Cortex.*;8(3):261-268.

Yuan, T., Yan, F., Ying, M., Cao, J., He, Q., Zhu, H., & Yang, B. (2018). Inhibition of

Ubiquitin-Specific Proteases as a Novel Anticancer Therapeutic Strategy. *Frontiers*

in Pharmacology, 9(September), 1–10. <https://doi.org/10.3389/fphar.2018.01080>

- Yuen, R.K., Merico, D., Cao, H., Pellecchia, G., Alipanahi, B., Thiruvahindrapuram, B., Tong, X., Sun, Y., Cao, D., Zhang, T., et al. (2016). Genome-wide characteristics of de novo mutations in autism. *NPJ genomic medicine* 1, 160271-1602710.
- Yuen, R. K. C., Merico, D., Bookman, M., Howe, J. L., Thiruvahindrapuram, B., Patel, R. V, ... Scherer, S. W. (2017). Whole genome sequencing resource identifies 18 new candidate genes for autism spectrum disorder. *Nat Neurosci*, 20, 21.
<https://doi.org/10.1038/nn.4524>
- Zarrei, M., Burton, C. L., Engchuan, W., Young, E. J., Higginbotham, E. J., Macdonald, J. R., ... Scherer, S. W. (2019). A large data resource of genomic copy number variation across neurodevelopmental disorders. *Npj Genomic Medicine*, 4(26).
<https://doi.org/10.1038/s41525-019-0098-3>.
- Zhang, S., Zhang, X., Ma, S., Purmann, C., Davis, K., Wong, W. H., ... Urban, A. (2020). Network effects of the neuropsychiatric 15q13.3 microdeletion on the transcriptome and epigenome in human induced neurons. *Biological Psychiatry*, 3223(20), 31710–31718. <https://doi.org/10.1101/77254>
- Zhang, X., Linder, S., & Bazzaro, M. (2020). Drug Development Targeting the Ubiquitin–Proteasome System (UPS) for the Treatment of Human Cancers. *Cancers (Basel)*, 12(4):902. doi: 10.3390/cancers12040902
- Zhou, Y., Kaiser, T., Monteiro, P., Zhang, X., Van der Goes, M. S., Wang, D., ... Feng, G. (2016). Mice with Shank3 Mutations Associated with ASD and Schizophrenia

Display Both Shared and Distinct Defects. *Neuron*, 89(1), 147–162.

<https://doi.org/10.1016/j.neuron.2015.11.023>

Zhu, S., Cordner, Z. A., Xiong, J., Chiu, C. T., Artola, A., Zuo, Y., ... Ross, C. A. (2017).

Genetic disruption of ankyrin-G in adult mouse forebrain causes cortical synapse alteration and behavior reminiscent of bipolar disorder. *PNAS*, 114(39), 10479–10484. <https://doi.org/10.1073/pnas.1700689114>

Ziats, M. N., Goin-Kochel, R. P., Berry, L. N., Ali, M., Ge, J., Guffey, D., ... Schaaf, C.

P. (2016). The complex behavioral phenotype of 15q13.3 microdeletion syndrome. *Genetics in Medicine*, 18(11), 1111–1118. <https://doi.org/10.1038/gim.2016.9>